PACIFIC EARTHQUAKE ENGINEERING
RESEARCH CENTER

Amplification Factors for Spectral Acceleration in Active Regions

Jonathan P. Stewart

Andrew H. Liu

Yoojoong Choi

and

Mehmet B. Baturay

Department of Civil and Environmental Engineering
University of California, Los Angeles

A report on research conducted under Grant No. EEC-9701568
from the National Science Foundation and Grant No. 1098-712
from the California Strong Motion Instrumentation Program

PEER 2001/10
DEC. 2001

Amplification Factors for Spectral Acceleration in Active Regions

Jonathan P. Stewart
Andrew H. Liu
Yoojoong Choi
and
Mehmet B. Baturay
Department of Civil and Environmental Engineering
University of California, Los Angeles

A report on research conducted under Grant No. EEC-9701568
from the National Science Foundation and Grant No. 1098-712
from the California Strong Motion Instrumentation Program

PEER Report 2001/10
Pacific Earthquake Engineering Research Center
College of Engineering
University of California, Berkeley

December 2001

EXECUTIVE SUMMARY

Empirical relationships are developed to predict amplification factors for 5% damped spectral acceleration (period range T = 0.01 – 5 s) as a function of site category. Amplification is evaluated by normalizing ground motion intensity measures from recordings by reference motions derived from modified attenuation relationships for active regions. The Abrahamson and Silva attenuation relationship for rock sites was used for the derivation of reference motions, with modifications to account for event terms and rupture directivity effects.

Strong motion sites are classified according to three geologic classification schemes: age-only, age + depositional environment, and age + material texture. Sites are also classified using the average shear wave velocity over the upper 30 m ($V_{s\text{-}30}$) and a recently proposed geotechnical classification scheme. Within each scheme, amplification of spectral acceleration is regressed against reference motion amplitude, and the magnitude-dependence of the residuals is evaluated.

The results of the regression indicate distinct levels of high-frequency spectral acceleration amplification across geologic age categories, but relatively modest variations between categories at long periods ($T \geq \sim 1$ s). Within the Quaternary age group, statistically significant variations in high-frequency amplification are observed between Holocene lacustrine/marine and Quaternary alluvial sediments, and also between Holocene coarse- and fine/mixed-texture sediments. Nonlinear ground response is evident in many categories from statistically significant decreases in low-period spectral amplification with increasing reference motion amplitude. Amplification of long-period ground motions is found to be less sensitive to the reference amplitude, but to increase significantly with magnitude.

We find spectral acceleration amplification functions for geologic classification schemes that incorporate information beyond age to have a smaller average residual dispersion than age-only schemes. Classification schemes based on $V_{s\text{-}30}$, and geotechnical data produced consistently higher dispersion than did detailed geologic classifications. However, the $V_{s\text{-}30}$-based classification scheme provides the clearest distinction between amplification factors in different categories. These findings have implications for the type of mapping that is most useful for regional ground motion characterizations.

Spectral acceleration amplification levels at all ground motion amplitudes and period ranges are found to be smaller than those in modern design codes (e.g., 2000 NEHRP Provisions). This

is attributed to differences in the characteristics of “rock” sites used to develop reference motions for the studies underlying the code provisions and this study. The rock site condition associated with this study is a composite average of rock sites in active regions — which most nearly corresponds to “soft rock.” Since the same rock site condition is inherent to rock attenuation relations, the amplification functions derived herein provide an appropriate means by which to adjust the statistical moments (median and standard error) from rock attenuation relations (applicable to active regions) for the effects of site conditions. Most previous studies, including the work that provides the empirical basis for the current NEHRP provisions, employ reference motions from relatively firm rock sites. The relatively large reference motion amplitudes from soft rock sites lead to the smaller amplification levels.

ACKNOWLEDGMENTS

Support for this study was provided by the Pacific Earthquake Engineering Research Center through the Earthquake Engineering Research Centers Program of the National Science Foundation under Award number EEC-9701568, and the California Department of Conservation, Division of Mines and Geology, Strong Motion Instrumentation Program, Contract 1098-712. This support is gratefully acknowledged. We would like to thank Drs. Moh Huang and Anthony Shakal of CSMIP, and the members of the CSMIP Advisory Committee, for their valuable advice and contributions of data. In particular, CSMIP staff provided accurate station locations that increased the quality of the site classifications. Charles Real of CDMG facilitated the acquisition of digital SCAMP maps for southern California. Drs. Walter Silva and Norman Abrahamson provided strong motion data for use in this study. James Chen of UCLA assisted with data synthesis and analysis. Steve Erickson of the UCLA Statistics Consulting Group provided consultation on the statistical processing of regression results. Dr. Roger Borcherdt of the U.S. Geological Survey provided valuable advice and suggestions during numerous conversations on this topic.

CONTENTS

LIST OF FIGURES

LIST OF TABLES

1 Introduction

Ground motion attenuation relationships are commonly used in seismic design practice to estimate earthquake ground motion intensity measures (*IM*s) such as spectral acceleration and duration. In particular, attenuation relationships provide statistical moments of a probabilistic distribution of *IM* conditioned on parameters such as magnitude, site-source distance, site condition, and style-of-faulting parameters. Ground motion data are often log-normally distributed, in which case the distribution can be represented by a median and standard deviation, σ (in natural logarithmic units).

Site condition is often characterized in attenuation relations as either rock or soil. Actual conditions at strong motion recording sites are variable with respect to local site conditions and underlying basin structure, and hence estimates from attenuation relationships necessarily represent averaged values across the range of possible site conditions within the "rock" or "soil" categories. The intent of this study is to evaluate the degree to which more detailed information on site conditions can be used to improve ground motion predictions relative to what is obtained with attenuation relationships. This "improvement" in ground motion prediction generally involves (1) removing potential bias in median ground motion estimates that might be present for a particular site condition, and (2) reducing the uncertainty in ground motion estimates, as measured by standard error term, σ.

Ground motion variations between a reference site condition and the actual site condition are described in terms of amplification factors that are a function of the amplitude of shaking on the reference site condition. We estimate ground motion amplification factors using a so-called "non-reference site" method in which amplification is defined as the ratio of *IMs* from recorded motions to reference motion *IMs*. The reference motion represents the ground motion that would have been expected at the site for the reference site condition. The reference motion *IMs* are defined using an attenuation relation for rock sites in active regions modified with an event term

and for rupture directivity effects. As such, this approach incorporates the observed, event-specific characteristics of source and path into the reference motions so that the ratio of recorded/reference *IMs* isolates (to the extent possible with a non-reference site approach) the effects of local geologic conditions on the ground motion. Additional details on the calculation of reference motion parameters are provided in Chapter 4.

A major thrust of the study was the classification of strong motion sites according to surface geology, average shear wave velocity in the upper 30 m ($V_{s\text{-}30}$, calculated as the ratio of 30 m to travel time for shear waves to travel from 30 m to the ground surface), and a geotechnical classification scheme. This work is discussed in Chapter 3, and resulted in surface geology classifications for 460 sites, $V_{s\text{-}30}$ classifications (established from local in situ measurements) for 185 sites, and geotechnical classifications for 183 sites. Data from the 1999 Chi-Chi (Taiwan) earthquake were not included in this compilation. However, using preliminary available site classifications, the Taiwan data are compared to the results of the present study in Chapter 6.

The process by which amplification factors are derived for a given recording is described in Chapter 4. Also described is the manner with which amplification factors within various site categories are regressed against ground motion amplitude. Median levels of amplification and the standard error of the residuals were compiled within site categories, the results of which are discussed in Chapter 5. We interpret the results in Chapter 6 to identify the relative merits of the variations classification schemes for estimating spectral acceleration. We also compare our results to those of previous investigators and discuss the practical implications of our findings.

2 Previous Studies

Site response effects associated with local ground response and/or basin response can be evaluated from ground motion recordings using amplification factors, which represent the ratio of an observed ground motion intensity measure to a reference value of that intensity measure for a particular site condition (e.g., intact rock or rock-average for active regions). Statistically robust empirical evaluations of site amplification generally cannot be performed on a site-specific basis due to lack of data. Accordingly, amplification factors for specific sites are assumed to be similar to those derived from strong motion recordings at other sites with similar geologic and/or geotechnical conditions. The following sections describe approaches used to derive amplification functions from accelerograms and the factors that have been found to control amplification in previous work. Classification schemes used to delineate ground conditions are described in Chapter 3.

2.1 TYPES OF OBSERVATIONAL STUDIES

Earthquake ground motions are affected by source, path, and site effects. Quantification of site effects from recorded motions requires the removal of source and path effects, which can be accomplished with two general categories of methods. The first compares motions on soil with those from a "reference" site, typically on rock. The second approach does not use a reference site.

Three types of reference site approaches have been commonly used:

1. If the rock recording is close to the soil site, both motions presumably contain similar source and path information, so a comparison of the two provides an estimate of site response effects. Investigations of this type have compared the motions using either response spectral ordinates (including peak horizontal acceleration) or Fourier amplitude spectra.

2. A variation on the first approach is to correct the reference and site recordings using a geometric spreading factor of $1/r$ (e.g., Borcherdt and Glassmoyer, 1994; Borcherdt, 1996) or frequency-dependant distance attenuation (e.g., Hartzell et al. 2000; Borcherdt 2001).

3. In a reference site approach developed by Andrews (1986), generalized inversions are performed using the Fourier spectra of observed motions adjusted for geometric spreading to evaluate source and site terms simultaneously. A weighted least-squares solution is developed in which the source term is allowed to have an arbitrary frequency dependence and the site response terms are taken as relative to the network average (Andrews, 1986) or relative to a single pre-determined "reference" site for which the site term is unity (e.g., Boatwright et al., 1991, Hartzell et al. 2000). Results of these studies have been found to compare favorably with more traditional reference site approaches (e.g., Field and Jacob, 1995). The principal advantage of this generalized inversion approach is that relatively large data sets can be utilized. However, results from most of the studies utilizing this approach are somewhat limited for engineering application, in that weak motions dominate the data sets; thus nonlinearities in sediment response are not represented in the identified amplification factors.

The second category of approaches for evaluating site amplification effects does not require the presence of a reference site. Such approaches have the advantage of being able to incorporate relatively large amounts of strong motion data. One such approach, termed horizontal-to-vertical spectral ratio (HVSR), involves normalizing the horizontal component spectra for a given site by the vertical component spectra for that same site, with the spectrum computed over the shear-wave dominated portion of the record (Lermo and Chavez-Garcia, 1993). The HVSR method has generally been found to extract the same spectral peaks as reference site methods, but different amplification levels, thus limiting its practical application (Field and Jacob, 1995; Bonilla et al., 1997). A second approach implements a generalized inversion scheme to identify source, path, and site effects for a given earthquake (Boatwright et al., 1991). The approach is similar to that of Andrews (1986) described above, but the source and path are now parameterized, and the site factor averaged across all frequencies and sites is constrained based on *a priori* information (Field and Jacob, 1995). While this approach, when properly implemented, can produce spectral ratios comparable to those observed from adjacent rock/soil sites (e.g., Field and Jacob, 1995), the aforementioned need for *a priori* information on ground response is a limitation.

A third non-reference site approach consists of evaluating amplification by normalizing the spectra of recorded motions by a reference (typically rock) spectrum obtained from an attenuation relationship. This approach has been applied to specific basins by Sokolov (1997) and Sokolov et al. (2000) using locally derived attenuation functions for Fourier amplitude spectra, and for the southern California region using attenuation relations for spectral acceleration (Field, 2000; Lee and Anderson, 2000; Steidl, 2000). This approach offers several advantages to others previously identified:

1. A much larger inventory of strong motion data can be utilized than for reference site approaches. For example, the southern California database used by the above-referenced researchers included 449 recordings from 281 stations and 28 earthquakes (Steidl and Lee, 2000).
2. No *a priori* assumptions about site effects are required.
3. Amplification factors derived in this way can be readily incorporated into hazard analyses as adjustments to predictions from rock attenuation relations.

The present study is based on this non-reference site approach, and like the cited studies for the southern California region, uses attenuation relations for spectral acceleration to derive reference motions.

2.2 OUTCOMES OF OBSERVATIONAL STUDIES

In this section, we review significant findings from observational studies of strong ground motion amplification at soil sites. Classification schemes used to categorize sites in these studies are presented in Chapter 3. Additional studies of weak-motion amplification are summarized by Field et al. (2000) and are not discussed here. An inherent feature of studies performed to date is that the influence of shallow, nearly one-dimensional ground response effects and the effects of deeper basin structure cannot be readily distinguished in recordings from sedimentary basins. Hence, empirical amplification factors necessarily incorporate both effects to varying degrees.

2.2.1 Studies Utilizing a Reference Site Approach

The 1989 Loma Prieta earthquake provided one of the first strong motion data sets with a sufficient number of recordings to evaluate amplification factors across a diverse array of surface geologic conditions. Borcherdt and Glassmoyer (1994) utilized 37 recordings from the San Francisco Bay region to evaluate site amplification factors as a function of $V_{s\text{-}30}$, which was generally evaluated from local downhole measurements. Amplification was evaluated relative to recordings from nearby rock sites, which consist of either Franciscan complex bedrock or well-consolidated sedimentary bedrock of Tertiary-Mesozoic age. Where the reference recording was from a sedimentary bedrock site, the amplification factor was adjusted (increased) to a common reference site condition of "firm to hard rock," represented by the Franciscan complex. The resulting amplification factors for the 37 sites are plotted in Figure 2.1 for the T = 0.1–0.5 and 0.4–2.0 s period range (amplification factors across these ranges are denoted F_a and F_v, respectively).

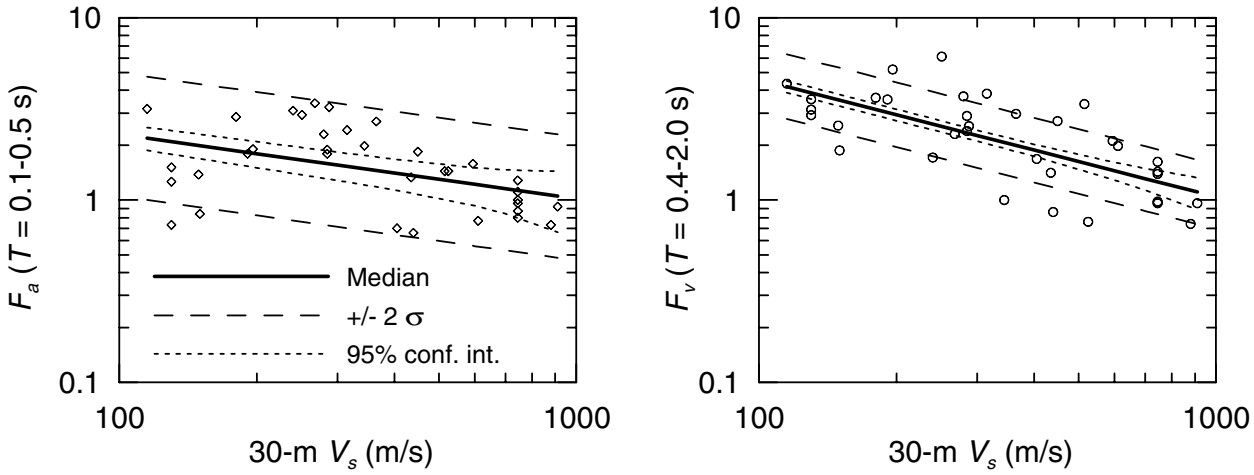

Fig. 2.1. Averaged spectral amplification vs. $V_{s\text{-}30}$ for 37 sites in the San Francisco Bay region that recorded the 1989 Loma Prieta earthquake (after Borcherdt and Glassmoyer, 1994)

Borcherdt (2001) performed a similar study using 125 recordings from the 1994 Northridge earthquake (mostly stiff soil and soft rock sites). Reference motions for the Northridge recordings were taken from local stations with metamorphic rock (e.g., weathered granite, gneiss) or sedimentary rock. Values of $V_{s\text{-}30}$ were estimated for the recording sites using local borehole measurements or correlations with surface geology. As shown in Figure 2.2, for relatively small ground motion levels (PHA ≤ 0.1g on rock), Northridge amplification factors for deep soil sites at small periods (i.e., F_a) are smaller than those obtained by Borcherdt and Glassmoyer (1994) for the Loma Prieta earthquake, but the amplification factors are comparable at longer periods (i.e., F_v). The Northridge results demonstrate decreasing amplification with increasing reference motion amplitude, which is evidence of nonlinearity in sediment response.

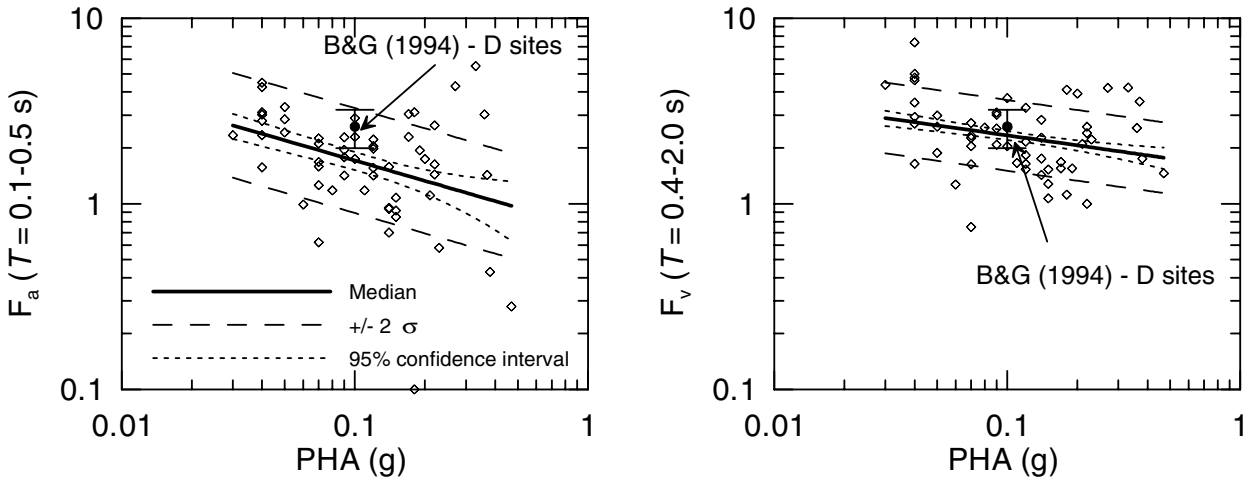

Fig. 2.2. Averaged spectral amplification vs. reference motion amplitude for Northridge earthquake stiff soil recordings (Borcherdt, 2001), as compared to low amplitude results of Borcherdt and Glassmoyer (1994) for Loma Prieta earthquake (symbol indicates median ± one standard error). Reference motion amplitude is taken as a scaled motion from a nearby rock site.

Harmsen (1997) evaluated mainshock recordings in the San Fernando Valley and Los Angeles basin from the 1971 San Fernando, 1987 Whittier, 1991 Sierra Madre, and 1994 Northridge events. Amplification factors relative to a single reference rock site (Caltech Seismic Lab) were derived using the inversion approach of Andrews (1986). The amplification factors were derived across intermediate (0.5–1.5 Hz) and high (2.0–6.0 Hz) frequency bands, and were correlated to site classes defined by $V_{s\text{-}30}$. As shown in Figure 2.3, the median fit through these data indicate slightly higher amplification levels than those of Borcherdt and Glassmoyer (1994), which is opposite to the finding of Borcherdt (2001). The results were found to be similar to amplification levels derived from weak-motion studies (e.g., Hartzell et al., 1996; Rogers et al., 1984). Based on this similarity, Harmsen suggested that amplification factors derived from weak-motion data could be used for strong motion applications (i.e., hazard analyses).

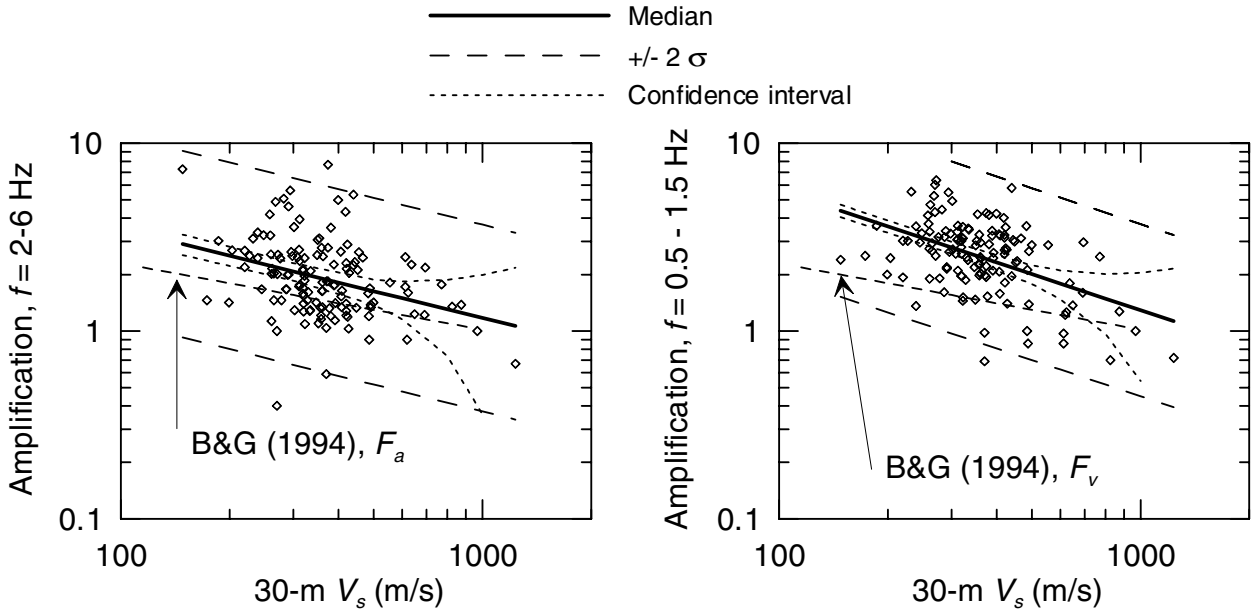

Fig. 2.3. Averaged spectral amplification vs. $V_{s\text{-}30}$ for Los Angeles region strong motion sites by Harmsen (1997), compared with results of Borcherdt and Glassmoyer (1994) for Loma Prieta earthquake

2.2.2 Studies Utilizing a Non-Reference Site Approach

Three recent projects coordinated through the Southern California Earthquake Center (SCEC) developed amplification factors by comparing recorded motions from the southern California region to predictions from attenuation relations (Field, 2000; Lee and Anderson, 2000; Steidl, 2000). The present study is utilizing a similar approach but a larger data set covering shallow crustal earthquakes in active regions. The following shows the attenuation relationships used to develop reference motions and the site classification systems used in these studies:

Investigator	Attenuation Relationship	Site Classification
Steidl (2000)	Sadigh (1993), rock	geology, basin depth, $V_{s\text{-}30}$
Lee and Anderson (2000)	Abrahamson and Silva (1997), soil or rock	geology, basin depth, wk. motion amp., etc.
Field (2000)	revised Boore et al. (1997), V_s = 760 m/s	$V_{s\text{-}30}$

In each study, amplification factors were inferred from residuals, i.e., differences between the natural logarithm of the data and the reference motion. Field (2000) and Lee and Anderson (2000) removed event terms before evaluating residuals, whereas Steidl (2000) used unadjusted predictions that map inter-event data variations into amplification factors.

The correlation between surface geology and amplification has been investigated by Steidl (2000) and Lee and Anderson (2000). Both classified strong motion stations using an age-based Q-T-M classification scheme. Steidl also investigated the relative merits of a more detailed classification scheme based on the mapping of Fumal and Tinsley (1985) and Tinsley and Fumal (1985) in which younger Quaternary (Qy) is separated from older Quaternary (Qo), with Tertiary added to the Qo class. Lee and Anderson utilized age and soil texture-based criteria (based on the Fumal and Tinsley mapping) to derive more detailed geological classifications.

Steidl evaluated mean amplification factors (relative to soft rock) for spectral periods T = 0 (PHA), 0.3, 1.0, and 3.0 s using data with reference motion PHA values in the following ranges: < 0.05g, 0.05-0.1g, 0.1-0.2g, >0.2g. The results at T = 0.3 and 1.0 s are compared to the findings

of Borcherdt (2001) for deep sedimentary sites in Figure 2.4. Noteworthy trends from this figure are (1) that Steidl, as Borcherdt, found significant nonlinear sediment response at low periods; (2) that Steidl's amplification factors are smaller than those of Borcherdt, particularly at long periods; and (3) that there are only small differences in amplification factors for the Q, Qo, and Qy site categories.

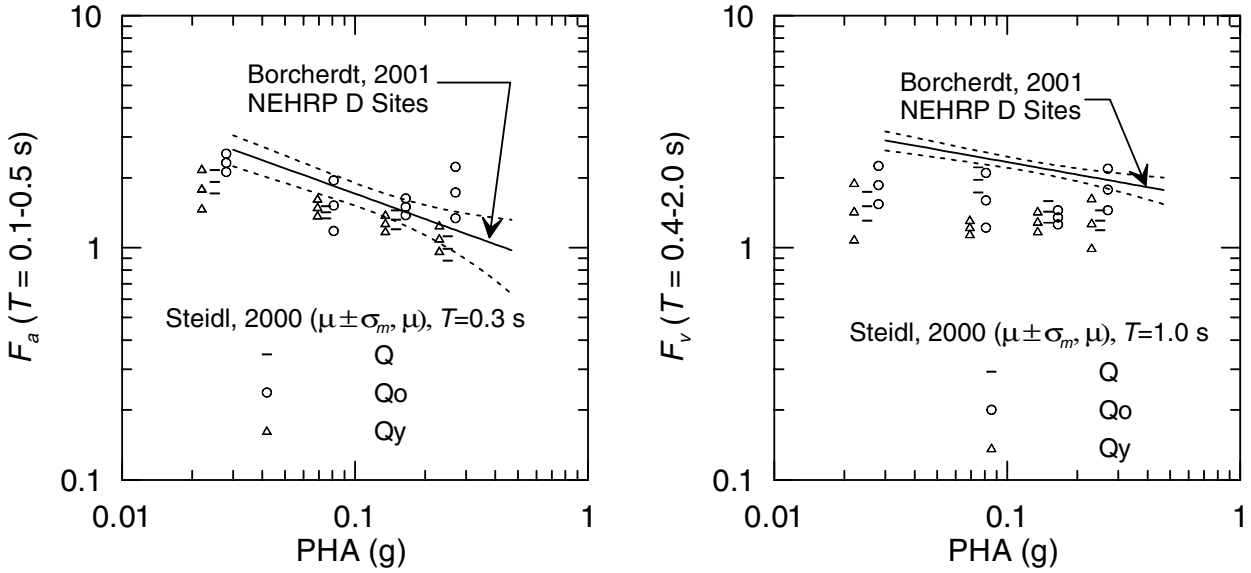

Fig. 2.4. Comparison of spectral amplification from Northridge earthquake (by Borcherdt, 2001) with results of Steidl (2000) for Quaternary sediments. Symbol μ denotes mean estimate by Steidl, σ_m denotes standard error of the mean.

Lee and Anderson (2000) derived amplification factors for the same spectral periods as Steidl, but used reference motions calculated from soil attenuation functions for Quaternary sites and rock attenuation functions for Tertiary and Mesozoic sites. Thus, amplification is not relative to rock for sites on soil. Their results generally indicate mean residuals within the various geologic categories that are not distinguishable from zero, with the notable exception of Tertiary sediments, for which the rock attenuation function underpredicted the observed motions at low periods.

Field (2000) and Steidl (2000) evaluated amplification factors as a function of V_{s-30}. The V_{s-30} site classifications used by Field (2000) are based on maps by Wills et al. (2000) that correlate V_{s-30} to surface geology obtained from 1:250,000 scale maps. The V_{s-30} site classifications used by Steidl (2000) are based on in situ measurements from boreholes within 1.0 km of the strong motion station. Field found relatively distinct weak-motion amplification levels in different NEHRP site categories (e.g., Figure 2.5). Steidl found a good correlation between amplification and V_{s-30} at long periods (T = 1.0 and 3.0 s); these results are similar to those of Harmsen (1997) previously reported (Figure 2.3). At smaller periods, the correlation between amplification and V_{s-30} was found to be relatively weak and dependent on shaking amplitude.

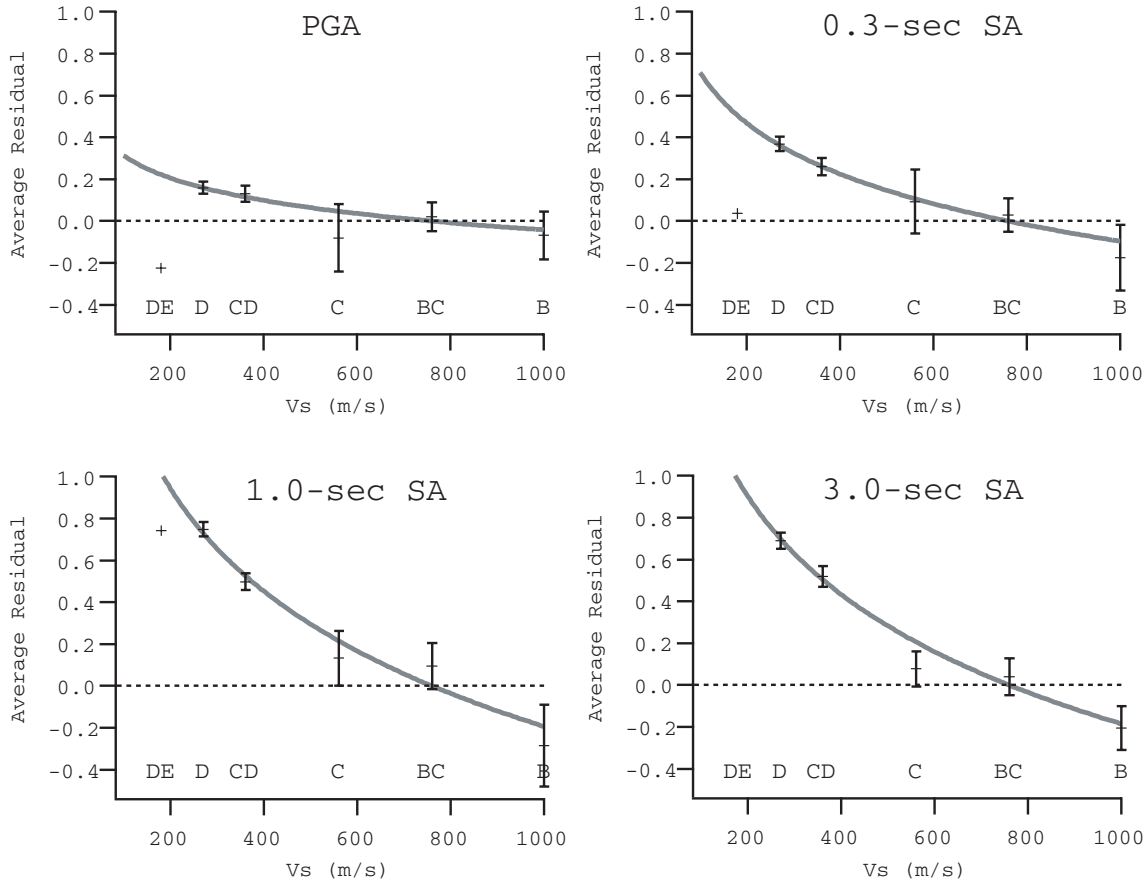

Fig. 2.5. Average residuals between southern California strong motion data and attenuation prediction for V_s = 760 m/s site condition as function of V_{s-30} (Field, 2000)

The studies by Steidl, Lee and Anderson, and Field found amplification to increase significantly with basin depth (defined as depth to V_s = 2.5 km/s isosurface), with representative results shown in Figure 2.6. The amplification factors in Figure 2.6 are defined relative to the prediction appropriate to each site class (i.e., not relative to a particular geologic formation or V_s = 760 m/s). Lee and Anderson attempted to correlate other parameters to amplification factors, the most promising and readily available of which is low-frequency amplification from basin modeling (i.e., 3D/1D amplification). However, this factor was found to be highly correlated to basin depth, and no trend could be identified in depth-adjusted data residuals. Hence, only basin depth was recommended as a parameter to supplement surface geology.

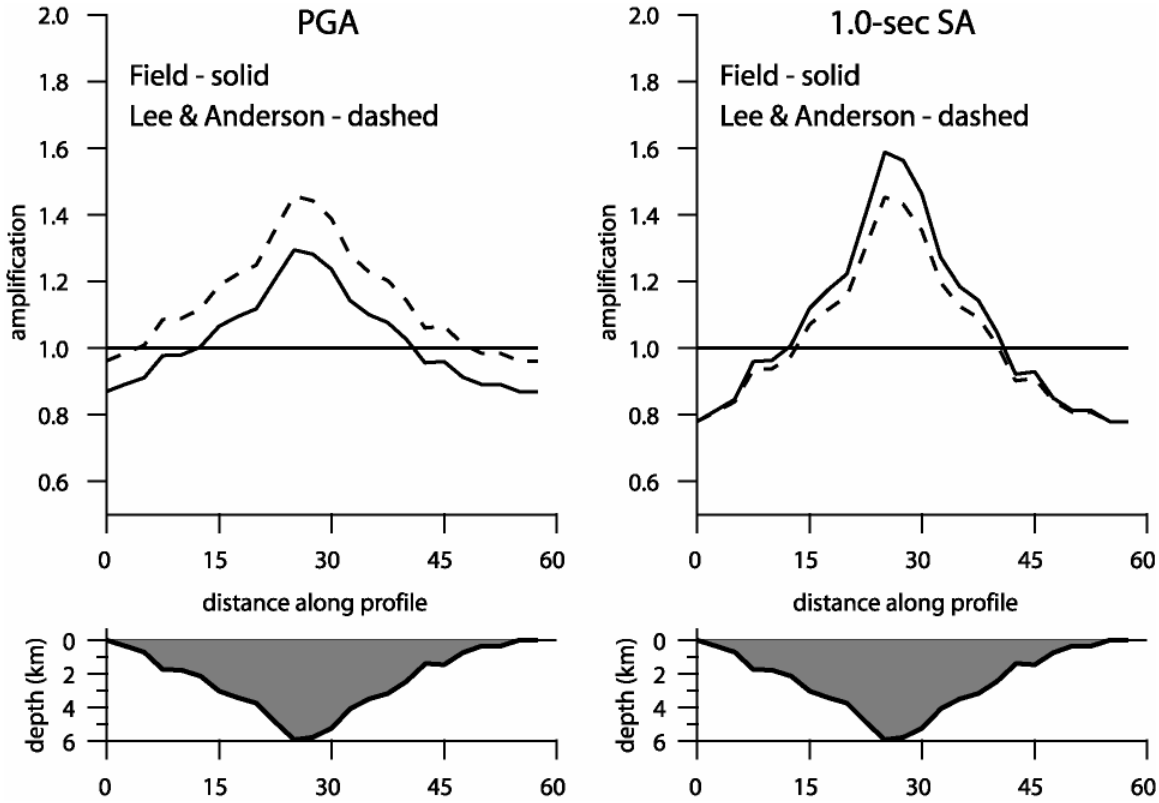

Fig. 2.6. Basin depth amplification factors implied by the attenuation relationships by Lee and Anderson (2000) and Field (2000), for sites along cross section through Los Angeles basin, after Field et al. (2000)

2.2.3 Discussion

Many of the observational studies outlined above quantified ground motion variations relative to a "hard rock" reference site condition. The attractiveness of this approach is obvious – ground response at the reference site should be small. The drawback is that reference motions for such site conditions cannot be readily evaluated because the data inventory is sparsely populated; hence, empirical attenuation relationships are difficult to develop. The ability to develop attenuation relations for the reference site condition is essential for practical application. Accordingly, for California, the most logical choice of a reference site condition may be weathered rock sites (primarily Tertiary in age), for which strong motion data are much more abundant than "hard" rock sites. The evaluation of amplification factors for this representative site condition is an important objective of this study.

3 Database

3.1 STRONG MOTION DATA SET

The database used in this study consists of 1828 recordings from 154 earthquakes. These recordings are from world-wide shallow crustal earthquakes near active plate margins. Subduction and inter-plate events are excluded. Event dates range from the 1933 Long Beach, California earthquake to the 1999 Duzce, Turkey, earthquake. Removed from the data set for this study were recordings from events with poorly defined magnitude or focal mechanism, recordings for which site-source distances are poorly constrained, and recordings for which problems were detected with one or more components. These removals reduced the data set to 1032 recordings from 51 events. The distribution of magnitude *(m)* and closest distance *(r)* parameters for the full data set are shown in Figure 3.1. The earthquakes contributing data to this study are listed in Table 3.1. Although listed in Table 3.1, data from the 1999 Chi-Chi, Taiwan, earthquake were not used in the main body of this study due to the preliminary nature of the site classifications. However, data from this earthquake are compared to the results of this study in Section 6.3.

The ground motion intensity measure for which amplification factors are derived in this study is 5% damped spectral acceleration. The spectral periods considered range from $T = 0.01$ to 5 s. Spectral ordinates with periods greater than $T = 1.25 \times 1/f_{HP}$ are not used, where f_{HP} = high-pass frequency used during data processing. We do not discard ordinates at frequencies higher than the low-pass frequency (f_{LP}) because of the saturation of S_a at high frequency. The distribution of spectral ordinates at $T = 0.01$ (PHA), 0.3, 1.0, and 3.0 s is presented in Figure 3.2. A significant amount of data has sufficiently large amplitude that sediment nonlinearity might be expected.

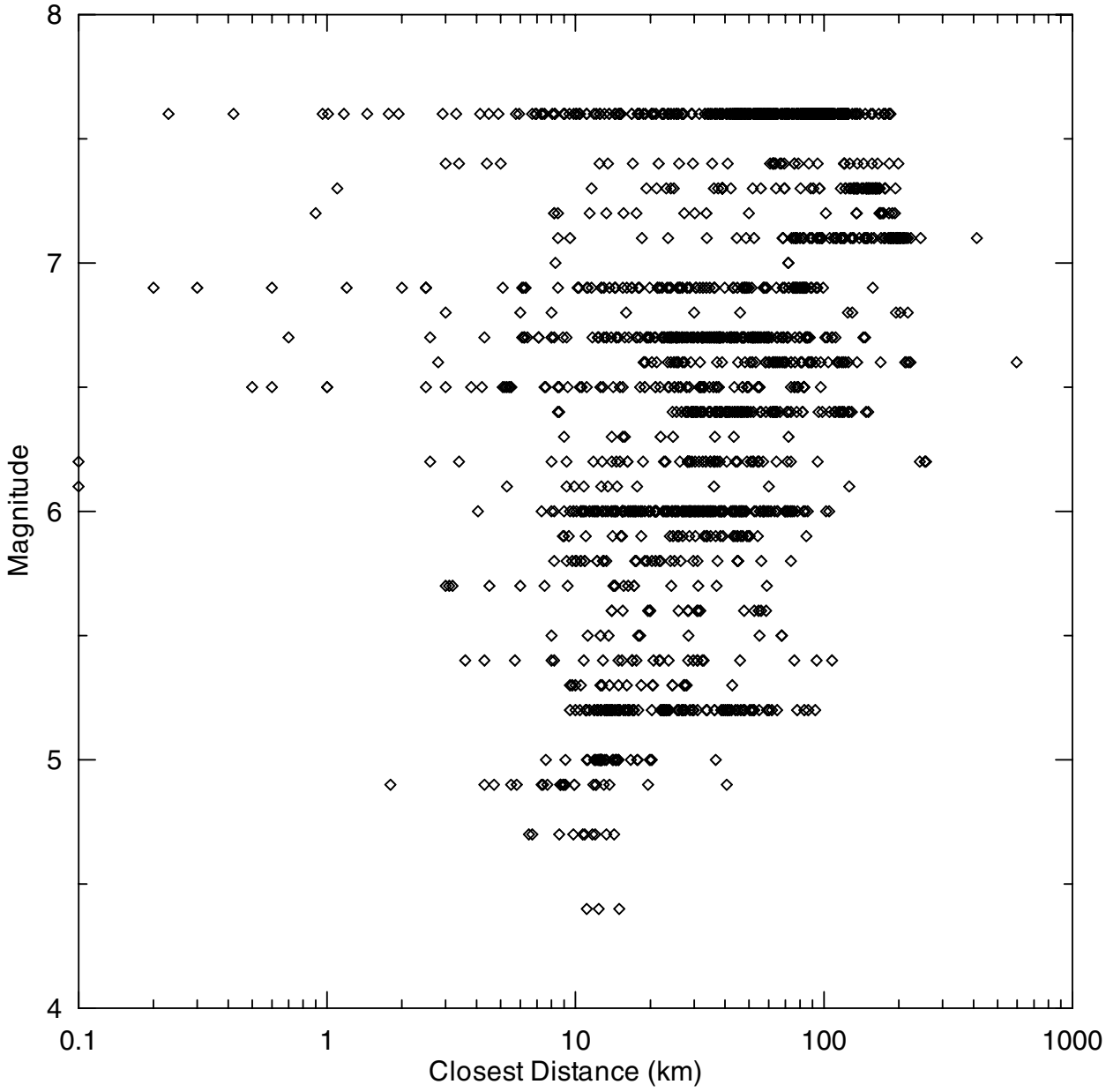

Fig. 3.1. Inventory of strong motion recordings from shallow crustal earthquakes in active tectonic regions; March 1933, Long Beach, California, earthquake to November 1999, Duzce, Turkey, earthquake (most data from PEER strong motion database)

Table 3.1. Earthquakes used in this study

Event	Year	Mo-Day	Time	Magnitude
Imperial Valley	1940	519	437	7.0
Kern County	1952	721	1153	7.4
San Francisco	1957	322	1944	5.3
Parkfield	1966	628	426	6.1
Borrego Mtn	1968	409	230	6.8
Lytle Creek	1970	912	1430	5.4
Hollister	1974	1128	2301	5.2
Oroville	1975	801	2020	6.0
Oroville	1975	802	2022	5.0
Oroville	1975	802	2059	4.4
Oroville	1975	808	700	4.7
Santa Barbara	1978	813		6.0
Tabas, Iran	1978	916		7.4
Coyote Lake	1979	806	1705	5.7
Imperial Valley	1979	1015	2316	6.5
Imperial Valley	1979	1015	2319	5.2
Imperial Valley	1979	1016	658	5.5
Livermore	1980	124	1900	5.8
Livermore	1980	127	233	5.4
Mammoth Lakes	1980	527	1901	4.9
Mammoth Lakes	1980	531	1516	4.9
Mammoth Lakes	1980	611	441	5.0
Westmoreland	1981	426	1209	5.8
Coalinga	1983	502	2342	6.4
Coalinga	1983	509	249	5.0
Coalinga	1983	611	309	5.3
Coalinga	1983	709	740	5.2
Coalinga	1983	722	239	5.8
Morgan Hill	1984	424	2115	6.2
Bishop (Rnd Val)	1984	1123	1912	5.8
Hollister	1986	126	1920	5.4
N. Palm Springs	1986	708	920	6.0
Chalfant Valley	1986	720	1429	5.9
Chalfant Valley	1986	721	1442	6.2
Chalfant Valley	1986	721	1451	5.6
Chalfant Valley	1986	731	722	5.8
Whittier Narrows	1987	1001	1442	6.0
Whittier Narrows	1987	1004	1059	5.3
Superstition Hills (A)	1987	1124	514	6.3
Superstition Hills (B)	1987	1124	1316	6.7
Loma Prieta	1989	1018	5	6.9
Cape Mendocino	1992	425	1806	7.1
Landers	1992	628	1158	7.3
Big Bear	1992	628	1506	6.4
Northridge	1994	117	1231	6.7
Northridge Aftershock	1994	117	431	5.9
Northridge Aftershock	1994	320	1320	5.2
Kobe, Japan	1995	116	2046	6.9
Kocaeli, Turkey	1999	817		7.4
Hector Mine	1999	1016	946	7.1
Duzce, Turkey	1999	1112		7.2

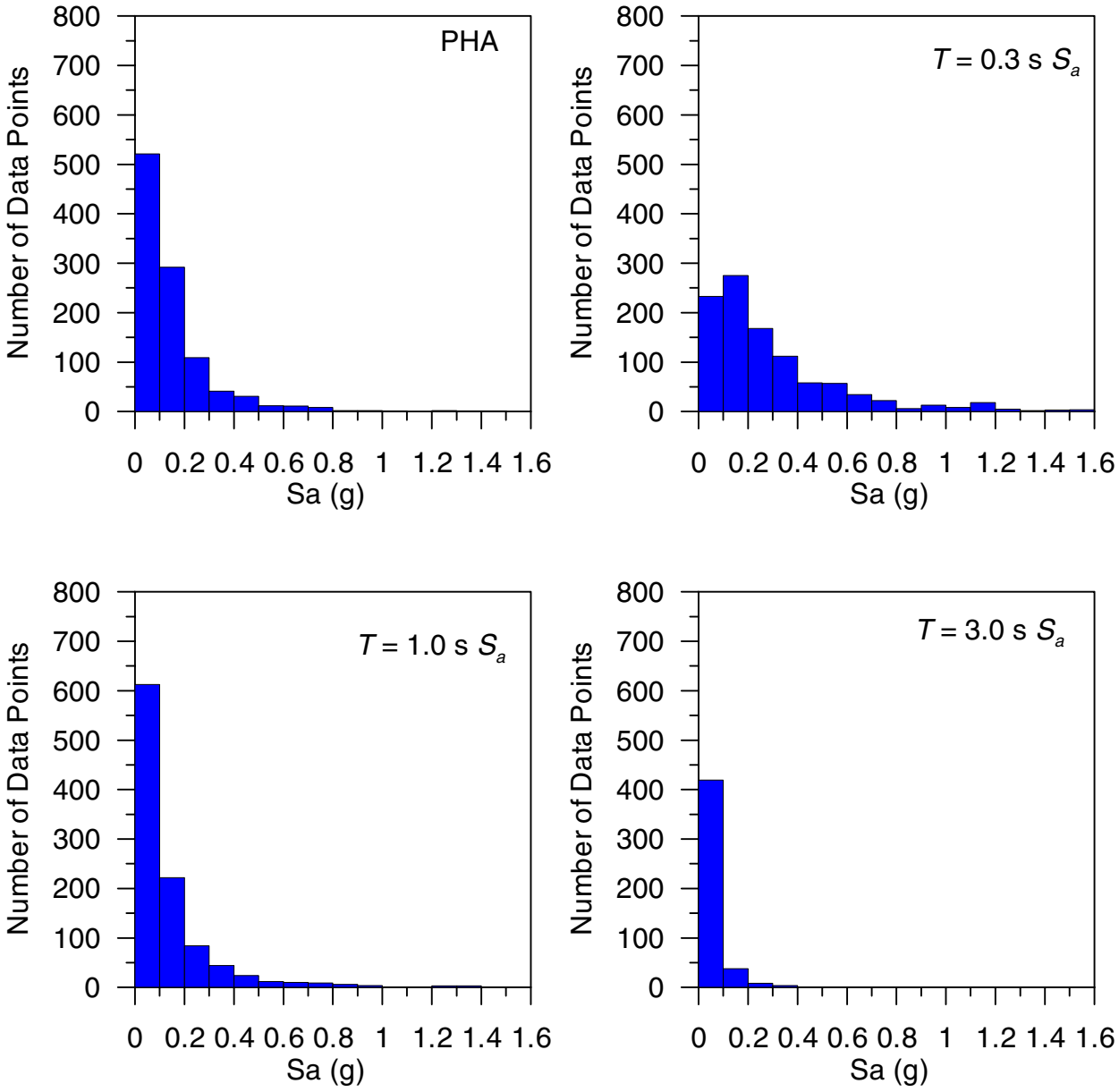

Fig. 3.2. Histograms of 5% damped spectral acceleration at various periods for strong motion data set used in this study

The western U.S. strong motion data were obtained from the California Strong Motion Instrumentation Program (CSMIP), the U.S. Geological Survey (USGS), the University of Southern California (USC), the California Division of Mines and Geology (CDMG), and the Los Angeles Department of Water and Power (LADWP). Additional data have been obtained for the 1999 Chi-Chi, Taiwan, earthquake from the National Center for Research in Earthquake Engineering (NCREE), and for the 1999 Kocaeli and Duzce, Turkey, earthquakes from the Kandilli Observatory and Earthquake Engineering Research Institute of Boğaçizi University (Kandilli), the Earthquake Research Department of the General Directorate of Disaster Affairs (ERD), and Istanbul Technical University (ITU). Most of the time histories used in this study can be obtained at the web site of the Pacific Earthquake Engineering Research Center (**www.peer.berkeley.edu**). All data were decimated to a common time step of 0.02 s by first low-pass filtering the data with a corner frequency of 25 Hz (using an 8^{th} order Chebyshev type-I filter), and then re-sampling the resulting signal at the time step of 0.02 s. Otherwise, the time signals were unaltered from their original processed form.

The distance measure used here is the closest distance to the rupture plane. Magnitude is taken as moment magnitude where available, and is otherwise taken as surface wave magnitude for $m > 6$ and local magnitude for $m < 6$.

3.2 SITE CLASSIFICATIONS

3.2.1 Surface Geology

A total of 394 California recording stations were classified based on mapped surface geology and used in this study. Classifications for these stations are listed in Appendix A. A number of additional sites were also classified, but were not used due to lack of suitable strong motion data (often because the instruments were in structures). Classifications for these sites are listed in Appendix B. Additional (non-California) sites listed in Appendix A include 21 stations near Kobe, Japan (classified by Fukushima et al., 2000), 8 stations near Tabas, Iran (classified by Shoja-Taheri and Anderson, 1978), 7 stations in northern Mexico (classified by Geomatrix, 1993), and 30 stations in Turkey (classified in the present study using data from Rathje, *pers. communication*).

The development of geologic classifications for California strong motion stations was a major thrust of this study. The level of mapping detail for Quaternary deposits is variable across the state. The geology of the entire state is documented on 27 maps at 1:250,000 scale by the California Division of Mines and Geology (CDMG, 1959–1998). These maps distinguish Quaternary deposits based on age (Holocene-Pleistocene) and generalized descriptions of depositional environment. The Southern California Aerial Mapping Project (SCAMP) is compiling more detailed geologic information for selected quadrangles in southern California. For example, data for the Santa Ana 30′ x 60′ quadrangle have been prepared at 1:100,000 scale by Morton et al. (1999) and were used in this study. In addition, we used preliminary digital geologic maps at 1:24,000 scale prepared through SCAMP of 7.5′ quadrangles in Los Angeles and Orange counties (CDMG staff, 2000, *pers. communication*). The SCAMP maps are the most detailed of the available geologic maps, providing basic information on the texture of Quaternary deposits (e.g., coarse/fine/mixed), and detailed information on depositional environment.

Despite the high quality of the geologic data sources used herein, classifications for some sites may be in error, particularly for strong motion sites near boundaries of geologic units. These errors occur because both the mapped boundaries, and the site locations, are subject to small errors. This could cause the mapped location of some sites to fall within the wrong geologic unit. Stations near dams are particularly subject to such errors, due to significant local variability in surface geology around dams. We sought to limit these mapping errors by checking our classifications against field geologic classifications made by Geomatrix (1993) and by the authors. However, these field classifications are not available for all sites, and thus we cannot guarantee the accuracy of all our geologic classifications.

Attempts were made to classify each California site according to schemes that make use of different levels of detail on geologic conditions. Three different schemes were used so that the sensitivity of ground motion amplification to various mapped geologic parameters could be investigated. Criteria used for the geologic classifications are presented in Table 3.2. The three classification schemes are as follows: age-only, age + depositional environment, age + material texture. Appendices A and B list the results of these classifications. It should be noted that all of these geologic classifications are based on surface conditions (hence the term “surface geology”). While borehole data are available for many sites that could be used, for example, to obtain additional information on material texture, we based our classifications for surface

geology strictly on the information on geologic maps. This was done so that the results would reflect the true data dispersion that could be expected when sites are classified using data from geologic maps. The breakdown of sites within geologic categories is shown in Figures 3.3–3.5.

Table 3.2. Criteria for surface geology classifications

Age	Depositional Environment	Sediment Texture
Holocene	Fan alluvium	Coarse
Pleistocene	Valley alluvium	Fine
	Lacustrine/marine	Mixed
	Aeolian	
	Artificial Fill	
Tertiary		
Mesozoic + Igneous		

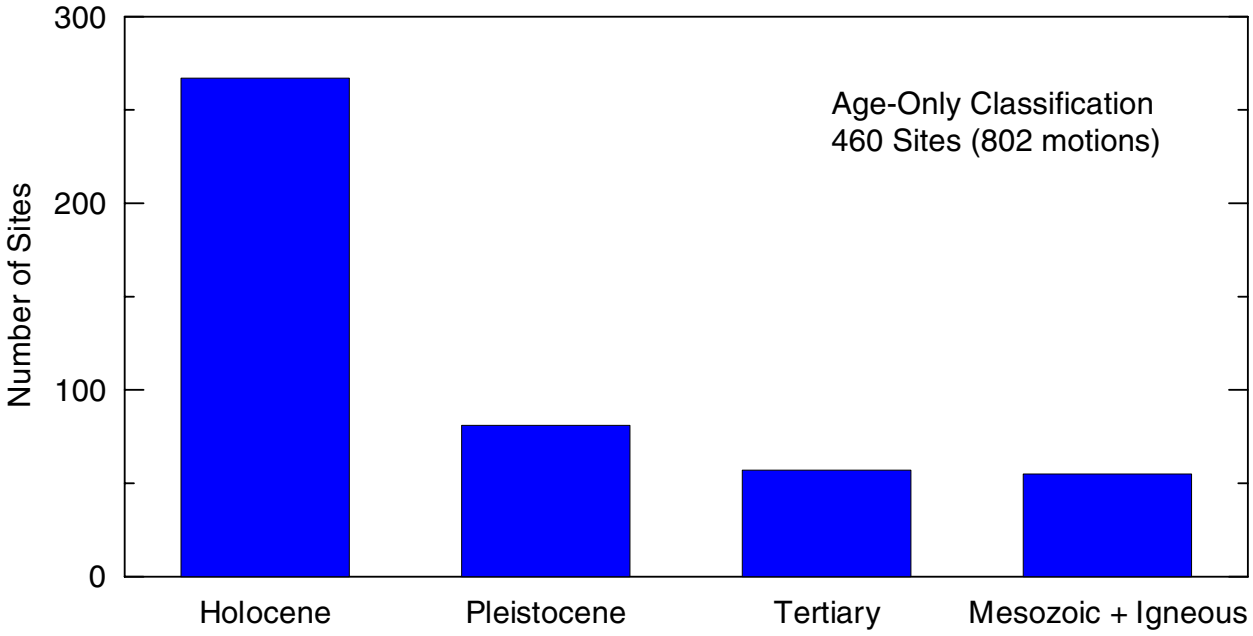

Fig. 3.3. Data breakdown for age-only geologic classification scheme

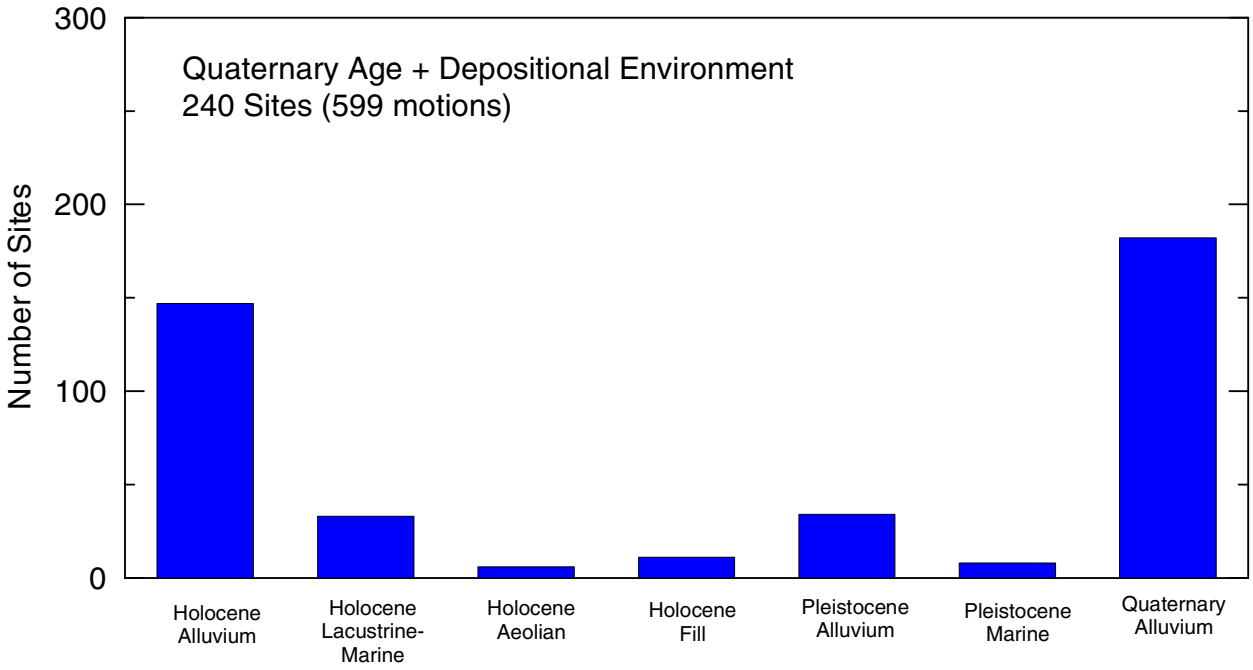

Fig. 3.4. Data breakdown for Quaternary geologic classification scheme incorporating age and depositional environment

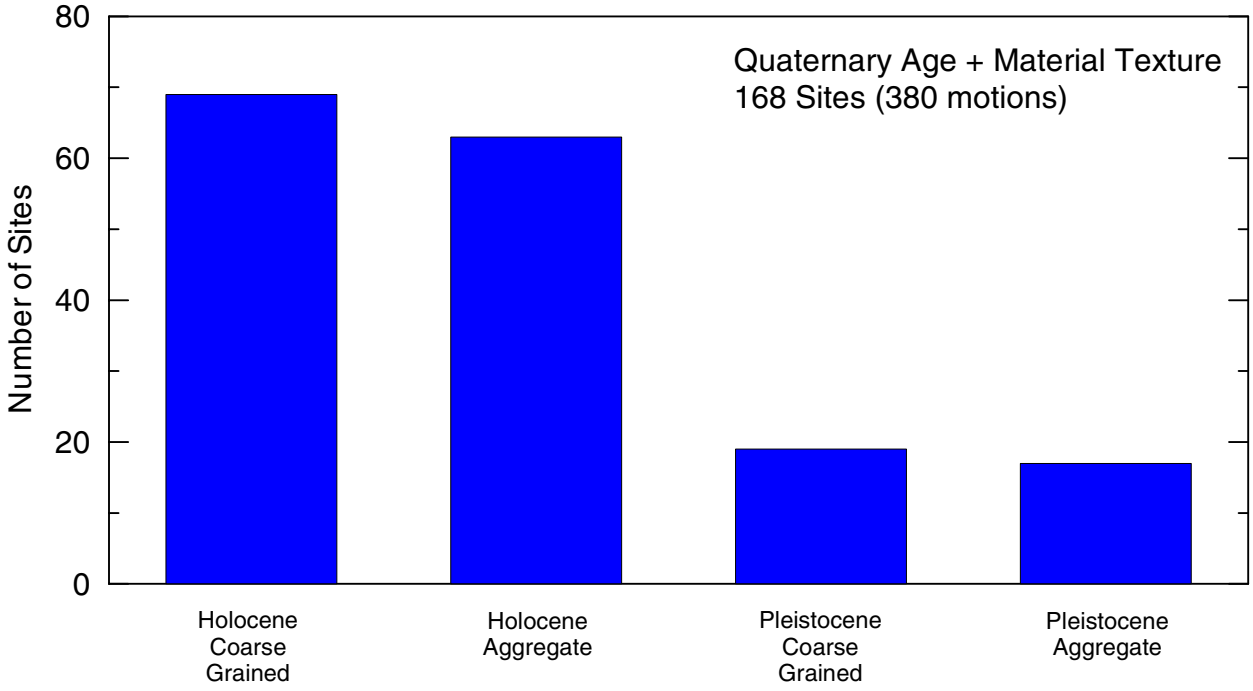

Fig. 3.5. Data breakdown for Quaternary geologic classification scheme incorporating age and sediment textural descriptions

3.2.2 Near-Surface Shear Wave Velocity

Wave propagation theory suggests that ground motion amplitude should depend on the density and shear wave velocity of near-surface media (e.g., Bullen, 1965; Aki and Richards, 1980). Density has relatively little variation with depth, and so shear wave velocity is the logical choice for representing site conditions. Two methods have been proposed for reducing depth-dependent velocity profiles to a single representative value. The first takes the velocity over the depth range corresponding to one-quarter wavelength of the period of interest (Joyner et al., 1981), which produces frequency-dependent depths. Fumal and Tinsley (1985) developed 1-Hz V_s maps for the Los Angeles region by relating quarter-wavelength velocities inferred from 33 boreholes to geologic units.

A practical problem with the quarter-wavelength V_s parameter is that the associated depths are often deeper than can economically be reached with boreholes. The $V_{s\text{-}30}$ parameter was proposed to overcome this difficulty, and has found widespread use in practice. Based on empirical studies by Borcherdt and Glassmoyer (1994), Borcherdt (1994) recommended $V_{s\text{-}30}$ as a means for classifying sites for building codes, and similar site categories were selected for the NEHRP seismic design provisions for new buildings (Martin, 1994). The site classification scheme in the NEHRP provisions is presented in Table 3.3.

Shear wave velocity has been found to be well correlated to detailed surface geology (age + texture for soil, age + weathering/fracture spacing for rock) by Fumal (1978). The $V_{s\text{-}30}$ parameter has been correlated with surface geology by Wills and Silva (1998), and this information has been used to generate state-wide maps of $V_{s\text{-}30}$ by Wills et al. (2000).

Table 3.3. Site categories in NEHRP Provisions (Martin, 1994)

NEHRP Category	Description	Mean Shear Wave Velocity to 30 m
A	Hard Rock	> 1500 m/s
B	Firm to hard rock	760-1500 m/s
C	Dense soil, soft rock	360-760 m/s
D	Stiff soil	180-360 m/s
E	Soft clays	< 180 m/s
F	Special study soils, e.g., liquefiable soils, sensitive clays, organic soils, soft clays > 36 m thick	

An extensive effort was made in this study to classify strong motion sites according to the V_{s-30} parameter. A GIS database was developed having the locations of both strong motion stations and boreholes in California. Each strong motion station location was checked with instrument owners (USGS and CSMIP), or against published reports (USC – Anderson et al., 1981), to optimize accuracy. Borehole locations were generally obtained from maps in reports. The borehole database is similar to that of Wills and Silva (1998), but also contains additional Caltrans boreholes, boreholes from selected consulting geotechnical engineers, and data recently compiled in the ROSRINE program (**http://geoinfo.usc.edu/rosrine/**). These databases were used to match boreholes with strong motion sites. The quality of the match was judged based on distance between the borehole and strong motion site as follows: A = 0–150 m, B = 150–450 m, C = 450–1600 m. Matches were only assigned if the borehole and strong motion site were on similar mapped surface geology. Appendices A and B indicate the borehole references used for classification, the borehole-station distance, the V_{s-30} value, and the NEHRP classification. The number of sites within the NEHRP categories is shown in Figure 3.6.

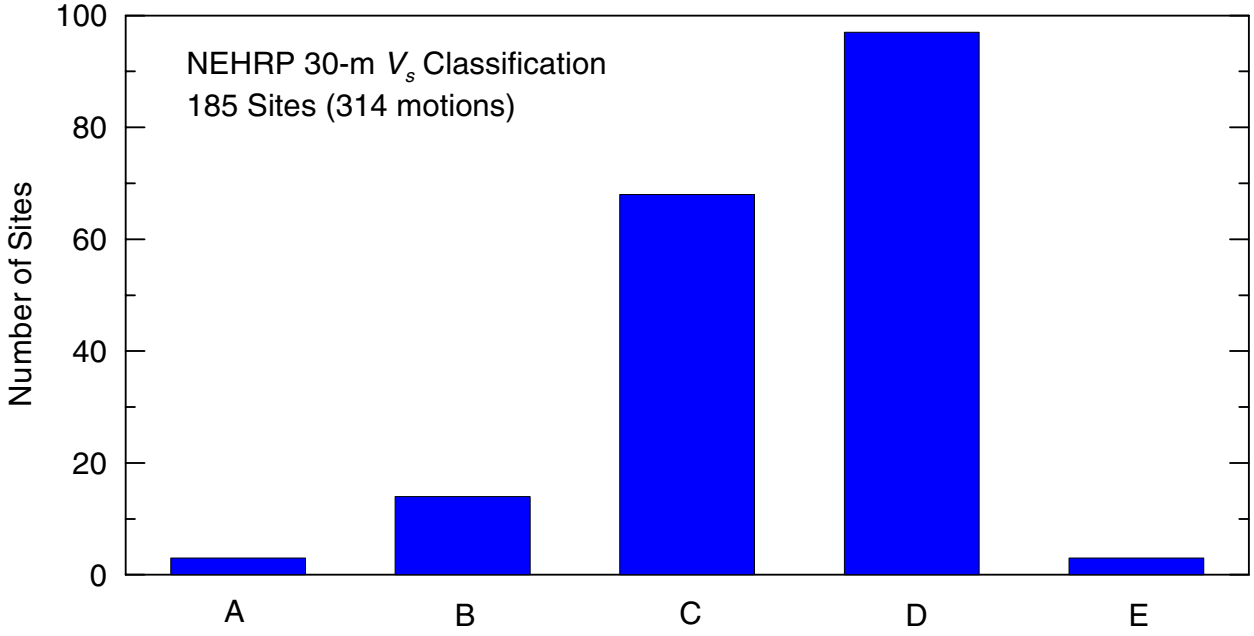

Fig. 3.6. Data breakdown for NEHRP classification scheme (all borehole-SMA distance ranges)

Classifications of V_{s-30} were obtained by these means for 185 sites. Of these sites, 149 have separation distances < 160 m, 12 from 160–300 m, and 24 from 300–1600 m. It should be noted that shear wave velocities for USC strong motion stations obtained by Rodriguez-Ordonez (1994) were not used due to apparent biases in such data as documented by Boore and Brown (1998) and Wills and Silva (1998).

3.2.3 Geotechnical Data

Geotechnical engineers have developed site classification schemes that can be used to estimate response spectra for soil sites. Early work on this topic is summarized in Seed and Idriss (1982), who recommended the following site classification scheme:

1. Rock sites
2. Stiff soil sites (< 60 m deep)
3. Deep cohesionless soil sites (> 75 m deep)
4. Sites underlain by soft to medium stiff clays

Response spectrum estimation procedures linked to this classification system were developed in which PHA on rock was first estimated, and then the ratio PHA(soil)/PHA(rock) and spectral shape were taken as a unique function of site condition (based on the work of Seed et al., 1976). Significant additional data gathered from the 1985 Mexico City, 1989 Loma Prieta, and 1994 Northridge earthquakes prompted revisions to the PHA rock-soil relations and spectral shapes, and the derivation of new site categories (e.g., Dickenson, 1994; Chang, 1996), which included information on sediment depth and near-surface shear wave velocity.

The most recent of the geotechnical classification schemes was proposed by Rodriguez-Marek et al. (2001) based on event-specific regressions of Loma Prieta and Northridge earthquake recordings. Data were grouped according to the categories in Table 3.4, and regressed using an attenuation function similar to that of Abrahamson and Silva (1997). Consistent trends were found for the Category D sites (deep stiff soil), as demonstrated by error terms smaller than those for the overall data population. However, the opposite was found for Category C sites (shallow stiff soil), prompting Rodriguez-Marek et al. to suggest that further subdivision of this category may be appropriate. Rodriguez-Marek et al. recommend use of their classification scheme over the V_{s-30} scheme as intra-category standard error terms were smaller for the geotechnical scheme.

Table 3.4. Geotechnical site categories proposed by Rodriguez-Marek et al. (2001)

Site	Description	Approx. Site Period (s)	Comments
A	Hard Rock	≤ 0.1	Crystalline Bedrock; $V_s \geq 1500$ m/s
B	Competent Bedrock	≤ 0.2	$V_s \geq 600$ m/s or < 6 m of soil. Most "unweathered" California Rock cases
C1	Weathered Rock	≤ 0.4	$V_s \approx 300$ m/s increasing to > 600 m/s, weathering zone > 6 m and < 30 m
C2	Shallow Stiff Soil	≤ 0.5	Soil depth > 6 m and < 30 m
C3	Intermediate Depth Stiff Soil	≤ 0.8	Soil depth > 30 m and < 60 m
D1	Deep Stiff Holocene Soil	≤ 1.4	Depth > 60 m and < 200 m
D2	Deep Stiff Pleistocene Soil	≤ 1.4	Depth > 60 m and < 200 m
D3	Very Deep Stiff Soil	≤ 2.0	Depth > 200 m
E1	Medium Thickness Soft Clay	≤ 0.7	Thickness of soft clay layer 3-12 m
E2	Deep Soft Clay	≤ 1.4	Thickness of soft clay layer > 12 m
F	Potentially Liquefiable Sand		Holocene loose sand with high water table ($z_w \leq 6$ m)

The effort to match boreholes and strong motion stations described in Section 3.2.2 was leveraged to develop geotechnical site classifications according to the Rodriguez-Marek et al. (2001) classification scheme. Geotechnical classifications were developed for all sites with a matched borehole. Developing the classification was straightforward if the borehole reached rock. If depth to rock is not known, but the site is located in an area with known deep sediments, D or D3 classifications are given. If the depth to rock is not known, and the sediment thickness could reasonably be expected to fall within several of the depth categories in Table 3.4, a range of possible classifications was given (e.g., C2–C3). The lower end of this depth range was constrained by the minimum known depth of sediments from the borehole (e.g., a site with a 30-m borehole that encounters only sediments must be C3 or D, and cannot be C2). Classifications

were obtained in this way for 183 sites, with the breakdown across categories shown in Figure 3.7. It should be noted that geotechnical classifications were not made in the absence of borehole data, with the exception of sites known from field mapping to be near outcropping rock, in which case B-C1 classifications were generally assigned.

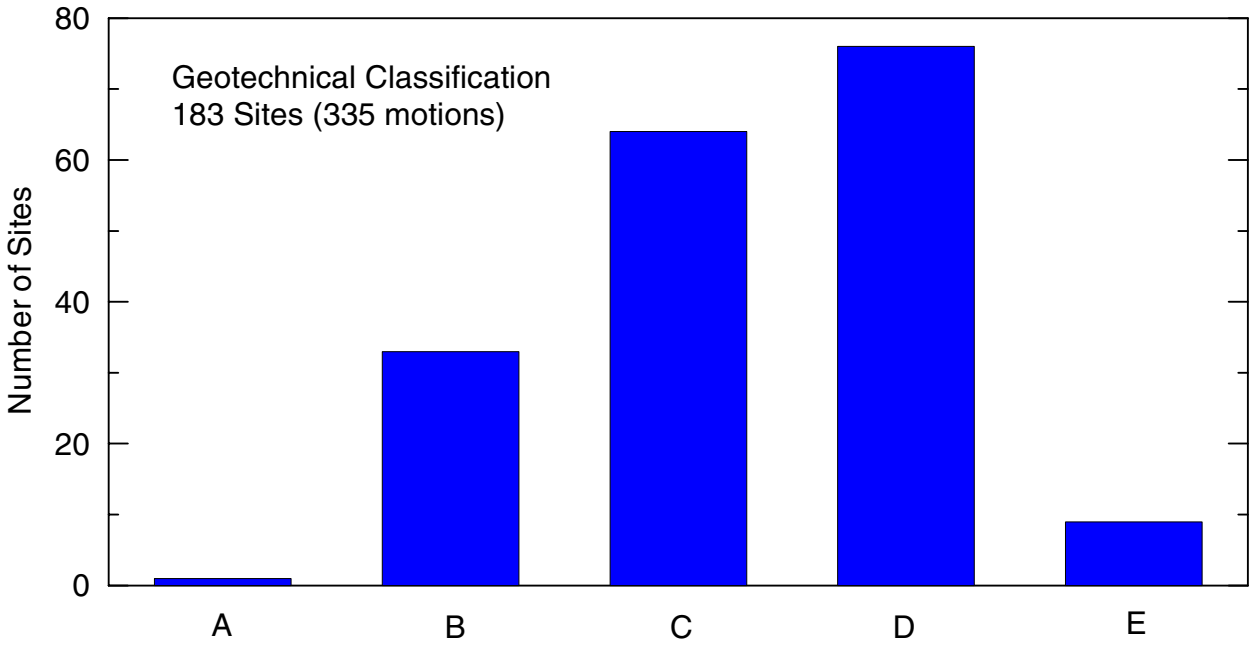

Fig. 3.7. Data breakdown for classification scheme based on geotechnical data

4 Analysis Procedures

4.1 AMPLIFICATION FACTORS FROM INDIVIDUAL RECORDINGS

Site-specific amplification factors, F_{ij}, are evaluated from the geometric mean of 5% damped acceleration response spectra for the two horizontal components of shaking, S_{ij}, and the reference ground motion for the site, $(S_r)_{ij}$, as follows:

$$F_{ij}(T) = S_{ij} / (S_r)_{ij} \tag{4.1}$$

where the indices refer to ground motion j within site category i, and T = spectral period. In Eq. 4.1, S_{ij} and $(S_r)_{ij}$ are computed at the same spectral period, which is varied from 0.01 to 5.0 s. Amplification factors are not evaluated for $T > 1.25 \times 1/f_{hp}$, where f_{hp} = high-pass corner frequency. Parameter $(S_r)_{ij}$ represents the reference spectral ordinate, and is an estimate of the ordinate that would have been expected at the recording site had the geology matched the reference condition.

A key step in evaluating F_{ij} is the analysis of the reference ground motion parameter, $(S_r)_{ij}$. Median spectral accelerations calculated using the Abrahamson and Silva (1997) attenuation relationship for rock sites provide a first-order estimate of $(S_r)_{ij}$ based on the following factors:

- Moment magnitude of causative earthquake, m.
- Closest distance from site to source, r.
- Rupture mechanism (reverse, oblique, strike-slip, or normal).
- Location of the site on or off the hanging wall of dip-slip faults.

This first-order estimate is then adjusted to correct for period-dependent average residuals between motions from a given event and the general attenuation model. This is accomplished with the use of period-dependent "event terms" computed during the regression of the Abrahamson and Silva (1997) attenuation model. For well-recorded events that occurred since the development of the Abrahamson and Silva attenuation relations (e.g., Hector Mine and

Turkey earthquakes), event terms were approximated as the average residual between the observed motions and predictions from the attenuation model. For sites that may have been influenced by rupture directivity effects, a second correction is made using the model by Somerville et al. (1997), later modified by Abrahamson (2000).

By evaluating reference motion parameters through the use of a rock attenuation relationship, the site condition associated with this motion is vaguely defined. This is because many site conditions are present at the recording sites represented within the "rock" category. Some sites have fresh, relatively hard rock, but most consist of deeply weathered, relatively soft rock. Ambiguity in the reference site condition can be smaller when amplification factors are derived using reference site approaches (described in Section 2.2.1). However, for practical purposes, what is most important is that the reference site condition is one for which attenuation relationships can be readily defined and one for which attenuation estimates of *IMs* are stable over time (i.e., as more earthquakes are added to the regression data set). Both criteria are satisfied through the approach taken here. First, use of the broad "rock" category provides ample recordings from which attenuation relations have previously been developed. Second, the use of event terms for well recorded events provide stability, because when coupled with the rock attenuation estimate of *IMs*, event terms for a given event define the rock average for that event, which should not change significantly in time. In other words, even if the attenuation estimate of an *IM* were to change as a result of additional data from future events, the event terms for well-recorded past events would similarly change so that the sum of the two would still provide a stable rock average for well-recorded past events. This rock average for past events will not change significantly provided that the relative numbers of recordings from hard rock and soft rock sites in the data set does not change significantly. Accordingly, the manner in which we define reference ground motions, while not unambiguously associated with any specific site condition, nonetheless should provide amplification factors that can be readily applied in practice and which should remain relatively stable over time.

The ground motion amplification estimate provided by $(S_r)_{ij}$ is subject to error as a result of the uncertainty associated with the modified attenuation model. Because S_{ij} is known, the standard error of the ground motion amplification for a particular site, $(\sigma_f)_{ij}$, is equivalent to the standard error of the reference motion estimate, $(\sigma_r)_{ij}$, i.e.,

$$\left(\sigma_f\right)_{ij} = \left(\sigma_r\right)_{ij} \tag{4.2}$$

Standard error terms from attenuation relationships are fairly large (≈0.4–0.9), and hence the uncertainty in individual estimates of amplification is also large. However, the central limit theorem in statistical theory (e.g., Ang and Tang, 1975) suggests that statistical moments (i.e., mean, standard deviation) estimated from *large* data populations are relatively insensitive to the probability density function associated with individual data points in the population. Accordingly, we surmise that the errors in point estimates of amplification can be accepted because relations for amplification factors are regressed upon using a large database.

Finally, it is acknowledged that the evaluation of amplification factors in terms of response spectral ordinates is less physically based than Fourier amplitude ratios, which have been used in many previous studies. The use of spectral ratios was prompted by two principal factors (1) state-of-the-art procedures for evaluating reference motions in terms of response spectral ordinates are more maturely developed than those for Fourier spectral ordinates, and (2) seismic hazard analyses are typically performed in terms of response spectral ordinates, and hence amplification factors expressed in term of spectral ordinates may have greater practical application.

4.2 REGRESSION PROCEDURE

Site-specific amplification factors defined in Eq. 4.1 were sorted into site categories defined by the schemes in Tables 3.2–3.4. For a particular scheme, within a given category i, regression analyses were performed to relate amplification factors, F_{ij}, to ground motion amplitude as follows:

$$\ln(F_{ij}) = a_i + b_i \ln(G_{ij}) \tag{4.3a}$$

where a_i and b_i are regression coefficients specific to category i, and G_{ij} is a parameter representing the reference ground motion for site j. This same regression equation has been used by Youngs (1993) and Bazzuro and Cornell (1999), with G_{ij} taken as PHA. Abrahamson and Silva (1997) also took G_{ij} as PHA, but added a constant term to G_{ij} as shown below.

$$\ln(F_{ij}) = a_i + b_i \ln(G_{ij} + c) \tag{4.3b}$$

where $c = 0.03g$ independent of period. This form of the regression equation was also investigated here, but was not found to decrease data dispersion, and so the c term was dropped.

We investigated the use of several G_{ij} parameters for evaluating amplification, including PHA, spectral acceleration at the same period used in the evaluation of F_{ij}, and peak velocity

(calculated using the attenuation relation by Campbell, 1997, 2000, 2001). As reported in Stewart and Liu (2000), these other G_{ij} parameters did not reduce data dispersion, and so in the following we take G_{ij} as PHA.

Due to the incorporation of event terms into the reference motions for spectral acceleration, systematic variations of amplification factors across events are not expected. Accordingly, least-square regression analyses are performed (which give equal weight to all points) in lieu of a random effects model such as that of Abrahamson and Youngs (1992).

Residuals (R_{ij}) between the amplification "prediction" of Eq. 4.3a and $\ln(F_{ij})$ values were evaluated ($R_{ij} = \ln(F_{ij})_{data} - \ln(F_{ij})_{pre}$) for all data in category i to enable evaluation of the mean residual, R_i, and the standard deviation of the residual, $(\sigma_R)_i$.

$$R_i = \frac{1}{N_i} \sum_{j=1}^{N_i} R_{ij} \tag{4.4a}$$

$$(\sigma_R)_i = \sqrt{\frac{\sum_{j=1}^{N_i} (R_{ij} - R_i)^2}{N_i - N_{dof,i}}} \tag{4.4b}$$

where N_i = number of data points in category i and $N_{dof,i}$ = number of degrees-of-freedom in regression equation for Category i (two in this case). Well defined site categories would be expected to have smaller values of $(\sigma_R)_i$ than relatively broad categories. It should be noted that we also investigated the magnitude-dependence of amplification factors, as described in Section 5.1.5.

5 Results

5.1 AGE-ONLY GEOLOGIC CLASSIFICATION SCHEME

Individual amplification factors for Holocene, Pleistocene, Tertiary, and Mesozoic + Igneous geology are plotted at four spectral periods in Figure 5.1 [PHA, T = 0.3 s, 1.0 s, and 3.0 s]. Also plotted are results of regression analyses performed according to Eq. 4.3a (solid lines), ± 95% confidence intervals on the median amplification (dotted lines), and median regression ± standard error, σ (dashed lines). The regression coefficients and standard error terms are listed in Table 5.1(a). Also provided in Table 5.1(a) are average amplification levels over the spectral period range of T = 0.1–0.5 s (denoted F_a) and T = 0.5–2.0 s (denoted F_v), respectively. The actual spectral ordinates used to evaluate F_a are from periods 0.1, 0.12, 0.15, 0.17, 0.20, 0.24, 0.3, 0.36, 0.4, 0.46, and 0.5 s; periods 0.4, 0.46, 0.5, 0.6, 0.75, 0.85, 1.0, 1.5, and 2.0 s were used to evaluate F_v.

Reduction of amplification factors with increasing rock PHA are inferred as evidence of sediment nonlinearity. This nonlinearity is quantified by the b_i parameter for each category i. The statistical significance of the PHA-dependence of amplification factors is assessed two ways. The first significance test consists of comparing the absolute value of b_i to the estimation error for b_i (both indicated in Table 5.1a). When $|b_i|$ exceeds the estimation error, the nonlinearity is considered significant. Secondly, sample 't' statistics are compiled to test the null hypothesis that b_i=0 and a_i = overall data median. This statistical testing provides a significance level = α that the null hypothesis cannot be rejected. For clarity of expression, we tabulate in Table 5.1(a) values of 1-α, which we refer to as a "rejection confidence for a b=0 model." Large rejection confidence levels (i.e., > 95%) suggest significant PHA-dependence in amplification factors. These results are also shown in Table 5.1(a).

A key issue when interpreting regression results for different site categories is the degree to which the data for different categories are distinct. Statistical F-tests (Cook and Weiberg, 1999) are performed to compare submodels with a full model. For example, a pair of submodels could be the regression results in Figure 5.1 and Table 5.1(a) for Holocene (H) and Pleistocene (P). The full model in this example would consist of a regression through all data in the H and P categories. The F-test is performed by calculating the residual sum of squares (based on misfit from the median model prediction) for the submodels (RSS_1 and RSS_2) and the full model (RSS_f). Since *RSS* measures lack of fit, the submodels and full model are compared by examining the difference $RSS_f - (RSS_1 + RSS_2)$. If this difference is small, then the submodels and full model fit the data about equally well. For well-populated submodel data spaces, this would imply that the submodels do not describe distinct data sets.

For normally distributed data sets, the F-statistic is calculated as

$$F = \frac{\left(RSS_f - \left(RSS_1 + RSS_2\right)\right) / \left(\left(df_1 + df_2\right) - df_f\right)}{\hat{\sigma}^2} \tag{5.1}$$

where df_i refers to the degree of freedom of regression fit i (two in this case), and

$$\hat{\sigma}^2 = \frac{RSS_1 + RSS_2}{N - \left(df_1 + df_2\right)} \tag{5.2}$$

where N = number of data points in the full model. This F statistic can be compared to the F distribution to evaluate a significance level (p) for the test. Large values of p (e.g., $p > 0.05$) are often taken to imply that the submodels are not distinct.

We compile the F statistic and significance level (p) for "adjacent" categories, i.e., Holocene-Pleistocene, Pleistocene-Tertiary, and Tertiary-Mesozoic. These statistics are compiled in Table 5.1(b) for the geologic age-only classification scheme. In the following, we judge the distinction between categories to be "significant" for $p < 0.05$, "moderate" for $0.05 < p < 0.15$, and "insignificant" for $p > 0.15$.

Table 5.1(a). Regression coefficients for S_a amplification factors, age-only classification scheme

Geology	Period	a	b	σ	Rejection confidence for b=0 model (%)
Holocene (H)	PHA	-0.25 ± 0.14	-0.17 ± 0.05	0.54	100
	0.3	-0.21 ± 0.13	-0.16 ± 0.05	0.52	100
	1	0.23 ± 0.15	-0.04 ± 0.06	0.59	90
	3	0.32 ± 0.21	-0.07 ± 0.09	0.64	90
	Fa	-0.21 ± 0.12	-0.14 ± 0.05	0.48	100
	Fv	0.14 ± 0.13	-0.09 ± 0.05	0.50	100
Pleistocene (P)	PHA	0.08 ± 0.27	0.00 ± 0.10	0.47	2
	0.3	0.18 ± 0.28	0.05 ± 0.11	0.48	68
	1	0.35 ± 0.33	0.04 ± 0.12	0.56	46
	3	-0.06 ± 0.43	-0.21 ± 0.18	0.50	98
	Fa	0.08 ± 0.25	0.00 ± 0.09	0.42	8
	Fv	0.26 ± 0.29	0.00 ± 0.11	0.50	6
Tertiary (T)	PHA	0.23 ± 0.36	-0.02 ± 0.14	0.62	25
	0.3	0.08 ± 0.37	-0.05 ± 0.14	0.64	55
	1	0.08 ± 0.35	-0.04 ± 0.14	0.61	48
	3	0.27 ± 0.37	-0.01 ± 0.18	0.47	7
	Fa	0.04 ± 0.34	-0.06 ± 0.13	0.59	62
	Fv	0.07 ± 0.34	-0.06 ± 0.13	0.58	54
Mesozoic + Igneous	PHA	-0.18 ± 0.35	-0.10 ± 0.14	0.54	85
(M + I)	0.3	-0.48 ± 0.38	-0.15 ± 0.15	0.59	95
	1	-0.66 ± 0.53	-0.17 ± 0.22	0.83	88
	3	-0.46 ± 0.61	-0.14 ± 0.27	0.66	70
	Fa	-0.35 ± 0.34	-0.13 ± 0.14	0.54	92
	Fv	-0.56 ± 0.46	-0.15 ± 0.19	0.73	89

Table 5.1(b). F-statistics indicating distinction between site categories, age-only classification scheme

	PHA		*T* = 0.3 s		*T* = 1.0 s		*T* = 3.0 s		F_a		F_v	
Categories	F	p	F	p	F	p	F	p	F	p	F	p
H-P	5.8	0.003	10.5	0.000	2.2	0.116	1.0	0.366	4.9	0.007	4.2	0.015
P-T	5.0	0.007	3.8	0.025	0.8	0.456	1.5	0.225	2.1	0.119	0.3	0.712
T-M+I	3.6	0.028	7.2	0.001	9.4	0.000	6.7	0.002	4.0	0.019	10.1	0.000

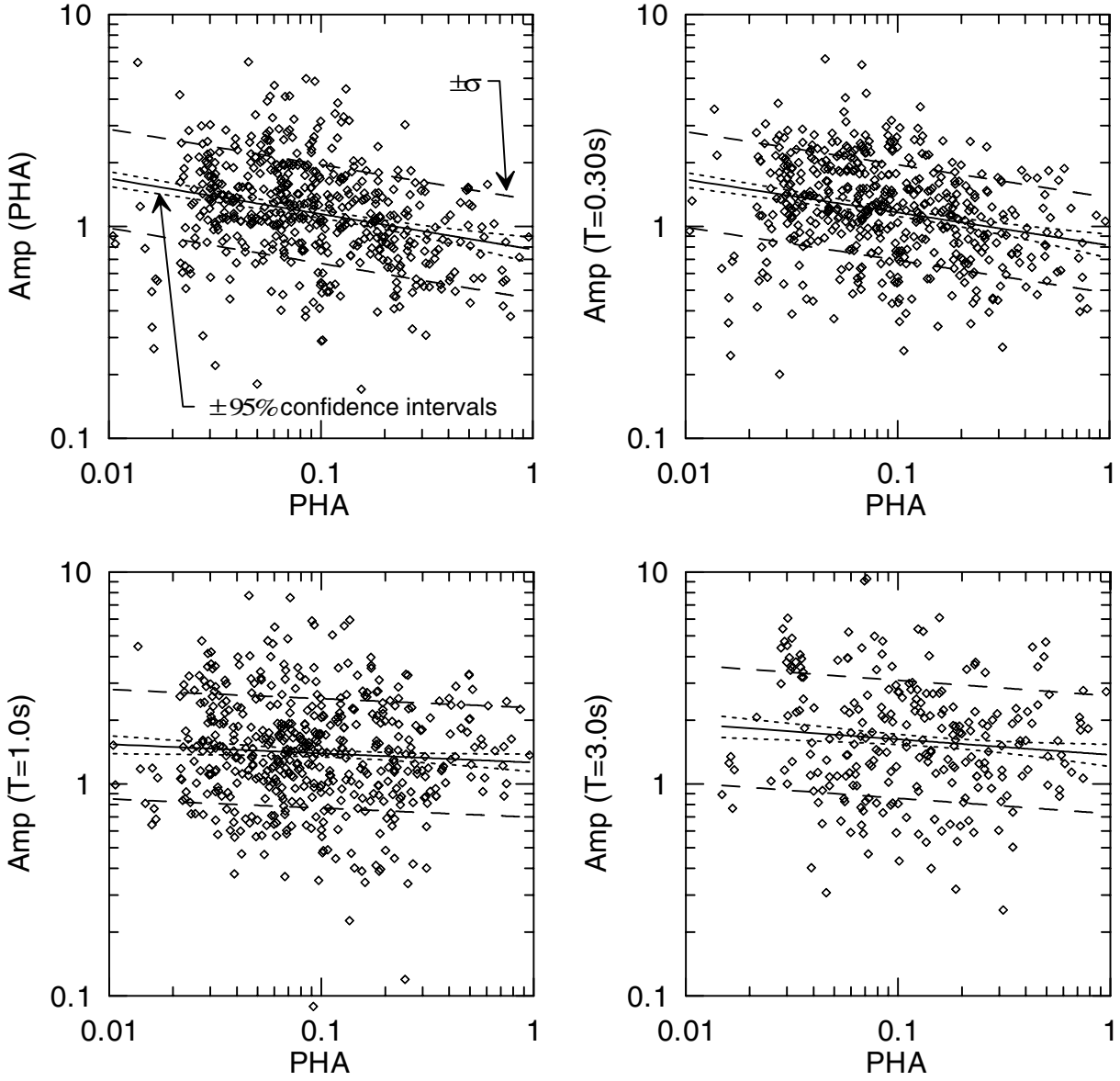

Fig. 5.1(a). Spectral acceleration amplification factors for Holocene geology plotted against regression results. PHA refers to peak horizontal acceleration of reference motion.

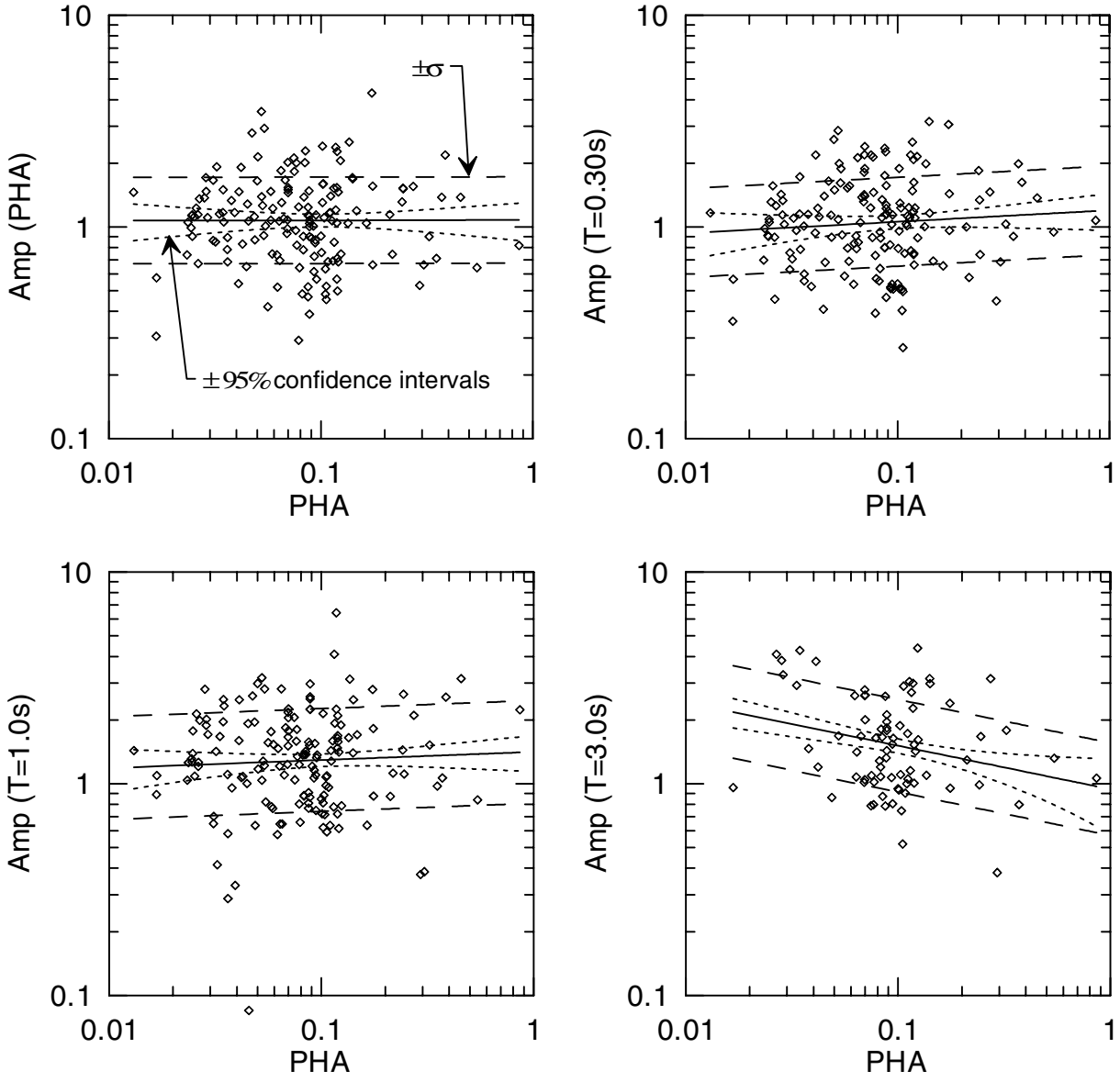

Fig. 5.1(b). Spectral acceleration amplification factors for Pleistocene geology plotted against regression results

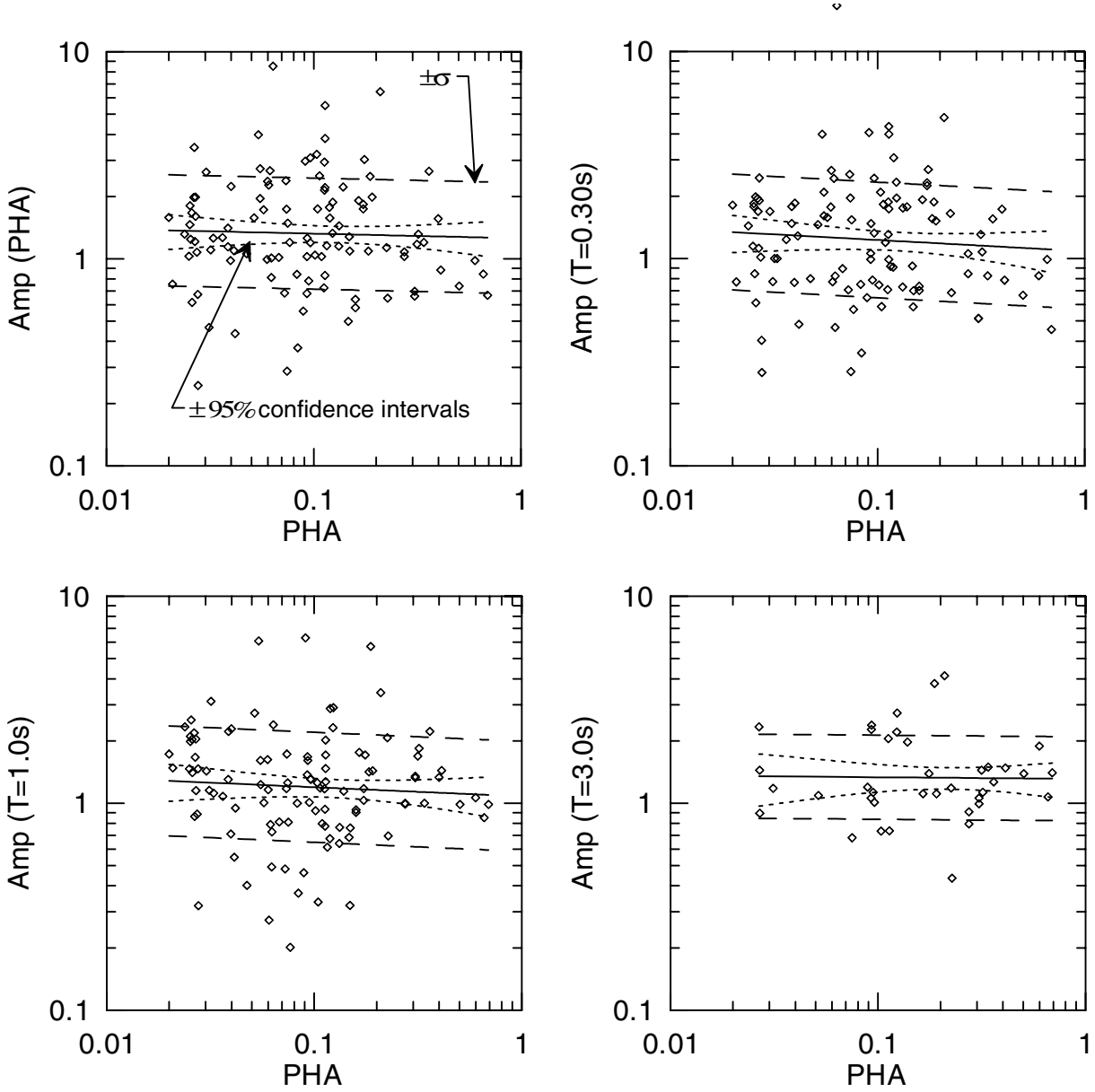

Fig. 5.1(c). Spectral acceleration amplification factors for Tertiary geology plotted against regression results

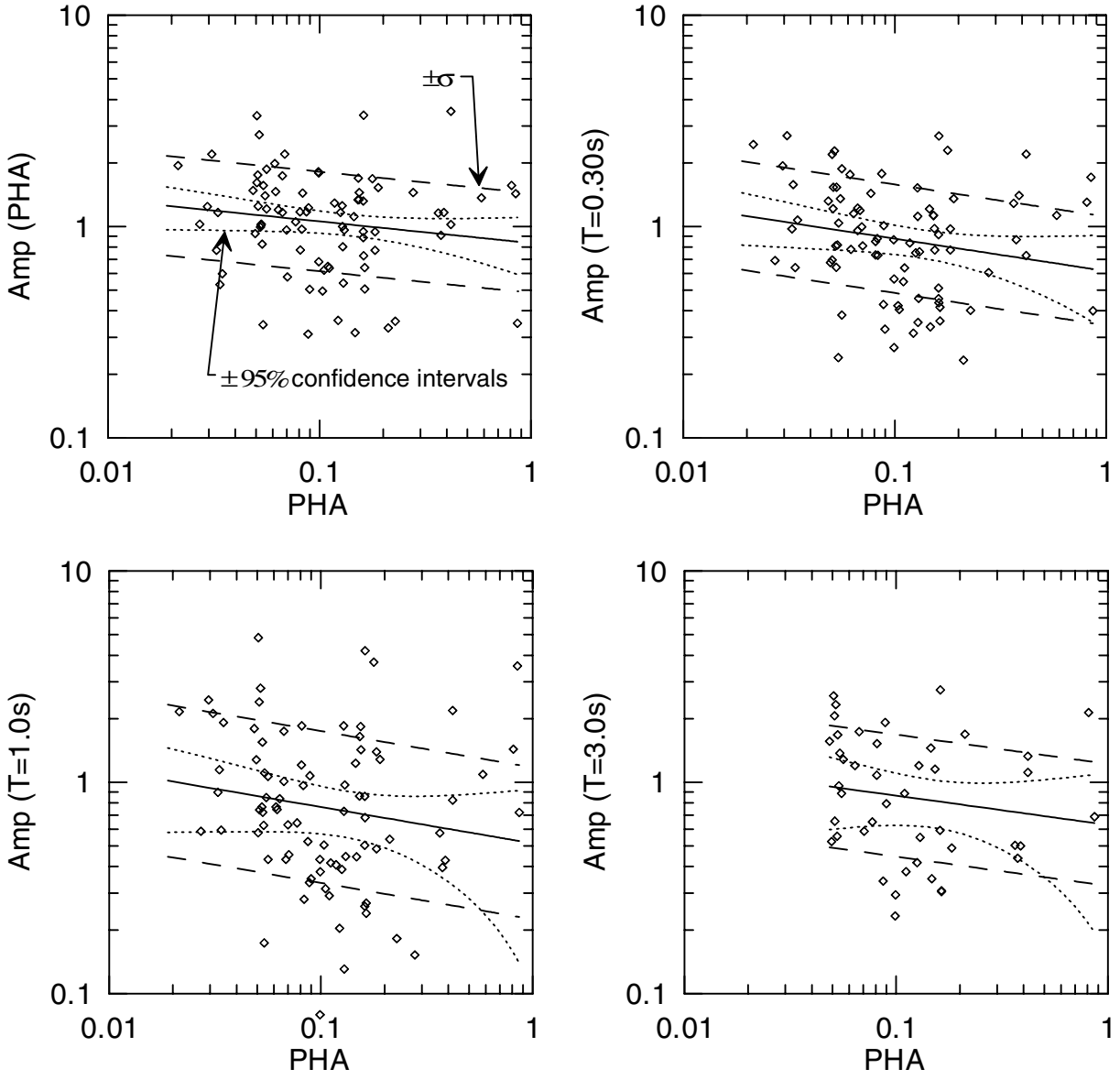

Fig. 5.1(d). Spectral acceleration amplification factors for Mesozoic and Igneous geology plotted against regression results

Significantly distinct values of low-period amplification factors (PHA and 0.3 s) are observed between Holocene and Pleistocene sediments. Low-period amplification in Holocene materials varies significantly with rock PHA, resulting in amplification at low levels of shaking (rock PHA < 0.2g), and de-amplification for stronger shaking (rock PHA >~0.2g). In contrast, low-period Pleistocene amplification is nearly unity and is essentially independent of rock PHA. Low-period Pleistocene amplification is significantly distinct from Tertiary, which has larger amplification factors. Long-period (T = 1.0 and 3.0 s) amplification levels for Holocene-Pleistocene and Pleistocene-Tertiary sediments are generally insignificantly distinct. The Tertiary and Mesozoic + Igneous (M+I) categories (i.e., the categories encompassing the materials that would generally be considered "rock") have significantly distinct amplification levels at all periods, with T amplification exceeding M+I.

The data in Table 5.1(a) indicate for Holocene sediments statistically significant PHA-dependence of amplification functions at small to intermediate periods. For PHA, T = 0.3 s, F_a, and F_v, the rejection confidence for the b=0 model is nearly 100%, and the estimated values of $|b_i|$ exceed their prediction errors. Nonlinearity is generally not statistically significant for other age categories.

The variation of standard error term (σ) with magnitude and site category is shown in Figure 5.2, with the magnitude-dependent error terms from Abrahamson and Silva (1997) also shown for comparison. We find no significant magnitude-dependence in the error terms, but do find an increase in σ with period. Values of σ at long period (T = 3 s) rise as high as σ ~ 0.7-0.8. The Abrahamson and Silva (1997) error terms decrease uniformly with magnitude for m = 5–7, and also increase with period. Typically, error terms from this study are smaller than the Abrahamson and Silva terms for m < 5.75 and larger for m > 5.75. No geologic category is found to have consistently large or small error terms.

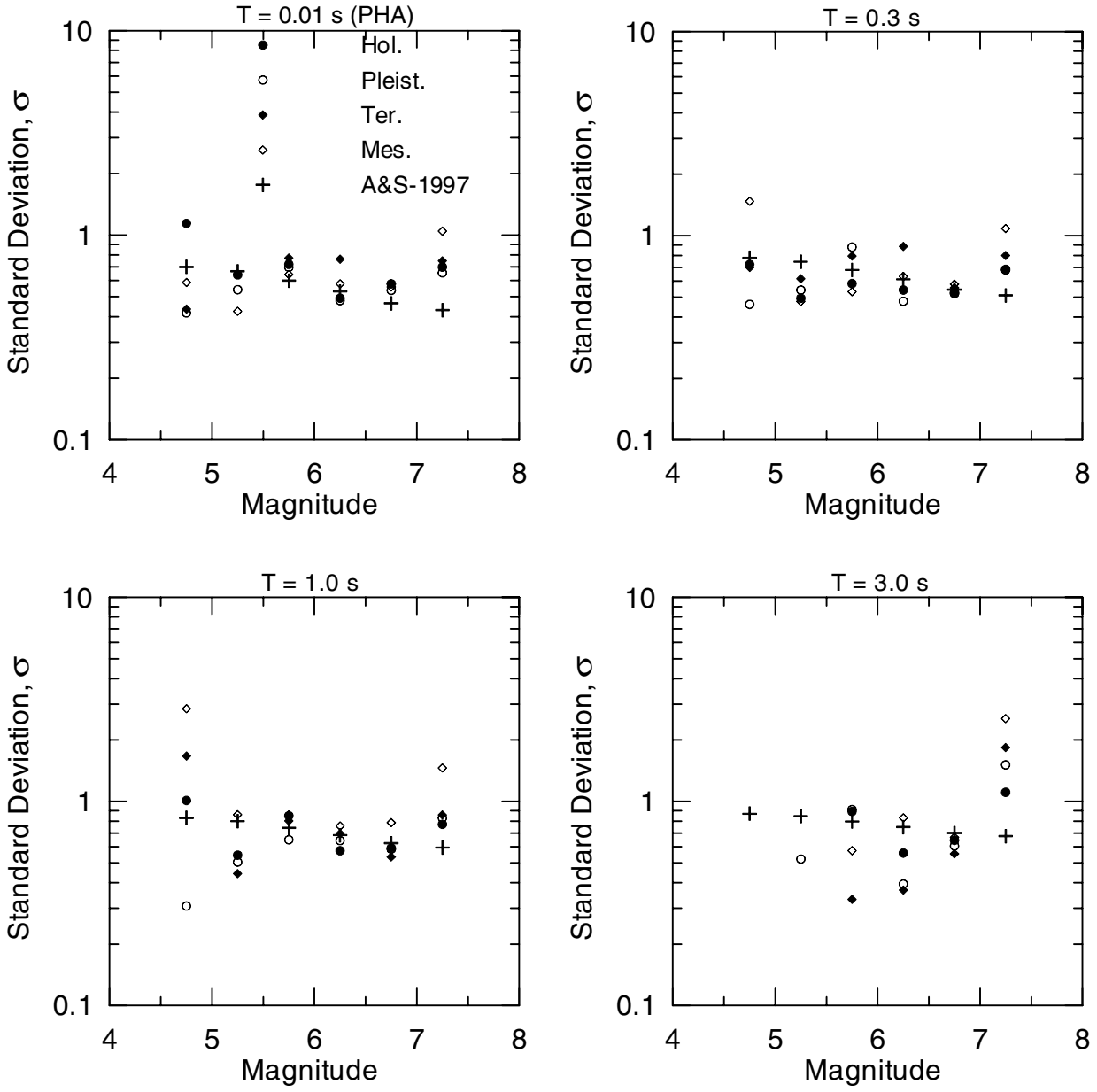

Fig. 5.2. Variation of standard error term σ with magnitude and geologic age. Compare to magnitude-dependent error term by Abrahamson and Silva (1997)

5.2 EFFECT OF GEOLOGIC SUB-CATEGORIZATION OF QUATERNARY SEDIMENTS

As indicated in Table 3.2, two additional geologic classification schemes were considered that incorporate information beyond age – depositional environment and material texture. Geologic data that enable classifications according to these criteria are most widely available for Quaternary sediments. The site breakdowns associated with these schemes are presented in Figures 3.4–3.5.

Figures 5.3 present results for Quaternary sediments segregated according to age and depositional environment. Individual amplification factors are shown along with regression results for Holocene sediments segregated into alluvial and lacustrine/marine depositional environments, and Pleistocene alluvial sediments. Due to a paucity of data, no regression analyses were performed for Pleistocene lacustrine/marine sediments, nor Aeolian and fill categories. Regression coefficients and error terms from these analyses are presented in Table 5.2(a), while F statistics on the distinctions between categories are provided in Table 5.2(b). Also shown in the figures for reference are regression results for the appropriate age-only category.

High levels of low- to moderate-period (T = 0.01−1.0 s, F_a, F_v) amplification and nonlinearity occur in the Holocene lacustrine/marine (Hlm) category (Figure 5.3b), which includes a significant number of sites from Imperial Valley and San Francisco bay-shore locations. As shown in Table 5.2(b), these Hlm amplification levels are significantly distinct from Holocene alluvium (Ha) for PHA, but are insignificantly distinct at longer periods. As can be seen from Figure 5.3(a), Ha deposits exhibit amplification levels consistent with those for the Holocene age-only category. In both the Hlm and Ha categories, amplification factors generally become less dependent on rock PHA as period increases.

Pleistocene alluvial sediments (Pa) generally exhibit similar amplification levels to those for the Pleistocene age-only category (Figure 5.3c). These amplification levels are generally insignificantly distinct from Ha (Table 5.2b); thus a fourth category is formed consisting of Quaternary alluvium (Qa). Regression results for Qa are provided in Figure 5.3(d) and Table 5.2(a). As shown in Table 5.2(b), Qa amplification factors are insignificantly distinct from Ha and Pa, and hence Qa is used in lieu of Ha and Pa. As shown in Table 5.2(b), Qa is significantly distinct from Hlm and T for PHA, but is generally insignificantly distinct at longer periods.

Table 5.2(a). Regression coefficients for S_a amplification factors, age + depositional environment classification scheme

Geology	Period	a	b	σ	Rejection confidence for b=0 model (%)
Hol. - alluvium	PHA	-0.21 ± 0.18	-0.15 ± 0.07	0.52	100
(Ha)	0.3	-0.15 ± 0.18	-0.14 ± 0.07	0.52	100
	1	0.20 ± 0.20	-0.06 ± 0.08	0.59	85
	3	0.07 ± 0.32	-0.18 ± 0.13	0.68	99
	Fa	-0.17 ± 0.16	-0.13 ± 0.06	0.48	100
	Fv	0.11 ± 0.17	-0.11 ± 0.07	0.50	100
Hol. - Lac/marine	PHA	-0.56 ± 0.31	-0.37 ± 0.14	0.47	100
(Hlm)	0.3	-0.36 ± 0.29	-0.23 ± 0.13	0.45	100
	1	0.10 ± 0.32	-0.15 ± 0.14	0.49	97
	3	0.39 ± 0.38	-0.09 ± 0.22	0.47	57
	Fa	-0.38 ± 0.30	-0.24 ± 0.13	0.46	100
	Fv	0.01 ± 0.28	-0.17 ± 0.12	0.43	99
Pleist. - alluvium	PHA	0.01 ± 0.40	-0.06 ± 0.15	0.48	53
(Pa)	0.3	0.04 ± 0.39	-0.02 ± 0.15	0.47	23
	1	0.44 ± 0.56	0.05 ± 0.21	0.67	36
	3	-0.27 ± 0.76	-0.32 ± 0.31	0.55	96
	Fa	-0.05 ± 0.35	-0.07 ± 0.13	0.42	70
	Fv	0.29 ± 0.50	0.00 ± 0.19	0.60	4
Quat. -alluvium	PHA	-0.18 ± 0.16	-0.14 ± 0.06	0.52	100
(Qa)	0.3	-0.12 ± 0.16	-0.12 ± 0.06	0.51	100
	1	0.23 ± 0.19	-0.04 ± 0.07	0.61	72
	3	0.04 ± 0.28	-0.19 ± 0.11	0.65	100
	Fa	-0.15 ± 0.15	-0.12 ± 0.06	0.47	100
	Fv	0.13 ± 0.16	-0.09 ± 0.06	0.52	99

Table 5.2(b). F-statistics indicating distinction between site categories, age + depositional environment classification scheme

	PHA		T = 0.3 s		T = 1.0 s		T = 3.0 s		F_a		F_v	
Categories	F	p	F	p	F	p	F	p	F	p	F	p
Hlm-Ha	5.0	0.007	0.7	0.517	1.1	0.338	0.9	0.393	1.1	0.344	0.5	0.608
Ha-Pa	0.6	0.532	2.8	0.065	0.7	0.516	0.3	0.767	0.6	0.551	1.3	0.261
Ha-Qa	0.1	0.940	0.3	0.706	0.1	0.927	0.0	0.987	0.1	0.922	0.2	0.833
Pa-Qa	0.5	0.636	1.8	0.171	0.4	0.649	0.2	0.793	0.4	0.679	0.8	0.447
Hlm-Qa	5.8	0.003	1.0	0.355	1.3	0.275	1.2	0.300	1.4	0.248	0.8	0.466
Qa-T	3.9	0.022	0.7	0.479	2.4	0.093	1.6	0.203	0.8	0.458	2.1	0.123

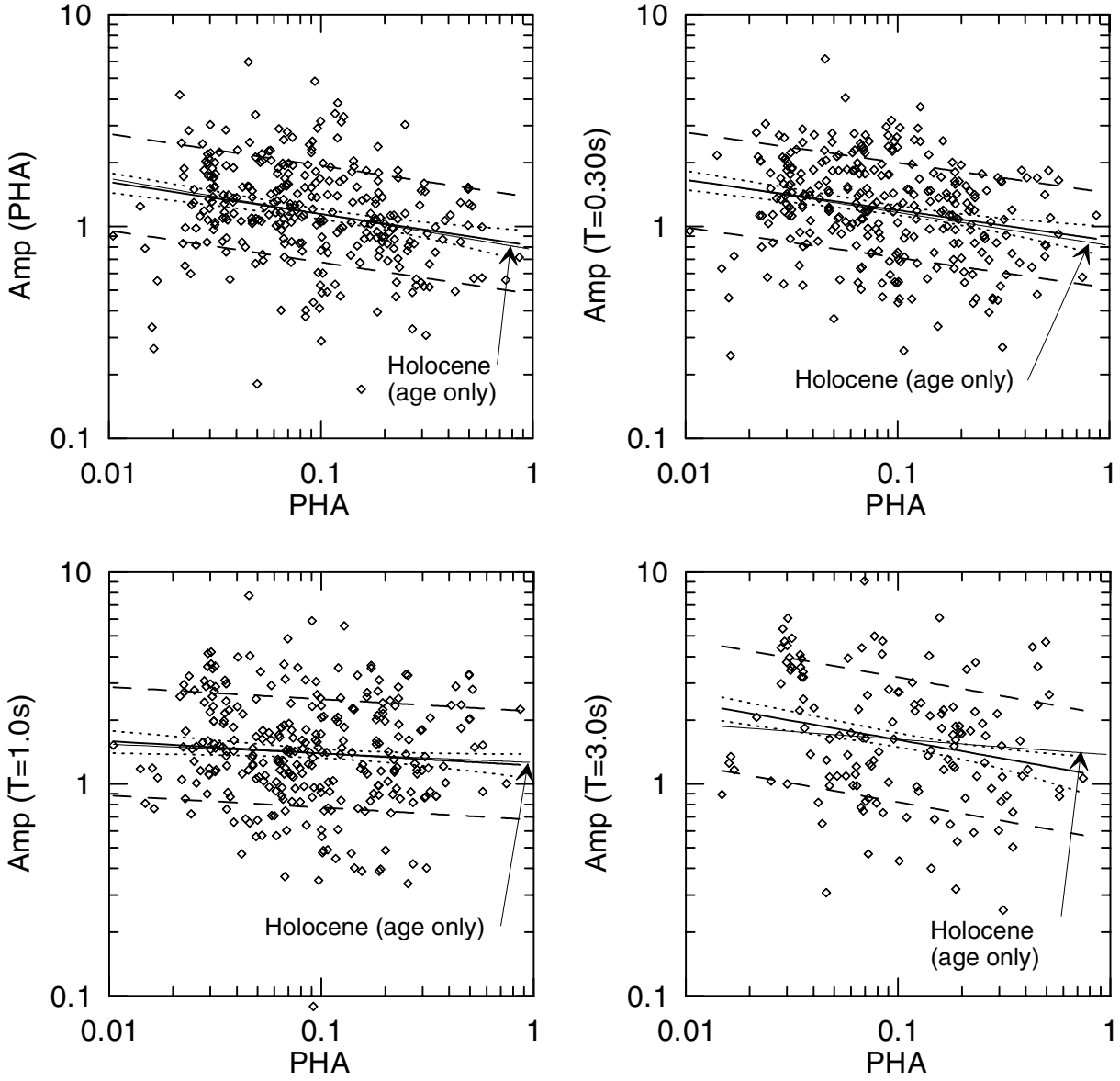

Fig. 5.3(a). Spectral acceleration amplification factors for Holocene alluvial sediments

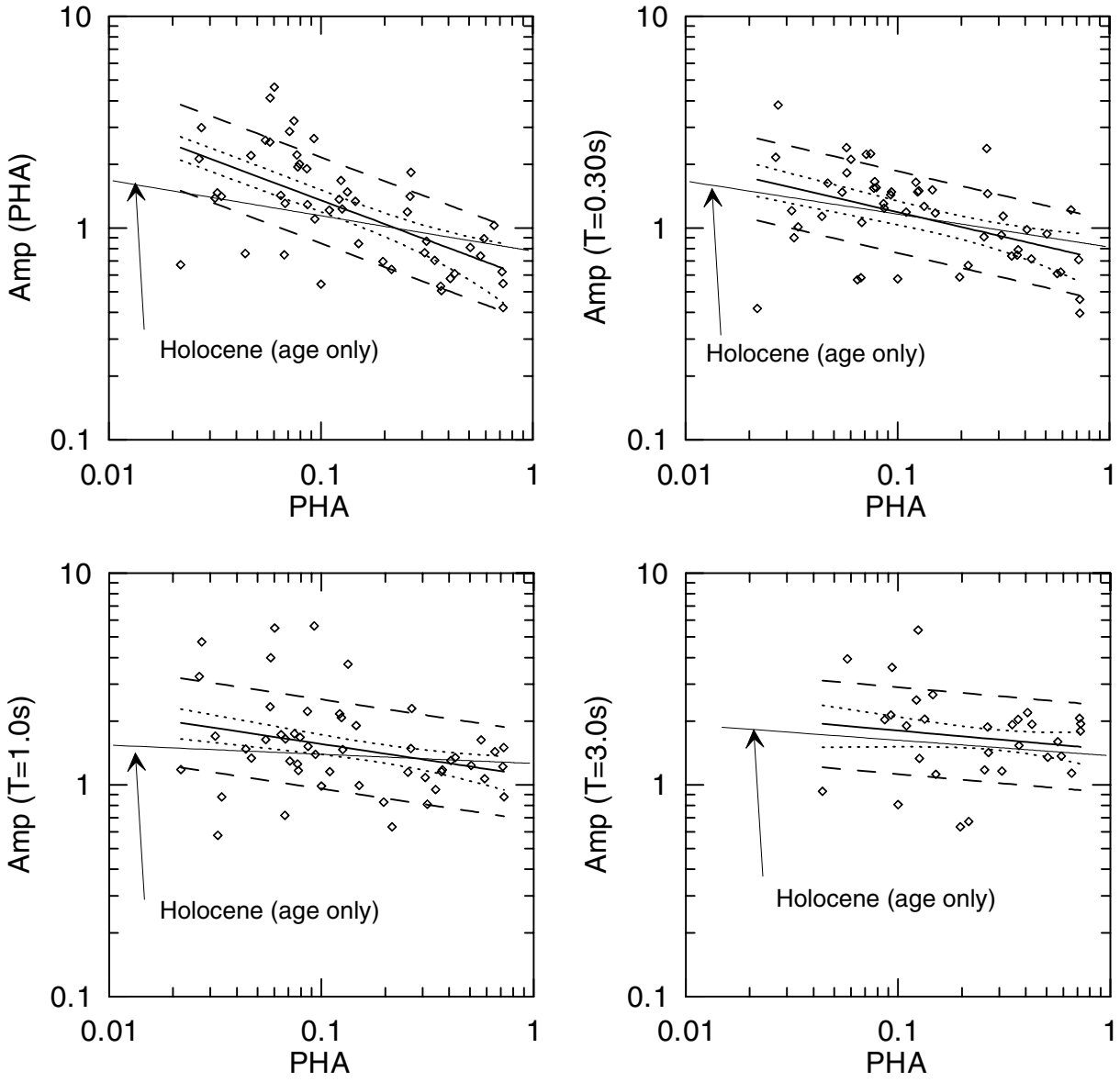

Fig. 5.3(b). Spectral acceleration amplification factors for Holocene lacustrine/marine sediments

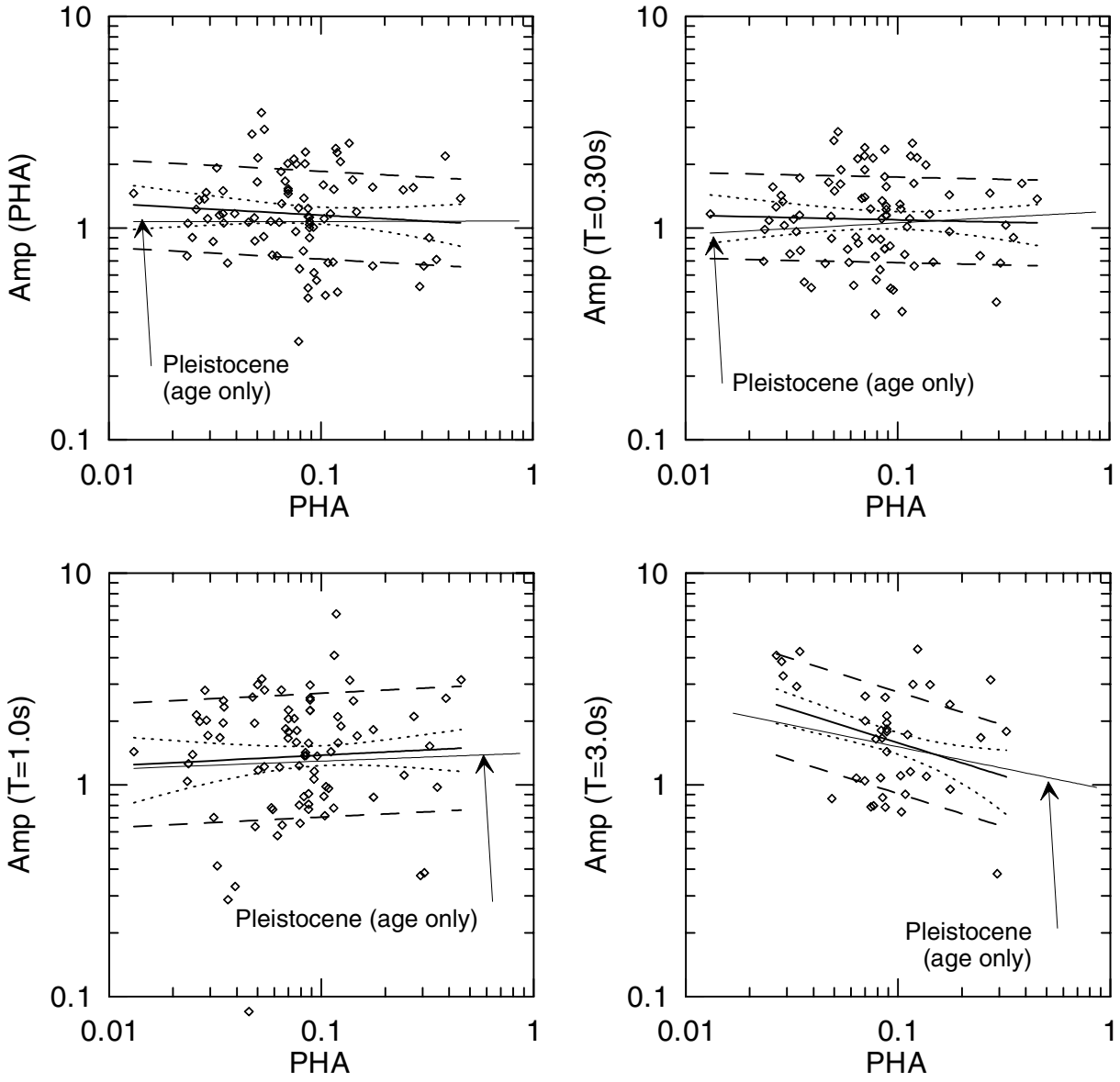

Fig. 5.3(c). Spectral acceleration amplification factors for Pleistocene alluvial sediments

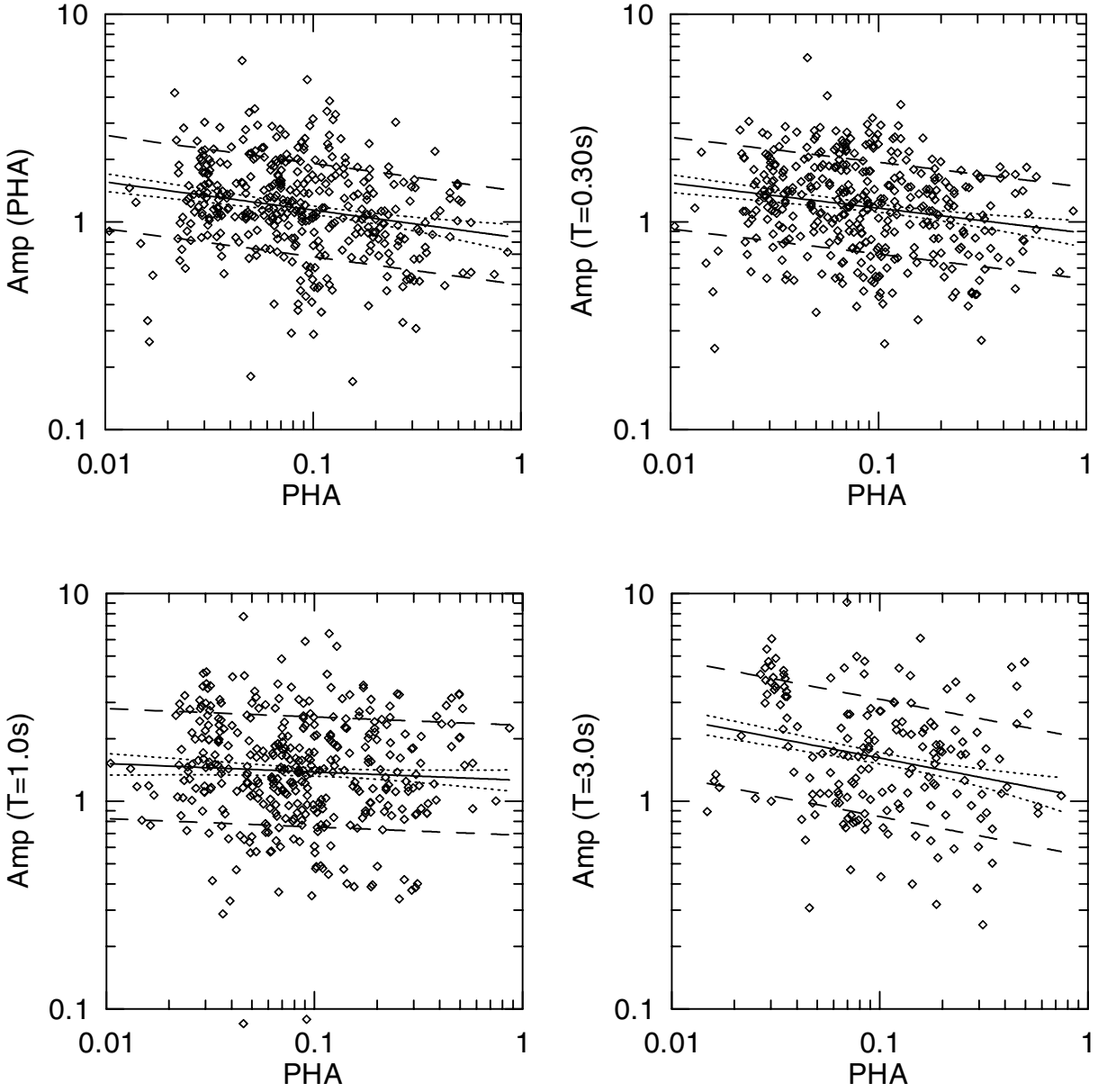

Fig. 5.3(d). Spectral acceleration amplification factors for Quaternary alluvial sediments

Figures 5.4 present amplification factors and regression results for Quaternary sediments segregated into coarse-grained and fine-grained/mixed soil types. Regression coefficients and error terms from these analyses are presented in Table 5.3(a), while F statistics on the distinction between categories are presented in Table 5.3(b). Fine-grained and mixed texture sediments exhibit similar amplification levels, which is why these categories were combined. As can be seen in Figure 5.4(a), Holocene coarse-grained sediments (Hc) exhibit amplification levels generally comparable to those for the Holocene age-only category. The same is true at short periods for Pleistocene coarse-grained sediments (Pc) and the Pleistocene age-only category (Figure 5.4c). The Holocene fine-grained/mixed category (Hm) has significantly distinct variations from Hc at low period (PHA and F_a), but the sub-categories are insignificantly distinct at longer periods ($T \geq 1.0$ s, F_v). Pleistocene categories Pc and Pm are insignificantly distinct at nearly all periods. Categories Hm and Pm (Figure 5.4b, d) exhibit higher levels of weak-motion amplification and low-period nonlinearity than Hc and Pc, respectively (Figures 5.4a, c). This is quantified by negative b-parameters that are generally larger and more statistically significant for mixed/fine-grained than coarse-grained sediments, and for Holocene than Pleistocene ages.

Based on the above, subdivision of Holocene according to material texture categories Hm and Hc is clearly justified both on the basis of F-statistics and on inter-category variations in nonlinearity. Subdivision of Pleistocene is not justified on the basis of the F-statistic, although variability in the nonlinearity of sediment response was observed between Pm and Pc. Based on these findings, for subsequent applications we take the geologic age + material texture scheme to consist of a single Pleistocene category and Holocene sub-categories Hc and Hm.

Figure 5.5 presents for the various Quaternary sub-categories the variation of standard error term (σ) with period. Values of σ for the Hm and Hlm categories are lower than those for the overall Holocene age group by about 0.05–0.2 in natural log units (a significant reduction). Error terms for Hc and Ha are comparable to those for the overall Holocene category. The results are less consistent for Pleistocene sediments, with the smallest errors occurring for the fine/mixed category at small periods and the coarse category at long periods. As noted previously, the Pc, Pm, and Pa categories are not carried forward.

Table 5.3(a). Regression coefficients for S_a amplification factors, age + material texture classification scheme

Geology	Period	a	b	σ	Rejection confidence for b=0 model (%)
Hol. - coarse (Hc)	PHA	-0.16 ± 0.26	-0.12 ± 0.10	0.51	99
	0.3	-0.14 ± 0.25	-0.11 ± 0.09	0.50	98
	1	0.15 ± 0.29	-0.06 ± 0.11	0.57	75
	3	-0.08 ± 0.46	-0.22 ± 0.17	0.63	99
	Fa	-0.11 ± 0.23	-0.09 ± 0.09	0.46	95
	Fv	0.05 ± 0.24	-0.11 ± 0.09	0.48	98
Hol. - mixed (Hm)	PHA	-0.50 ± 0.26	-0.31 ± 0.11	0.51	100
	0.3	-0.34 ± 0.23	-0.23 ± 0.10	0.47	100
	1	0.12 ± 0.28	-0.11 ± 0.12	0.56	93
	3	0.33 ± 0.32	-0.11 ± 0.15	0.57	84
	Fa	-0.39 ± 0.22	-0.24 ± 0.10	0.45	100
	Fv	0.03 ± 0.24	-0.16 ± 0.11	0.48	100
Pleist. - coarse (Pc)	PHA	-0.25 ± 0.65	-0.11 ± 0.24	0.46	54
	0.3	0.07 ± 0.60	-0.02 ± 0.23	0.43	13
	1	0.66 ± 0.73	0.11 ± 0.27	0.51	57
	3	0.49 ± 1.12	-0.03 ± 0.45	0.43	10
	Fa	-0.26 ± 0.50	-0.13 ± 0.19	0.35	85
	Fv	0.20 ± 0.58	-0.04 ± 0.22	0.41	32
Pleist. - mixed (Pm)	PHA	-0.53 ± 0.54	-0.23 ± 0.22	0.39	96
	0.3	-0.31 ± 0.55	-0.17 ± 0.22	0.40	87
	1	-0.54 ± 0.68	-0.35 ± 0.27	0.49	99
	3	-0.34 ± 0.81	-0.34 ± 0.35	0.47	94
	Fa	-0.35 ± 0.51	-0.19 ± 0.21	0.37	93
	Fv	-0.31 ± 0.58	-0.27 ± 0.24	0.42	97

Table 5.3(b). F-statistics indicating distinction between site categories, age + material texture classification scheme

	PHA		T = 0.3 s		T = 1.0 s		T = 3.0 s		F_a		F_v	
Categories	F	p	F	p	F	p	F	p	F	p	F	p
Hc-Hm	4.2	0.016	2.1	0.123	0.8	0.452	1.6	0.205	3.2	0.044	1.3	0.285
Hc-Pc	3.1	0.048	0.9	0.429	1.6	0.210	1.4	0.249	0.4	0.682	0.6	0.533
Pc-Pm	0.3	0.758	0.5	0.622	3.1	0.054	0.8	0.440	0.2	0.802	1.2	0.313
Hm-Pm	0.8	0.450	0.3	0.742	0.8	0.441	0.4	0.686	0.1	0.888	0.2	0.860

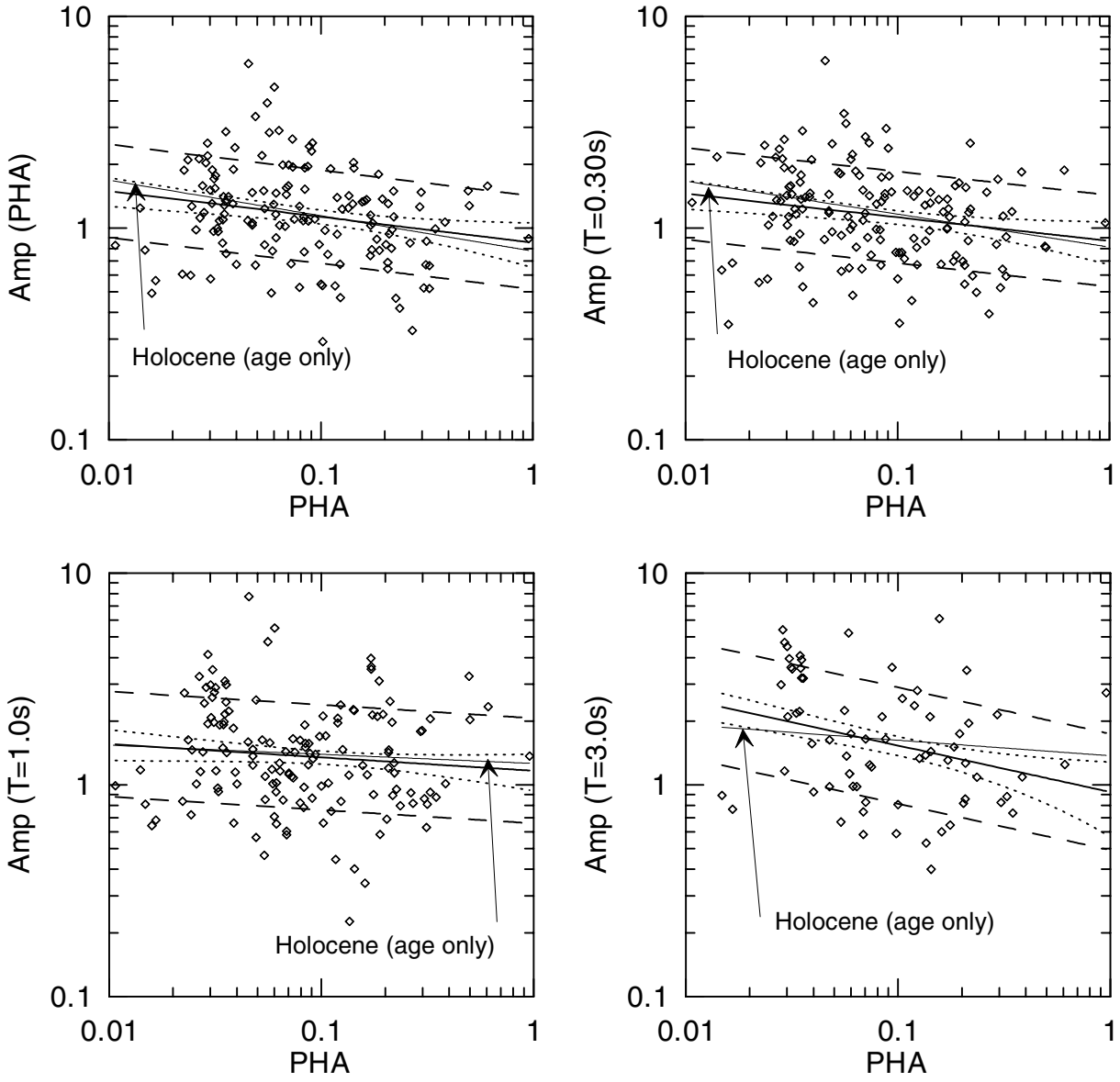

Fig. 5.4(a). Spectral acceleration amplification factors for Holocene coarse-grained sediments

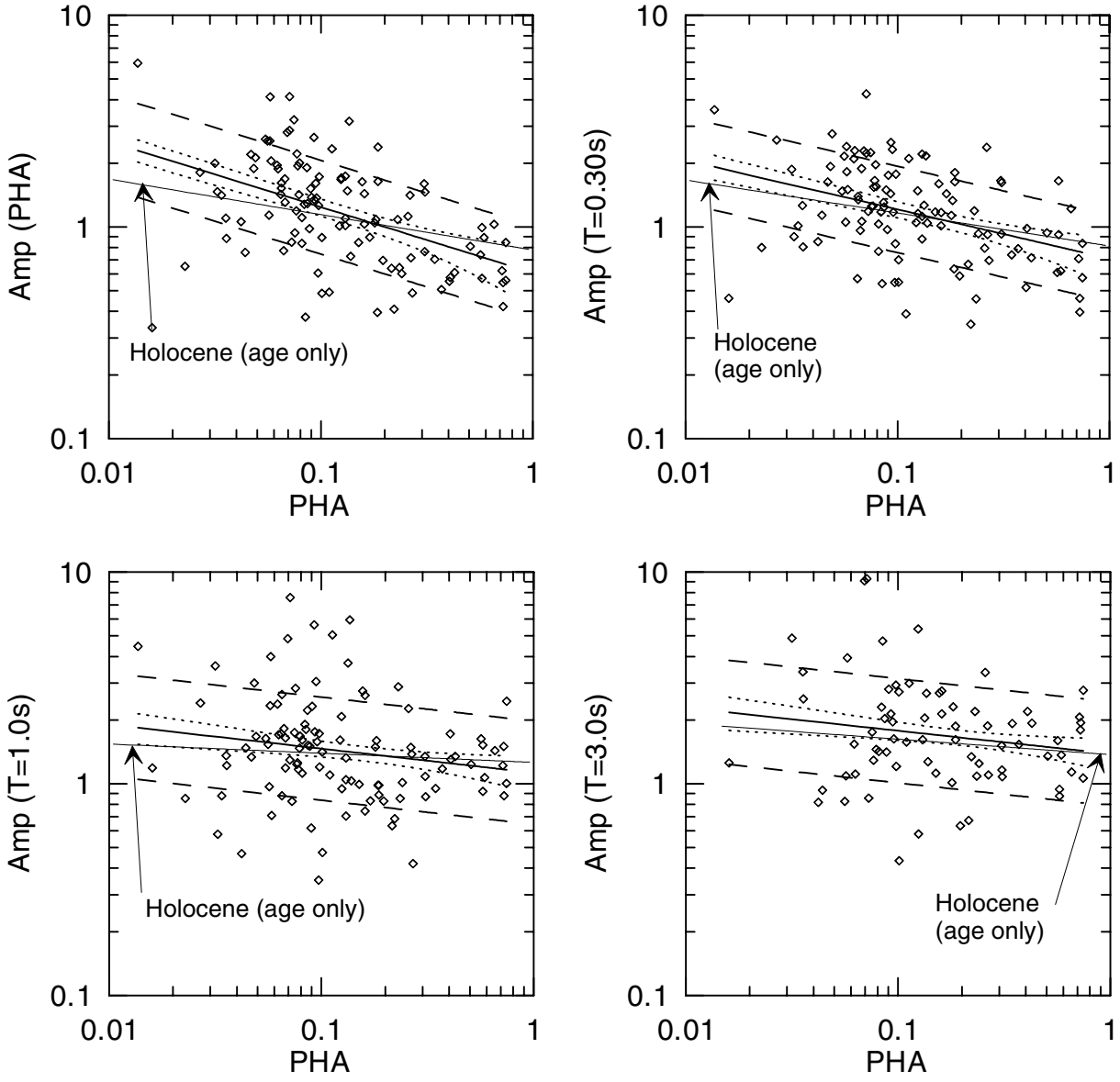

Fig. 5.4(b). Spectral acceleration amplification factors for Holocene fine-grained/mixed sediments

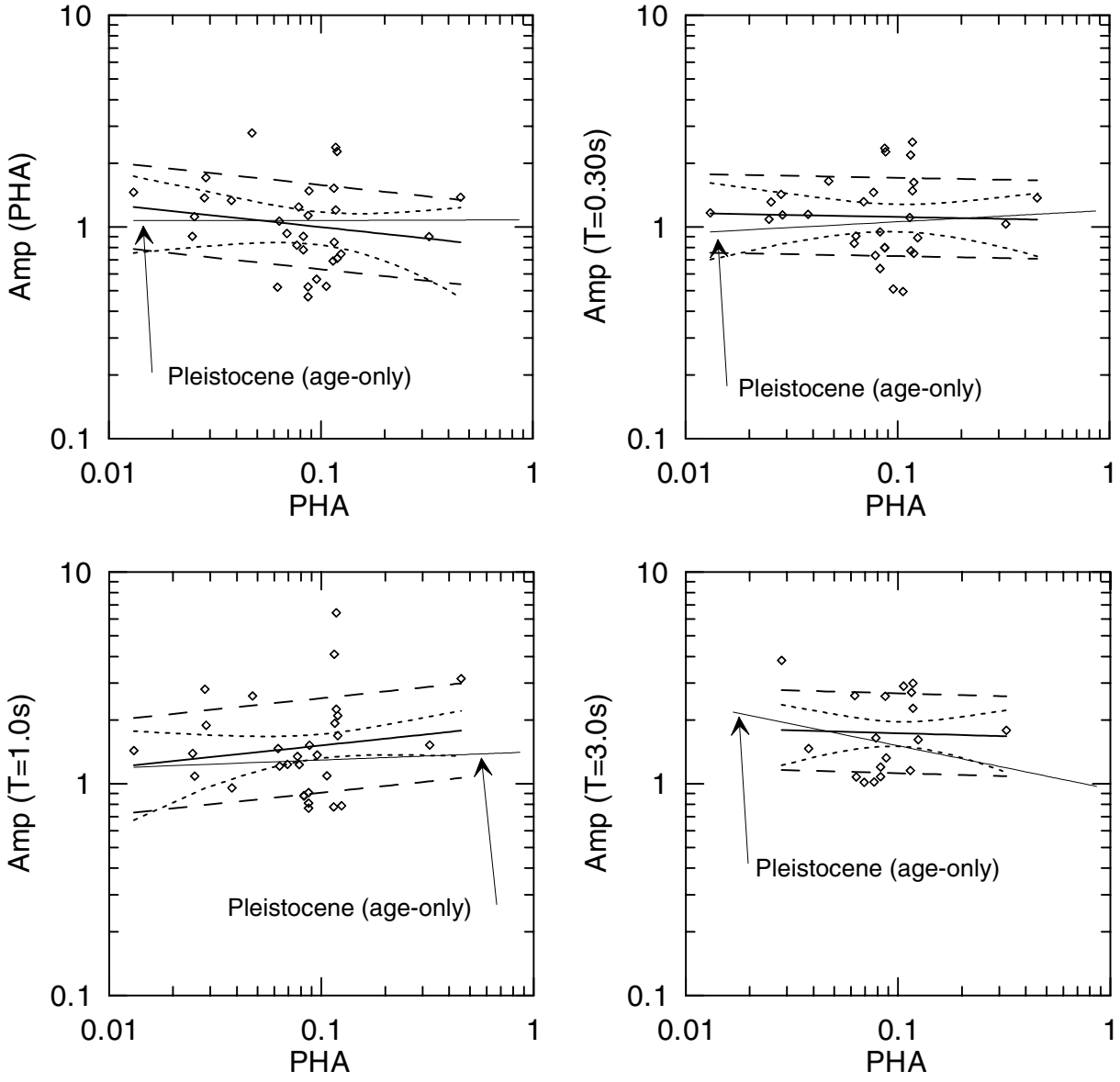

Fig. 5.4(c). Spectral acceleration amplification factors for Pleistocene coarse-grained sediments

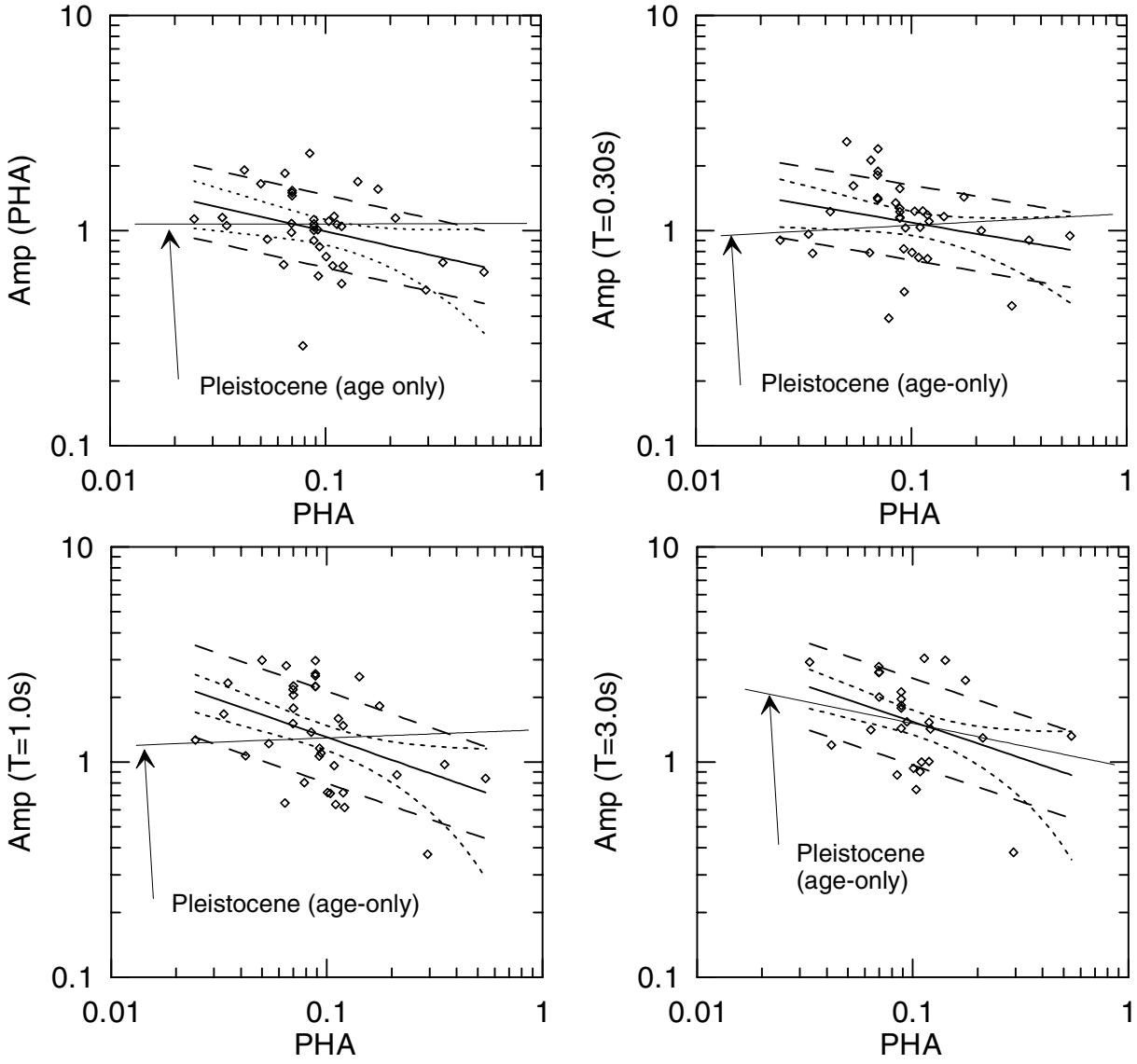

Fig. 5.4(d). Spectral acceleration amplification factors for Pleistocene fine-grained/mixed sediments

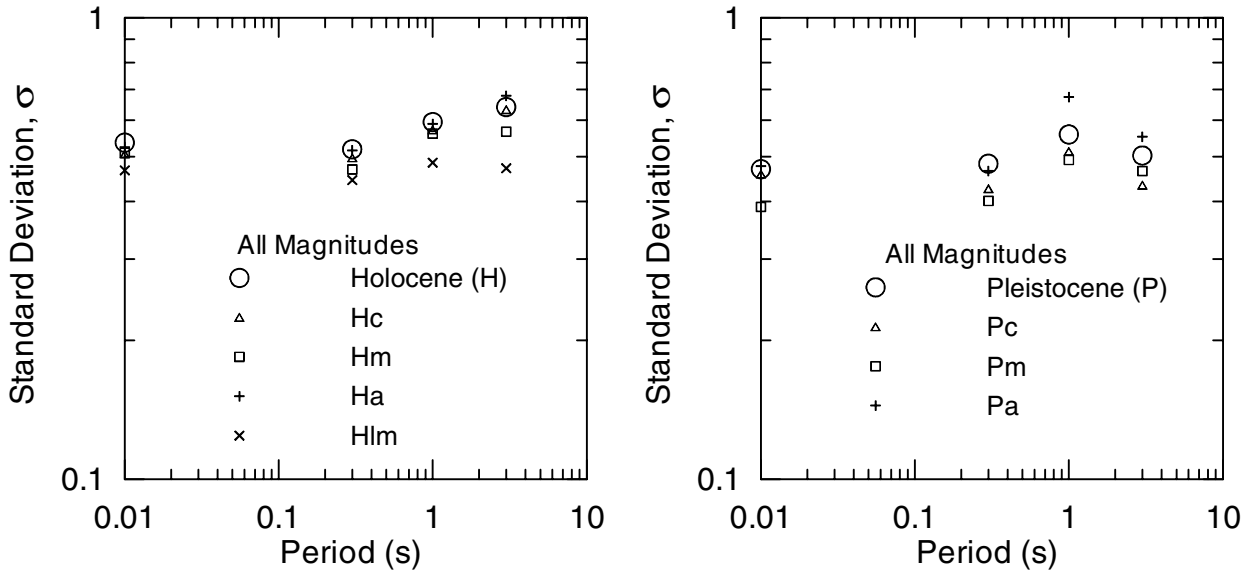

Fig. 5.5. Variation of standard error term σ with period for Quaternary sub-categories

5.3 AMPLIFICATION WITHIN SITE CATEGORIES DEFINED BY $V_{s\text{-}30}$

As noted in Section 3.2.2, shear wave velocity profiles were matched to strong motion stations for 185 sites with strong motion recordings. The site breakdowns associated with the $V_{s\text{-}30}$-based NEHRP classification scheme (Table 3.3) are presented in Figure 3.6. Only Categories B–D have a sufficient number of sites to enable a stable regression of amplification factors. Individual amplification factors and the results of regression analyses performed according to Eq. 4.3(a) are presented in Figures 5.6 and Tables 5.4 for NEHRP Categories B–D.

Amplification levels between NEHRP Categories C–D are moderately or significantly distinct at all periods, with the amplification being larger for NEHRP D than for C. Amplification levels for Categories B and C are not distinct for some individual periods, but are distinct for parameters F_a and F_v, with C amplification exceeding B. The PHA-dependence of amplification in NEHRP B is statistically insignificant. For C, the PHA-dependence is moderate to strong at low periods (T = 0.01 s and 0.3 s, F_a), and insignificant at longer periods. The NEHRP D category has weak-motion amplification levels that are comparable to C at low periods (T = 0.01 s and 0.3 s, F_a) and moderate nonlinearity. For relatively strong shaking, D amplification clearly exceeds C. At longer periods, amplification of D is large but the PHA-dependence of the amplification is negligible.

Table 5.4(a). Regression coefficients for S_a amplification factors, NEHRP (V_{s-30}) classification scheme

Category	Period	a	b	σ	Rejection confidence for b=0 model (%)
NEHRP B	PHA	-0.16 ± 1.26	-0.04 ± 0.51	0.51	13
	0.3	-0.41 ± 1.15	-0.02 ± 0.47	0.47	7
	1	-1.03 ± 1.84	-0.22 ± 0.75	0.75	46
	3	-1.77 ± 1.79	-0.65 ± 0.66	0.32	95
	Fa	-0.25 ± 1.08	0.02 ± 0.44	0.44	8
	Fv	-0.93 ± 1.50	-0.21 ± 0.61	0.61	51
NEHRP C	PHA	-0.11 ± 0.26	-0.08 ± 0.10	0.56	86
	0.3	-0.29 ± 0.30	-0.14 ± 0.12	0.63	97
	1	0.05 ± 0.37	-0.05 ± 0.15	0.77	48
	3	0.09 ± 0.57	0.00 ± 0.27	0.76	2
	Fa	-0.27 ± 0.27	-0.13 ± 0.11	0.57	98
	Fv	0.00 ± 0.32	-0.07 ± 0.13	0.68	71
NEHRP D	PHA	0.07 ± 0.22	-0.07 ± 0.08	0.57	88
	0.3	0.07 ± 0.21	-0.05 ± 0.08	0.54	77
	1	0.37 ± 0.21	-0.01 ± 0.08	0.54	15
	3	0.47 ± 0.26	0.00 ± 0.12	0.56	4
	Fa	0.02 ± 0.19	-0.06 ± 0.07	0.50	91
	Fv	0.34 ± 0.18	-0.02 ± 0.07	0.46	50

Table 5.4(b). F-statistics indicating distinction between site categories, NEHRP (V_{s-30}) classification scheme

	PHA		T = 0.3 s		T = 1.0 s		T = 3.0 s		F_a		F_v	
Categories	F	p	F	p	F	p	F	p	F	p	F	p
NEHRP B-C	0.49	0.614	3.01	0.052	5.78	0.004	0.73	0.487	3.09	0.049	5.93	0.003
NEHRP C-D	2.7	0.068	3.7	0.026	5.0	0.007	6.1	0.003	3.1	0.049	7.2	0.001

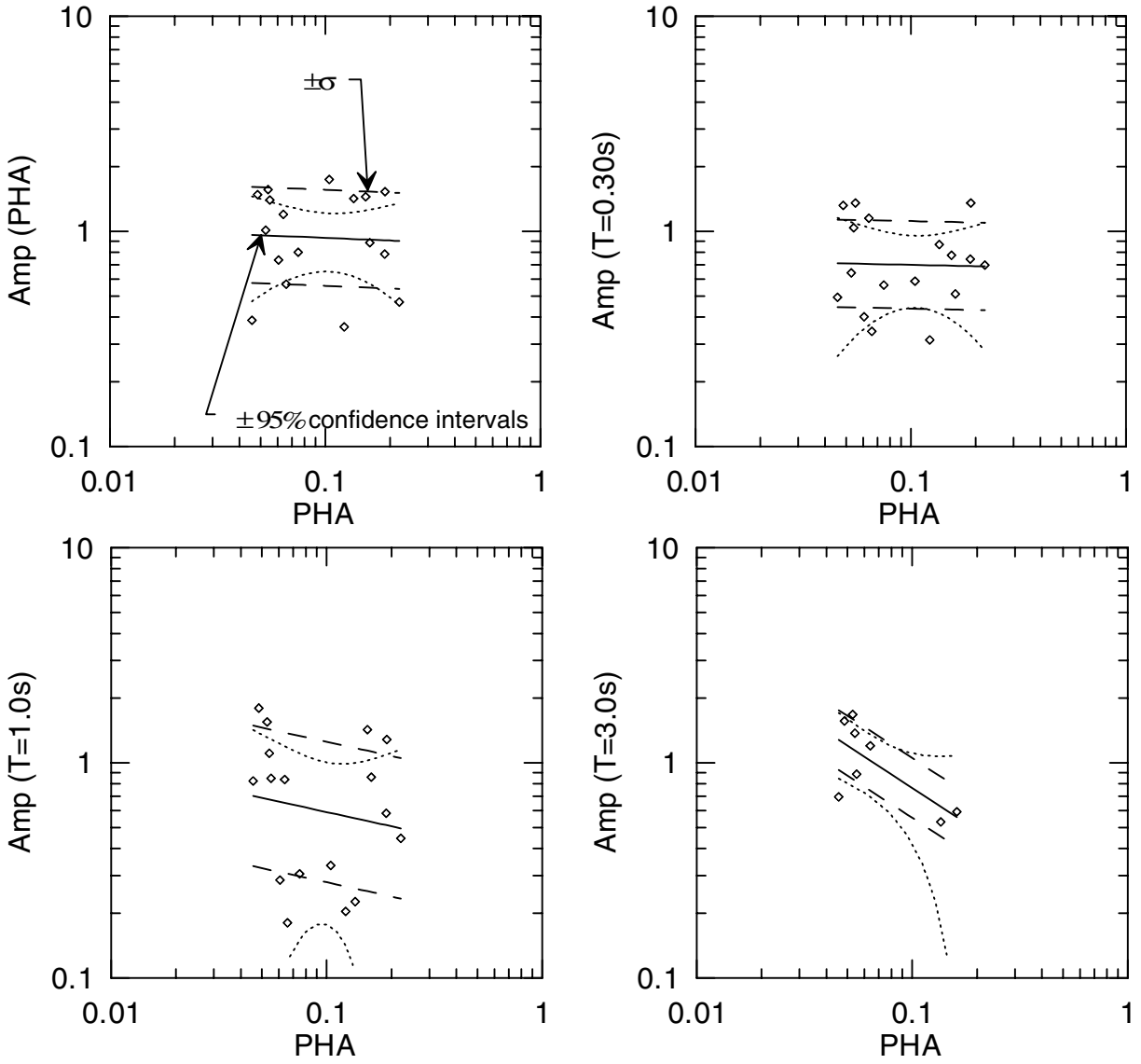

Fig. 5.6(a). Spectral acceleration amplification factors for NEHRP Category B materials

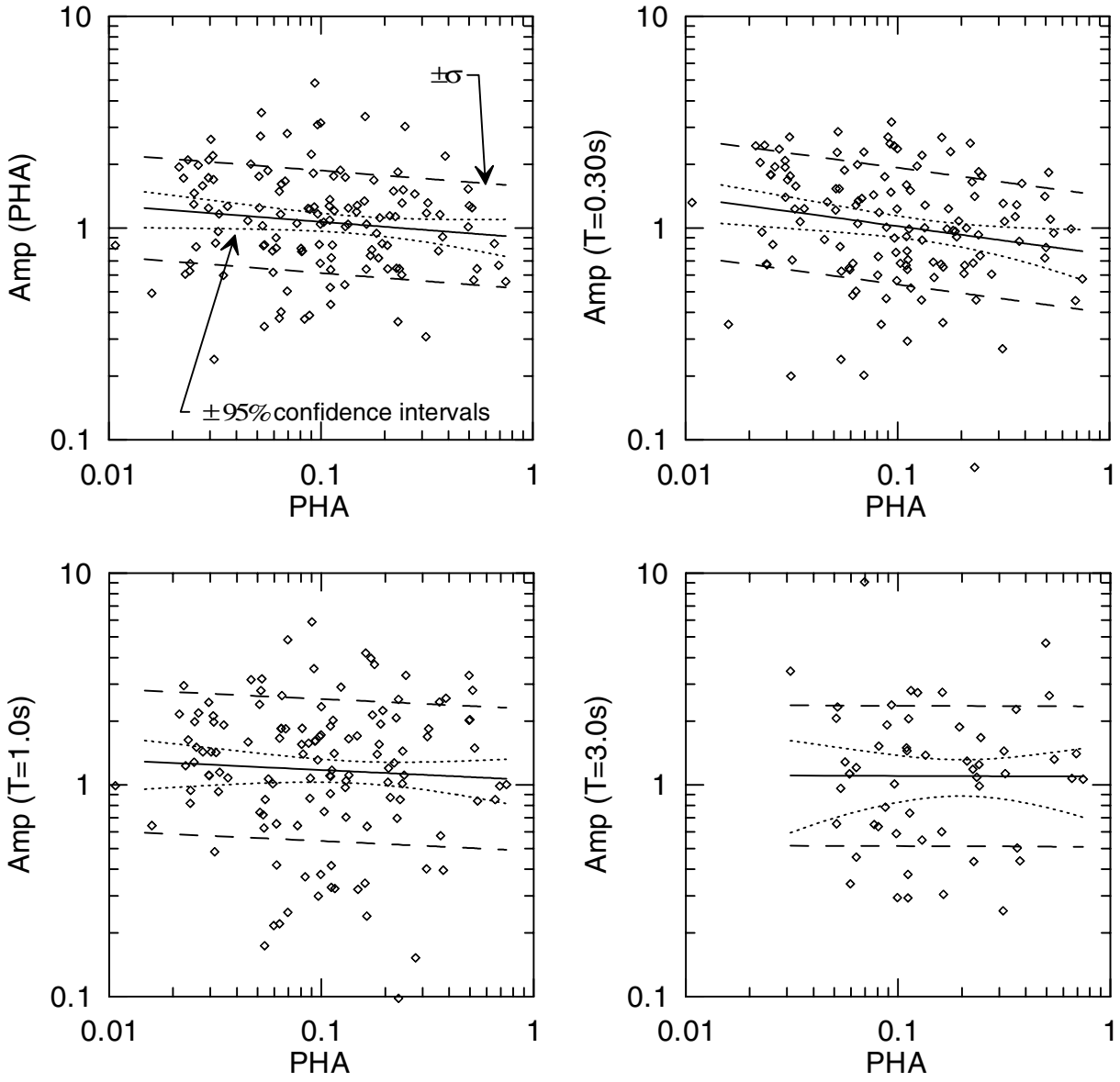

Fig. 5.6(b). Spectral acceleration amplification factors for NEHRP Category C materials

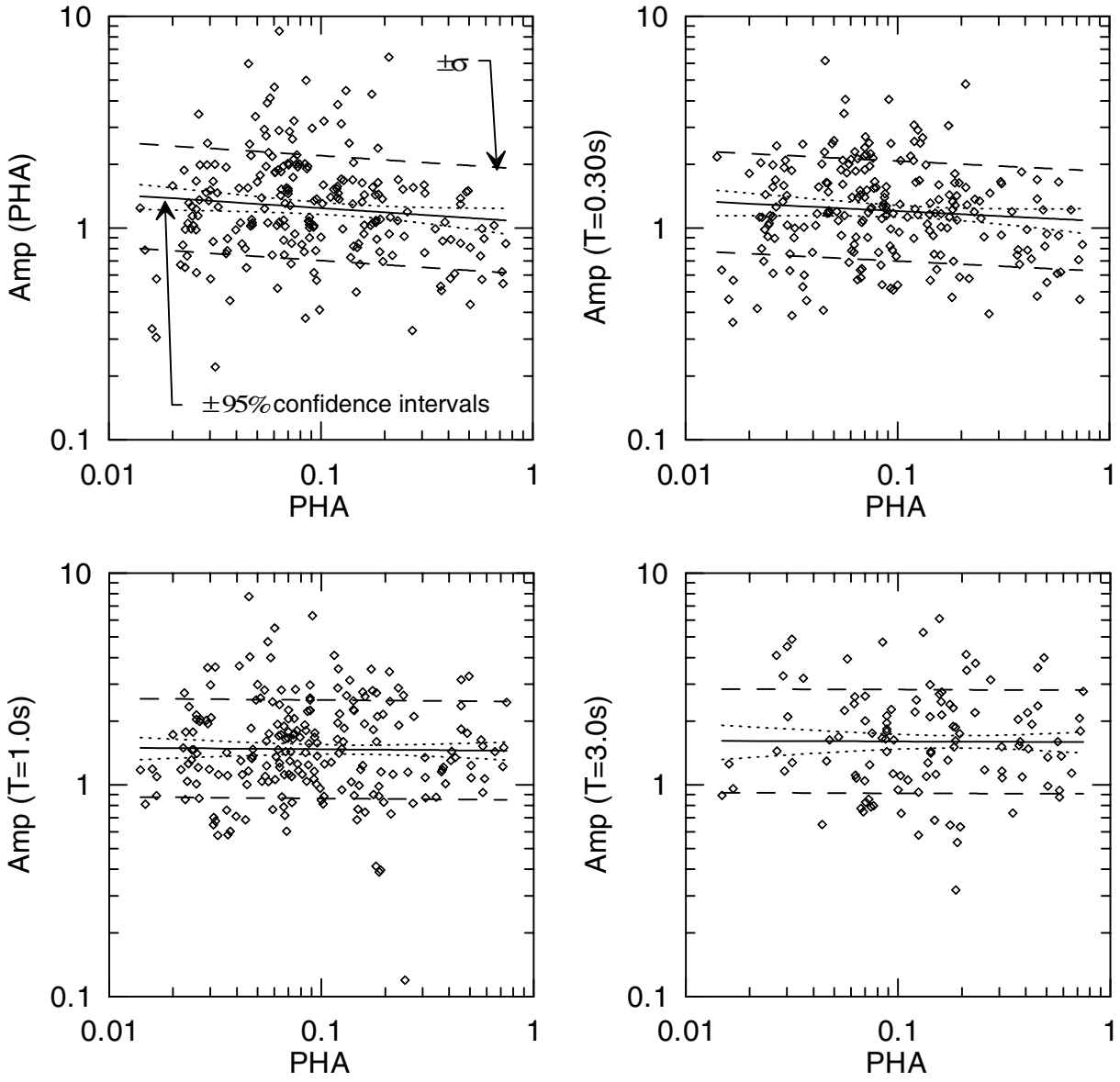

Fig. 5.6(c). Spectral acceleration amplification factors for NEHRP Category D materials

The amplification factors for NEHRP categories do not exactly match those for surface geology categories because there is not a one-to-one correspondence between V_{s-30} and surface geology. NEHRP B amplification factors are generally smaller than Mesozoic, which likely occurs because many of the Mesozoic geology sites in our database have V_{s-30} smaller than the lower-bound NEHRP B threshold of 760 m/s (e.g., among the 24 Mesozoic sites with NEHRP classifications, 13 are C, 8 are B, and 3 are A). The results for NEHRP C sites are generally intermediate between results for the geologic Pleistocene and Tertiary categories (except at long period). Results for NEHRP D sites are generally intermediate between those for Holocene and Pleistocene sediments. Data dispersion, as measured by intra-category standard deviations, is generally larger than the values obtained for detailed surface geology schemes. This is a significant outcome, as it suggest that the NEHRP scheme has less ability to distinguish site-to-site variations in spectral acceleration than the geology scheme.

We investigated whether revising the velocities that define the NEHRP boundaries would improve the intra-category data dispersion. To define new velocities for this exercise, we attempted to align the revised NEHRP categories with typical V_{s-30} values for geologic units in California (Wills and Silva, 1998). The following revised categories were investigated:

Category	**Current NEHRP**	**Possible Revision**
E	< 180 m/s	< 200 m/s
D	180 – 360 m/s	200 – 340 m/s
C	360 – 760 m/s	340 – 530 m/s
B	760 – 1500 m/s	530 – 1300 m/s

The revised boundaries correspond roughly to 84th and 16th percentile V_{s-30} values for the following geologic units, as determined by Wills and Silva (1998): NEHRP E-D boundary, Hlm and Qa; D-C boundary, Qa and Tertiary; C-B boundary, Tertiary and Mesozoic (Franciscan formation).

To investigate whether the revised NEHRP categories are worthwhile from the standpoint of dispersion reduction, we categorized all sites according the revised boundaries shown above, and performed regression of data within the categories. For soil categories (C + D), the outcome of the analyses is that the new site categories do not produce significant changes in standard error terms and the dispersion remains significantly higher than for detailed surface geology schemes. For rock categories (B + C), the new B-C boundary provides a small improvement. A

presentation of the numerical results that support these conclusions is deferred to Section 6.1, where the results are presented as inter-category standard error terms (i.e., averaged error terms across categories within a scheme).

A significant outcome of the work presented in this section is that the NEHRP classification scheme appears to be less effective at predicting site-to-site variations in ground motion at soil sites than detailed surface geology schemes. This is evidenced by the relative high intra-category dispersion terms at small period for the NEHRP categories (in Table 5.4b) as compared to those for the detailed surface geology schemes (Tables 5.2a and 5.3a). Further support for this conclusion is provided by the inter-category error terms discussed in Section 6.1.

To further investigate the degree to which surface geology can provide an improved representation of site effects relative to the NEHRP categories, we compiled sites classified into the NEHRP C and D categories, and for sites within a given category, compute F statistics to test the level of distinction between sites within Quaternary alluvium (Qa) and Tertiary (T) sub-categories. These results are presented in the top two rows of Table 5.4(c), and show that Qa and T sites have distinct amplification levels at low period within the NEHRP D category but not within the NEHRP C category. The above analyses were performed in reverse as well, to evaluate the degree to which amplification levels within the Qa and T categories can be distinguished on the basis of NEHRP category C or D. These results are shown in the bottom two rows of Table 5.4(c), and show that NEHRP C and D sites do not have distinct amplification levels for multiple periods within either the Qa and T categories. To the extent that the low-period distinction between Qa and T within NEHRP D is greater than that obtained from subdivision of geology categories, the results of the sets of analyses in Table 5.4(c) weakly support the use of surface geology-based categories over NEHRP categories.

Table 5.4(c). F-statistics indicating distinction between sub-categories within NEHRP and surface geology categories

	PHA		T = 0.3 s		T = 1.0 s		T = 3.0 s		F_a		F_v	
Categories	**F**	**p**	**F**	**p**	**F**	**p**	**F**	**p**	**F**	**p**	**F**	**p**
NEHRP C: Qa - T	0.3	0.727	0.4	0.699	2.3	0.110	0.3	0.722	0.3	0.721	2.6	0.088
NEHRP D: Qa - T	2.4	0.100	3.5	0.034	0.1	0.883	0.5	0.600	1.9	0.156	0.9	0.395
Qa: NEHRP C - D	1.5	0.223	2.3	0.102	1.1	0.328	0.4	0.665	3.2	0.044	0.8	0.451
T: NEHRP C - D	1.5	0.241	2.1	0.136	1.2	0.326	0.6	0.542	1.3	0.275	2.5	0.100

5.4 AMPLIFICATION WITHIN SITE CATEGORIES DEFINED BY GEOTECHNICAL DATA

As noted in Section 3.2.3, geotechnical site classifications were developed for 183 strong motion stations based on nearby boreholes, and 335 recordings have been made at these sites. The site breakdown associated with the geotechnical classification scheme developed by Rodriguez-Marek et al. (2001) (Table 3.4) is presented in Figure 3.7. Individual amplification factors and the results of regression analyses performed according to Eq. 4.3(a) are presented in Figures 5.7 and Tables 5.5 for Categories B–E.

Category B (intact rock) has substantial de-amplification that is significantly distinct from Category C at low- to moderate-periods ($T \leq 1.0$ s, F_a, F_v). De-amplification factors for B do not vary significantly with rock PHA, and are generally lower than those for the Mesozoic + Igneous category in the age-only geology classification scheme. The general levels of C and D amplification at small periods are comparable to those for Holocene alluvial sediments. As demonstrated by the regression and hypothesis test results in Table 5.5(a), nonlinearity is generally weak to modest in Categories C and D. Data for Category E indicate much larger weak-motion amplification and nonlinearity than C or D for $T \leq 1.0$ s. However, this trend is based on a small number of recordings (12) and is considered tentative.

Interestingly, for Categories C and D, low-period amplification levels ($T = 0.01$ and 0.3 s) are not distinct, while intermediate to long-period amplification factors are significantly distinct with D exceeding C. This result is a reversal of trends discussed above in which inter-category distinction was generally greater at smaller period, and may be associated with a sediment depth effect on long-period spectral ordinates (the geotechnical scheme is the only one that incorporates depth in the definition of the site categories).

Data dispersion for Categories B and C, as measured by intra-category standard error terms, is comparable to that obtained for Tertiary and Mesozoic + Igneous geology or for NEHRP C. Category D error terms are similar to those for Holocene alluvium and NEHRP D. Category E error terms are relatively small. As with the other classification schemes, dispersion generally tends to increase with period.

Table 5.5(a). Regression coefficients for S_a amplification factors, geotechnical data classification scheme

Category	Period	a	b	σ	Rejection confidence for b=0 model (%)
Geotech. - B	PHA	-0.03 ± 0.50	0.02 ± 0.22	0.56	11
	0.3	-0.17 ± 0.59	0.06 ± 0.26	0.67	70
	1	-0.14 ± 0.70	0.12 ± 0.31	0.79	89
	3	-0.24 ± 0.77	-0.08 ± 0.35	0.63	36
	Fa	-0.15 ± 0.53	0.04 ± 0.24	0.60	27
	Fv	-0.15 ± 0.62	0.10 ± 0.28	0.70	52
Geotech. - C	PHA	0.10 ± 0.30	-0.04 ± 0.11	0.61	56
	0.3	-0.10 ± 0.30	-0.12 ± 0.11	0.63	97
	1	0.20 ± 0.35	-0.02 ± 0.13	0.71	23
	3	0.41 ± 0.47	0.13 ± 0.21	0.69	77
	Fa	-0.07 ± 0.27	-0.11 ± 0.10	0.56	96
	Fv	0.24 ± 0.30	-0.03 ± 0.11	0.63	37
Geotech. - D	PHA	-0.04 ± 0.24	-0.09 ± 0.09	0.57	94
	0.3	0.04 ± 0.21	-0.05 ± 0.08	0.51	76
	1	0.35 ± 0.22	-0.03 ± 0.09	0.54	50
	3	0.42 ± 0.29	-0.04 ± 0.13	0.58	45
	Fa	-0.01 ± 0.20	-0.06 ± 0.08	0.49	87
	Fv	0.28 ± 0.20	-0.05 ± 0.08	0.47	79
Geotech. - E	PHA	-0.88 ± 0.75	-0.62 ± 0.33	0.41	100
	0.3	-1.00 ± 0.68	-0.62 ± 0.30	0.38	100
	1	-0.28 ± 0.80	-0.42 ± 0.35	0.44	98
	3	0.28 ± 0.97	-0.23 ± 0.48	0.46	70
	Fa	-0.93 ± 0.63	-0.55 ± 0.27	0.35	100
	Fv	-0.21 ± 0.69	-0.36 ± 0.30	0.38	97

Table 5.5(b). F-statistics indicating distinction between site categories, geotechnical data classification scheme

	PHA		T = 0.3 s		T = 1.0 s		T = 3.0 s		F_a		F_v	
Categories	F	p	F	p	F	p	F	p	F	p	F	p
Geot. B-C	3.1	0.048	10.0	0.000	12.8	0.000	1.4	0.258	8.7	0.000	16.6	0.000
Geot. C-D	0.3	0.729	0.8	0.468	2.9	0.056	6.9	0.001	0.6	0.532	1.3	0.276
Geot. D-E	5.0	0.007	5.7	0.004	2.9	0.055	1.0	0.380	4.5	0.013	2.4	0.095

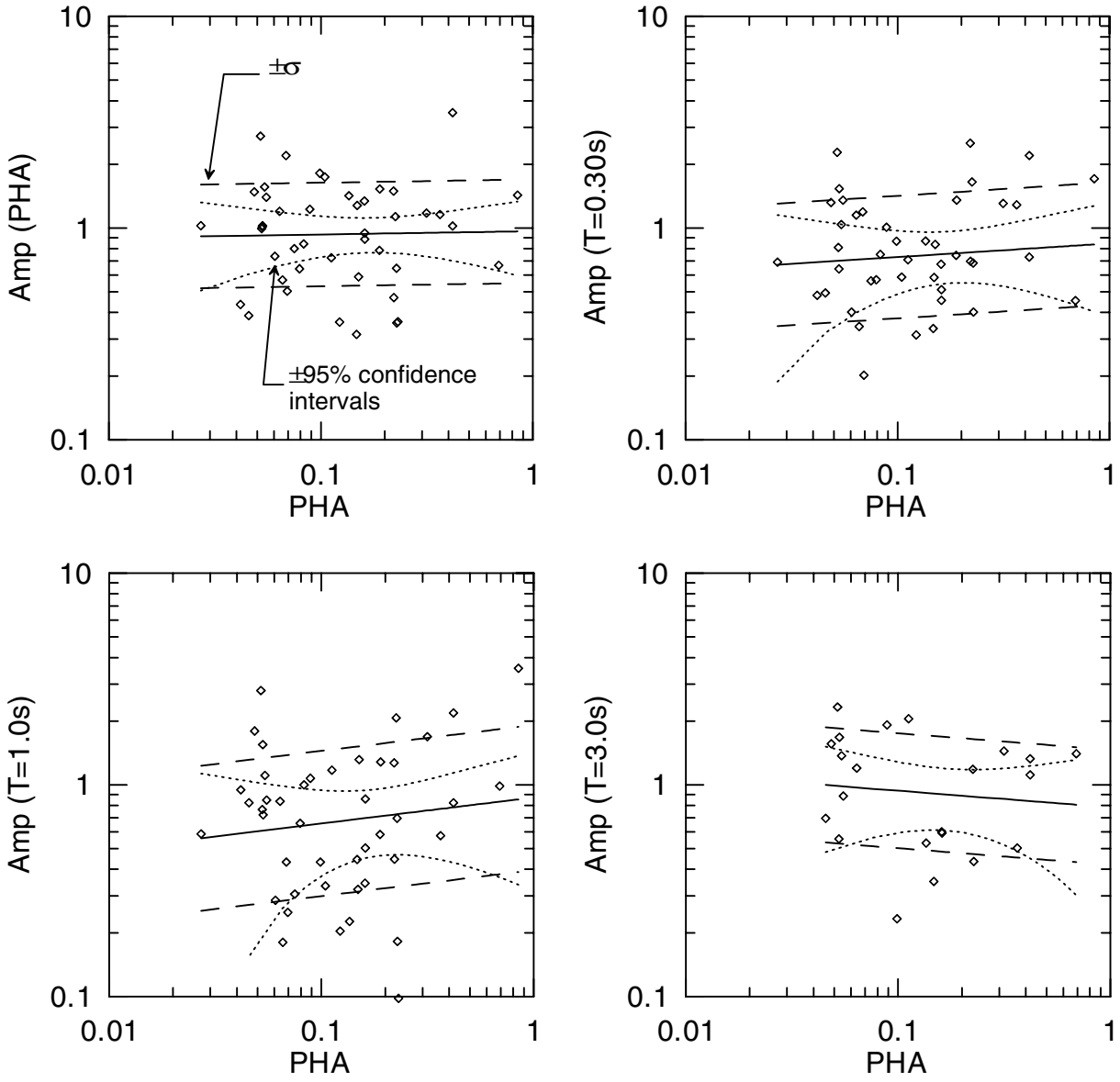

Fig. 5.7(a). Spectral acceleration amplification factors for Geotechnical B materials

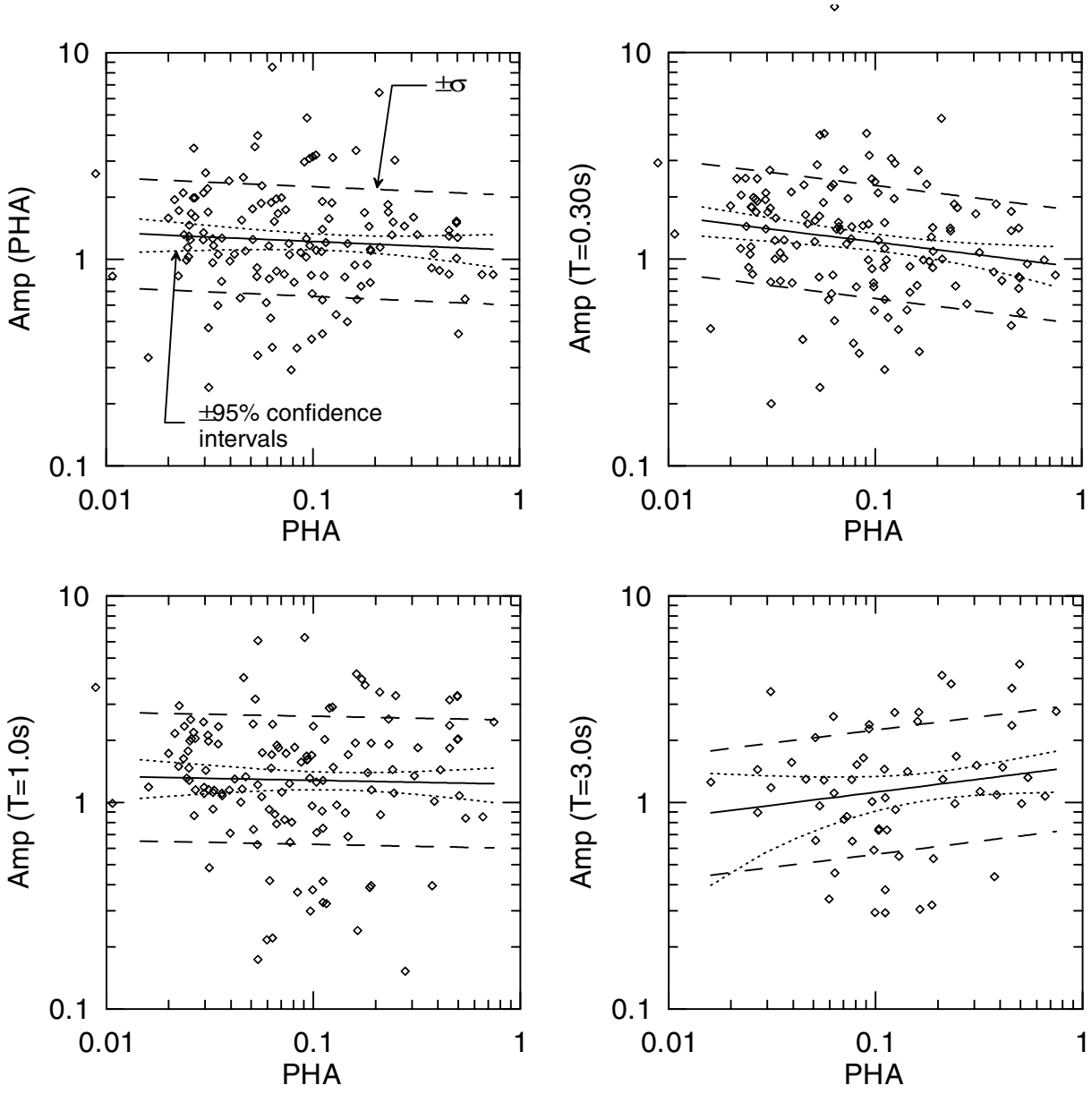

Fig. 5.7(b). Spectral acceleration amplification factors for Geotechnical C materials

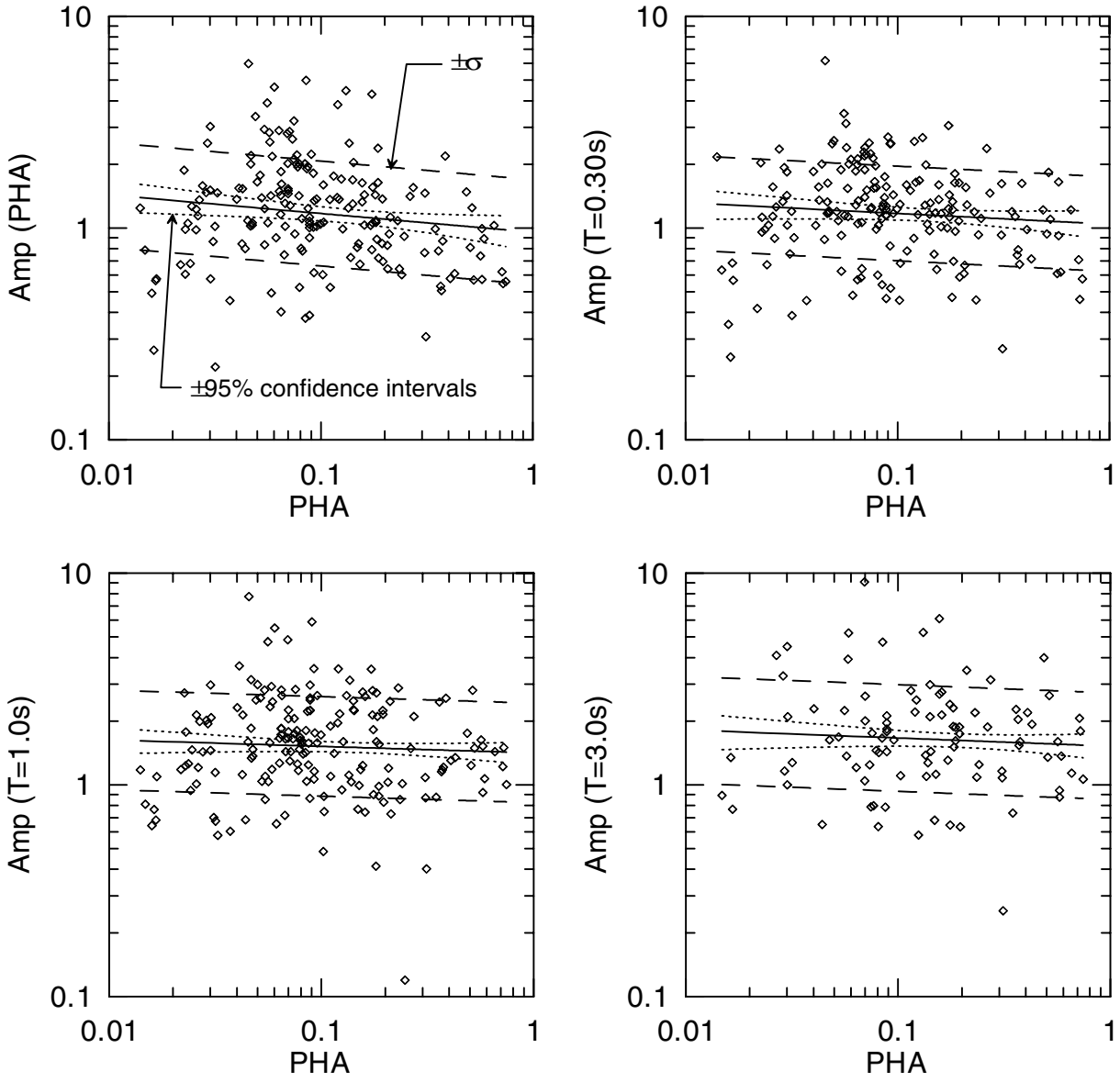

Fig. 5.7(c). Spectral acceleration amplification factors for Geotechnical D materials

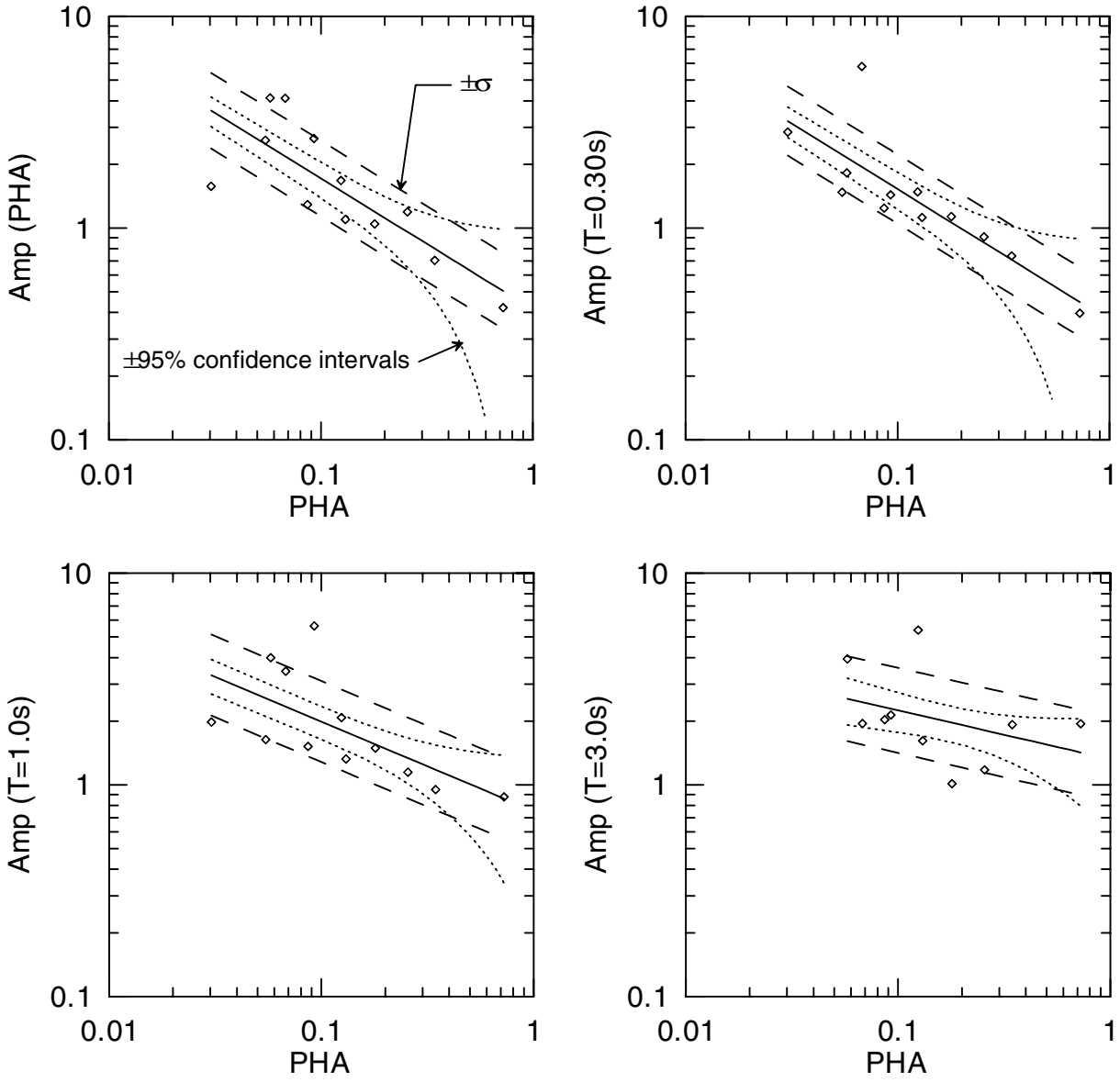

Fig. 5.7(d). Spectral acceleration amplification factors for Geotechnical E materials

The distinction between C and D sites is made based on depth to rock. Information on sediment stiffness is not directly incorporated into the geotechnical classification scheme, with the exception of the special category for soft soil (E). Accordingly, for Categories C and D we evaluate the dependence of amplification factors on stiffness using the $V_{s\text{-}30}$ parameter, which is available for many of the geotechnically classified sites. This evaluation is performed by regressing residual R_{ij} for motion j in scheme i against $V_{s\text{-}30}$ as follows:

$$\ln(R_{ij}) = c_i + d_i V_{s-30} \tag{5.3}$$

where c_i and d_i represent regression coefficients for category i. These analyses are performed for period-averaged spectral ordinates F_a and F_v. The results are presented in Figure 5.7(e)–(f) and Table 5.5(c). These results indicate moderate variability of the residuals with $V_{s\text{-}30}$ in the C category for F_v and in the D category for F_a. Dispersion is not significantly reduced from the values given in Table 5.5(a).

Our judgment is that these results do not support modification of the geotechnical categorization scheme to include information on $V_{s\text{-}30}$. We base this opinion on the lack of dispersion reduction associated with the introduction of this parameter, and the lack of a significant effect of $V_{s\text{-}30}$ on F_a values for Category C (where the greatest effect might have been expected given the limited depth of Category C sites). For Category C, our lack of dispersion reduction differs from the findings of Rodriguez-Marek et al. (2001), who found use of the $V_{s\text{-}30}$ parameter to reduce dispersion for Category C. Like the present study, Rodriguez-Marek et al. found the use of $V_{s\text{-}30}$ to not reduce dispersion for Category D.

Table 5.5(c). Regression coefficients for variation of residual in geotechnical categories C and D with 30 m V_s

Category	Period	c	d (s/m)	σ
Geotech C	Fa	0.07 ± 0.37	-0.0002 ± 0.0009	0.56
	Fv	0.45 ± 0.40	-0.0010 ± 0.0010	0.61
Geotech D	Fa	0.28 ± 0.29	-0.0009 ± 0.0009	0.48
	Fv	0.14 ± 0.27	-0.0005 ± 0.0009	0.47

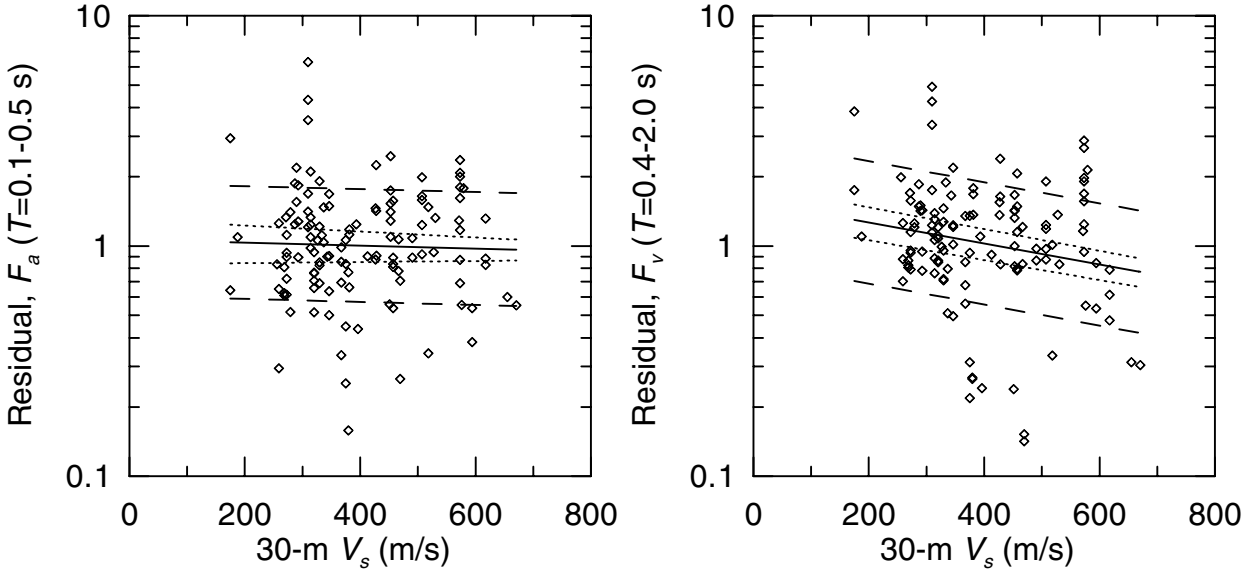

Fig. 5.7(e). Variation of residual for Geotechnical Category C with V_{s-30}

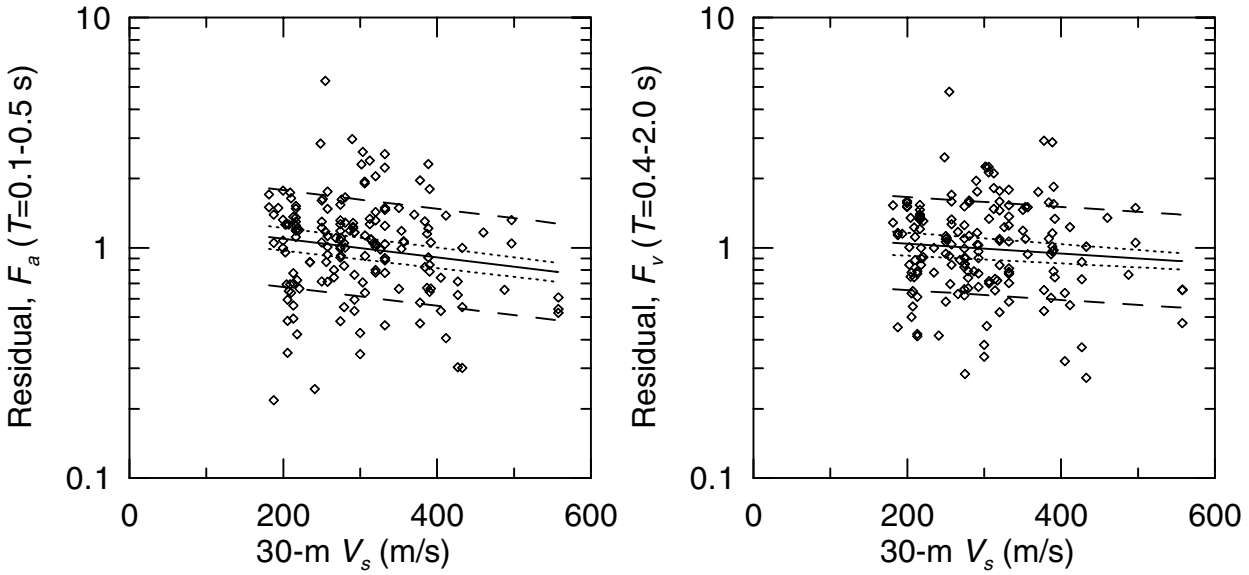

Fig. 5.7(f). Variation of residual for Geotechnical Category D with V_{s-30}

5.5 MAGNITUDE-DEPENDENCE OF AMPLIFICATION FACTORS

The regression equation used in the above analyses (Eq. 4.3a) is based on the assumption that amplification for a given site category is a function of only reference motion amplitude. Due to the finite time required for soil profiles to reach their steady-state resonant response, some dependence of amplification on the magnitude/duration of strong shaking might be expected. In Figure 5.8 we present residuals between individual amplification factors for Holocene sites and amplification-adjusted reference motions (using the regression results in Figure 5.1a). The results indicate no significant magnitude-dependence in the sediment response for spectral accelerations at T = 0.01 and 0.3 s. However, magnitude-dependent residuals are observed at T = 1.0 and 3.0 s. The increase of residual with magnitude in Figure 5.8 indicates larger long-period sediment response in large magnitude earthquakes as compared to small magnitude events. Similar results are obtained for other site categories.

We perform linear regression analyses to relate residuals such as those shown in Figure 5.8 to magnitude for T=3.0 s amplification factors and F_v. The regression was performed according to:

$$\ln(R_{ij}) = e_i + f_i m \tag{5.4}$$

where e_i and f_i are regression coefficients for category i and m = moment magnitude. Values of the regression coefficients and standard error terms are shown in Table 5.6. Parameters e_i and f_i can be taken as zero for T = 0.01 and 0.3 s. The standard error terms at long periods are reduced slightly from the values indicated in Table 5.1.

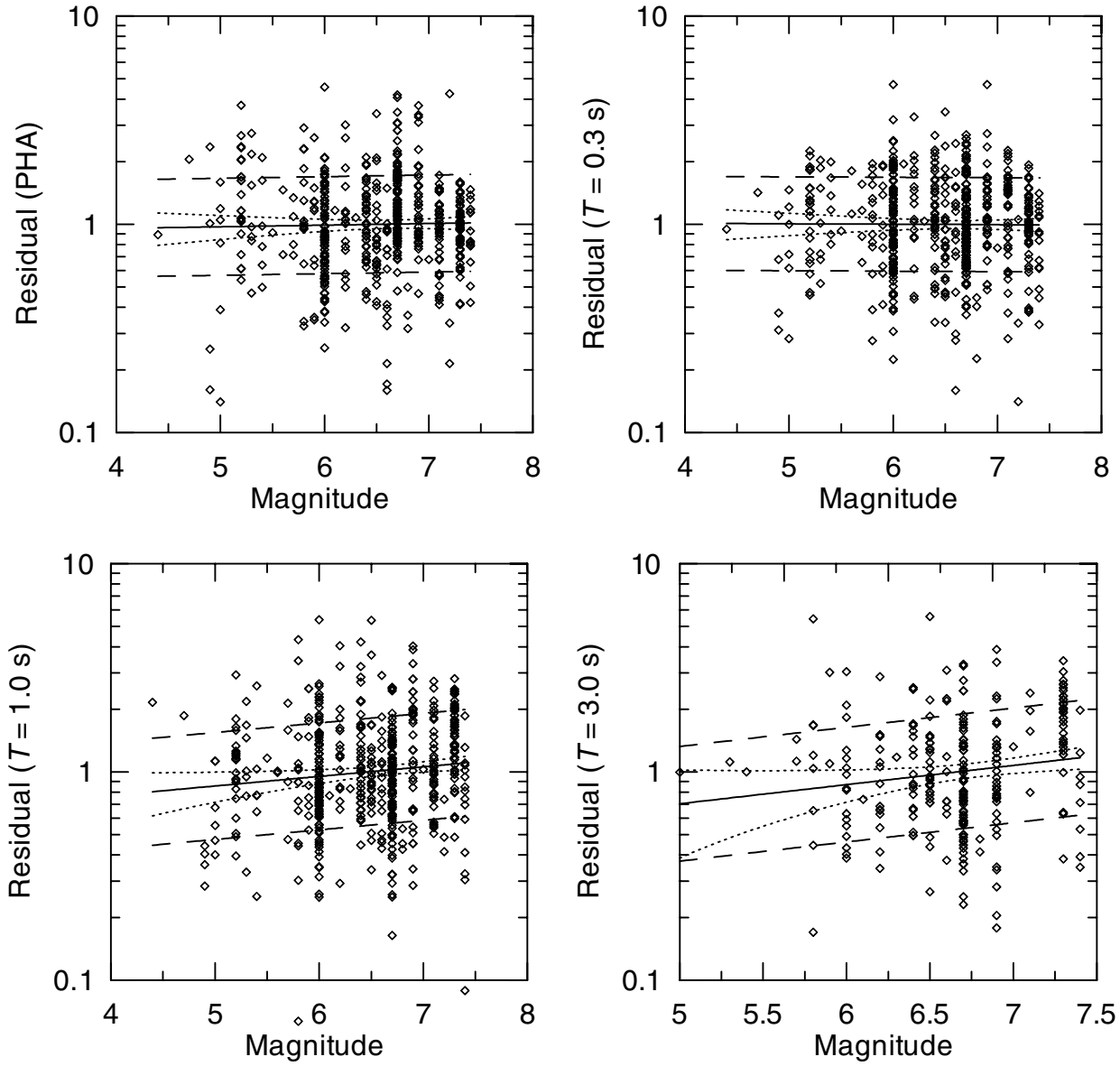

Fig. 5.8. Variation with magnitude of spectral acceleration residuals calculated using amplification-adjusted reference motions. Data are for Holocene soil sites.

Table 5.6. Regression coefficients for magnitude-dependence of residual for amplification of T=3 s S_a and F_v

Geology	Period	e	f	σ
Holocene	3	-1.41 ± 1.19	0.21 ± 0.18	0.63
	Fv	-0.77 ± 0.45	0.12 ± 0.07	0.49
Pleistocene	3	-0.61 ± 1.82	0.09 ± 0.28	0.50
	Fv	-0.02 ± 0.80	0.00 ± 0.13	0.50
Tertiary	3	-1.78 ± 1.98	0.27 ± 0.30	0.45
	Fv	-0.55 ± 0.87	0.09 ± 0.14	0.58
Mesozoic	3	-1.28 ± 3.75	0.19 ± 0.56	0.66
	Fv	-1.39 ± 1.63	0.22 ± 0.25	0.72
Hol. - alluvium	3	-1.37 ± 1.51	0.21 ± 0.23	0.67
	Fv	-1.26 ± 0.59	0.20 ± 0.09	0.48
Hol. - Lac/marine	3	-6.00 ± 4.96	0.91 ± 0.75	0.43
	Fv	-1.28 ± 1.10	0.21 ± 0.18	0.41
Pleist. - alluvium	3	-0.79 ± 2.47	0.12 ± 0.37	0.55
	Fv	0.70 ± 1.43	-0.11 ± 0.22	0.59
Quat. - alluvium	3	-1.26 ± 1.28	0.19 ± 0.19	0.64
	Fv	-0.93 ± 0.56	0.14 ± 0.09	0.51
Hol. - coarse	3	-2.14 ± 2.32	0.31 ± 0.34	0.62
	Fv	-0.66 ± 0.93	0.10 ± 0.14	0.48
Hol. - mixed	3	-0.85 ± 2.22	0.13 ± 0.34	0.56
	Fv	-0.47 ± 1.01	0.08 ± 0.16	0.48
Pleist. - coarse	3	-2.88 ± 5.67	0.44 ± 0.87	0.42
	Fv	0.62 ± 2.32	-0.10 ± 0.36	0.41
Pleist. - mixed	3	1.50 ± 2.92	-0.23 ± 0.46	0.46
	Fv	1.67 ± 1.76	-0.27 ± 0.28	0.40
NEHRP - C	3	-0.71 ± 3.19	0.11 ± 0.48	0.76
	Fv	1.76 ± 1.33	-0.27 ± 0.20	0.66
NEHRP - D	3	-1.46 ± 1.67	0.22 ± 0.25	0.56
	Fv	0.01 ± 0.60	0.00 ± 0.09	0.46
Geotech. - B	3	1.69 ± 6.84	-0.25 ± 1.02	0.62
	Fv	0.12 ± 2.53	-0.02 ± 0.38	0.70
Geotech. - C	3	-2.60 ± 3.47	0.39 ± 0.52	0.68
	Fv	0.96 ± 1.18	-0.15 ± 0.18	0.62
Geotech. - D	3	-1.01 ± 1.65	0.15 ± 0.25	0.58
	Fv	0.06 ± 0.68	-0.01 ± 0.11	0.47
Geotech. - E	3	-4.25 ± 6.38	0.64 ± 0.96	0.41
	Fv	-2.62 ± 2.70	0.40 ± 0.41	0.31

6 Discussion

6.1 COMPARISON OF CLASSIFICATION SCHEMES

One of the objectives of this research was to quantify the ability of different classification schemes to capture site-to-site variations of spectral acceleration. Five classification schemes were considered, three of which are based on surface geology, one on near-surface shear wave velocity ($V_{s\text{-}30}$), and one on geotechnical data. One measure of the quality of a classification scheme is inter-category, or scheme, median residuals (R) and standard errors (σ_R), which are calculated as follows:

$$R = \frac{1}{M}\sum_{i=1}^{M} R_i \tag{6.1a}$$

$$\sigma_R = \sqrt{\frac{\sum_{i=1}^{M}\sum_{j=1}^{N_i}\left(R_{ij} - R_i\right)^2}{\left(\sum_{i=1}^{M} N_i\right) - N_{dof}}} \tag{6.1b}$$

where M = the number of categories in scheme i and N_{dof} = total number of degrees-of-freedom in regression equations for the scheme ($2 \times$ M) (other terms were defined in Section 4.2). All median residuals (R) are zero. Inter-category standard error σ_R represents the average dispersion of data within all categories belonging to a given scheme.

Inter-category standard error terms for the soil and rock categories are plotted as a function of period in Figures 6.1a and 6.1b, respectively. The error terms for T=3 s spectral acceleration apply for non-magnitude corrected amplification factors. The error terms for the geotechnical scheme are those without a $V_{s\text{-}30}$ adjustment. Error terms based on $V_{s\text{-}30}$ classifications are shown for the NEHRP categories, and newly-defined categories with velocity boundaries adjusted to be more correlated with geologic age (as discussed in Section 5.3).

For soil sites (Figure 6.1a), the largest error terms at all periods except $T = 3.0$ s are obtained from the V_{s-30} -based and geotechnical classification schemes. The smallest error terms are from detailed geology schemes such as age + depositional environment or age + material texture. Maximum differences in the category dispersion values are as large as 0.1 in natural logarithmic units, which is a significant variation. Also shown for reference are the error terms from the Abrahamson and Silva (1997) attenuation relationship. Note that these error terms are strongly magnitude dependent, an effect not observed in this study (see Figure 5.2).

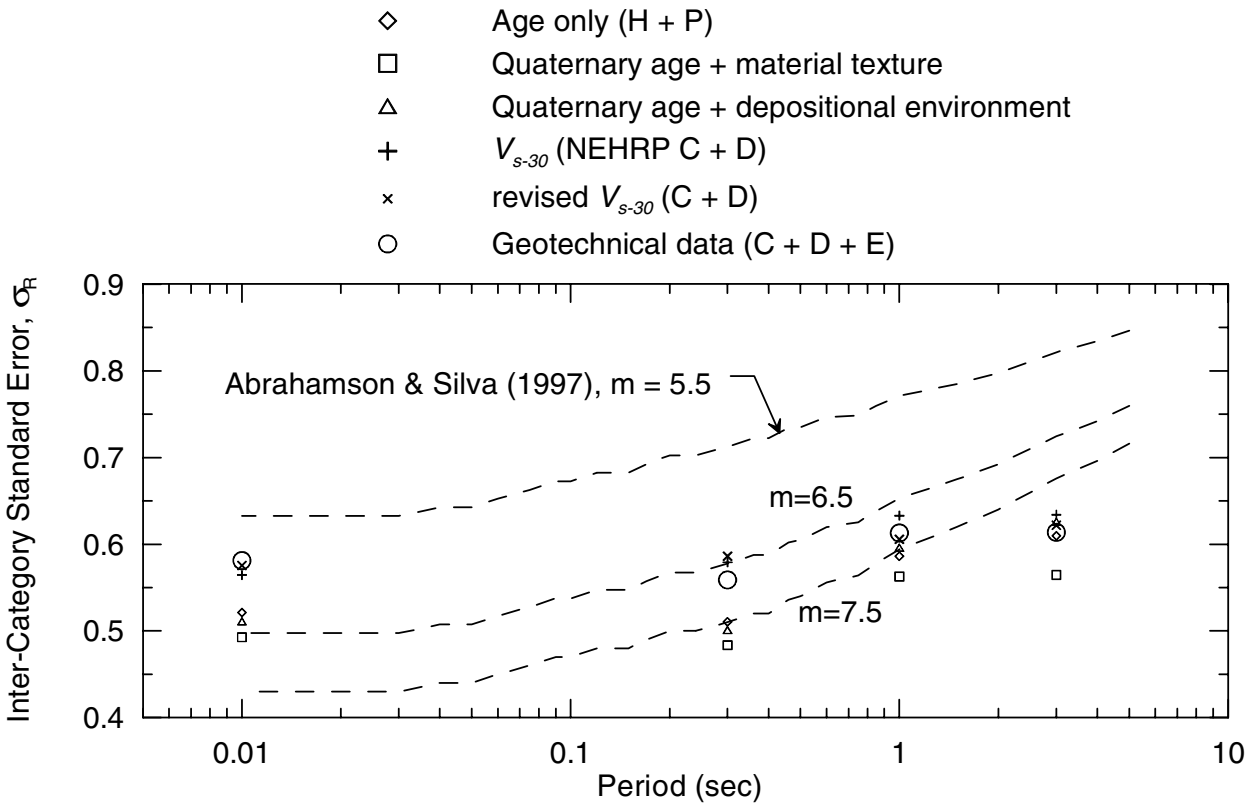

Fig. 6.1(a). Inter-category standard error terms for spectral acceleration (this study) and error terms derived by Abrahamson and Silva (1997). Results apply for categories within the respective schemes associated with poorly consolidated sediments (soil).

For rock sites (Figure 6.1b), the error terms are generally minimized at intermediate to long period for the geology scheme (which is age-only for rock) and at short period for the V_{s-30} -based schemes. The rock error terms for all schemes are larger than those for soil. Detailed information on the geology of rock sites (i.e., information beyond age such as fracture spacing or degree of weathering) is not available on most geologic maps. Incorporation of such information into site classification schemes might reduce intra-category dispersion for rock categories.

As shown in Figures 6.1a-b, the inter-category error terms for the two $V_{s\text{-}30}$ –based schemes are not significantly different for soil sites. For rock sites, the revised B-C boundary produces slightly smaller error terms. For this reason, adjustment of the NEHRP B-C boundary may be advisable.

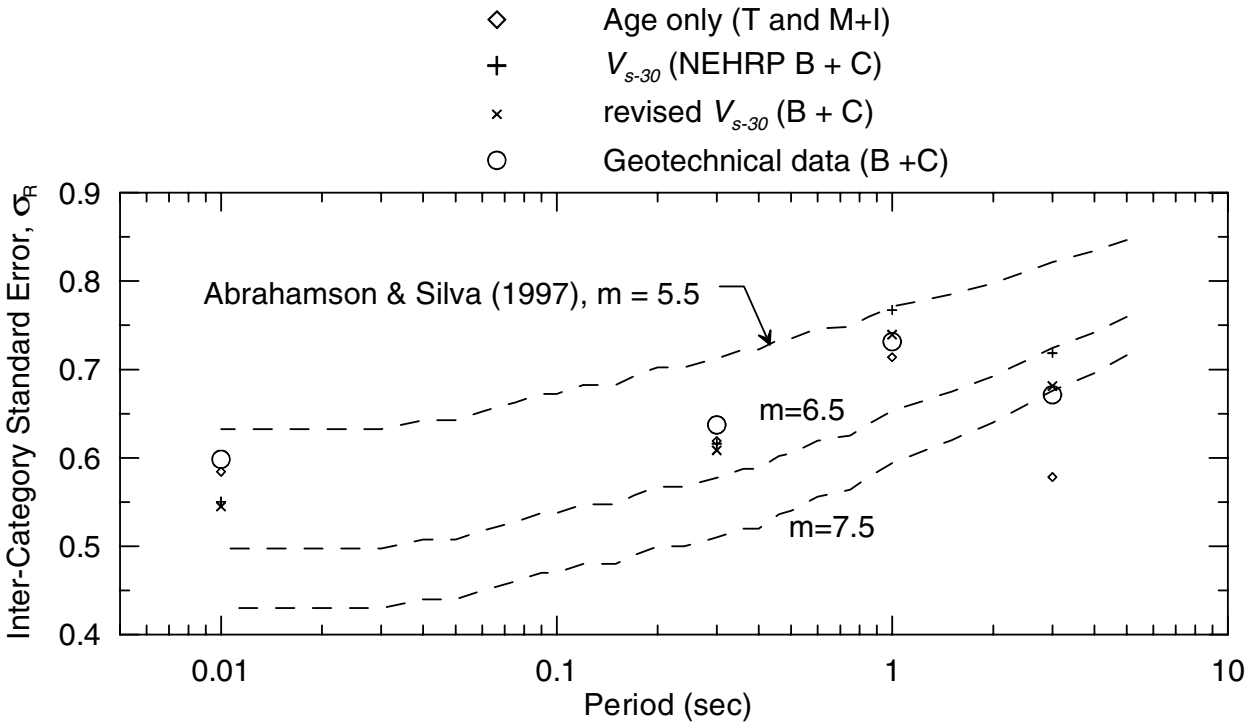

Fig. 6.1(b). Inter-category standard error terms for spectral acceleration (this study) and error terms derived by Abrahamson and Silva (1997). Results apply for categories within the respective schemes associated with rock conditions.

The data used to compile the inter-category error terms in Figures 6.1(a)–(b) include motions from all classified sites. These data sets are inconsistent to the extent that the various schemes have different numbers of classified sites. Accordingly, we compiled a list of 109 sites (with 187 recordings) for which classifications are available by all five of the categorization schemes considered herein. Using this data set, inter-category error terms for the soil and rock categories are compared in Figures 6.1(c)–(d). The general trends in the error terms from this reduced data set are similar to those for the full data set (Figures 6.1a–b). Detailed surface geology schemes minimize inter-category error for soil. NEHRP minimizes inter-category error for rock at small period ($T \leq 0.3$ s) and age-only geology is more effective at longer periods.

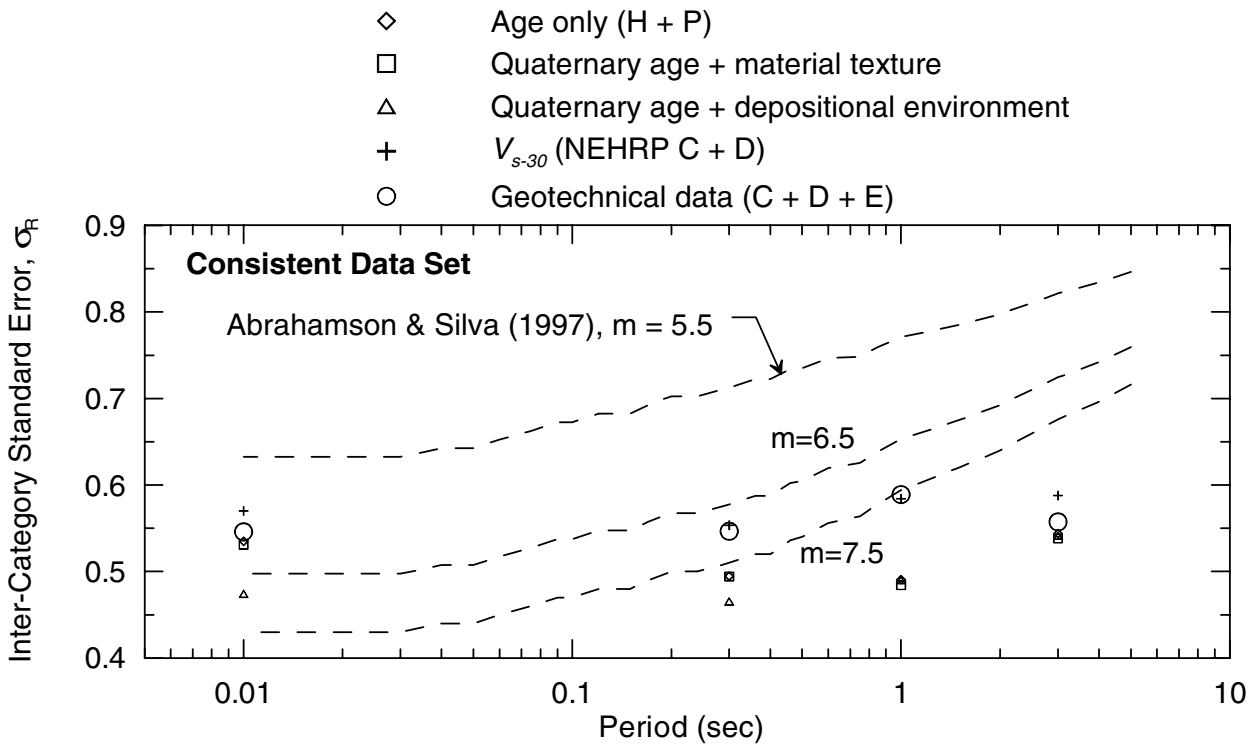

Fig. 6.1(c). Inter-category standard error terms derived using consistent data set, categories associated with soil conditions

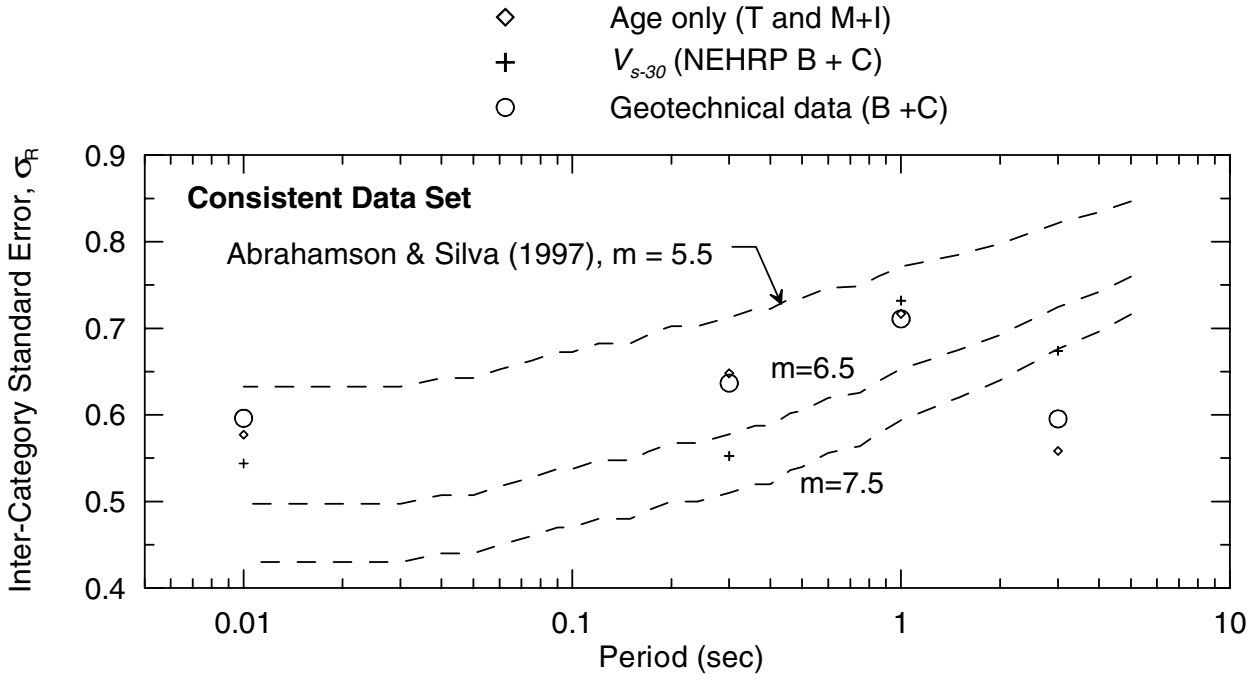

Fig. 6.1(d). Inter-category standard error terms derived using consistent data set, categories associated with rock conditions

6.2 COMPARISON TO PREVIOUS STUDIES

It is of interest to compare the results of this study to the findings of previous research. In the following sections we compare our results for amplification of spectral acceleration to those from previous empirical work (Section 6.2.1) and analytical work (6.2.2).

6.2.1 Empirical Studies

Several previous studies have developed amplification factors suitable for comparison to the results of this study. In Figure 6.2(a) we compare our results for Quaternary alluvium to those of Steidl (2000) for Quaternary sediments in the southern California region. In Figure 6.2(b), we compare our results for NEHRP D sites to those of Borcherdt (2001), which were derived using data from the 1994 Northridge earthquake for NEHRP D sites. We find our amplification factors to be similar to those of Steidl for the Q (all Quaternary) and Qy (young Quaternary) categories, but to show lower amplification levels and less variation with rock PHA than was found by Borcherdt.

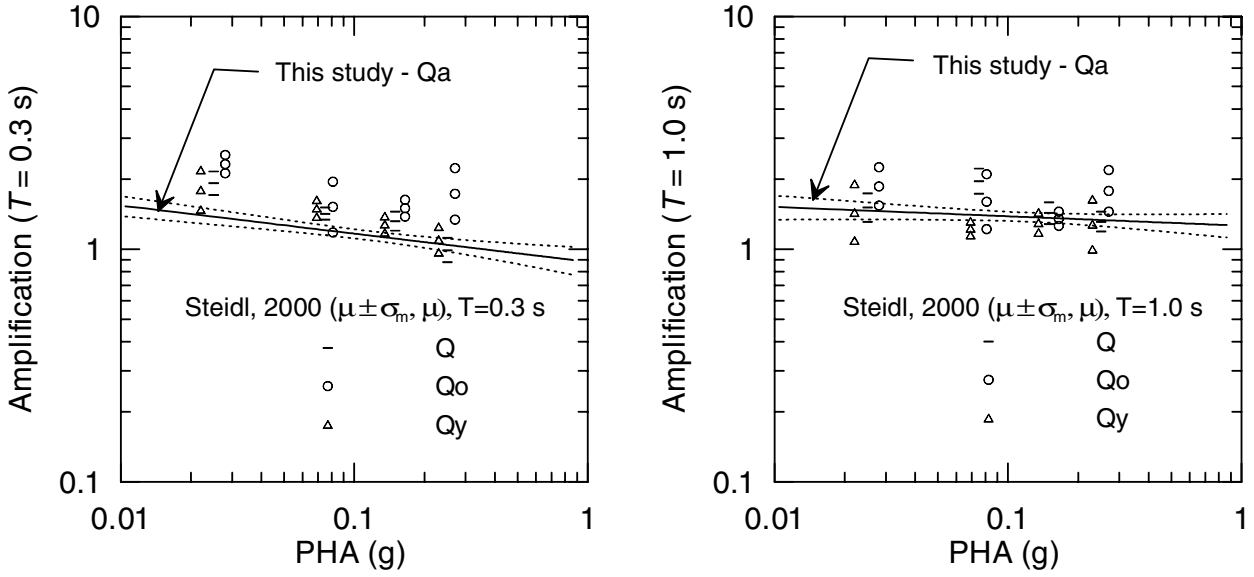

Fig. 6.2(a). Comparison of results from this study and Steidl (2000) for Quaternary alluvium. For Steidl results, symbol μ denotes median, symbol σ_m denotes standard error of the median.

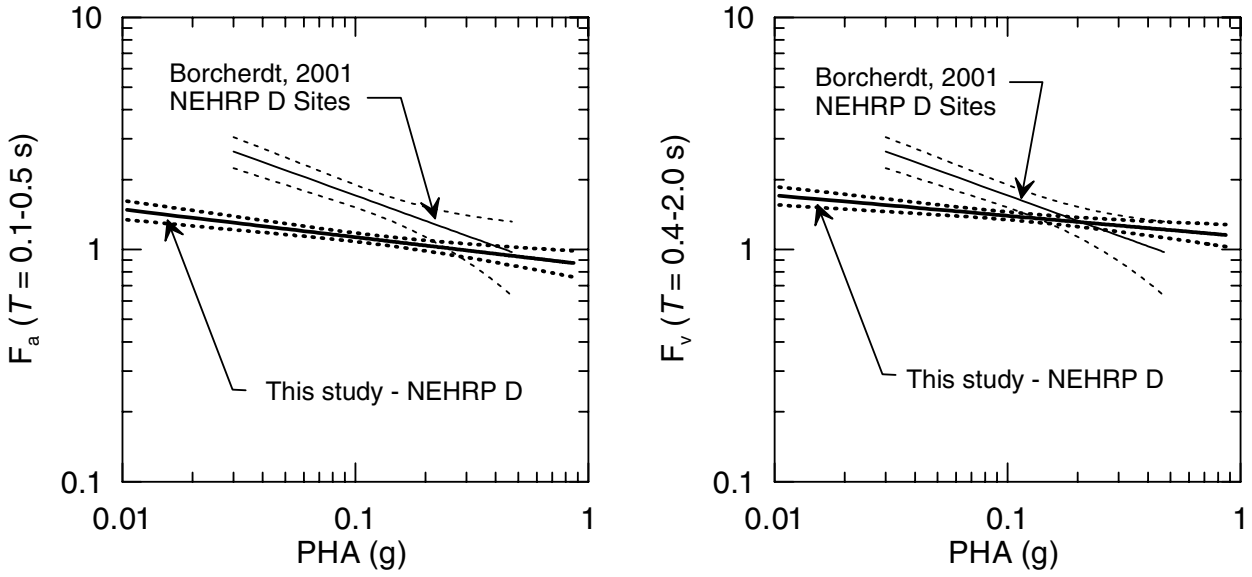

Fig. 6.2(b). Comparison of results from this study and Borcherdt (2001) for NEHRP D sites

Figure 6.3(a) compares our results to those of Steidl (2000) for Tertiary sites. Figure 6.3(b) compares our results to those of Borcherdt (2001) for NEHRP C sites. Our results indicate similar levels of amplification, although a lower degrees of low-period nonlinearity, to those of Steidl. As before, our results show lower amplification levels and less variation with rock PHA than was found by Borcherdt.

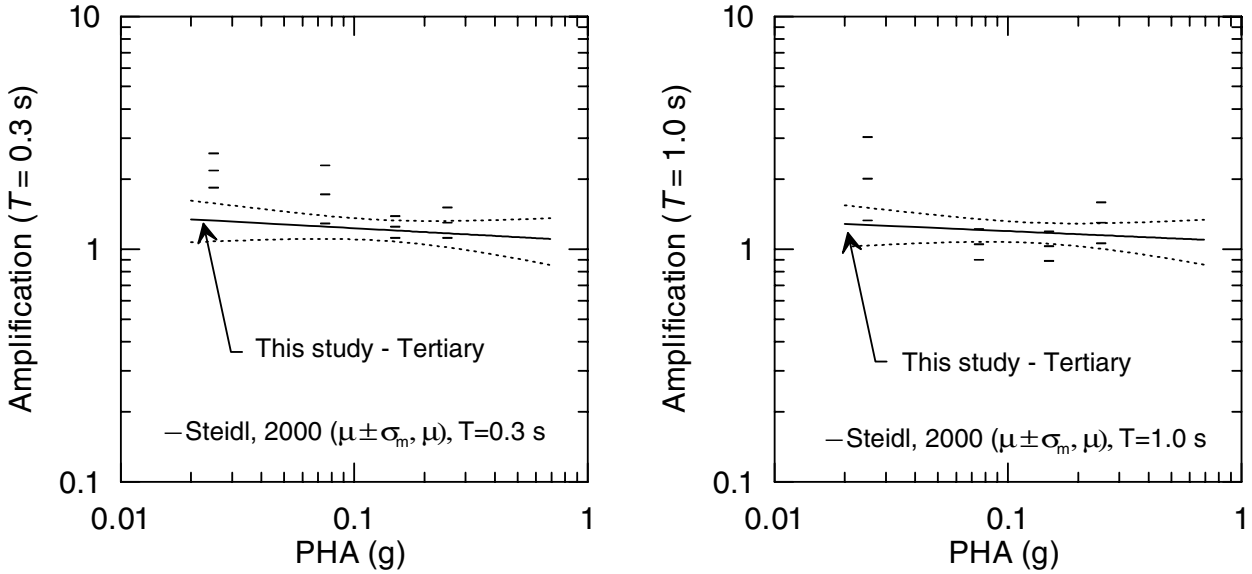

Fig. 6.3(a). Comparison of results from this study and Steidl (2000) for Tertiary sediments

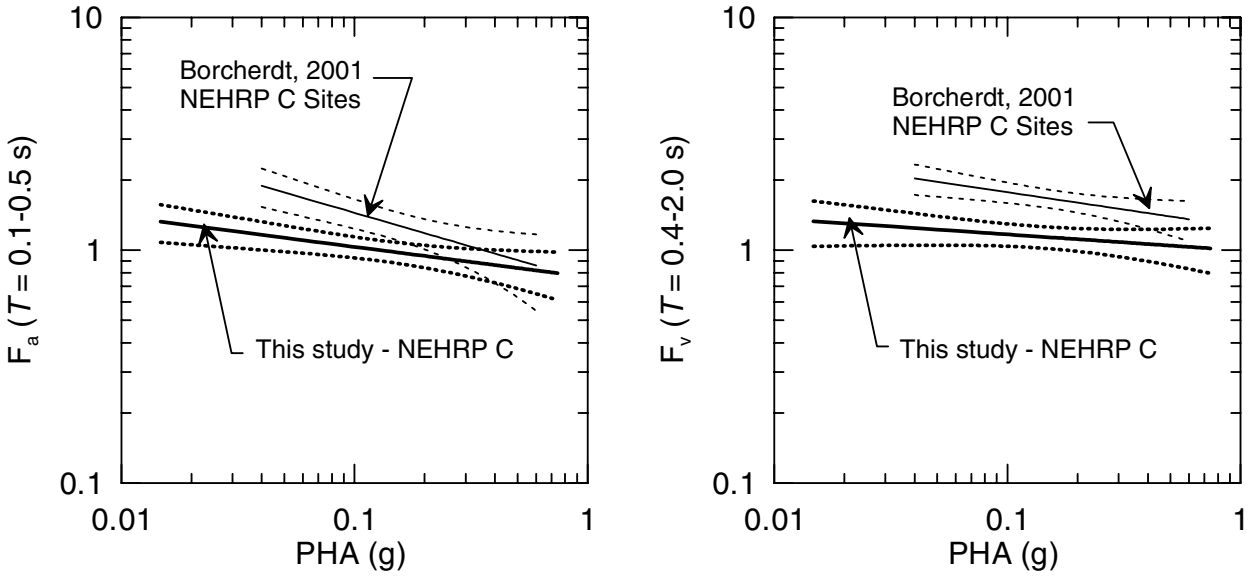

Fig. 6.3(b). Comparison of results from this study and Borcherdt (2001) for NEHRP C sites

We compare in Figure 6.3(c) our results for Mesozoic materials to those of Steidl, and find comparable overall amplification levels and degrees of apparent nonlinearity. As noted previously, nonlinearity in the response of Mesozoic materials is not statistically significant because of the weak trend in the data relative to the large data scatter.

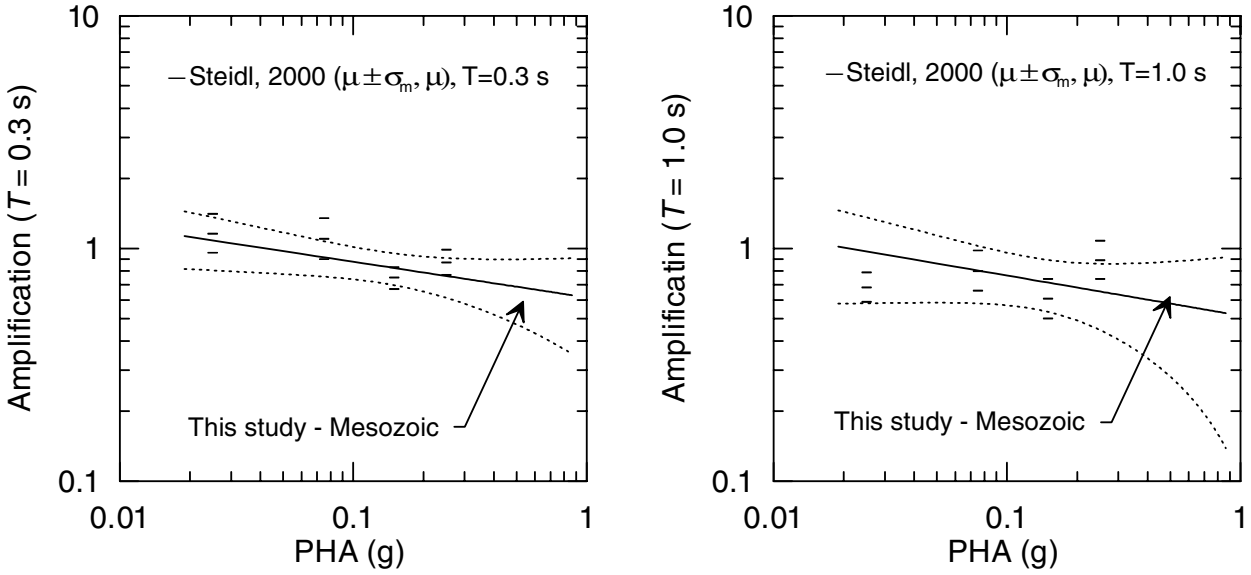

Fig. 6.3(c). Comparison of results from this study and Steidl (2000) for Mesozoic and Igneous geology

Another existing source of amplification factors is the site term in the Abrahamson and Silva, 1997 (A&S) attenuation relationship. The form of this term was given in Eq. 4.3(b). Regression coefficients for Eq. 4.3(b) were derived by A&S using all "soil" sites, which generally include Holocene and Pleistocene sediments. In Figure 6.4 we compare this site term to the data for Quaternary alluvial sediments (Qa) and Holocene lacustrine/marine sediments (Hlm). For Qa, low-period amplification levels are similar to the A&S site term. At longer periods (e.g., T = 3.0 s), A&S predicts increases in amplification with PHA, an effect not observed in the data trend. The A&S site term at long periods and high PHA therefore appears to be biased high. For Hlm, our results indicate for T = 0.01 s larger low-period amplification levels and rock PHA-dependence than the A&S site term. Differences at longer periods are much smaller.

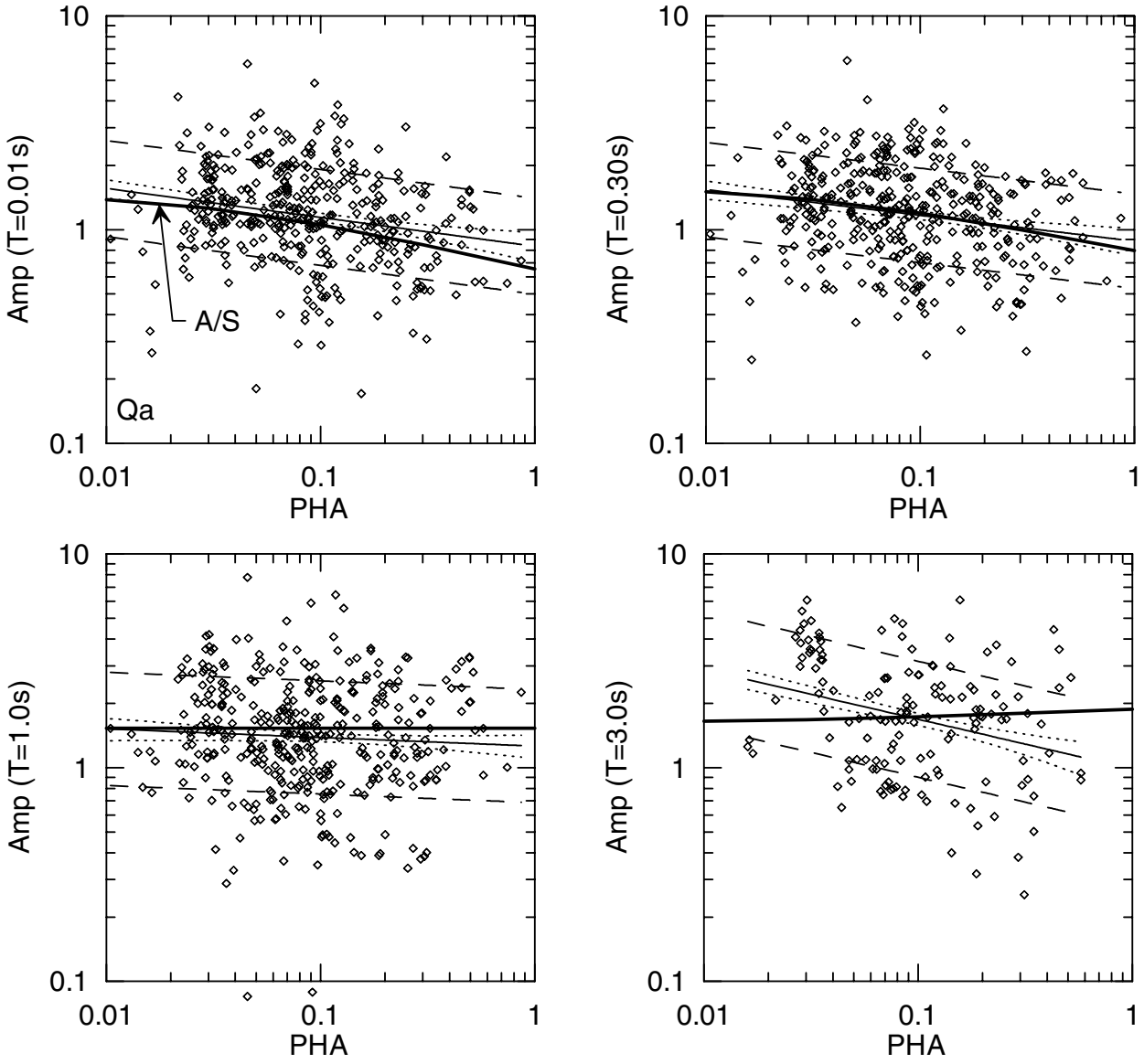

Fig. 6.4(a). Comparison of results for Quaternary alluvium (this study) with site term in Abrahamson and Silva (1997) attenuation relationship

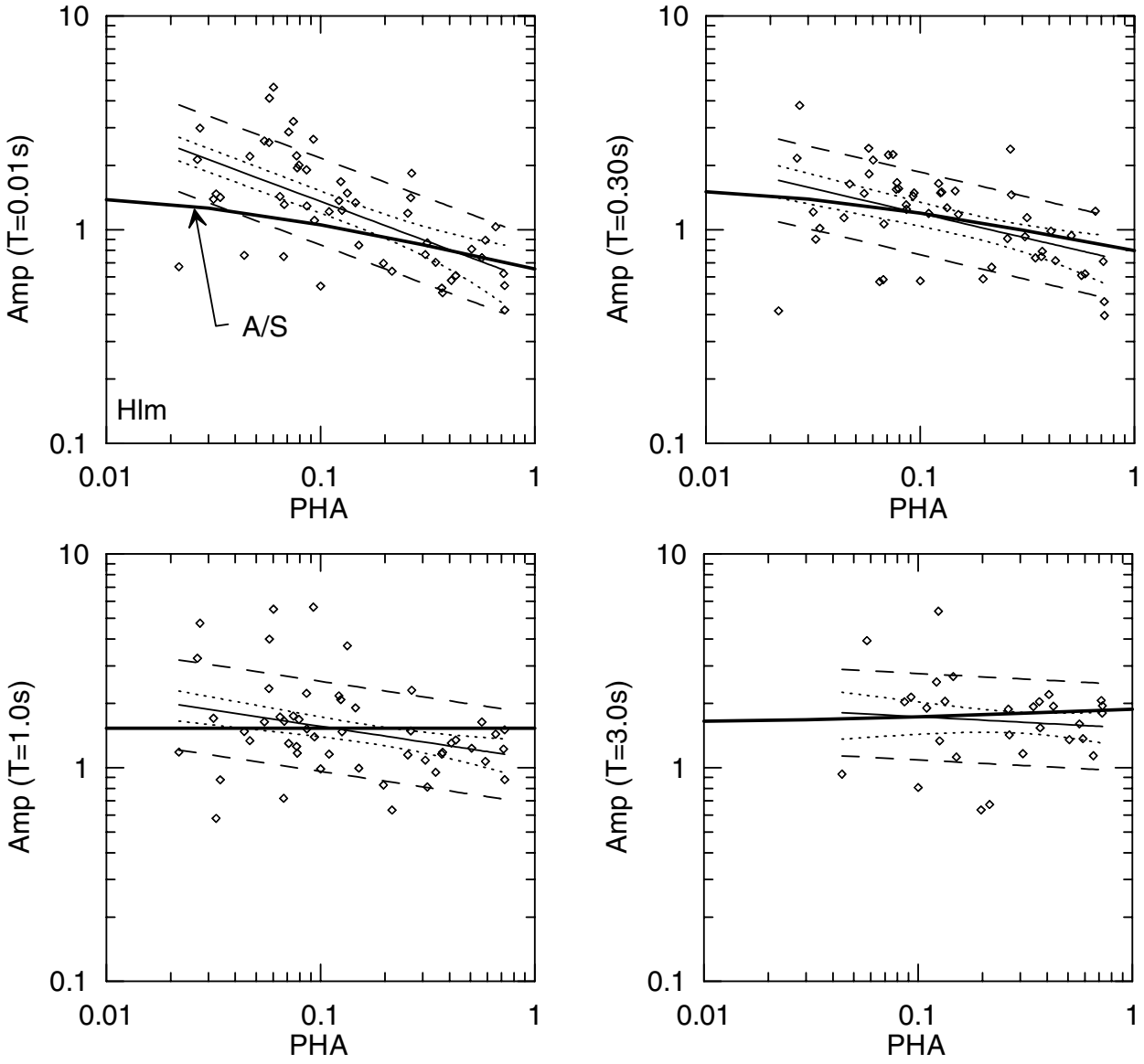

Fig 6.4(b). Comparison of results for Holocene lacustrine/marine sediments (this study) with site term in Abrahamson and Silva (1997) attenuation relationship

6.2.2 Analytical Studies

Equivalent-linear ground response analyses have been extensively used to estimate amplification factors F_a and F_v for use in seismic design codes. The F_a and F_v factors in the NEHRP provisions for new buildings (BSSC, 2000) are empirically based up to PHA ≈ 0.1g (from Borcherdt, 1994), and are based on ground response analysis results at stronger levels of shaking (Dobry et al., 2000). In Figure 6.5 we compare the results of this study for the $V_{s\text{-}30}$ classification scheme to the NEHRP amplification factors. Our amplification levels are generally smaller than those given in the code provisions. This can be attributed to the use of a rock-average reference site condition (corresponding approximately to soft rock) in the derivation of reference ground motions for this study, as compared to a relatively competent reference rock condition that applies for the code-based amplification factors. Ground motion amplitude on soft rock is generally larger than on firm rock, therefore producing smaller amplification factors. The PHA-dependence of our factors and the NEHRP factors are comparable for the F_a parameter in Class C. For both parameters in Class D and the F_v parameter in Class C, the NEHRP factors have larger nonlinearity than our factors.

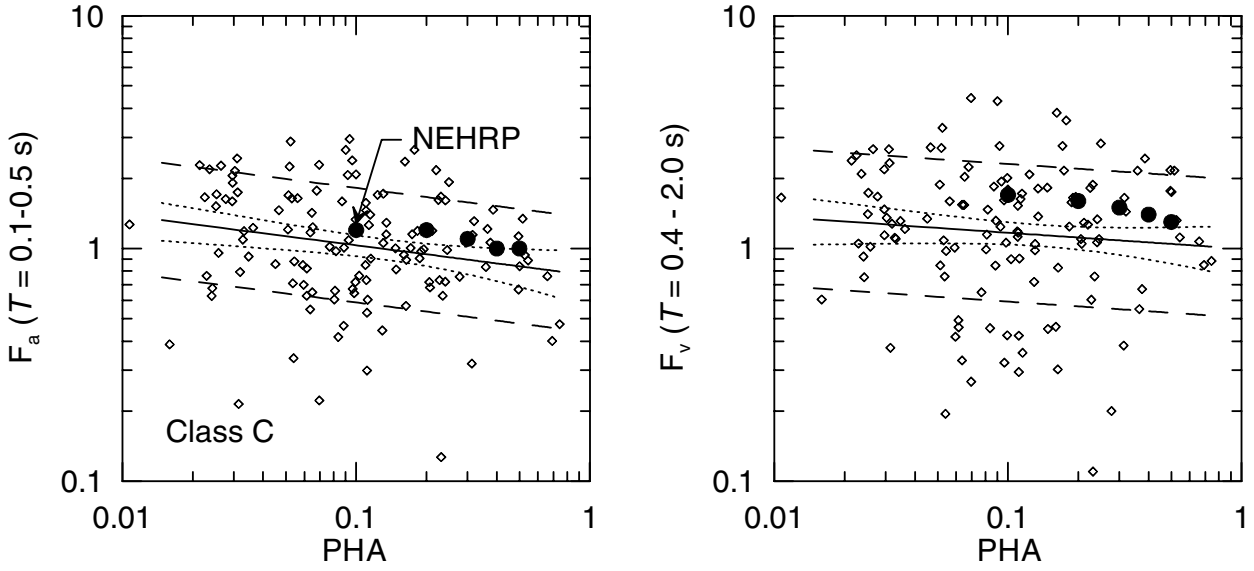

Fig. 6.5(a). Comparison of results for NEHRP Class C soils (this study) with site factors in NEHRP provisions (BSSC, 2000)

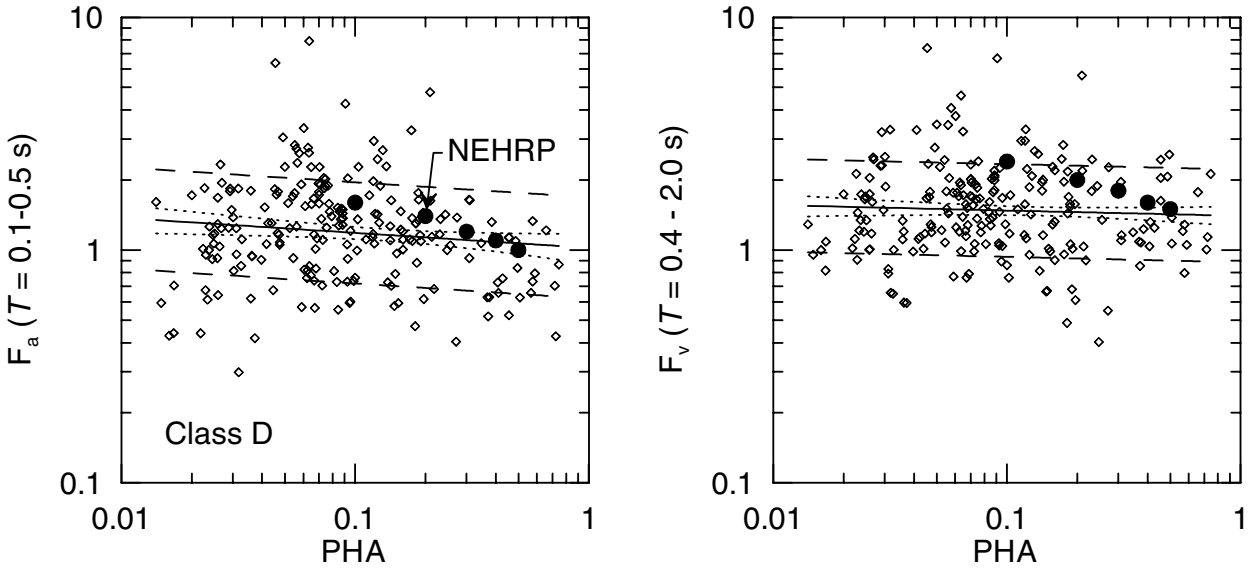

Fig. 6.5(b). Comparison of results for NEHRP Class D soils (this study) with site factors in NEHRP provisions (BSSC, 2000)

Silva et al. (1999) developed amplification factors for the San Francisco Bay (SFB) and Los Angeles (LA) areas as a function of surface geology, depth to basement (defined as V_s = 1 km/s), and control motion amplitude. Amplification is defined relative to Franciscan rock in SFB and granite in LA, both being Mesozoic in age. The amplification factors were developed using randomized ground conditions (velocity profiles, modulus reduction, and damping curves, etc.) and hence incorporate significant parametric uncertainty. Shown in Figure 6.6 are results by Silva for the San Francisco Bay region vs. results of this study. Comparisons are made within comparable geology categories [i.e., Silva Bay Mud is compared to Hlm; Silva Quaternary materials (Qa/QT) are compared to Qa; direct Tertiary comparison]. The empirical amplification factors from this study are smaller than the calculated factors by Silva et al., with the exception of F_a for the Hlm category. The deviation is likely a result of the different reference rock conditions. The PHA-dependence of the amplification factors are similar, with the exception of Silva's F_a factors for Bay Mud, which have much higher PHA-dependence than our results for Hlm.

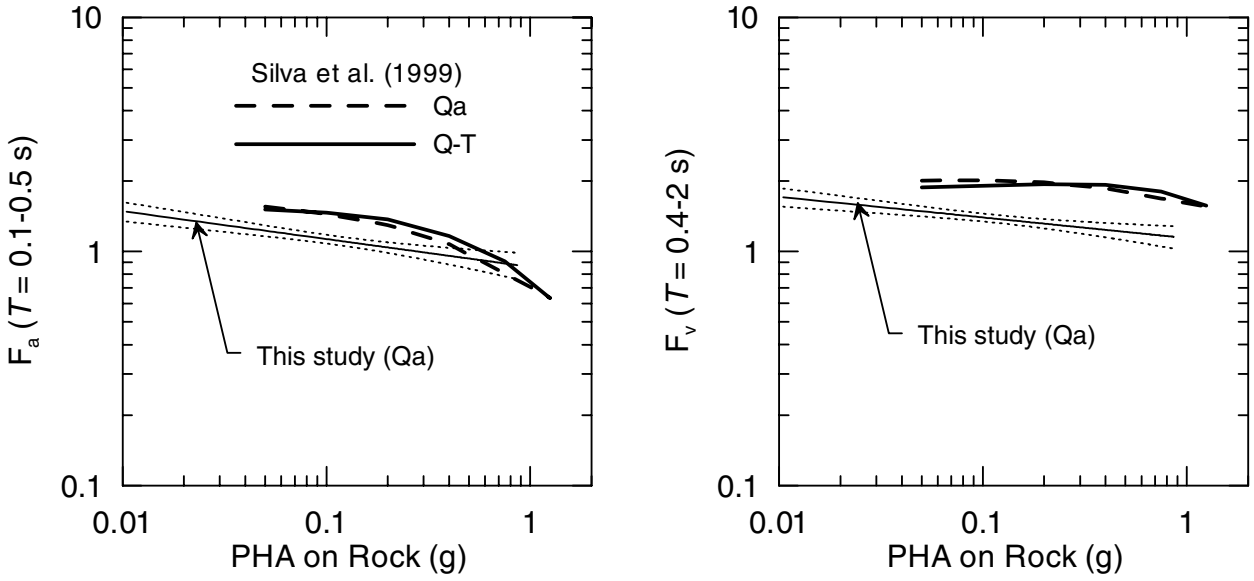

Fig. 6.6(a). Comparison of results for Quaternary alluvial sediments (this study) with analytical results by Silva et al. (1999) for San Francisco Bay Area Quaternary sediments

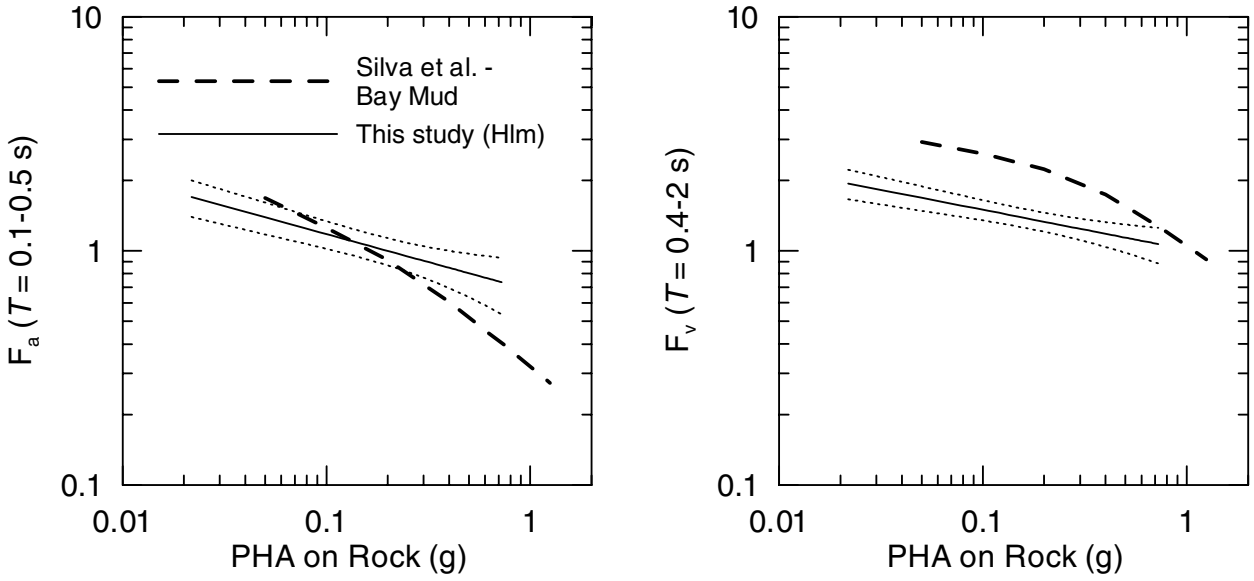

Fig. 6.6(b). Comparison of results for Holocene lacustrine/marine sediments (this study) with analytical results by Silva et al. (1999) for San Francisco Bay Mud

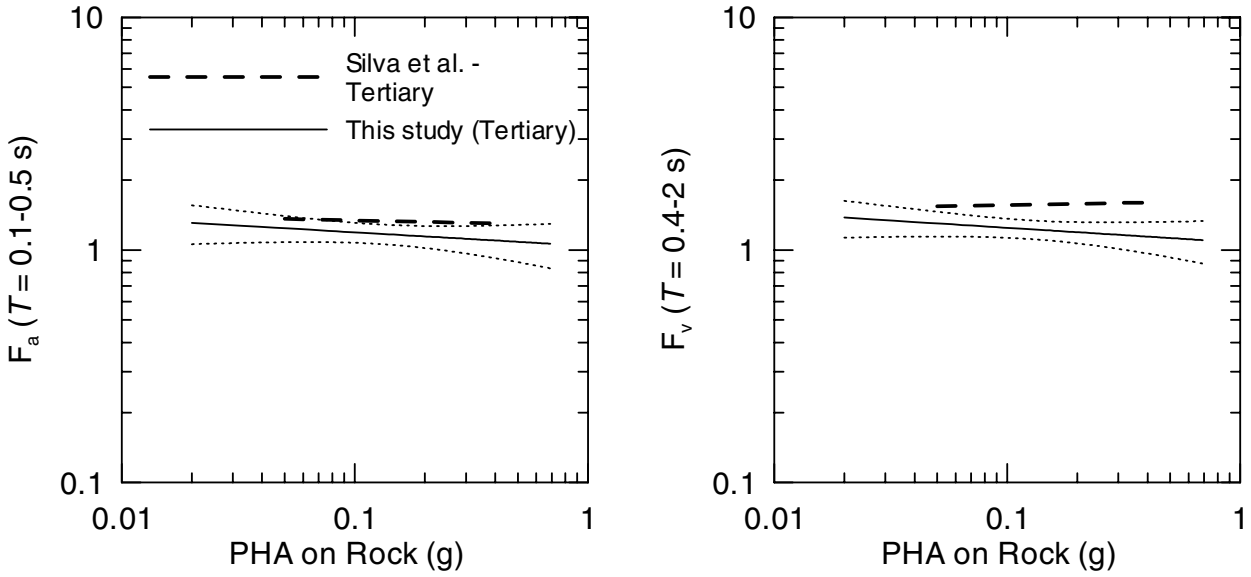

Fig 6.6(c). Comparison of results for Tertiary sediments (this study) with analytical results by Silva et al. (1999) for Tertiary

Figure 6.7 compares recommended PHA amplification factors for soft soil sites by Idriss (1990) to PHA amplification factors for the Hlm category. The amplification factors by Idriss were derived from a combination of observation and equivalent-linear ground response analysis. Median amplification factors from this study are near the lower bound of the "Loma Prieta" and "Mexico City" bands given by Idriss, and are below Idriss's recommended relation (labeled as "Idriss, 1990" in Figure 6.7). There are two possible explanations for this. First, some sites in the Hlm category are not "soft soil," and hence would be expected to produce smaller amplification levels. Second, Idriss's site factors are based on reference recordings from sites with more competent bedrock than the rock-average condition used in this study.

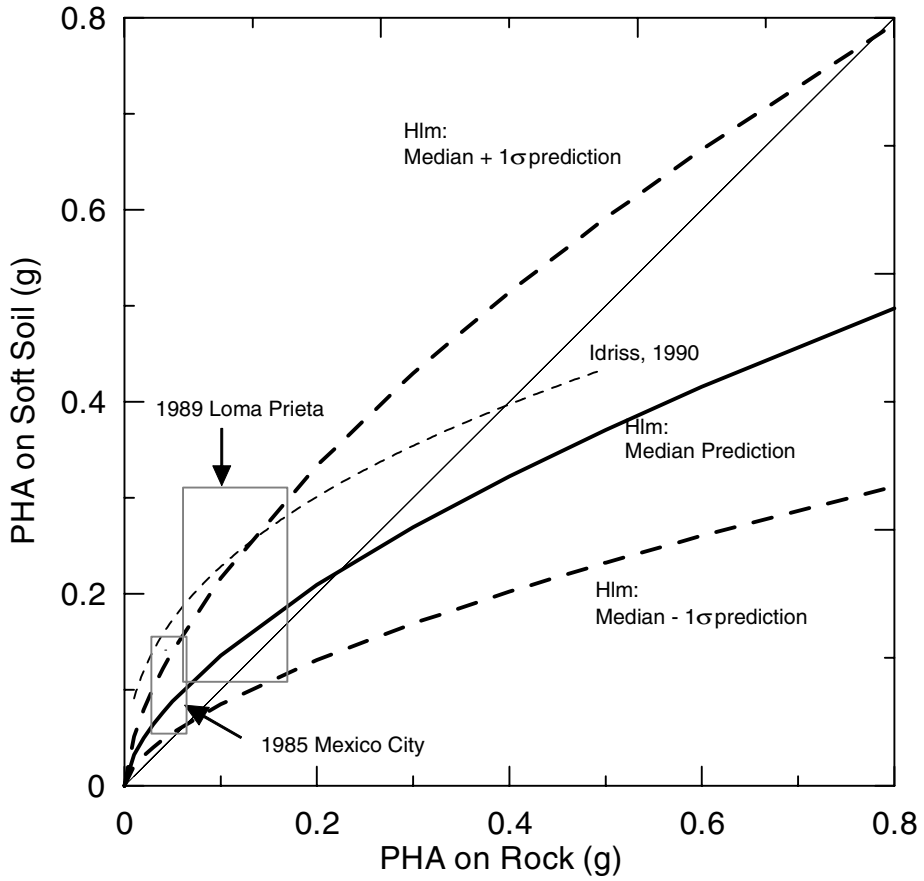

Fig 6.7. Comparison of regression results for Holocene lacustrine/marine sediments to findings of Idriss (1990) for soft clay sites

6.3 COMPARISON TO PRELIMINARY DATA FROM 1999 CHI-CHI (TAIWAN) EARTHQUAKE

The 1999 Chi-Chi (Taiwan) earthquake provided a large number of strong motion recordings that were not included in the regression analyses discussed previously. Preliminary geologic classifications of these data have been compiled by Lee et al. (2001), and subdivide the sites according to the following classification scheme:

- B: Pliocene and older, igneous, and metamorphic, and limestone
- C: Pliocene and Pleistocene, conglomerate, pyroclastic rocks, geomorphologic lateritic terraces
- D: Late Pleistocene and Holocene strata, geomorphologic fluvial terraces, stiff clays and sandy soils with standard penetration test blow count, $N > 17$ in upper 30 m
- E: Holocene and fills, $N < 17$ in upper 30 m

Amplification factors were computed for the stations in these categories, and the results are compared in Figure 6.8 to median amplification factors derived in this study. The amplification factors shown in Figure 6.8 were calculated using an event term that is the median residual of the Abrahamson and Silva (1997) attenuation relation. Comparisons of the Taiwan data to the results of this study are made as follows: B — Mesozoic, C — Tertiary, D — Quaternary alluvium, E — Holocene lacustrine/marine.

The results indicate significant positive bias for large rock PHAs and long periods for each site category. Results are generally more satisfactory at lower rock PHAs and periods.

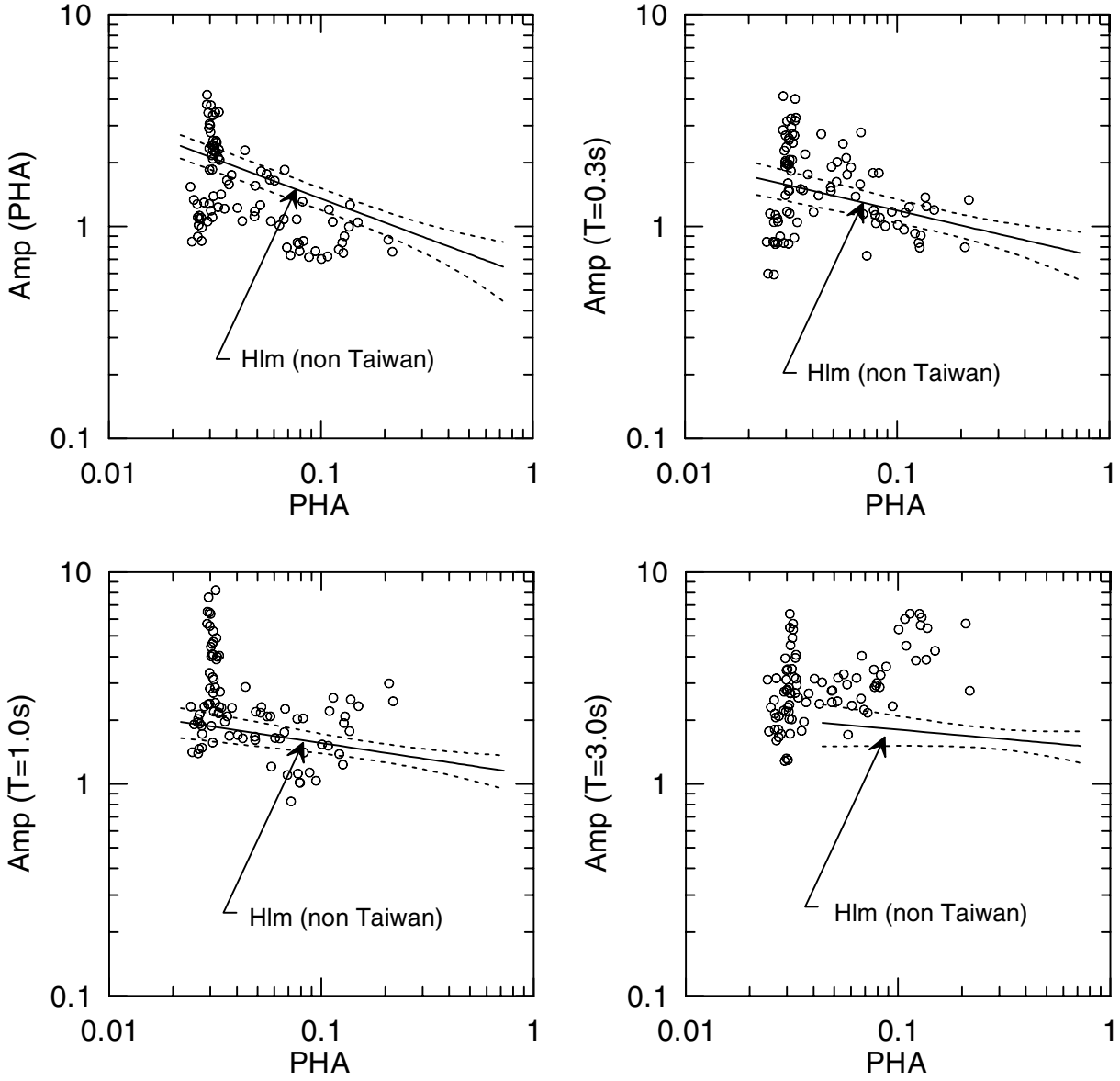

Fig. 6.8(a). Comparison of Chi-Chi, Taiwan, data for 'E' sites to regression results for Holocene lacustrine/marine sediments (Hlm) from this study

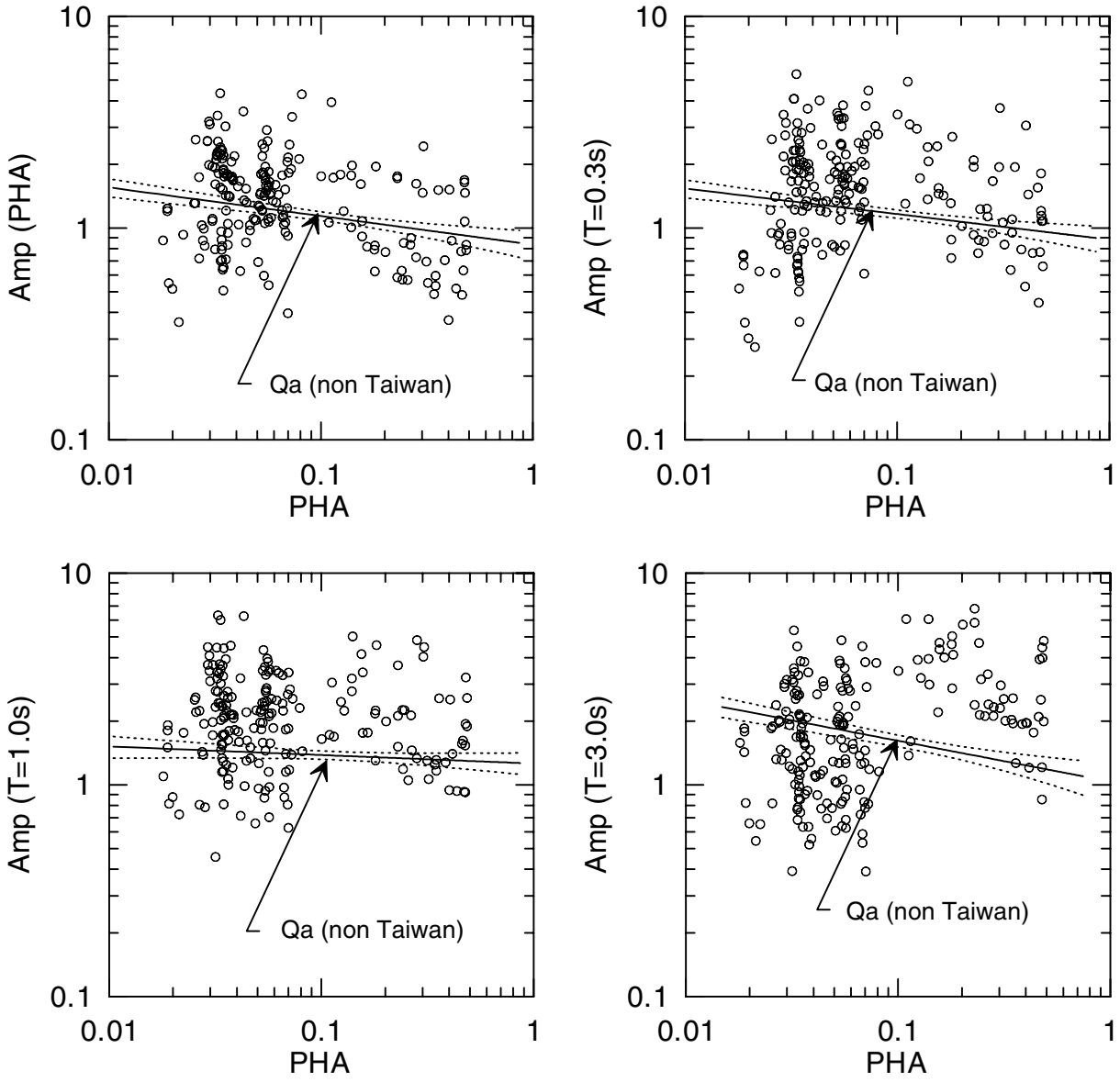

Fig. 6.8(b). Comparison of Chi-Chi, Taiwan, data for 'D' sites to regression results for Quaternary alluvium (Qa) sites from this study

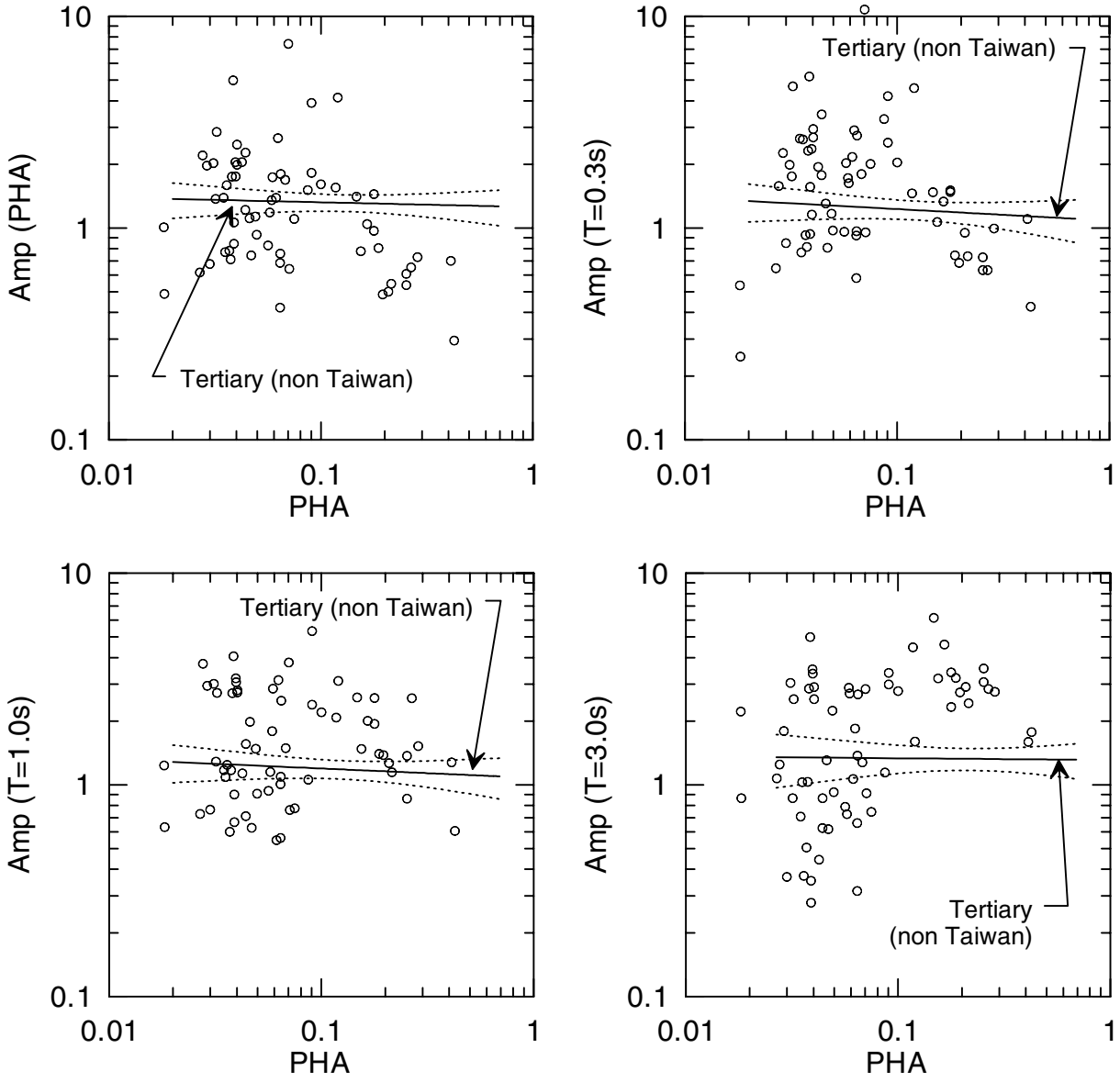

Fig. 6.8(c). Comparison of Chi-Chi, Taiwan, data for 'C' sites to Tertiary regression results from this study

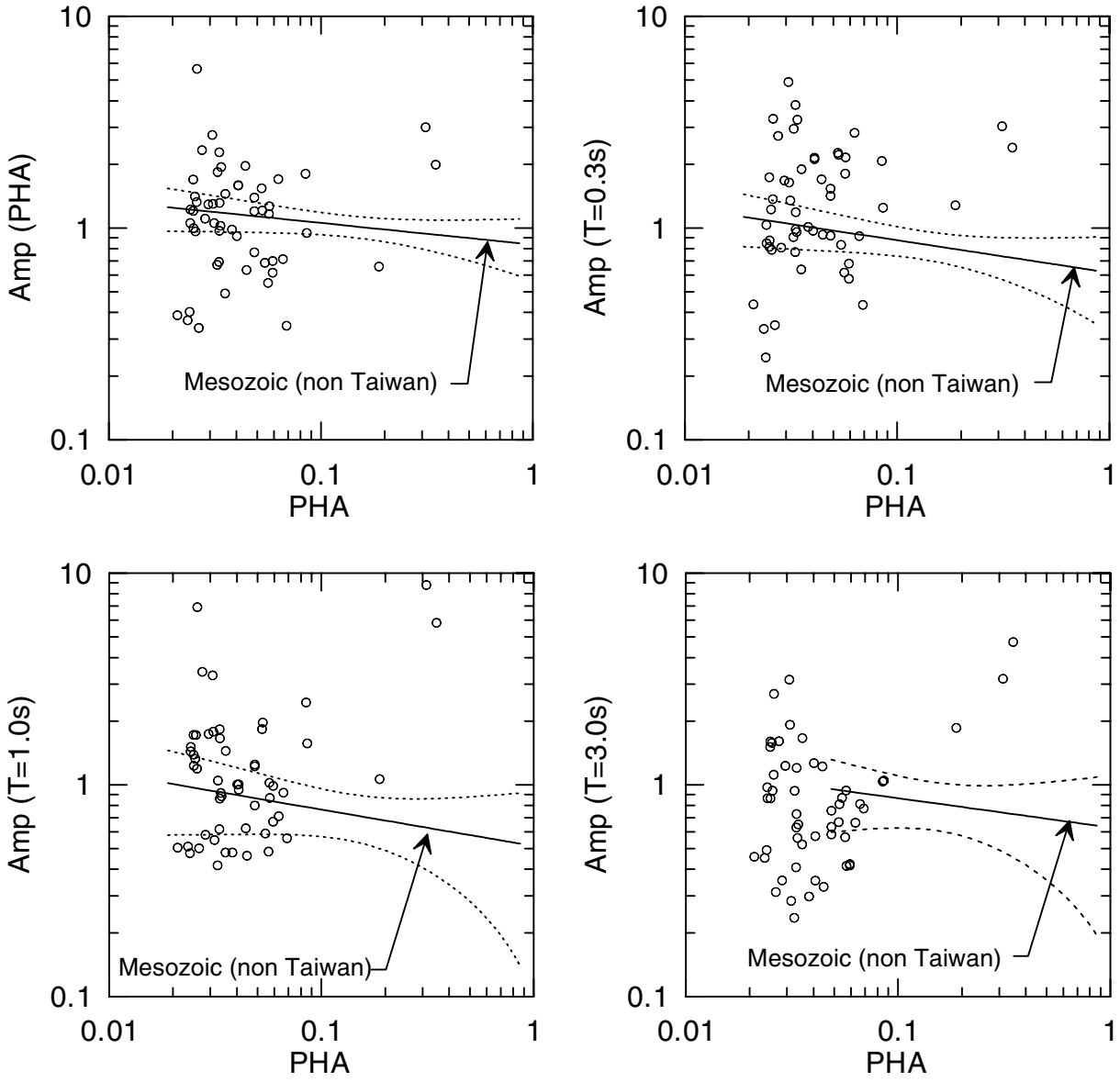

Fig. 6.8(d). Comparison of Chi-Chi, Taiwan, data for 'B' sites to Mesozoic regression results from this study

7 Conclusions and Recommendations

7.1 SUMMARY OF FINDINGS

Many current strong motion attenuation relations (e.g., Abrahamson and Silva, 1997; Sadigh, 1997) sub-divide site conditions into two broad categories: rock and soil. This project has developed amplification factors that can be used to modify predictions of rock attenuation relations for spectral acceleration on the basis of mapped surface geology, $V_{s\text{-}30}$, or a geotechnical site classification.

Low-period spectral acceleration amplification in geologically defined categories is found to be strongly a function of the age, material texture, and depositional environment of the surface deposits. Materials of Holocene age are found to have the highest levels of weak shaking amplification and soil nonlinearity, particularly when deposited in lacustrine or marine environments. The nonlinearity in such materials is typically sufficiently pronounced that high-frequency spectral ordinates are de-amplified at strong levels of shaking (PHA >~ 0.2g). Quaternary alluvial sediments experience less weak shaking amplification, but less nonlinearity as well. Amplification of Quaternary alluvial sediments is not significantly age-dependent. In all Quaternary categories, ground motion amplification is found to be strongly period-dependant, with less nonlinearity, and often more amplification, at longer spectral periods. “Rock-like” materials of pre-Pleistocene age (i.e., Tertiary or Mesozoic + Igneous categories) generally experience less amplification than Quaternary sediments and statistically insignificant nonlinearity. Amplification levels in the Tertiary and Mesozoic categories are significantly distinct at all periods, with Tertiary amplification factors exceeding unity, and Mesozoic generally being less than unity.

Available data from sites that can be classified on the basis of $V_{s\text{-}30}$ indicate spectral acceleration amplification levels for NEHRP B that are less than Mesozoic, NEHRP C

amplification levels intermediate between those for Pleistocene and Tertiary sediments (except at long period), and NEHRP D amplification levels that are intermediate between Holocene and Pleistocene sediments. Amplification factors for sites classified on the basis of the geotechnical classification scheme are distinctly lower for B than C, and are significantly differentiated between C and D only at intermediate to long periods. Preliminary results for E sites show significantly lower dispersion and higher PHA-dependence than for other categories.

One of the objectives of this study is to identify the "optimal" classification scheme among the options of surface geology, NEHRP categories, and categories defined from geotechnical data. We judge the relative effectiveness of these schemes based on the level of distinction between categories within the scheme, and on the inter-category standard error term. The NEHRP scheme is the most effective of those considered from the standpoint of inter-category distinction across a broad period range (e.g., Figures 5.6, Table 5.4b). Detailed surface geology provides the minimum values of inter-category error terms, although the distinction between categories is insignificant at long periods.

Further advances in the characterization of site effects on intensity measures may require use of parameters associated with features of the site other than near-surface sediments. We speculate that such parameters may include basin depth and distance to basin edge. Some promising preliminary results on basin depth have been obtained recently by Field et al. (2000) and Steidl (2000) for sites in the Los Angeles basin. Further study of these effects is needed.

Insight was gained in this study into the critical influence of reference site condition on amplification factors. In concept, any reference site condition could be used to define amplification factors, provided that subsequent use of such factors is coupled with design motions appropriate for the reference site condition. In California, the predominant condition of consolidated (non-soil) geologic materials in urban areas is weathered "soft rock." Accordingly, attenuation models based on "rock" recordings in California are more nearly applicable to a soft rock condition than to a hard rock condition. The reference site condition in this study was selected to match the composite rock average for active regions, so that amplification factors would be appropriate for use with standard rock attenuation models. The use of amplification factors defined with respect to a relatively firm rock reference site condition coupled with these same rock attenuation models may produce overly conservative design ground motions.

7.2 RECOMMENDATIONS

Based on the analyses completed to date, classification schemes based on detailed surface geology appear to provide an effective means by which to delineate site conditions for the evaluation of site amplification factors. Recommended categories for materials of Quaternary age are delineated on the basis of depositional environment or material texture as follows:

Depositional Environment	Material Texture
Quaternary alluvium	Holocene coarse-grained
Holocene lacustrine/marine	Holocene fine/mixed texture
	Pleistocene

Based on the data analyzed to date, we are unable to unambiguously identify one of the detailed surface geology schemes as superior to the other. For pre-Quaternary materials (i.e., rock-like), classifications are based only on age (T and M+I), and the dispersion of amplification factors is relatively large. For each of the categories, the recommended regression equation is Eq. 4.3(a), with the coefficients in Table 5.2(a) or 5.3(a) (Quaternary) or 5.1(a) (Tertiary and Mesozoic).

NEHRP site categories distinguished on the basis of $V_{s\text{-}30}$ have distinct variations in amplification levels between categories, but higher inter-category dispersion than detailed surface geology schemes. It was possible to slightly reduce this dispersion for rock sites by revising the V_s boundary between the B-C categories to better reflect the velocity transition between Tertiary and Mesozoic sediments, as discussed in Section 5.3. No such dispersion reduction was observed for sites in soil categories. Regression coefficients and error terms for the NEHRP categories are presented in Table 5.4(a).

A correction to the results of Eq. 4.3(a) is appropriate at long periods (i.e., T = 3 s, F_v). The correction can be made using Eq. 5.4, with the coefficients in Table 5.6. Additional refinements to these recommendations are likely as information on basin depth and other basin geometric parameters is analyzed.

If the amplification factors derived herein are used to estimate probabilistic distributions of ground motions within the context of a hazard analysis, the median of the distribution should be taken as the product of the median of rock attenuation and the appropriate amplification factor. The corresponding standard error term (σ_{haz}) can be taken as

$$\sigma_{haz} = \sqrt{\sigma^2 + 0.23^2} \tag{7.1}$$

where σ is taken from the appropriate row of Table 5.1(a), 5.2(a), 5.3(a), or 5.4(a). The additional error term of 0.23 accounts for inter-event variability, which was removed by use of the event term during the derivation of reference motion in this study. The value of 0.23 was obtained during the data regressions of Abrahamson and Silva (1997).

REFERENCES

Abrahamson, N. A. (2000). "Effects of rupture directivity on probabilistic seismic hazard analysis," *Proc. 6th Int. Conf. on Seismic Zonation*, Palm Springs.

Abrahamson, N. A., and Silva, W. J. (1997). "Empirical response spectral attenuation relations for shallow crustal earthquakes," *Seism. Res. Letters* 68(1): 94–127.

Abrahamson, N. A., and Youngs, R. R. (1992). "A stable algorithm for regression analyses using the random effects model," *Bull. Seism. Soc. Am.* 82: 505–10.

Aki, K., and Richards, P. G. (1980). *Quantitative seismology*, Vol. 1, W.H. Freeman, San Francisco, CA.

Anderson, J. G., Trifunac, M. D., Teng, T.-L., Amini, A., and Moslem, K. (1981). *Los Angeles vicinity strong motion accelerograph network,* Report No. CE 81-04, Univ. of Southern California.

Anderson, J. G. (2000). "Expected shape of regressions for ground motion parameters on rock," *Bull. Seism. Soc. Am.* 90: S43–S52.

Andrews, D. J. (1986). "Objective determination of source parameters and similarity of earthquakes of different size," in *Earthquake source mechanics*, S. Das, J. Boatwright, and C. H. Scholz (eds.), American Geophysical Union, Washington D.C., pp. 259–68.

Ang, A. H.-S., and Tang, W. H. (1975). *Probability Concepts in Engineering Planning and Design, Volume I — Basic Principles*, John Wiley & Sons, New York.

Bazzuro, P., and Cornell, A. C. (1999). *Efficient PSHA for nonlinear soil sites with uncertain properties,* Report, Civil Engineering Dept., Stanford University (in progress).

Boatwright, J., Seekins, L. C., and Mueller, C. S. (1991). "Ground motion amplification in the Marina," *Bull. Seism. Soc. Am.* 81: 1980–1997.

Bonilla, L .F., Lavallee, D., and Archuletta, R. J. (1997). "Site amplification in the San Fernando Valley, California," *Bull. Seism. Soc. Am*. 87: 710–30.

Boore, D. M., Joyner, W. B., and Fumal, T. E. (1997). "Equations for estimating horizontal response spectra and peak acceleration from western North American earthquakes: A summary of recent work," *Seism. Res. Letters* 68(1): 128–53.

Boore, D. M., and Brown, L. T. (1998). "Comparing shear wave velocity profiles from inversion of surface wave phase velocities with downhole measurements: systematic differences between the CXW method and down hole measurements at six USC strong motion sites," *Seism. Res. Letters* 69: 222–29.

Borcherdt, R. D. (1994). "Estimates of site-dependent response spectra for design (methodology and justification)," *Earthquake Spectra* 10(4): 617–53.

Borcherdt, R. D. (1996). "Preliminary amplification estimates inferred from strong ground motion recordings of the Northridge earthquake of January 17, 1994," *Proc. Int. Workshop on Site Response Subjected to Strong Ground Motion*, Vol. 1, Port and Harbor Research Institute, Yokosuka, Japan.

Borcherdt, R. D. (2001-in press). "Empirical evidence for acceleration-dependent amplification factors," submitted to *Bull. Seism. Soc. Am.*

Borcherdt, R. D., and Glassmoyer, G. (1994). "Influences of local geology on strong and weak ground motions recorded in the San Francisco Bay region and their implications for site-specific building-code provisions," The Loma Prieta, California Earthquake of October 17, 1989—Strong Ground Motion, U. S. Geological Survey Professional Paper 1551-A, A77-A108

Building Seismic Safety Council, BSSC (2000). *NEHRP Recommended Provisions for Seismic Regulations for New Buildings and Other Structures, Part 1 — Provisions and Part 2 — Commentary*, Federal Emergency Management Agency, Washington D.C., February.

Bullen, K. E. (1965). *An introduction to the theory of seismology*, Cambridge Univ. Press, Cambridge, U.K.

Campbell, K. W. (1997). "Empirical near-source attenuation relations for horizontal and vertical components of peak ground acceleration, peak ground velocity, and pseudo-absolute acceleration response spectra," *Seism. Res. Letters* 68(1): 154–79.

Campbell, K. W. (2000). Erratum to Campbell, 1997, *Seism. Res. Letters* 71(3): 352–54.

Campbell, K. W. (2001). Erratum to Campbell, 2000, *Seism. Res. Letters*, 72(4), p. 474.

Cook, R. D., and Weisberg, S. (1999). *Applied regression including computing and graphics*, John Wiley & Sons, Inc., New York.

Chang, S. W. (1996). "Seismic response of deep stiff soil deposits," Ph.D. Dissertation, Univ. of California, Berkeley.

Dickenson, S. E. (1994). "The dynamic response of soft and deep cohesive soils during the Loma Prieta earthquake of October 17, 1989," Ph.D. Dissertation, Univ. of California, Berkeley.

Dobry, R., Borcherdt, R. D., Crouse, C. B., Idriss, I. M., Joyner, W. B., Martin, G. R., Power, M.S., Rinne, E. E., and Seed, R. B. (2000). "New site coefficients and site classification system used in recent building seismic code provisions," *Earthquake Spectra*, 16 (1): 41–67.

Field, E. H. (2000). "A modified ground motion attenuation relationship for southern California that accounts for detailed site classification and a basin depth effect," *Bull. Seism. Soc. Am.* 90: S209–S221.

Field, E. H. et al. (2000). "Accounting for site effects in probabilistic seismic hazard analyses of southern California: Overview of the SCEC Phase III report," *Bull. Seism. Soc. Am*. 90: S1–S31.

Field, E. H., and Jacob, K. H. (1995). "A comparison and test of various site-response estimation techniques, including three that are not reference-site dependent" *Bull. Seism. Soc. Am*. 85: 1127–43.

Fukushima, Y., Irikura, K., Uetake, T., and Matsumoto, H. (2000). "Characteristics of observed peak amplitude for strong ground motion from the 1995 Hyokoken Nanbu (Kobe) earthquake," *Bull. Seism. Soc. Am.* 90: 545–65.

Fumal, T. E. (1978). *Correlations between seismic wave velocities and physical properties of near-surface geologic materials in the southern San Francisco Bay region, California,* Open-File Report 78-1067, U.S. Geological Survey, Menlo Park, California, 114 pp.

Fumal, T. E., and Tinsley, J. C. (1985). "Mapping shear-wave velocities of near-surface geologic materials," *U.S. Geological Survey Prof. Paper 1360*, 127–50.

Geomatrix Consultants (1993). *Compilation of geotechnical data for strong motion stations in the Western United States,* Report to Lawrence Livermore National Lab., Project No. 2256.

Harmsen, S. C. (1997). "Determination of site amplification in the Los Angeles urban area from inversion of strong motion records," *Bull. Seism. Soc. Am.* 87: 866–87.

Hartzell, S. A., Carver, D., Cranswick, E., and Frankel, A. (2000). "Variability of site response in Seattle, Washington," *Bull. Seism. Soc. Am.* 90 1237–50.

Hartzell, S. A., Leeds, A., Frankel, A., and Michael, J. (1996). "Site response for urban Los Angeles using aftershocks of the Northridge earthquake," *Bull. Seism. Soc. Am.*, 86: S168–S192.

Idriss, I. M. (1990). "Response of soft soil sites during earthquakes," *Proc. H. Bolton Seed Memorial Symposium*, J. M. Duncan (ed.), Vol. 2, pp. 273–90.

Joyner, W. B., Warrick, R. E., and Fumal, T. E. (1981). "The effect of Quaternary alluvium on strong ground motion in the Coyote Lake, California earthquake of 1979," *Bull. Seism. Soc. Am.* 71: 1333–49.

Lee, C.-T., Cheng, C.-T., Liao, C.-W., and Tsai, Y.-B.(2001) "Site classification of Taiwan free-field strong motion stations," *Bull. Seism. Soc. Am*. 91: 1283–97.

Lee, Y., and Anderson, J. G. (2000). "A custom southern California ground motion relationship based on analysis of residuals," *Bull. Seism. Soc. Am.* 90: S170–S187.

Lermo, J., and Chavez-Garcia, F. J. (1993). "Site effect evaluation using spectral ratios with only one station," *Bull. Seism. Soc. Am.* 83: 1574–94.

Martin, G. M., ed. (1994). *Proceedings of the NCEER/SEAOC/BSSC Workshop on Site Response during Earthquakes and Seismic Code Revisions*, Univ. of Southern Calif.

Morton, D. M., Hauser, R. M., and Ruppert, K. R. (1999). *Preliminary digital geologic map of the Santa Ana 30' x 60' Quadrangle, Southern California,* Open-File Report 99-172, U.S. Geological Survey, Menlo Park, CA.

Rodriguez-Marek, A., Bray, J. D., and Abrahamson, N. A. (2001). "An empirical geotechnical seismic site response procedure," *Earthquake Spectra* 17(1): 65–87.

Rodriquez-Ordonez, J. A. (1994). "A new method for interpretation of surface wave measurements in soils," Ph.D. Dissertation, North Carolina State University, Raleigh.

Rogers, A. M., Borcherdt, R. D., Covington, P. A., and Perkins, D. M. (1984). "A comparative ground response study near Los Angeles using recordings of Nevada nuclear tests and the 1971 San Fernando earthquake," *Bull. Seism. Soc. Am.* 74: 1925–49.

Sadigh, K. (1993). "A review of attenuation relationships for rock site conditions from shallow crustal earthquakes in an interplate environment," *Proc. Int. Workshop on Strong Motion Data*, 2, 179–236, Menlo Park, CA.

Sadigh, K., Chang, C.-Y., Egan, J. A., Makdisi, F., and Youngs, R. R. (1997). "Attenuation relations for shallow crustal earthquakes based on California strong motion data," *Seism. Res. Letters* 68(1): 180–9.

Seed, H. B. and Idriss, I. M. (1982) *"*Ground motions and soil liquefaction during earthquakes*"* Monograph Series, Vol. 5, Earthquake Engineering Research Institute.

Seed, H. B., Ugas, C., and Lysmer, J. (1976). "Site-dependant spectra for earthquake resistant design," *Bull. Seism. Soc. Am*. 66: 221–43.

Shoja-Taheri, J., and Anderson, J. G. (1988). "The 1978 Tabas, Iran, earthquake: an interpretation of the strong motion records," *Bull. Seism. Soc. Am*. 78: 142–71.

Silva, W. J., Li, S., Darragh, R., and Gregor, N. (1999). *"Surface geology based strong motion amplification factors for the San Francisco Bay and Los Angeles areas,"* Report to Pacific Earthquake Engineering Research Center.

Silva, W. J., Darragh, R., Gregor, N., Martin, G., Abrahamson, N., and Kircher, C. (2000). *"Reassessment of site coefficients and near-fault factors for building code provisions,"* Report to U.S. Geological Survey, National Earthquake Hazards Reduction Program.

Sokolov, V. Y. (1997). "Empirical models for estimating Fourier-amplitude spectra of ground acceleration in the northern Caucasus (Racha seismogenic zone)," *Bull. Seism. Soc. Am.* 87: 1401–12.

Sokolov, V. Y., Loh, C.-H., and Wen, K.-L. (2000). "Empirical study of sediment-filled basin response: The case of Taipei City," *Earthquake Spectra* 16(3): 681–707.

Somerville, P. G., Smith, N. F., Graves, R. W. and Abrahamson, N. A. (1997). "Modification of empirical strong ground motion attenuation relations to include the amplitude and duration effects of rupture directivity," *Seismological Research Letters* 68: 199–222.

Steidl, J. H. (2000). "Site response in southern California for probabilistic seismic hazard analysis," *Bull. Seism. Soc. Am.* 90: S149–S169.

Steidl, J. H., and Lee, Y. (2000). "The SCEC Phase III strong-motion database," *Bull. Seism. Soc. Am.* 90: S113–S135.

Stewart, J.P., and Liu, A. H. (2000). "Ground motion amplification as a function of surface geology," *Proc. SMIP2000 Seminar on Utilization of Strong Motion Data*, California Strong Motion Instrumentation Program, Sacramento, CA, 1–22.

Tinsley, J. C., and Fumal, T. E. (1985). "Mapping Quaternary sedimentary deposits for areal variations in shaking response," U.S. Geological Survey Prof. Paper 1360, pp. 101–126.

Wills, C. J., Petersen, M., Bryant, W. A., Reichle, M., Saucedo, G. J., Tan, S., Taylor, G., and Treiman, J. (2000). "A site conditions map for California based on geology and shear wave velocity," *Bull. Seism. Soc. Am.* 90: S187–S208.

Wills, C. J., and Silva, W. (1998). "Shear wave velocity characteristics of geologic units in California," *Earthquake Spectra* 14(3): 533–56.

Youngs, R. R. (1993). "Soil amplification and vertical to horizontal ratios for analysis of strong motion data from active tectonic regions," Appendix 2C in *Guidelines for determining design basis ground motions, vol. 2,* Electrical Power Research Institute, Report No. TR-102293.

Appendix A Classification of Strong Motion Accelerograph Sites Used in This Study

Location	Station Name	Agency	Station #	Latitude	Longitude	Geology				30-m V_s and Geotechnical Data				
						Age	Grain Size	Depositional History	Reference	Boring	V_s (m/s)	NEHRP	Geot.	Reference
Agnew	Agnews State Hospital	CSMIP	57066	37.239	121.952	Holo	Fine	Alluvial Fan	DOC, Geomatrix	A	274	D	D3	AA 9225-6427
Alameda	Naval Air Station	US Navy				Holo	Fine	Marine	boring	A	188	D	E	
Alhambra	Fremont School	CSMIP	24461	34.070	118.150	Pleist			Geomatrix	C	340	D	C2-D	Law/Crandall 82031
Altadena	Eaton Canyon Park	CSMIP	24402	34.177	118.096	Holo	Coarse	Alluvial Fan	CDMG, Geomatrix					
Amboy		CSMIP	21081	34.560	115.743	Holo		Alluvium	CDMG					
Anacapa Island		CSMIP	25169	34.0160	119.3620	Tertiary			CDMG					
Anaheim	W. Ball Rd	USC	90088	33.817	117.951	Holo	Coarse	Alluvial Fan	CDMG					
Anaverde Valley	City Ranch	CSMIP	24576	34.5800	118.1990	Holo/Pleist ?			CDMG					
Angeles Nat. Forest	Big Tujunga	USC	90061	34.2860	118.2250	Mesoz			CDMG					
Antioch	510 G Street	CSMIP	67070	38.015	121.813	Holo		Alluvial Valley	DOC					
Anza	Red Mountain	USGS	5224	33.6304	116.848	Mesoz			CDMG					
Arcadia	Arcadia av	USC	90099	34.127	118.059	Holo	Coarse	Alluvial Fan	CDMG					
Arcadia	Campus Dr.	USC	90093	34.130	118.036	Holo	Coarse	Alluvial Valley	CDMG					
Arcadia	Santa Anita Resevoir	CIT	104	34.185	118.018	Mesoz			Boring				B	Nureg/CR-0055
Arleta	Nordhoff Fire Sta #	CSMIP	24087	34.236	118.439	Holo		Alluvial Fan	CDMG, Geomatrix	A	293	D	D1S	ROSRINE
Baker	Fire Station	CSMIP	32075	35.272	116.066	Holo		Alluvium	CDMG					
Bakersfield*	Harvey Auditorium	CIT	4	35.370	119.020	Holo			CDMG	A	241	D	D	UCLA rpt. 62-55, Law/Crandall 76238
Baldwin Park	N. Holly Ave	USC	90069	34.100	117.974	Holo	Coarse	Alluvial Fan	CDMG	C	288	D	C-D	Law/Crandall 77042
Barstow	Vineyard & H St.	CSMIP	23559	34.887	117.047	Holo			Geomatrix					
Bell Gardens	Jaboneria	USC	90094	33.965	118.158	Holo	Coarse	Alluvial Fan	CDMG					
Belmont	Envirotech Bldg. (2 story)	CSMIP	58262	37.512	122.308	Mesoz			DOC, Geomatrix	A	628	C	B	AA 9225-6427
Benton	Caltrans Maintennance Yard	CSMIP	54100	37.818	118.475	Holo		Alluvial Fan	DOC, Geomatrix					
Berkeley	Lawrence Berkely Lab	CSMIP	58471	37.876	122.249	Tertiary			DOC					
Beverly Hills	12520 Mulholland	USC	90014	34.127	118.405	Tertiary			CDMG					
Beverly Hills	14145 Mulholland	USC	90013	34.132	118.439	Tertiary			CDMG					
Beverly Hills	Pac Bell	USGS	5402	34.076	118.395	Holo	Fine	Alluvial Valley	CDMG	A	341	D	C2-D	Law/Crandall 81373
Bishop	LADWP South Street Garage	CSMIP	54171	37.360	118.396	Holo		Alluvial Fan	DOC, Geomatrix					
Bishop	Paradise Lodge	CSMIP	54424	37.481	118.602	Pleist			DOC					
Bombay Beach		USGS	5271	33.353	115.732	Holo		Lacustrine	DOC					
Boron	Fire Station	CSMIP	33083	35.002	117.650	Holo		Alluvium	CDMG					
Borrego Springs	Borrego Air Ranch	USGS	5049	33.190	116.280	Pleist/Holo ?			CDMG					
Borrego Springs*	Fire Station	CIT	105	33.258	116.371	Holo		Alluvium	CDMG					
Brawley	Airport	USGS	5060	32.990	115.510	Holo	Aggregate	Lacustrine	DOC, Geomatrix	A	213	D	D	USGS OFR 84-562
Brea	Brea Dam (downstream)	ACOE	951	33.889	117.926	Holo	Fine	Non-marine	CDMG, Geomatrix	C	396	C	C-D	USGS OFR 80-378
Brea	Brea Dam (left abutment)	ACOE	951	33.889	117.926	Holo	Fine	Non-marine	CDMG, Geomatrix	C	396	C	C-D	USGS OFR 80-378
Brea	Carbon Canyon Dam (left abutment)	ACOE/CIT	108	33.914	117.839	Holo	Coarse	Alluvial Fan	CDMG, Geomatrix				C2	Nureg/CR-0055
Brea	Carbon Canyon Dam (right abutment)	ACOE/CIT	108	33.914	117.839	Holo	Coarse	Alluvial Fan	CDMG, Geomatrix				C2	Nureg/CR-0055
Brea	S. Flower Ave	USC	90087	33.916	117.896	Pleist		Alluvial Valley	CDMG					
Buena Park	La Palma	USC	90086	33.847	118.018	Holo	Coarse	Alluvial Fan	CDMG					
Burbank	Howard Road	USC	90059	34.2040	118.3020	Mesoz			Dibblee Map					
Burbank	N Buena Vista	USC	90012	34.168	118.331	Holo		Alluvium	Dibblee Map	C	320	D		Law/Crandall 78383
Cabazon	Post Office	USGS	5073	33.9176	116.7833	Holo		Alluvium	CDMG					
Calabasas	N Las Virg	USC	90052	34.150	118.696	Holo	Coarse	Alluvial Fan	CDMG					
Calabasas	Pac Bell	USGS	5404	34.155	118.640	Tertiary			CDMG					
Calexico	Fifth & Mary (Fire Station)	USGS	5053	32.670	115.490	Holo	Fine	Lacustrine	DOC, Geomatrix	A	235	D	D3	USGS OFR 84-562
Calipatria	Fire Station	USGS	5061	33.130	115.520	Holo	Fine		Geomatrix	A	207	D	D3	USGS OFR 84-562
Camarillo	Fire Station	CSMIP	25282	34.208	119.079	Holo	Fine		DOC					
Canoga Park	Topanga Canyon	USC	90053	34.212	118.606	Holo		Alluvial Fan	CDMG	A	287	D	C3	USGS OFR 96-740
Cantua Creek	Cantua Creek School	CDMG	46314	36.503	120.320	Holo		Alluvial Fan	DOC, Geomatrix					
Canyon Country	W Lost Cany	USC	90057	34.419	118.426	Holo		Floodplain	CDMG					
Capitola	Fire Station	CSMIP	47125	36.974	121.952	Holo		Alluvium	DOC	A	290	D	C2	AA 9225-6427
Carson	Catskill Ave	USC	90040	33.812	118.270	Pleist		Alluvial Valley	CDMG					
Carson	Water St	USC	90081	33.836	118.240	Holo		Alluvial Valley	CDMG					
Castaic	Old Ridge Route #	CSMIP	24278	34.564	118.642	Mesoz			Geomatrix	A	578	C	C1	NUREG/CR-0055, V2, USGS OFR 84-681
Castaic*	Castaic Dam	CIT	110	34.560	118.630	Holo			CDMG	C	573	C	C1	USGS OFR 84-681
Cedar Springs*	Allen Ranch	CIT	111	34.278	117.335	Pleist/Mesoz ?			CDMG	A	832	B	B	USGS OFR 84-681
Century City	LACC North	CSMIP/CDM	24389	34.063	118.418	Pleist	Aggregate	Alluvial Valley	CDMG, Geomatrix	B	306	D	D3	UCB/EERC-97/01
Century City	LACC South	CSMIP/CDM	24390	34.062	118.416	Pleist	Aggregate	Alluvial Valley	CDMG, Geomatrix	A	306	D	D3	Law/Crandall 79294, Law/Crandall 80038
Chalfant	Zack Brothers Ranch	CSMIP	54428	37.662	118.398	Holo		Alluvial Valley	DOC					

Chatsworth	Devonshire	USC	90004	34.358	118.571	Tertiary			CDMG					
Cholame *	Temblor pre 1969	CDMG	1438	35.752	120.264	Pleist			DOC	A	518	C	C1	USGS OFR 82-407
Cholame Array	Cholame-Limb Station 12W	CDMG	36229	35.639	120.404	Holo	Coarse		Geomatrix	A	402	C	C3-D	USGS OFR 82-407
Cholame Array	Cholame-Limb Station 1E	CDMG	36452	35.743	120.277	Holo	Aggregate	Alluvial Fan	DOC, Geomatrix	C	187	D	D	NUREG-0029,V1
Cholame Array	Cholame-Limb Station 2E	CDMG	36230	35.752	120.264	Tertiary			Boring	A	518	C	C1	USGS OFR 82-407
Cholame Array	Cholame-Limb Station 2WA	CDMG	36228	35.733	120.290	Holo	Fine	Non-marine	DOC, Geomatrix	A	187	D	D1	NUREG-0029,V1
Cholame Array	Cholame-Limb Station 3E	CDMG	36450	35.770	120.247	Tertiary			DOC, Geomatrix					
Cholame Array	Cholame-Limb Station 3W	CDMG	36410	35.724	120.294	Holo	Aggregate	Alluvium	DOC, Geomatrix	C	187	D	C	NUREG-0029,V1
Cholame Array	Cholame-Limb Station 4AW	CDMG	36412	35.707	120.316	Holo	Aggregate	Alluvium	DOC, Geomatrix	C	293	D	C	USGS OFR 82-407
Cholame Array	Cholame-Limb Station 4W	CDMG	36411	35.718	120.304	Pleist		Non-marine	DOC, Geomatrix					
Cholame Array	Cholame-Limb Station 5W	CDMG	36227	35.697	120.328	Holo	Coarse	Alluvium	DOC, Geomatrix	A	293	D	C2	USGS OFR 82-407
Cholame Array	Cholame-Limb Station 6W	CDMG	36451	35.684	120.342	Holo	Aggregate	Alluvium	DOC, Geomatrix					
Cholame Array	Cholame-Limb Station 8W	CDMG	36226	35.671	120.359	Holo	Fine	Alluvium	DOC	A	259	D	C3	USGS OFR 82-407
Cholame Array	Fault Zone Station 1	CDMG	36407	35.758	120.307	Holo		Alluvium	DOC, Geomatrix					
Cholame Array	Fault Zone Station 10	CDMG	36444	35.872	120.422	Pleist	Coarse	Non-marine	DOC, Geomatrix					
Cholame Array	Fault Zone Station 11	CDMG	36453	35.896	120.398	Pleist	Coarse		DOC, Geomatrix					
Cholame Array	Fault Zone Station 12	CDMG	36138	35.899	120.433	Holo	Coarse	Alluvium	DOC, Geomatrix					
Cholame Array	Fault Zone Station 14	CDMG	36456	35.908	120.458	Pleist	Coarse	Alluvial Fan	DOC, Geomatrix					
Cholame Array	Fault Zone Station 15	CDMG	36445	35.921	120.481	Pleist	Coarse		DOC, Geomatrix					
Cholame Array	Fault Zone Station 16	CDMG	36457	35.927	120.456	Holo	Coarse	Marine	DOC, Geomatrix					
Cholame Array	Fault Zone Station 2	CDMG	36413	35.787	120.334	Holo	Aggregate	Alluvial Fan	DOC, Geomatrix					
Cholame Array	Fault Zone Station 3	CDMG	36408	35.803	120.344	Holo	Aggregate	Alluvium	DOC, Geomatrix					
Cholame Array	Fault Zone Station 4	CDMG	36414	35.836	120.395	Holo	Aggregate	Alluvial Fan	DOC, Geomatrix					
Cholame Array	Fault Zone Station 6	CDMG	36454	35.859	120.420	Pleist	Coarse	Non-marine	DOC, Geomatrix					
Cholame Array	Fault Zone Station 7	CDMG	36431	35.871	120.404	Pleist	Aggregate	Non-marine	DOC, Geomatrix					
Cholame Array	Fault Zone Station 8	CDMG	36449	35.878	120.381	Pleist	Aggregate		DOC, Geomatrix					
Cholame Array	Fault Zone Station 9	CDMG	36443	35.879	120.445	Holo	Aggregate	Non-marine	DOC, Geomatrix					
Cholame Array	Gold Hill Limb Station 1W	CDMG	36415	35.818	120.378	Holo		Alluvial Fan	DOC					
Cholame Array	Gold Hill Limb Station 2E	CDMG	36421	35.843	120.348	Pleist	Aggregate	Alluvium	DOC, Geomatrix					
Cholame Array	Gold Hill Limb Station 2W	CDMG	36416	35.812	120.391	Pleist	Aggregate	Marine	DOC, Geomatrix					
Cholame Array	Gold Hill Limb Station 3E	CDMG	36439	35.870	120.334	Pleist	Aggregate		DOC, Geomatrix					
Cholame Array	Gold Hill Limb Station 3W	CDMG	36420	35.796	120.411	Pleist	Coarse	Non-marine	DOC, Geomatrix					
Cholame Array	Gold Hill Limb Station 4W	CDMG	36433	35.785	120.444	Pleist	Coarse	Non-marine	DOC, Geomatrix					
Cholame Array	Gold Hill Limb Station 5W	CDMG	36434	35.770	120.477	Pleist	Coarse	Non-marine	DOC, Geomatrix					
Cholame Array	Gold Hill Limb Station 6W	CDMG	36432	35.738	120.507	Pleist	Coarse	Non-marine	DOC, Geomatrix					
Cholame Array	Stone Corral Limb Station 2E	CDMG	36422	35.810	120.282	Pleist	Aggregate		DOC, Geomatrix					
Cholame Array	Stone Corral Limb Station 3E	CDMG	36437	35.833	120.270	Pleist	Aggregate		DOC, Geomatrix					
Cholame Array	Stone Corral Limb Station 4E	CDMG	36438	35.855	120.281	Pleist	Aggregate		DOC, Geomatrix					
Cholame Array	Vineyard Canyon Limb Station 1E	CDMG	36455	35.957	120.481	Holo	Aggregate	Marine	DOC, Geomatrix					
Cholame Array	Vineyard Canyon Limb Station 1W	CDMG	36448	35.934	120.497	Pleist	Coarse	Marine	DOC, Geomatrix					
Cholame Array	Vineyard Canyon Limb Station 2E	CDMG	36177	35.973	120.467	Mesoz			DOC, Geomatrix					
Cholame Array	Vineyard Canyon Limb Station 2W	CDMG	36447	35.927	120.509	Pleist	Coarse	Alluvial Fan	DOC, Geomatrix					
Cholame Array	Vineyard Canyon Limb Station 4W	CDMG	36446	35.905	120.550	Holo	Coarse	Marine	DOC, Geomatrix					
Cholame Array	Vineyard Canyon Limb Station 5W	CDMG	36440	35.885	120.565	Tertiary		Marine	DOC, Geomatrix					
Cholame Array	Vineyard Canyon Limb Station 6W	CDMG	36441	35.861	120.600	Pleist	Coarse	Alluvium	DOC, Geomatrix					
Cholame Array*	Shandon 2	CIT		35.731	120.286	Holo		Alluvium	DOC	A	187	D	D	NUREG-0029,V1
Cholame Array*	Shandon 8	CIT		35.671	120.360	Holo	Fine	Alluvium	DOC, Geomatrix	A	259	D	C3	USGS OFR 82-407
Coachella Canal	Canal Sta 4 - Siphon 15	USGS	5066	33.360	115.590	Holo	Aggregate		Geomatrix					
Coalinga	Anticline Ridge	USGS	1607	36.230	120.330	Tertiary			DOC					
Coalinga	Burnett Construction	USGS	1606	36.138	120.357	Holo		Alluvial Fan	DOC					
Coalinga	Oil City	USGS	1604	36.229	120.360	Tertiary		Marine	DOC					
Coalinga	Skunk Hollow	USGS	1605	36.275	120.306	Tertiary		Marine	DOC					
Coalinga	Transmitter Hill	USGS	1651	36.249	120.343	Tertiary		Marine	DOC					
Cogswell Resevoir	Cogswell Dam	CSMIP	23210	34.245	117.964	Holo		Fill	DOC					
Colton*	Edison Company	CIT	113	34.059	117.312	Holo		Alluvium	CDMG	A	314	D	D3	UCLA Rpt. 62-55, USGS OFR 84-681
Compton	Castlegate St	USC	90078	33.899	118.196	Holo	Coarse	Alluvial Fan	CDMG					
Convict Creek	UC Experimental Station	CSMIP	54099	37.614	118.831	Holo		Alluvial Fan	DOC					
Corralitos	Eureka Canyon Road	CSMIP	57007	37.046	121.803	Tertiary			DOC, Geomatrix	A	466	C	C1	USGS OFR 93-376, ROSRINE
Covina	S. Grand Ave.	USC	90068	34.078	117.871	Holo	Fine	Alluvial Fan	CDMG					
Covina	W. Badillo	USC	90070	34.087	117.915	Holo	Coarse	Alluvial Fan	CDMG					
Crystal Springs	APEEL Array Stn. 9 - Residence	USGS	1161	37.470	122.320	Tertiary			DOC, Geomatrix	A	343	D	C3?	USGS OFR 79-1619
Desert Hot Springs	Fire Station	CSMIP	12149	33.962	116.509	Holo		Alluvium	CDMG	A	389	C	D	Rosrine
Downey	Birchdale	USC	90079	33.920	118.137	Holo	Coarse	Alluvial Fan	CDMG	A	255	D	D3	ROSRINE
Downey	Co Maint Bldg.	CSMIP	14368	33.924	118.167	Holo	Coarse	Alluvial Fan	CDMG, Geomatrix	C	258	D	D	Law/Crandall 90391
Duarte	Mel Canyon Rd.	USC	90067	34.150	117.939	Holo		Alluvial Fan	CDMG					

El Centro	Array 1 - Borchard Ranches	USGS	5056	32.960	115.320	Holo	Fine	Lacustrine	DOC, Geomatrix					
El Centro	Array 10 - Community Hospital	USGS	412	32.780	115.567	Holo		Lacustrine	DOC, Geomatrix	A	206	D	D3	USGS OFR 84-562
El Centro	Array 11 - Mc Cabe School	USGS	5058	32.750	115.590	Holo	Fine	Lacustrine	DOC, Geomatrix	A	181	E	D1C	USGS OFR 84-562
El Centro	Array 13 - Strobel Residence	USGS	5059	32.710	115.680	Holo	Aggregate	Lacustrine	DOC, Geomatrix	A	256	D	D3	USGS OFR 84-562
El Centro	Array 2 - Keystone Rd	USGS	5115	32.920	115.370	Holo	Fine	Lacustrine	DOC, Geomatrix	A	194	D	D3	USGS OFR 84-562
El Centro	Array 3 - Pine Union School	USGS	5057	32.890	115.380	Holo	Aggregate	Lacustrine	DOC, Geomatrix	A	166	E\F	E	USGS OFR 84-562
El Centro	Array 4 - 2905 Anderson Rd	USGS	955	32.860	115.430	Holo	Aggregate	Lacustrine	DOC, Geomatrix	A	210	D	D3	USGS OFR 84-562
El Centro	Array 5 - 2801 James Rd	USGS	952	32.860	115.470	Holo	Fine	Lacustrine	DOC, Geomatrix	A	209	D	D3	USGS OFR 84-562
El Centro	Array 7 - Imperial Valley Col	USGS	5028	32.830	115.500	Holo	Aggregate	Lacustrine	DOC, Geomatrix	A	218	D	D3	USGS OFR 84-562
El Centro	Array 8 - 95 E Cruickshank Rd	USGS	958	32.810	115.530	Holo	Fine	Lacustrine	DOC, Geomatrix	A	213	D	D3	USGS OFR 84-562
El Centro	Array 9 - 302 Commercial Av	USGS	117	32.790	115.550	Holo	Aggregate	Lacustrine	DOC, Geomatrix	A	218	D	D3	USGS OFR 84-562
El Centro	EC County Center FF	CDMG	5154	33.792	115.564	Holo	Fine		DOC					
El Centro	EC Differential Array - Dogwood Rd.	USGS	5165	32.800	115.540	Holo	Aggregate	Lacustrine	DOC, Geomatrix	A	203	D	D3	USGS OFR 84-562
El Centro	Hwys 98 & I15 - Bonds Corner	USGS	5054	32.693	115.338	Holo	Aggregate	Lacustrine	DOC, Geomatrix	A	221	D	D3	USGS OFR 84-562
El Centro	Imperial County Center - Ground	CDMG	01335	32.793	115.562	Holo		Lacustrine	DOC, Geomatrix	A	195	D	E	USGS OFR 84-562
El Centro	Parachute Test Site	USGS	5051	32.930	115.700	Holo	Aggregate	Alluvium	DOC, Geomatrix	A	378	C	D	USGS OFR 84-562
El Centro	Rte 8 / Meloland overcrossing	CDMG	01336	32.773	115.448	Holo	Fine	Lacustrine	DOC, Geomatrix	A	165	E\F	E	ROSRINE
El Monte	Fairview Ave	USC	90066	34.093	118.019	Holo	Coarse	Alluvial Fan	CDMG					
Eureka	Myrtle & West Avenue	CSMIP	89509	40.801	124.148	Holo		Marine	DOC, Geomatrix	C	274	D	D2	NUREG/CR-0055, V3
Fairmont Resevoir*		CIT	121	34.704	118.426	Mesoz/Pleist ?			CDMG	A			B	NUREG/CR-0055, V1
Featherly Park	Pk Maint. Bldg	CSMIP	13122	33.869	117.709	Holo		Colluvium	DOC					
Fort Irwin		CSMIP	24577	35.268	116.684	Holo/Pleist ?			CDMG					
Fortuna	701 S. Fortuna Blvd.	CSMIP	89486	40.584	124.145	Holo			DOC, Geomatrix					
Foster City	Menhaden Court	USGS	1515	37.555	122.248	Holo	Fine	Marine	DOC, Geomatrix	A	126	E\F	E	USGS OFR 94-222
Fountain Valley	Euclid	USC	90002	33.719	117.937	Holo	Aggregate	Alluvial Fan	CDMG	C	204	D	D?	Law/Crandall 79295
Fremont	Emerson Court	USGS	1686	37.535	121.929	Pleist		Alluvial Fan	DOC	A	287	D	D1	USGS OFR 94-222
Fremont	Mission San Jose	CSMIP	57064	37.530	121.919	Pleist	Aggregate	Alluvial Fan	DOC, Geomatrix	A	367	C	C1	AA 9225-6427
Fun Valley	Fun Valley Resevoir	USGS	5069	33.9249	116.3899	Holo		Alluvium	CDMG					
Garden Grove	Santa Rita	USC	90085	33.790	118.012	Holo	Fine	Alluvial Fan	CDMG					
Gilroy	Gavilan Coll., Phys. Sc. Bldg.	CSMIP	47006	36.973	121.568	Mesoz			DOC, Geomatrix	A	744	C	C2	USGS OFR 91-311
Gilroy	Gilroy 1; Gavilian Coll. Water Tank	CSMIP	47379	36.973	121.572	Mesoz			DOC, Geomatrix	A	1582	A	A	USGS OFR 82-407
Gilroy	Gilroy 2; Hwy 101/Bolsa Rd. Motel	CSMIP	47380	36.982	121.556	Holo	Coarse	Alluvium	DOC	A	274	D	D1	USGS OFR 92-287
Gilroy	Gilroy 3; Sewage Plant	CSMIP	47381	36.987	121.536	Holo	Fine	Alluvial Fan	DOC, Geomatrix	A	274	D	D1	USGS OFR 82-407
Gilroy	Gilroy 6; San Ysidro	CSMIP	57383	37.026	121.484	Tertiary			DOC, Geomatrix	A	613	C	B	USGS OFR 91-311
Gilroy	Gilroy 7; Mantelli Ranch	CSMIP	57425	37.033	121.434	Holo		Alluvial Fan	DOC, Geomatrix	A	337	D	C2	USGS OFR 93-376
Gilroy	Historic Comm. Bldg (2-story)	CSMIP	57476	37.009	121.569	Holo		Alluvial Fan	DOC, Geomatrix					
Glendale	Las Palmas	USC	90063	34.200	118.231	Holo	Coarse	Alluvial Fan	CDMG					
Glendora	N. Oakbank	USC	90065	34.137	117.883	Holo	Coarse	Alluvial Fan	CDMG					
Gorman*	Oso Pumping Plant	CIT	52	34.800	118.720	Holo	Coarse		Geomatrix	A	314	D	C3	USGS OFR 84-681
Hacienda Hts	Colima Rd	USC	90073	33.990	117.943	Pleist		Alluvial Valley	CDMG					
Halls Valley	Grant Park	CSMIP	57191	37.388	121.714	Holo			DOC, Geomatrix	A	268	D	C2	AA 9225-6427
Hayward	APEEL 1E-Pt. Eden Way	CSMIP	58376	37.623	122.130	Holo	Fine	Marine	DOC				D?	USGS OFR 76-731
Hayward	APEEL 2E-Muir School	CSMIP	58393	37.657	122.082	Pleist		Alluvial Fan	DOC	A	251	D	D2	USGS OFR 79-1619
Hayward	APEEL 3E-CSUH Stadium Grounds	CSMIP	58219	37.657	122.061	Mesoz			DOC	A	617	C	C1	USGS OFR 79-1619
Hayward	BART Station Parking Lot	CSMIP	58498	37.670	122.086	Pleist		Alluvial Fan	DOC	C	276	D	D2	BART
Hayward	City Hall - Free Field	USGS	1129	37.679	122.082	Pleist		Alluvial Fan	DOC	A	745	C	B	USGS OFR 94-222
Hemet	Ryan Airfield #	CDMG	13660	33.731	117.023	Holo		Alluvium	CDMG					
Hemet	Stetson Ave Fire Station	CSMIP	12331	33.729	116.979	Holo			Geomatrix					
Hesperia	4th and Palm	CSMIP	23583	34.405	117.311	Pleist		Alluvium						
Hesperia		CSMIP	23321	34.448	117.327	Holo		Alluvium	CDMG					
Hollister	City Hall	USGS	1028	36.850	121.400	Holo	Aggregate		DOC, Geomatrix	A	200	D	D	USGS OFR 91-311
Hollister	Hollister Airport-differential Array	USGS	1656	36.888	121.413	Pleist	Aggregate	Alluvial Valley	DOC, Geomatrix	A	216	D	D	USGS 94-552
Hollister	SAGO Vault	USGS	1032	36.765	121.446	Mesoz			DOC, Geomatrix				B	USGS OFR 91-311
Hollister	SAGO-South	CSMIP	47189	36.753	121.396	Mesoz			DOC, Geomatrix	A	594	C	C1	AA 9225-6427
Hollister	South & Pine	CSMIP	47524	36.848	121.397	Holo	Aggregate		DOC, Geomatrix	C	200	D	D1	USGS OFR 91-311
Hollywood	Willoughby Ave	USC	90018	34.088	118.365	Holo	Coarse	Alluvial Fan	CDMG	C	326	D	D	Law/Crandall 84182
Holtville	Post Office	USGS	5055	32.810	115.380	Holo	Aggregate	Lacustrine	DOC, Geomatrix	A	204	D	D3	USGS OFR 84-562
Humboldt Bay	Power Plant	PGE		40.741	124.209	Holo		Alluvium	CDMG	A	317	D	D	UCB EERC 97-01
Huntington Bch	Lake St. Fire Station	CSMIP	13197	33.662	117.997	Pleist	Aggregate	Marine	CDMG, Geomatrix					
Huntington Bch	Waikiki	USC	90083	33.727	118.044	Holo	Coarse	Alluvial Fan	CDMG					
Hyoken-Nanbu	Abeno	CEOR				Holo		Alluvium	Ref. 1					
Hyoken-Nanbu	Amagasaki	CEOR				Holo		Reclaimed	Ref. 1					
Hyoken-Nanbu	Chihaya	CEOR				Mesoz			Ref. 1					
Hyoken-Nanbu	FUK					Holo		Alluvium	Ref. 1					
Hyoken-Nanbu	Fukushima	CEOR				Holo		Alluvium	Ref. 1					
Hyoken-Nanbu	Kakogawa	CUE				Holo		Alluvium	Ref. 1					
Hyoken-Nanbu	Kobe University	CEOR				Mesoz			Ref. 1					

Hyoken-Nanbu	Kobe-KJMA					Pleist		Dilluvium	Ref. 1					
Hyoken-Nanbu	Morigawachi	CEOR				Holo		Alluvium	Ref. 1					
Hyoken-Nanbu	MZH					Holo		Reclaimed	Ref. 1					
Hyoken-Nanbu	Nishi-Akashi	CUE				Pleist		Dilluvium	Ref. 1					
Hyoken-Nanbu	OKA					Holo		Alluvium	Ref. 1					
Hyoken-Nanbu	Port Island 0m	CEOR				Holo		Reclaimed	Ref. 1					
Hyoken-Nanbu	Sakai	CEOR				Holo		Alluvium	Ref. 1					
Hyoken-Nanbu	Shin-Osaka	CUE		34.690	135.500	Holo		Alluvium	Ref. 1					
Hyoken-Nanbu	Tadoka	CEOR				Pleist		Dilluvium	Ref. 1					
Hyoken-Nanbu	Takatori	CUE				Holo		Alluvium	Ref. 1					
Hyoken-Nanbu	TOT					Holo		Alluvium	Ref. 1					
Hyoken-Nanbu	Yae	CEOR				Holo		Alluvium	Ref. 1					
Indio	Coachella Canal	CSMIP	12026	33.717	116.156	Holo	Aggregate		Geomatrix					
Indio	So Calif Gas Co	USGS	5067	33.7473	116.2152	Holo			CDMG					
Inglewood	LAX	USGS	5399	33.943	118.411	Holo	Coarse	Aeolian	CDMG					
Inglewood	Union Oil #	CSMIP	14196	33.905	118.279	Pleist	Coarse	Alluvial Valley	CDMG, Geomatrix					
Joshua Tree	Fire Station	CSMIP	22170	34.131	116.314	Holo			Geomatrix	A?	390	C	D	ROSRINE
LA	116th St. School	CSMIP	14403	33.929	118.260	Pleist		Alluvial Valley	CDMG, Geomatrix	C	320	D	D3	ROSRINE
LA	Baldwin Hills#	CSMIP	24157	34.009	118.361	Holo		Fill	CDMG, Geomatrix	A	291	C	D2	ROSRINE
LA	Brentwood VA Hospital	USGS	638	34.058	118.457	Pleist		Alluvial Valley	CDMG	A	427	C	C3	ROSRINE
LA	Centinela St	USC	90054	34.001	118.431	Holo		Alluvial Valley	CDMG					
LA	Chalon Rd.	USC	90015	34.086	118.481	Mesoz			CDMG					
LA	City Terrace #	CSMIP	24592	34.053	118.171	Tertiary			DOC	C	507	C	C1	Law/Crandall 77200
LA	Cypress Ave.	USC	90033	34.088	118.222	Holo		Alluvial Valley	DOC					
LA	E Vernon Ave	USC	90025	34.004	118.230	Holo		Alluvium	DOC					
LA	Fletcher Dr	USC	90034	34.115	118.244	Holo		Alluvium	Dibblee Map					
LA	Hollywood Stor FF #	CSMIP, CIT	24303, 135	34.090	118.339	Holo	Coarse	Alluvial Valley	CDMG, Geomatrix	A	332	D	D	NUREG/CR-0985, V5
LA	Jensen Filter Plant #	USGS	655	34.309	118.499	Holo		Alluvial Fan	CDMG	A	381	C	C2	ROSRINE
LA	LA Dam	USGS	0	34.293	118.484	Tertiary			CDMG	A	640	C	B	USGS OFR 96-740
LA	N Faring Rd	USC	90016	34.089	118.435	Mesoz			CDMG					
LA	N Westmoreland	USC	90021	34.082	118.298	Holo		Alluvial Valley	CDMG	C	314	D	C1	ROSRINE
LA	N. Figueroa St.	USC	90032	34.111	118.189	Holo		Alluvium	Dibblee Map					
LA	Obregon Park #	CSMIP	24400	34.037	118.178	Holo		Alluvial Valley	Geomatrix	A	453	C	C3	ROSRINE
LA	Pico & Sentous	CSMIP	24612	34.043	118.271	Holo		Fill	CDMG	B	393	C	C3-D	Law/Crandall 80268.03
LA	S Grand Ave	USC	90022	34.005	118.279	Holo		Alluvial Valley	CDMG					
LA	S. Vermont Ave (6 story)	USC	90096	34.021	118.287	Holo		Alluvial Valley	CDMG	B	387	C	D	Law/Crandall 78051
LA	Saturn St	USC	90091	34.046	118.355	Holo		Alluvial Valley	CDMG	A	303	D	D	ROSRINE
LA	Sepulveda VA	VA	637	34.249	118.475	Pleist		Alluvial Fan	CDMG	A	370	C	D2	USGS OFR 96-740
LA	Stone Canyon #	MWD	78	36.633	121.234	Tertiary			DOC					
LA	Temple & Hope #	CSMIP	24611	34.059	118.246	Pleist			DOC	B	320	D	C1	Law/Crandall 83282
LA	UCLA Grounds	CSMIP	24688	34.068	118.439	Pleist		Alluvial Valley	CDMG	B	428	C	C2	Law/Crandall 76124
LA	Univ. Hospital	CSMIP	24605	34.062	118.198	Tertiary			DOC	A	329	D	C1	UCB/EERC-97/01
LA	W 15th St	USC	90020	34.045	118.298	Pleist		Alluvial Valley	CDMG					
LA	W 70th St	USC	90023	33.976	118.289	Holo		Alluvial Valley	CDMG					
LA	Wonderland	USC	90017	34.114	118.380	Mesoz			CDMG	A	1309	B	B	ROSRINE
La Canada	Paulette Place	USGS	5408	34.209	118.186	Holo		Alluvial Fan	CDMG	C	488	C	C-D?	NUREG/CR-0055, V2
LA County	Whittier Narrows Dam (upstream)	ACOE	289	34.020	118.053	Holo	Coarse	Alluvial Fan	CDMG					
La Crescenta	New York	USC	90060	34.238	118.254	Pleist			Dibblee Map	B	671	C		UCLA-ENG-7206
La Habra	Briarcliff	USC	90074	33.921	117.973	Holo			CDMG					
La Puente	504 Rimgrove Ave	USC	90072	34.026	117.918	Holo	Fine	Alluvial Fan	CDMG					
Lake Crowley	Long Valley Dam (downstream)	CSMIP	54214	37.588	118.705	Pleist			DOC, Geomatrix					
Lake Crowley	Long Valley Dam (left abutment)	CSMIP	54214	37.588	118.705	Mesoz			DOC, Geomatrix					
Lake Crowley	Shehorn Residence	CSMIP	54T03	37.561	118.743	Mesoz			DOC					
Lake Hughes	#1 - Fire Station #78	CSMIP/CIT	24271	34.674	118.430	Holo	Coarse		Geomatrix	A	457	C	C2	USGS OFR 82-833
Lake Hughes	#12 - Elizabeth Lake	CSMIP/CIT	24607	34.571	118.560	Holo	Coarse		Geomatrix	A	622	C	B	USGS OFR 84-681
Lake Hughes	#4 - Camp Mendenhall (near water tank)	CSMIP/CIT	24469	34.650	118.478	Mesoz			Geomatrix	A	375	C	C2	USGS OFR 82-833
Lake Hughes	#4B - Camp Mendenhall	CSMIP	24523	34.6505	118.4777	Mesoz/Holo ?			CDMG	B	375	C	C2	USGS OFR 82-833
Lake Hughes	#9 - Warm Springs Camp	USGS/CIT	127	34.608	118.558	Holo	Coarse		Geomatrix	A	853	B	B	ROSRINE, Nureg/CR-0055,v1
Lakewood	Del Amo Blvd	USC	90084	33.846	118.099	Holo		Alluvial Valley	DOC					
Lancaster	15th & J, Hospital Grounds	CSMIP	24526	34.6883	118.1572	Holo		Alluvium	CDMG	A	313	D		UCB EERC 97/01
Lancaster	Fox Airfield	CSMIP	24475	34.739	118.214	Holo		Alluvium	CDMG	A	305	D		UCB EERC 97/01
Landers	Fire Station	CSMIP	22t13	34.274	116.392	Holo	Coarse		Geomatrix					
Lawndale	Osage Ave	USC	90045	33.897	118.346	Pleist		Alluvial Valley	CDMG					
Leona Valley	#1	CSMIP	24305	34.594	118.242	Pleist			Bray					
Leona Valley	#2	CSMIP	24306	34.595	118.243	Holo			Bray					
Leona Valley	#4	CSMIP	24308	34.598	118.242	Pleist			Bray					

Leona Valley	#5	CSMIP	24055	34.600	118.241	Holo			Bray					
Leona Valley	#6	CSMIP	24309	34.604	118.244	Holo			Bray					
Littlerock	Post Office	USGS	5030	34.5213	117.9917	Holo		Alluvium	CDMG	A	436	C		USGS OFR 82-833
Livermore	Fagundes Ranch	CSMIP	57528	37.753	121.772	Holo		Alluvial Fan	DOC					
Livermore	Morgan Territory Park	CSMIP	Temp	37.819	122.215	Mesoz			DOC	C	893	B		AA 9225-6427, USGS OFR 93-502
Long Beach	City Hall	CSMIP	14560	33.768	118.195	Pleist		Alluvial Valley	CDMG, Geomatrix	B	347	D	C3-D	USGS OFR 80-378
Long Beach	Harbor Plaza	CSMIP	14395	33.754	118.200	Holo	Coarse	Fill	CDMG, Geomatrix	A	247	D	D?	UCB EERC-97/01
Long Beach	Orange Ave.	USC	90080	33.881	118.176	Holo	Coarse	Alluvial Valley	CDMG					
Long Beach	Rancho Los Cerritos	CSMIP	14242	33.840	118.194	Pleist	Coarse	Alluvial Valley	CDMG, Geomatrix	C	271	D	C3-D	Law/Crandall 85005-858
Long Beach	Recreation Park	CSMIP	14241	33.778	118.133	Pleist	Coarse	Alluvial Valley	CDMG, Geomatrix	B	302	D	C3-D?	Law/Crandall 79207
Long Valley	Fire Station	USC	35	37.568	118.748	Holo		Alluvial Fan	DOC					
Los Banos		CSMIP	56012	37.106	120.825	Holo			CDMG					
Los Gatos	LGPC	UCSC	16	37.022	122.010	Tertiary			DOC					
Malibu	Point Dume School	CSMIP	24396	34.077	118.800	Tertiary			Dibblee Map					
Malibu	W. Pacific Coast Hwy	USC	90051	34.024	118.788	Pleist			Dibblee Map					
Mammoth Lakes	Sheriff Substation	CSMIP	54T04	37.638	118.892	Tertiary			DOC					
Manhattan Beach	Manhattan	USC	90046	33.886	118.389	Holo	Coarse	Aeolian	CDMG					
Mecca	CVWD Yard	CSMIP	11625	33.564	115.987	Holo		Alluvial Fan	DOC					
Mojave	Hwys 14 and 58	CSMIP	34093	34.070	118.175	Holo		Alluvium	Dibblee Map					
Montebello	Bluff Rd	USC	90011	33.990	118.114	Pleist	Fine	Alluvial Fan	CDMG					
Monterey	City Hall	CSMIP	47377	36.597	121.897	Mesoz			DOC, Geomatrix	A	655	C	C1	AA 9225-6427
Monterey Park	Garvey Resevoir (abutment building)	MWD	709	34.050	118.110	Tertiary			CDMG, Geomatrix	B	393	C	C1	Stokoe SASW (1995)
Moorpark	Fire Station	CSMIP	24283	34.288	118.881	Holo/Pleist ?		Alluvium	Dibblee Map					
Morongo Valley	Fire Station	USGS	5071	34.0486	116.5781	Holo		Alluvium	CDMG					
Mt. Wilson	CIT Seism. Sta #	CSMIP	24399	34.224	118.057	Mesoz			CDMG, Geomatrix				B	UCLA 62-55
N. Hollywood	Coldwater Canyon	USC	90009	34.194	118.412	Holo		Alluvial Fan	CDMG					
Neenach	Sacatara Ck.	CSMIP	24586	34.848	118.536	Holo		Alluvium	CDMG					
Newhall	LA County Fire Station	CSMIP	24279	34.390	118.530	Holo		Alluvial Fan	CDMG	A	273	D	C2	ROSRINE
Newhall	W Pico Canyon	USC	90056	34.391	118.622	Holo		Alluvial Fan	CDMG	A	279	D	C2	ROSRINE
Newport Beach	Irvine Ave	CSMIP	13160	33.634	117.902	Pleist	Coarse	Marine	CDMG					
Newport Beach	Newport Blvd. & Coast Highway	CSMIP	13610	33.623	117.931	Holo	Coarse	Aeolian	CDMG				C2	UCB/EERC-97/01 A31
Niland	Fire Station	CSMIP	11023	33.239	115.512	Holo	Aggregate		Geomatrix					
North Palm Springs	Post Office	USGS	5070	33.9246	116.5436	Holo		Alluvium	CDMG	A	384	C	D	Rosrine
Northridge	17645 Saticoy St	USC	90003	34.209	118.517	Pleist		Alluvial Fan	CDMG	A	280	D	D1	USGS OFR 96-740
Norwalk	12400/12440 Imperial Highway - FF1	USGS	634	33.916	118.065	Holo	Coarse	Alluvial Valley	CDMG, Geomatrix	A	266	D	D	UCB EERC-97/01
Oakland	Outer Harbor Wharf	CSMIP	58472	37.816	122.314	Holo	Coarse	Marine	DOC, Geomatrix	A	248	D	D1	USGS OFR 92-287
Oakland	Title & Trust Bldg.. (2-story)	CSMIP	58224	37.806	122.267	Holo	Coarse	Aeolian	DOC	A	302	D	D1	UJLPE/BCS/CURe 16
Oroville	Aiport	CIT	1545	39.496	121.614	Pleist			DOC					
Oroville	Duffy Residence	CDMG	1550	39.445	121.574	Pleist			DOC					
Oroville	DWR Garage	CIT	1543	39.510	121.504	Mesoz			DOC					
Oroville	Johnson Ranch	CDMG	1493	39.425	121.521	Tertiary			DOC					
Oroville	Medical Center	CIT	1544	39.507	121.541	Tertiary			DOC					
Oroville	Pacific Heights	CDMG	1549	39.456	121.603	Pleist			DOC					
Oroville	Seismograph Station	CDWR	1051	39.550	121.500	Mesoz			DOC, Geomatrix				B	USGS OFR 78-1005
Oroville	Summit Ave	CDMG	1551	39.449	121.490	Tertiary			DOC					
Oroville	Up & Down Café	CDMG	1546											
Pacific Palisades	Sunset Blvd	USC	90049	34.042	118.554	Tertiary			CDMG					
Pacoima	Pacoima Dam (downstream)	CSMIP/CIT	24207	34.334	118.396	Mesoz			CDMG, Geomatrix	A	1859	A	B	ROSRINE
Pacoima	Pacoima Dam (upper left)	CSMIP/CIT	24207	34.334	118.396	Mesoz			CDMG, Geomatrix	A	1859	A	B	ROSRINE
Pacoima	Pacoima Kagel Canyon	CSMIP	24088	34.288	118.375	Tertiary			CDMG, Geomatrix	A	346	D	C1	ROSRINE
Pacoima	Pacoima Kagel Canyon	USC	90005	34.250	118.420	Holo	Coarse	Alluvial Fan	CDMG					
Palm Springs	Aiport	CSMIP	12025	33.829	116.501	Holo	Coarse		Geomatrix					
Palmdale	Fire Station	USGS	262	34.580	118.110	Holo	Coarse		Geomatrix	A	497	C	D	USGS OFR 82-833
Palmdale	Hotel free field	CSMIP	24521	34.581	118.135	Holo/Pleist ?			CDMG	A	558	C	D	USGS OFR 82-833, UCB EERC-97/01
Palo Alto	1900 Embarcadero (2-story)	CSMIP	58264	37.453	122.112	Holo	Fine	Marine	DOC, Geomatrix	A	207	D\F	E	USGS OFR 93-376
Palo Alto	Stanford Park Garage	USGS	17	37.432	122.172	Pleist		Alluvium	DOC					
Palo Alto	Stanford Univ. - SLAC Test Lab	USGS	1601	37.419	122.205	Tertiary			DOC, Geomatrix	A	427	C	C2	USGS OFR 94-222
Palos Verdes*	Estates - Via Tejon	USGS/CIT	411	33.801	118.387	Pleist	Coarse	Aeolian	CDMG	A	259	D	C2	USGS OFR 84-681
Pasadena	535 S. Wilson	USGS	5291	34.136	118.127	Pleist		Alluvial Fan	CDMG	A	411	C	D	NUREG-0029, V2
Pasadena	CIT Athenaeuem	CDMG	80053	34.139	118.121	Holo	Coarse		Geomatrix	A	427	C	D3	USGS OFR 84-681
Pasadena	CIT Keck Lab	CDMG	80049	34.200	118.170	Holo		Alluvial Fan	CDMG	B	488	C	D2	NUREG/CR-0055, V2
Pasadena	N Sierra Madre	USC	90095	34.168	118.078	Holo	Coarse	Alluvial Fan	CDMG					
Pearblossom	Pallet Creek	CSMIP	23584	34.458	117.909	Holo	Coarse		DOC					
Pearblossom*	Pumping Plant	CIT	269	34.500	117.920	Pleist/Mesoz ?			CDMG	A	530	C	C2	USGS OFR 82-833
Petrolia	Cape Mendocino	CSMIP	89005	40.348	124.352	Mesoz			DOC, Geomatrix					

Petrolia		CSMIP	89156	40.324	124.286	Holo	Fine		DOC, Geomatrix	A	343	D	C2	NUREG/CR-0985, V5
Phelan	Wilson Ranch	CSMIP	23597	34.467	117.520	Holo		Alluvium	CDMG					
Piedmont	Piedmont Junior High	CSMIP	58338	37.823	122.233	Mesoz			DOC	A	893	B	B	AA 9225-6427
Plaster City	Storehouse	USGS	5052	32.790	115.860	Holo	Aggregate	Alluvium	DOC, Geomatrix					
Playa Del Rey	Saran	USC	90047	33.960	118.432	Holo	Coarse	Aeolian	CDMG					
Pleasant Valley	Pumping Plant	USGS	1162	36.308	120.249	Holo	Aggregate	Alluvial Fan	DOC, Geomatrix	A	250	D	D3	Sholtis (1999)
Point Bonita		CSMIP	58043	37.820	122.520	Mesoz			DOC	A	1303	B	B	AA 9225-6427
Point Mugu	Laguna Peak	CSMIP	25148	34.109	119.065	Tertiary			Dibblee Map					
Pomona	4th & Locust	CSMIP	23525	34.056	117.748	Holo		Alluvial Fan	DOC				D	UCB/EERC-97/01
Port Hueneme	Naval lab	CSMIP	25281	34.145	119.206	Holo		Alluvium	CDMG	A	433	C	D2	UCLA Rpt. 62-55
Rancho Cucamonga	Law and Justice Center Parking Lot	CSMIP	23497	34.104	117.574	Holo	Coarse		Geomatrix	A	404	C	D	UCB/EERC-97/01 A37
Rancho Palos Verdes	30840 Hawthorne Blvd.	CSMIP	14404	33.746	118.396	Tertiary			CDMG					
Rancho Palos Verdes	Luconia	USC	90044	33.740	118.335	Tertiary			CDMG					
Redwood City	APEEL Array Stn. 2	USGS	1002	37.520	122.250	Holo	Fine	Marine	DOC, Geomatrix	A	136	E\F	E	USGS OFR 93-376
Richmond	City Hall Parking Lot	CSMIP	58505	37.935	122.342	Holo		Alluvial Fan	DOC	A	271	D	C3	AA 9225-6427
Rinaldi	Receiving Station	DWP	5968 (77)	34.281	118.477	Pleist	Coarse	Alluvial Fan	CDMG	A	334	D	C2	USGS OFR 96-740
Rio Dell	Hwy 101/ Painter St. Overpass	CSMIP	89324	40.503	124.100	Holo		Alluvial Fan	DOC, Geomatrix					
Riverside	Airport	CSMIP	13123	33.951	117.446	Pleist		Alluvium	CDMG					
Rolling Hills	Rancho Vista School	CSMIP	14405	33.787	118.356	Tertiary			CDMG					
Rosamond	Aiport	CSMIP	24092	34.870	118.206	Holo		Alluvium	CDMG					
Rosamond	Godde Ranch	CSMIP	24274	34.827	118.265	Holo		Alluvium	CDMG					
Salinas	John and Work St	CSMIP	47179	36.671	121.642	Holo		Alluvial Fan	DOC					
Salton City		CSMIP	11628	33.280	115.984	Holo		Alluvial Fan	DOC					
Salton Sea	Salton Sea State Park HQ	CSMIP	11613	33.504	115.913	Holo		Lacustrine	DOC					
Salton Sea	Salton Sea Wildlife Refuge	USGS	5062	33.178	115.615	Holo	Fine		Geomatrix	A	171	E	E	USGS OFR 84-562
Salton Sea	Wildlife Liquefaction array	USGS	5210	33.100	115.530	Holo		Lacustrine	DOC					
San Bernadino	2nd & Arrowhead	CSMIP	23522	34.1030	117.2892	Holo		Alluvium	CDMG	A	460	C	D	UCB/EERC-97/01, UCLA Rpt.62-55
San Bernadino	CSUSB Grounds	CSMIP	23672	34.1834	117.3222	Holo			CDMG	B			C?	UCB/EERC-97/01
San Bernadino	E & Hospitality	CSMIP	23542	34.065	117.289	Holo		Alluvium	DOC	A			D	UCB/EERC-97/01
San Bernadino	Mill Creek Ranger Station	UGSS	5076	34.080	117.114	Holo		Alluvium	CDMG					
San Bernadino	Mill Creek, Angeles Nat'l Forest	USC	90062	34.389	118.080	Mesoz			CDMG					
San Diego	San Diego Gas & Electric Bldg.	CSMIP/CIT	03300/277	32.719	117.163	Pleist		Marine	DOC	C	326	D	C3-D	Law/Crandall 79300
San Dimas	Puddingstone Dam	CSMIP/CIT	23328	34.091	117.808	Tertiary			CDMG, Geomatrix				B	NUREG/CR-0055, V2
San Francisco	Cliff House	CSMIP	58132	37.780	122.510	Mesoz			DOC	C	527	C	C2	UJLPE/BCS/CURe 28
San Francisco	Diamond Heights	CSMIP	58130	37.740	122.430	Mesoz			DOC	A	572	C	C1	AA 9225-6427
San Francisco	Golden Gate Bridge	USGS	1678	37.806	122.472	Mesoz			DOC					
San Francisco	International Airport	CSMIP	58223	37.622	122.398	Holo		Fill	DOC	A	227	D\F	E	USGS OFR 92-287
San Francisco	Pacific Heights	CSMIP	58131	37.790	122.430	Mesoz			DOC	A	1241	B	B	AA 9225-6427
San Francisco	Presidio	CSMIP	58222	37.792	122.457	Mesoz			DOC	A	597	C	B	USGS OFR 93-376
San Francisco	Rincon Hill	CSMIP	58151	37.790	122.390	Mesoz			DOC	A	875	B	B	AA 9225-6427
San Francisco	Telegraph Hill	CSMIP	58133	37.800	122.410	Mesoz			DOC	A			B	UJLPE/BCS/CURe 27
San Francisco*	Golden Gate Park	USGS	1117	37.770	122.478	Holo		Aeolian	DOC	A	914	B	B	USGS OFR 77-850
San Gabriel	E Grand Ave	USC	90019	34.091	118.093	Pleist	Fine	Alluvial Fan	CDMG					
San Jacinto	CDF Fire Station	CSMIP	12673	33.787	116.958	Holo		Alluvium	CDMG					
San Jacinto	Soboba	CSMIP	12204	33.797	116.880	Pleist			CDMG					
San Jacinto	Valley Cemetery	CSMIP	12202	33.760	116.960	Holo		Alluvium	CDMG					
San Juan Bautista	24 Polk St.	CDMG	1377	36.860	121.540	Pleist			DOC					
San Marino	SW Academy	CSMIP	24401	34.115	118.130	Pleist			Geomatrix	C	328	D	D?	Law/Crandall 85240
San Martin	Coyote Lake Dam (abutment)	CSMIP	57217	37.118	121.550	Holo	Coarse	Landslide	DOC, Geomatrix					
San Martin	Coyote Lake Dam (downstream)	CSMIP	57504	37.124	121.551	Holo	Coarse		DOC, Geomatrix					
San Onofre*	Nuclear Power Plant	CIT	280	33.367	117.555	Tertiary			CDMG	B			C2	NUREG/CR-0055, V2
San Pedro	Palos Verdes	CSMIP	14159	33.722	118.309	Tertiary			CDMG					
San Ramon	Kodak Bldg.	CSMIP	57187	37.729	121.928	Holo		Alluvial Fan	DOC					
Sandberg	Bald Mtn	CSMIP	24644	34.743	118.724	Mesoz			CDMG					
Santa Ana	Orange County Resevoir Abutment	USGS	697	33.936	117.884	Tertiary			Geomatrix					
Santa Barbara	Courthouse	USGS	283	34.420	119.700	Holo	Aggregate		Geomatrix	A	392	C	D1	NUREG-0029, V2
Santa Barbara	UCSB Goleta	CSMIP	25091	34.422	119.851	Holo	Coarse		Geomatrix	C	351	D	D	Law/Crandall 80172
Santa Clara County	Anderson Dam (downstream)	USGS	1652	37.166	121.628	Pleist	Aggregate		DOC	A	491	C	C2	USGS OFR 94-552
Santa Clara County	Anderson Dam (left abutment)	USGS	1652	37.166	121.628	Mesoz			DOC, Geomatrix					
Santa Cruz	UCSC/ Lick Obs. Elect. Lab	CSMIP	58135	37.001	122.060	Mesoz			DOC	A	732	C	B	AA 9225-6427
Santa Fe Springs	E. Joslin	USC	90077	33.944	118.087	Holo	Coarse	Alluvial Fan	CDMG					
Santa Monica	City Hall	CSMIP	24538	34.011	118.490	Holo			DOC	A	312	D	D3	Stokoe SASW (1995), Chang(1996)
Santa Monica	Second St.	USC	90048	34.005	118.485	Pleist		Marine	CDMG	C	411	C	D	USGS OFR 82-833
Santa Susana	ETEC, Freefield	USGS	5108	34.230	118.710	Mesoz			CDMG	A	914	B	B	ROSRINE
Saratoga	Aloha Ave	CSMIP	58065	37.255	122.031	Tertiary			DOC, Geomatrix					

Saratoga	W. Valley College (1-story Gym)	CDMG	58235	37.262	122.009	Pleist	Coarse	Alluvial Fan	DOC, Geomatrix					
Seal Beach	Office Bldg #	CSMIP	14578	33.757	118.084	Pleist			DOC	A	279	D	D	Law/Crandall 86097
Shelter Cove	Airport	CSMIP	89530	40.026	124.069	Mesoz			DOC, Geomatrix					
Silent Valley	Poppet Flat	CSMIP	12206	33.851	116.852	Mesoz			Geomatrix					
Simi Valley	Katherine Road	USC	90055	34.264	118.666	Holo		Alluvial Fan	CDMG	A	579	C	C2	USGS OFR 96-740
Slack Canyon		CDMG	46175	36.034	120.590	Mesoz			DOC, Geomatrix					
So. San Francisco	Sierra Point	CSMIP	58539	37.674	122.388	Mesoz			DOC	A	1018	B	B	AA 9225-6427
Studio City	Coldwater Canyon	USC	90010	34.146	118.412	Holo		Alluvial Fan	CDMG					
Sun Valley	Glenoaks	USC	90008	34.235	118.366	Holo		Alluvium	Dibblee Map					
Sun Valley	Roscoe Blvd	USC	90006	34.221	118.421	Holo	Coarse	Alluvial Fan	CDMG					
Sunland	Mt. Gleason Ave	USC	90058	34.269	118.303	Holo	Coarse	Alluvial Fan	CDMG					
Sunnymead		USGS	5038	33.946	117.1508	Holo		Alluvium	CDMG					
Sunnyvale	Colton Ave	USGS	1695	37.402	122.024	Holo	Coarse	Alluvial Valley	DOC, Geomatrix	A	268	D	D1	USGS OFR 94-222
Superstition Mtn	USAF Camera Site	USGS/CIT	286	32.920	115.820	Mesoz			DOC					
Sylmar	Converter Station	DWP	74	34.312	118.489	Holo	Coarse	Alluvial Fan	CDMG	A	256	D	C2	ROSRINE
Sylmar	Converter Station East	DWP	75	34.313	118.485	Holo	Coarse	Alluvial Fan	CDMG	A	375	C	C2	ROSRINE
Sylmar	Olive View Med FF	CSMIP	24514	34.326	118.444	Holo		Fill	CDMG, Geomatrix	A	357	D	D	USGS OFR 96-740
Sylmar	Sayre St	USC	90001	34.306	118.437	Holo	Coarse	Alluvial Fan	CDMG	B	328	D	C3-D	UCLA-ENG-7206
Tabas	Bajestan		69			Holo	Coarse		Ref 2					
Tabas	Boshrooyeh		70			Holo	Coarse		Ref 2					
Tabas	Dayhook		9102			Tertiary			Ref 2					
Tabas	Ferdows		71			Holo	Coarse		Ref 2					
Tabas	Kashmar		72			Holo	Coarse		Ref 2					
Tabas	Sedeh		73			Holo	Coarse		Ref 2					
Tabas	Tabas		9101			Holo	Coarse		Ref 2					
Taft*	Taft High	CIT	94	35.146	119.459	Holo	Coarse		Geomatrix	A	386	C	D1	NUREG-0029,V2
Tarzana	Cedar Hill Nursery	CSMIP	24436	34.160	118.534	Tertiary			CDMG, Geomatrix	A	309	D	C2	ROSRINE
Tehachapi*	Pumping Plant	CIT	27	34.942	118.827	Holo/Oligocene/Mesoz ?			CDMG	A	671	C	C1	USGS OFR 84-681
Tejon*	Fort Tejon	CIT	96	34.870	118.900	Mesoz/Holo ?			CDMG	A	396	C	C2	USGS OFR 84-681
Temecula	6th & Mercedes/CDF Fire Station	CSMIP	13172	33.496	117.149	Holo/Pleist ?			CDMG					
Terminal Island	S Seaside	USC	90082	33.765	118.225	Holo	Coarse	Fill	CDMG				D3	UCLA Rpt. 62-55
Terwilliger Valley	Snodgrass Residence	USGS	5045	33.4797	116.5874	Mesoz			CDMG					
Tinehama Resevoir	Free Field	CSMIP	54101	37.054	118.229	Holo		Alluvial Fan	DOC					
Topanga	Fire Station	USGS	5081	34.084	118.600	Holo		Land Slide	CDMG					
Torrance	W 226th St	USC	90038	33.822	118.356	Holo		Alluvial Valley	CDMG					
Tracy	Sewage Plant	CSMIP	57458	37.766	121.421	Pleist		Marine	DOC					
Tracy	Sewage Plant	CSMIP	63	37.766	121.421	Pleist		Marine	DOC					
Treasure Island	Naval Base Fire Station	CSMIP	58117	37.825	122.373	Holo		Fill	DOC	A	174	E\F	E\F	USGS OFR 92-287
Turkey	Ambarli Termik Santrali	Kandilli		40.981	28.692	Tertiary			MTA-Turkey	A	175	E	C2-C3	Rathje 2000
Turkey	Arcelik ARGE Lab.	Kandilli								A	380	C	C2-C3	Rathje 2000
Turkey	Atakoy	ITU								A		D	D	Rathje 2000
Turkey	Balikesir Huzur Evi	ERD		39.650	27.857	Mesoz			MTA-Turkey					
Turkey	Bolu Bayindirlik ve Iskan Mudurlugu	ERD		40.745	31.610	Pleist			MTA-Turkey	A	290	D	D	Rathje 2000, DSI
Turkey	Botas	Kandilli		40.993	27.979	Tertiary			MTA-Turkey					
Turkey	Bursa Sivil Savunma Mudurlugu	ERD		40.183	29.131	Holo			MTA-Turkey					
Turkey	Cekmece Nukleer Santral Binasi	Kandilli		41.025	28.759	Tertiary			MTA-Turkey	A	300	D		Rathje 2000
Turkey	Cekmece Nukleer Santral Binasi(silva)	ERD		40.970	28.700	Tertiary			MTA-Turkey	A	300	D		Rathje 2000
Turkey	Duzce Meteoroloji Istasyonu	ERD		40.844	31.149	Holo			MTA-Turkey	A	275	D	D1-D2	Rathje 2000, DSI
Turkey	Fatih Tur.	Kandilli		41.054	28.950	Tertiary			MTA-Turkey					
Turkey	Gebze Tubitak Marmara Aras, Merkezi	ERD		40.820	29.440	Tertiary			MTA-Turkey	A	750	C	A-B	Rathje 2000
Turkey	Goynuk Devlet Hastanesi	ERD		40.396	30.783	Mesoz			MTA-Turkey					
Turkey	Havaalani	Kandilli		40.982	28.820	Pleist			MTA-Turkey					
Turkey	Istanbul Bayindirlik ve Iskan Mudurlugu	ERD		41.058	29.013	Tertiary			MTA-Turkey				B-C2	MTA-Turkey
Turkey	Izmit Meteoroloji Istasyonu	ERD		40.790	29.960	Tertiary			MTA-Turkey	A	800	B	A-B	Rathje 2000
Turkey	Iznik Karayollari Sefligi	ERD		40.440	29.750	Holo			MTA-Turkey	A	225	D		Rathje 2000
Turkey	Kutahya Sivil Savunma Mudurlugu	ERD		39.419	29.997	Tertiary			MTA-Turkey					
Turkey	Lam0362	Lamont								A	600	C	A-B	Rathje 2000
Turkey	Lam1058	Lamont								A	450	C	A-B	Rathje 2000
Turkey	Lam1060	Lamont								A	800	B	A-B	Rathje 2000
Turkey	Lam1061	Lamont								A	450	C	C2-C3	Rathje 2000
Turkey	Maslak	ITU								A		B	A-B	Rathje 2000
Turkey	Mecidiyekoy	ITU								A		C	C2-C3	Rathje 2000
Turkey	Sakarya Bayindirlik ve Iskan Mudurlugu	ERD		40.737	30.384	Mesoz			MTA-Turkey	A	470	C	C2	Rathje 2000
Turkey	Yarimca Petkim	Kandilli		40.764	29.762	Holo			MTA-Turkey	A	300	D	D	Rathje 2000
Turkey	Zeytinburnu	ITU								A	230	D		Rathje 2000
Tustin	Sycamore	USC	90089	33.728	117.824	Holo	Coarse	Alluvial Fan	CDMG					
Twentynine Palms	Park Maint. Bldg.	CSMIP	22161	34.021	116.009	Mesoz			Geomatrix					

Upper Crystal Springs Res.	APEEL 10; Skyline Blvd.	CSMIP	58373	37.465	122.343	Tertiary			DOC, Geomatrix	A	320	D	C1	USGS OFR 79-1619
Upper Crystal Springs Res.	APEEL 7; Pulgas Temple	CSMIP	58378	37.490	122.310	Tertiary			DOC, Geomatrix	A	413	C	C1	USGS OFR 91-311
Ventura	Harbor and California	CSMIP	25340	34.2766	119.2942	Holo			Dibblee Map	A	309	D		UCB/EERC-97/01
Villa Park	Serrano Ave	USC	90090	33.821	117.818	Holo	Aggregate	Alluvial Fan	CDMG					
West Covina	S. Orange Ave	USC	90071	34.064	117.952	Holo	Coarse	Alluvial Fan	CDMG					
Westmorland	Fire Station	CSMIP	11369	33.037	115.623	Holo	fine		Geomatrix					
Wheeler Ridge*	Tejon Hills oil Field	CIT	102	35.027	118.791	Holo/Pleist ?			CDMG					
Whittier	S. Alta Drive	USC	90075	34.015	118.029	Tertiary			CDMG					
Whittier	Whittier Narrows Dam (baseyard)	USGS/CIT	289	34.030	118.050	Holo	Coarse	Lacustrine	CDMG, Geomatrix					
Winchester	Bergman Ranch	CSMIP	13199	33.640	117.094	Mesoz			CDMG					
Winchester	Page Bros. Ranch	CSMIP	13201	33.718	117.022	Holo			Geomatrix					
Woodside	Fire Station	CSMIP	58127	37.429	122.258	Tertiary			DOC	A	454	C	B	USGS OFR 93-376
Wrightwood	Jackson Flat	CSMIP	23590	34.381	117.737	Mesoz			CDMG					
Wrightwood	Nielson Ranch	CSMIP	23573	34.314	117.545	Holo			CDMG					
Wrightwood	Swarthout	CSMIP	23574	34.369	117.658	Holo			CDMG					
Yerba Buena Island	USCG Foghorn Bldg.	CSMIP	58163	37.810	122.360	Mesoz			DOC	A	576	C	C1	USGS OFR 92-287
Yermo	Fire Station	CSMIP	22074	34.903	116.823	Holo			Geomatrix	A	354	D	D	ROSRINE
	Agragrias	UNAM	6618	32.620	115.300	Holo	Aggregate		Geomatrix					
	Cerro Prito	UNAM	6604	32.420	115.300	Tertiary			Geomatrix					
	Chihuahua	UNAM	6621	32.480	115.230	Holo	Aggregate		Geomatrix					
	Compuertas	UNAM	6622	32.370	115.080	Holo	Aggregate		Geomatrix					
	Delta	UNAM	6605	32.350	115.180	Holo	fine		Geomatrix					
	McGee Creek	USC	45	37.553	118.793	Holo		Alluvium	DOC					
	McGee Creek	USC	52	37.553	118.793	Holo								
	Oil Fields Fire Station	USGS	1608	36.247	120.314	Tertiary			DOC					
	Palmer Ave	USGS	1609	36.209	120.292	Tertiary			DOC					
	San Justo Dam	USGS	1655	36.815	121.447	Pleist	Aggregate		DOC, Geomatrix					
	Santa Felicia Dam (Outlet)	CIT	285							A	326	D	C2	NUREG/CR-0055, V2, Law/Crandall 81259
	Victoria	UNAM	6610	32.289	115.103	Holo	Aggregate		Geomatrix					
	WAHO	UCSC	14	36.970	121.995	Holo		Marine	DOC					

[1] Boring-SMA distance index: A = < 150 m; B = 150 - 450 m; C = 450 - 1600 m

1: Fukushima et al., 2000

2: Shoja-Taheri and Anderson, 1988

Rathje 2000 = personal communication

References

Appendix B Classification of Strong Motion Accelerograph Sites Not Used in This Study

Location	Station Name	Agency	Station #	Latitude	Longitude	Geology				30-m V_s and Geotechnical Data				
						Age	Grain Size	Depositional History	Reference	Boring	V_s (m/s)	NEHRP	Geot.	Reference
Alhambra	900 South Fremont Ave	USGS/CIT	482	34.090	118.150	Holo	Coarse		Geomatrix	B	421	C	C3-D	USGS OFR 82-833
Almiros	Almiros													
Alpine	Fire Station	CSMIP	02467	32.838	116.724	Mesoz			DOC					
Anaheim	Lakeview & Riverdale	CSMIP	13849	33.854	117.817	Holo	Coarse	Alluvial Fan	CDMG					
Antellope Buttes		CSMIP	24310	34.7580	118.3610	Mesoz/Holo ?			CDMG					
Anza	Anza Fire Station	USGS	5160	33.555	116.661	Holo/Mesoz ?			CDMG					
Anza	Rancho de Anza	USGS		33.3484	116.4005	Holo/Mesoz ?			CDMG					
Anza	Tule Canyon	USGS	5231	33.4618	116.6452	Pleist/Mesoz ?			CDMG					
Anza*	Post Office	CIT	103	33.556	116.674	Holo/Mesoz ?			CDMG					
Banning	Twin Pines Rd.	CSMIP	12674	33.869	116.824	Mesoz/Holo ?			CDMG					
Bear Valley	Stn. 10; Webb Residence	USGS	1479	36.532	121.143	Holo		Alluvium	DOC	A	305	D	C2	USGS OFR 94-552
Bear Valley	Stn. 12; Williams Ranch	USGS	1481	36.658	121.249	Holo		Alluvial Fan	DOC	A	332	D	D1C	USGS OFR 94-552
Bear Valley	Stn. 3; Almaden G H	USGS	1472	36.670	121.280	Mesoz			DOC					
Bear Valley	Stn. 5; Callens Ranch	USGS	1474	36.673	121.195	Pleist			DOC	A	381	C	C2	USGS OFR 94-552
Bear Valley	Stn. 7; Pinnacles Nat'l mon.	USGS	1476	36.483	121.180	Tertiary			DOC				B	USGS OFR 91-311
Berkeley	2168 Shattuck Ave. (bsmt east)	USGS	1103	37.870	122.270	Pleist		Alluvial Fan	DOC					
Berkeley	Hospital (2 story)	CSMIP	58496	37.855	122.256	Pleist		Alluvial Fan	DOC				C ?	USGS OFR 91-311
Berkeley	UCB Memorial Stadium Grounds	CSMIP	58000	37.870	122.250	Pleist		Alluvial Fan	DOC	A	479	C	C1	AA 9225-6427
Berkeley	UCB-Haviland Hall (bsmt)	USGS	1006	37.870	122.260	Tertiary			Boring	A	1219	B	B	AA 9225-6427
Berkeley	UCB-Strawberry Cyn.	USGS	1005	37.870	122.240	Mesoz			DOC					
Beverly Hills*	435 Oakhurst	CIT	452	34.078	118.391	Holo	Fine	Alluvial Valley	CDMG, Geomatrix	C	320	D	C2-D	Law/Crandall 83053
Beverly Hills*	450 N. Roxbury	CIT	455	34.069	118.406	Holo	Aggregate	Alluvial Valley	CDMG, Geomatrix	C	320	D	C2-D	Law/Crandall 83053
Beverly Hills*	9100 Wilshire	CIT	416	34.066	118.389	Holo	Fine	Alluvial Valley	CDMG, Geomatrix					
Big Bear Lake	Civic Center Grounds	CSMIP	22561	34.238	116.935	Holo/Mesoz ?			CDMG					
Big Dalton	Big Dalton Dam	CSMIP	23247	34.170	117.808	Holo		Fill	CDMG					
Big Sur	Pfeiffer State Park	CSMIP	47136	36.255	121.782	Mesoz			DOC					
Bishop	North Main Street Office Building	CSMIP	54388	37.370	118.396	Holo		Alluvial Fan	DOC					
Bitterwater Valley		CDMG/CSMI	46173	36.395	120.982	Tertiary			DOC					
Blythe	Fire Station	CSMIP	10021	33.611	114.710	Holo		Alluvial Valley	DOC					
Bodega Head	Doran Beach	CSMIP	69039	38.311	123.052	Holo	Coarse	Wind Blown	DOC					
Bunker Hill		USGS		40.498	124.294	Mesoz			DOC					
Burbank	Airport	USGS	5398	34.195	118.3583	Holo		Alluvium	Dibblee Map					
Burbank	Cal. Fed. Savings (6-story)	CSMIP	24370	34.185	118.308	Holo			Geomatrix	B	445	C	C2-D	Law/Crandall 78188
Calaveras	Calaveras Resevoir S.	USGS	1687	37.452	121.807	Holo		Alluvium	DOC, Geomatrix	A	480	C	D2S	USGS OFR 94-552
Castaic	Halsey Canyon	CSMIP	24277	34.459	118.650	Holo/Plio-Pleist ?			CDMG					
Cedar Springs*	Abutment	CIT	112											
Centerville		CSMIP	45045	36.734	119.486	Holo		Alluvial Fan	DOC					
Centerville Beach		USGS		40.563	124.348	Holo		Nonmarine	DOC					
Cherry Flat	Calaveras Array - Resevoir	USGS	1696	37.396	121.756	Mesoz			DOC, Geomatrix				B	USGS OFR 91-311
Cholame *	Temblor II	CIT	97	35.752	120.264	Pleist			DOC, Geomatrix	A	518	C	C1	USGS OFR 82-407
Cholame Array	Gold Hill Limb Station 1E	CDMG	36137	35.831	120.353	Mesoz			DOC					
Cholame Array	Stone Corral Limb Station 1E	CDMG	36419	35.788	120.294	Pleist	Aggregate		DOC, Geomatrix					
Cholame Array	Vineyard Canyon Limb Station 3W	CDMG	36176	35.922	120.534	Tertiary		Marine	DOC, Geomatrix					
Coachella Canal	Canal Sta 2 - Demosser	USGS	5064	33.560	115.950	Holo		Alluvial Fan	DOC					
Coachella Canal	Canal Sta 3 - Siphon 24	USGS	5065	33.510	115.770	Holo		Alluvial Fan	DOC					
Colton	1 story School Gym	CSMIP	23540	34.072	117.335	Holo	Coarse	Aeolian	CDMG	C	381	C	D3	Law/Crandall 82224
Colton	Colton Interchange	CDOT	754	34.060	117.300	Holo		Alluvium	DOC	C	314	D	D3	USGS OFR 84-681
Concord	Residential Bldg. (8 story)	CSMIP	58492	37.979	122.032	Holo		Alluvium	DOC					
Coolwater		SCE	23											
Costa Mesa	Fire Station #4 (Placentia)	USGS	5286	33.658	117.931	Pleist	Coarse	Marine	CDMG					
Costa Mesa	John Wayne Airport	USGS	5287	33.677	117.869	Pleist	Fine	Alluvial Valley	CDMG	C	268	D	C3-D	Law/Crandall 79334
Costa Mesa*	666 W 19th Street	CIT		33.644	117.926	Pleist	Coarse	Marine	CDMG				C1	Nureg/CR-0055
Covelo		CSMIP	79036	39.806	123.247	Holo		Alluvium	DOC					
Death Valley	Grapevine	CSMIP	43080	36.983	117.357	Holo		Alluvial Fan	DOC					
Desert Shores		CSMIP	12626	33.426	116.078	Holo		Alluvium	CDMG					
Devore	Devore Water Dept.	USGS	5265	34.235	117.407	Holo/Mesoz ?			CDMG					
Dos Amigos	Pumping Plant	CDWR	1142	36.920	120.830	Tertiary			DOC					
Dublin	Calaveras Array - Fire Stn.	USGS	1689	37.709	121.932	Holo		Alluvium	DOC					
East LA	La Calandria Wy	USGS	5396	34.072	118.176	Tertiary			DOC					
El Centro	Array 12 - 907 Brockman Rd	USGS	931	32.720	115.640	Holo	Fine	Lacustrine	DOC, Geomatrix	A	209	D	D	USGS OFR 84-562

El Centro	Array 6 - Huston Rd	USGS	942	32.840	115.490	Holo	Fine	Lacustrine	DOC, Geomatrix	A	203	D	E	USGS OFR 84-562
El Centro	Meadows Union School	USGS	464	32.800	115.470	Holo	Fine	Lacustrine	DOC, Geomatrix					
El Cerrito	Capwell Store (2-story)	CSMIP	58188	37.899	122.298	Holo		Alluvium	DOC					
El Segundo	14 story Office Bldg	CSMIP	14654	33.920	118.390	Holo	Coarse	Aeolian	CDMG	A	338	D	D	Law/Crandall 83307
El Segundo*	909 Sepulveda Blvd	CIT	494	33.927	118.389	Holo	Coarse	Aeolian	CDMG	A	305	D	D	Law/Crandall 88044-22
Elizabeth Lake		CSMIP	24575	34.6620	118.3870	Pliocene/Holo ?			CDMG					
Emeryville	6363 Christie Ave. - gnd. Site. S.	USGS	1662	37.844	122.295	Holo		Alluvial Valley	DOC, Geomatrix	A	198	D\F	E	USGS OFR 94-222
Eureka	5th & H Federal Bldg.	CSMIP	89327	40.802	124.163	Holo	Aggregate	Non-marine	DOC, Geomatrix	A	274	D	D2	NUREG/CR-0055, V3
Fairmont Resevoir	Fairmont Dam Right Abutment	CSMIP	24270	34.704	118.426	Holo	Aggregate		Geomatrix				C1	Nureg/CR-0055
Ferndale	City Hall	USGS	1023	40.566	124.250	Pleist		Alluvial Valley	CDMG, Geomatrix	A	183	D	D2	NUREG-0029, V1
Fillmore		USGS	5401	34.397	118.917	Holo		Alluvium	CDMG					
Forest Falls	Post Office	USGS	5075	34.088	116.921	Holo/Miocene ?			CDMG					
Fort Bragg		CSMIP	79016	39.452	123.803	Holo		Marine	DOC					
Fortuna		USGS		40.599	124.219	Holo		Alluvium	DOC					
Foster City	APEEL 1; Redwood Shores	CSMIP	58375	37.550	122.230	Holo	Fine	Fill	DOC, Geomatrix	A	114	E\F	E	USGS OFR 93-376
Fresno	California State University	SMIP/CDM	45010	36.813	119.746	Pleist		Non-marine	DOC					
Frink		CSMIP	11684	33.398	115.657	Holo		Lacustrine	DOC					
Fullerton*	2600 Nutwood	CIT	476	33.877	117.881	Holo	Fine	Non-marine	CDMG					
Gilroy	Gilroy 4; San Ysidro School	CSMIP	57382	37.005	121.522	Holo	Aggregate	Alluvial Fan	DOC, Geomatrix	A	226	D	D1	USGS OFR 91-311
Glendale*	633 E. Broadway	CIT	122	34.150	118.247	Holo	Coarse	Alluvial Fan	CDMG, Geomatrix	A	387	C	D2	NUREG/CR-0055, V1
Greenfield	Green-field A	CSMIP	47460	36.321	121.243	Holo		Alluvium	DOC					
Hawthorne	FAA Bldg.	USGS	5243	33.896	118.377	Holo	Coarse	Aeolian	CDMG	C	320	D	D	Law/Crandall 88044-04
Hayward	CSUH Science Bldg. (4-story)	CSMIP	58488	37.657	122.053	Mesoz			DOC	C	617	C	C1	USGS OFR 79-1619
Hayward	Southlands office bldg. (6 story)	CSMIP	58462	37.635	122.104	Holo		Alluvium	DOC					
Huntington Bch	18401 Springdale	USGS	p 76	33.697	118.023	Holo	Coarse	Alluvial Fan	CDMG					
Huntington Bch	Adams & Bushard	CSMIP	13887	33.676	117.963	Holo	Coarse	Alluvial Fan	CDMG					
Hyoken-Nanbu	HIK					Holo		Alluvium	Ref. 1					
Hyoken-Nanbu	Takarazuka	CUE				Pleist		Dilluvium	Ref. 1					
Independence	LADWP Building	CSMIP	44298	36.800	118.199	Holo		Alluvium	DOC					
Independence		CSMIP	44102	36.831	118.161	Mesoz			DOC					
Indio	County Services Bldg Grounds	CSMIP	12543	33.714	116.221	Holo			CDMG	A	250	D		UCB EERC 97/01
Inglewood	Hollywood Park	CSMIP	14537	33.952	118.335	Pleist		Alluvial Valley	CDMG	B	332	D	D	Law/Crandall 83199
Irvine	19900 MacArthur Blvd	USGS	80	33.656	117.859	Pleist	Fine	Alluvial Valley	CDMG	B	245	D	C3	Law/Crandall 85213
Irvine	2603 Main Street	USGS	p 75	33.682	117.842	Holo	Fine	Alluvial Fan	CDMG	A	268	D	C3-D	Law/Crandall 84145
Irvine	8-story UCI Engineering Bldg.	CSMIP	13329	33.645	117.840	Tertiary			CDMG					
Joshua Tree	Keys View	CSMIP	12647	33.925	116.172	Mesoz								
June Lake	Fire Station	CSMIP	55429	37.783	119.075	Holo		Glacial	DOC					
Kings Canyon	Cedar Grove	CSMIP	46	36.788	118.674	Holo		Alluvium	DOC					
LA	1100 Wilshire Blvd - Bsmt 3 NE	USGS	5233	34.052	118.263	Pleist		Alluvial Valley	CDMG	A	390	C	C1	Law/Crandall 82247
LA	1111 Sunset Blvd.	MWD	872	34.070	118.250	Tertiary			CDMG	C	320	D	C1	Law/Crandall 83282
LA	12-story Commercial/Office Bldg.	CSMIP	24581	34.048	118.260	Holo		Alluvial Valley	CDMG	A	354	D	C2	Law/Crandall 85310
LA	13-story Office Bldg.	CSMIP	24567	34.050	118.247	Holo		Alluvial Valley	DOC	B	431	C	C2	USGS OFR 82-833
LA	17-story Residential	CSMIP	24601	34.053	118.248	Tertiary			DOC	B	368	C	C1	Law/Crandall 80268.08
LA	1955 1/2 Purdue Ave (bsmt)	USGS		34.040	118.445	Holo	Fine	Alluvial Valley	CDMG	B	285	D	D2	Law/Crandall 84280
LA	2-story fire Command Control Bldg	CSMIP	24580	34.053	118.171	Tertiary			DOC	C	507	C	C1	Law/Crandall 77200
LA	52-story Office Bldg.	CSMIP	24602	34.051	118.259	Holo		Alluvial Valley	CDMG	A	354	D	C1	Law/Crandall 81190
LA	54-story Office Bldg.	CSMIP	24629	34.048	118.260	Holo		Alluvial Valley	CDMG	A	360	D	C2	Law/Crandall 81040
LA	6301 Owensmouth Ave	USGS		34.185	118.584	Holo		Alluvial Fan	CDMG	C	259	D	D?	Law/Crandall 84034
LA	8-story CSULA Admin. Bldg.	CSMIP	24468	34.067	118.168	Tertiary			Geomatrix					
LA	9-story Office Bldg.	CSMIP	24579	34.044	118.261	Holo		Alluvial Valley	CDMG	A	354	D	D	Law/Crandall 85005-037
LA	Bulk Mail Facility	USGS	5129	33.990	118.160	Holo	Coarse	Alluvial Fan	CDMG, Geomatrix	A?	302	D	D2	ROSRINE
LA	Century City Bullock Store (3-story)	CSMIP	24332	34.058	118.417	Holo	Aggregate	Alluvial Valley	CDMG, Geomatrix	B	287	D	D3	Law/Crandall 84277
LA	Chantry flat Forest Station 1	USGS		34.196	118.021	Holo	Fine	Non-marine	CDMG					
LA	Chantry flat Forest Station 2	USGS		34.196	118.021	Holo	Fine	Non-marine	CDMG					
LA	Chantry flat Forest Station 3	USGS		34.196	118.021	Holo	Fine	Non-marine	CDMG					
LA	Griffith Observatory	USGS	141	34.118	118.299	Mesoz			CDMG, Geomatrix	A	783	B	B	USGS OFR 84-681
LA	I10/405 Interchange Bridge	CSMIP	24670	34.031	118.433	Holo		Alluvial Valley	CDMG	C	303	D	D	Law/Crandall 81273
LA	Sears Warehouse (5-story)	CSMIP	24463	34.028	118.223	Holo		Alluvial Valley	Geomatrix					
LA	Sepulveda Canyon Spillway Bldg	USGS	757	34.100	118.480	Mesoz			CDMG					
LA	Subway Terminal			34.050	118.250	Holo	Aggregate	Alluvial Valley	CDMG, Geomatrix	B	431	C	C3-D	USGS OFR 82-833
LA	Vincent Thomas Bridge	CSMIP	14406	33.750	118.271	Holo	Coarse	Alluvial Valley	DOC					
LA	Wadsworth VA Hospital (N gnd)	USGS	5082	34.050	118.452	Pleist		Alluvial Valley	CDMG	A	427	C	C3	ROSRINE
LA	Wadsworth VA Hospital (S gnd)	USGS	5082	34.050	118.452	Pleist		Alluvial Valley	CDMG	A	405	C	D2	ROSRINE
LA County	Leona Valley - Fire Station	USGS	5029	34.620	118.290	Pliocene/Holo ?			CDMG	A	334	D		USGS OFR 82-833
LA County	Sepulveda Dam (downstream)	ACOE	949	34.170	118.470	Holo		Alluvial Fan	CDMG					
LA*	1150 S. Hill	CIT	437	34.044	118.259	Holo		Alluvium	CDMG, Geomatrix	C	329	D	D	Law/Crandall 82264

LA*	11661 San Vicente	CIT	250	34.050	118.450	Pleist		Alluvial Valley	CDMG	C	454	C	D3	Law/Crandall 79189
LA*	1177 Beverly Drive	CIT	413	34.060	118.400	Holo		Alluvial Valley	CDMG, Geomatrix	A	393	C	D	Law/Crandall 80099
LA*	120 N. Robertson	CIT	142	34.070	118.380	Holo	Fine	Alluvial Valley	CDMG, Geomatrix	C	276	D	D	Law/Crandall 76198
LA*	14724 Ventura	CIT	253	34.152	118.455	Holo		Alluvial Fan	CDMG, Geomatrix	C	332	D	C-D?	NUREG/CR-0074
LA*	15250 Ventura	CIT	466	34.154	118.464	Holo	Aggregate	Alluvial Fan	CDMG, Geomatrix	A	296	D	C2	Law/Crandall 81384
LA*	15433 Ventura	CIT	256	34.150	118.470	Holo		Alluvial Fan	CDMG	B	262	D	C2	Law/Crandall 78044
LA*	15910 Ventura	CIT	461	34.160	118.480	Holo	Aggregate	Alluvial Fan	CDMG, Geomatrix	B	302	D	C2	Law/Crandall 79086
LA*	1625 S. Olympic Blvd.	CIT	469	34.049	118.273	Holo	Aggregate	Alluvial Valley	CDMG, Geomatrix	A	366	C	D?	Law/Crandall 78297
LA*	1640 Marengo	CIT	181	34.060	118.213	Holo		Alluvium	Geomatrix	B	320	D	C1	Law/Crandall 78046
LA*	1760 N. Orchid Ave.	CIT	446	34.100	118.330	Holo		Alluvial Valley	CDMG, Geomatrix	B	354	D	D	Law/Crandall 81073
LA*	1800 Century Park E	CIT	425	34.063	118.414	Pleist	Aggregate	Alluvial Valley	CDMG, Geomatrix	A	320	D	D3	NUREG/CR-0074
LA*	1900 Avenue of Stars	CIT	184	34.059	118.415	Pleist	Aggregate	Alluvial Valley	CDMG, Geomatrix	A	287	D	D2	Law/Crandall 84277
LA*	1901 Avenue of Stars	CIT	187	34.053	118.416	Pleist	Aggregate	Alluvial Valley	CDMG, Geomatrix	A	287	D	D2	Law/Crandall 84277
LA*	2011 Zonal	CIT	190	34.050	118.200	Holo	Fine	Alluvium	Geomatrix	B	320	D	C1	Law/Crandall 78046
LA*	222 S. Figueroa (Bunker Hill Towers)	CIT	145	34.050	118.250	Holo	Fine	Alluvial Valley	CDMG, Geomatrix	A	300	D	C1	NUREG/CR-0055, V1
LA*	234 S. Figueroa	CIT	148	34.050	118.250	Holo		Alluvial Valley	CDMG, Geomatrix	A	300	D	C1	NUREG/CR-0055, V1
LA*	250 E. First	CIT	151	34.050	118.241	Holo	Coarse	Alluvium	Geomatrix	A	482	C	C2	Law/Crandall 74024
LA*	2500 Wilshire	CIT	449	34.059	118.279	Pleist		Alluvial Valley	CDMG, Geomatrix				C2	NureG/CR-0055
LA*	3345 Wilshire	CIT	196	34.062	118.295	Pleist		Alluvial Valley	CDMG, Geomatrix	A	392	C	C1	NUREG/CR-0074
LA*	3407 W. Sixth Street	CIT	199	34.060	118.300	Pleist		Alluvial Valley	CDMG, Geomatrix	A	410	C	C1	Law/Crandall 79156
LA*	3411 Wilshire	CIT	202	34.050	118.280	Pleist		Alluvial Valley	CDMG, Geomatrix	A	392	C	C1	NUREG/CR-0055, V1
LA*	3440 University (USC)	CIT	205	34.022	118.283	Holo	Coarse	Alluvial Valley	CDMG, Geomatrix				D?	LAw/Crandall 73004
LA*	3470 Wilshire	CIT	208	34.061	118.299	Holo		Alluvial Valley	CDMG, Geomatrix	B	384	C	C2	NUREG/CR-0055, V1
LA*	3550 Wilshire	CIT	211	34.050	118.300	Holo	Fine	Alluvial Valley	CDMG, Geomatrix	A	384	C	C1	NUREG/CR-0055, V1
LA*	3710 Wilshire	CIT	217	34.061	118.306	Pleist		Alluvium	CDMG, Geomatrix	B	384	C	C1	NUREG/CR-0055, V1
LA*	3838 Lankershim	CIT	220	34.137	118.360	Holo	Coarse		Geomatrix	A	454	C	C1	NUREG/CR-0055, V2
LA*	420 S. Grand	CIT	154	34.050	118.251	Holo		Alluvial Valley	CDMG	A	363	C	C1	Law/Crandall 79351
LA*	445 S. Figueroa	CIT	157	34.053	118.257	Pleist		Alluvial Valley	CDMG, Geomatrix	B	325	D	C1	NUREG/CR-0055, V1
LA*	4680 Wilshire	CIT	223	34.061	118.330	Pleist		Alluvial Valley	CDMG, Geomatrix	C	460	C	C1	Law/Crandall 77283
LA*	4867 Sunset	CIT	226	34.098	118.294	Pleist		Alluvial Valley	CDMG, Geomatrix	A	379	C	C1	NUREG/CR-0055, V2
LA*	5260 Century Blvd.	CIT	229	33.930	118.370	Pleist		Alluvial Valley	CDMG	A	355	D	D	Law/Crandall 79252
LA*	533 S. Fremont	CIT	160	34.052	118.257	Pleist		Alluvial Valley	CDMG, Geomatrix	B	325	D	C1	NUREG/CR-0055, V1
LA*	5900 Wilshire	CIT	428	34.050	118.350	Pleist		Alluvial Valley	CDMG	B	320	D	C1	Law/Crandall 84199
LA*	611 W. Sixth Street	CIT	163	34.049	118.254	Holo	Fine	Alluvial Valley	CDMG, Geomatrix	B	379	C	C1	Law/Crandall 78256
LA*	616 S. Normandie	CIT	431	34.062	118.298	Holo	Aggregate	Alluvial Valley	CDMG, Geomatrix	B	312	D	C2	Law/Crandall 82046
LA*	6200 Wilshire	CIT	443	34.050	118.350	Pleist	Fine	Alluvial Valley	CDMG, Geomatrix	C	322	D	D	Law/Crandall 81230
LA*	6430 Sunset	CIT	232	34.097	118.329	Holo		Alluvial Valley	CDMG, Geomatrix	C	354	D	C-D?	Law/Crandall 81073
LA*	646 S. Olive	CIT	166	34.050	118.250	Holo		Alluvial Valley	CDMG, Geomatrix	B	376	C	C1	Law/Crandall 79304
LA*	6464 Sunset	CIT	235	34.097	118.331	Holo		Alluvial Valley	CDMG, Geomatrix	C	354	D	C-D?	Law/Crandall 81073
LA*	750 S. Garland	CIT	169	34.050	118.266	Pleist		Alluvial Valley	CDMG	B	328	D	C1	Law/Crandall 85001
LA*	800 W. First	CIT	172	34.050	118.250	Holo		Alluvial Valley	CDMG, Geomatrix	B	283	D	C1	Law/Crandall 82004
LA*	808 S. Olive	CIT	175	34.050	118.260	Pleist		Alluvial Valley	CDMG, Geomatrix	A	515	C	C1?	Law/Crandall 77249
LA*	8244 Orion	CIT	241	34.221	118.471	Holo		Alluvial Fan	CDMG	B	308	D	D	UCLA-ENG-7206
LA*	8639 Lincoln Blvd.	CIT	244	33.960	118.419	Holo	Coarse	Aeolian	CDMG, Geomatrix	C	341	D	D	Law/Crandall 83049
LA*	930 Hilgard	CIT	407	34.050	118.430	Holo		Alluvial Valley	CDMG	B	299	D	C3	Law/Crandall 80057
LA*	945 Tiverton	CIT	178	34.062	118.442	Pleist		Alluvial Valley	CDMG	B	299	D	C3	Law/Crandall 80057
LA*	9841 Airport Blvd	CIT	247	33.946	118.385	Pleist		Alluvial Valley	CDMG, Geomatrix	A	335	D	D	Law/Crandall 81322
LA*	UCLA (Boelter Hall)	CIT	140	34.068	118.439	Holo	Coarse	Alluvial Valley	CDMG, Geomatrix	B	315	D	C2	Law/Crandall 77171
LA*	Water and Power (111 S. Hope St.)	CIT	137	34.050	118.250	Holo	Fine	Alluvial Valley	CDMG, Geomatrix	B	302	D	C1	NUREG/CR-0055, V1
Lafayette	Briones Dam	CSMIP	58183	37.914	122.208	Tertiary			DOC					
Lake Cahuilla		CSMIP	12624	33.628	116.280	Mesoz/Holo ?			CDMG					
Lake Edison	Vermilion Dam	CSMIP	54362	37.369	118.982	Mesoz			DOC, Geomatrix					
Lake Edison	Vermilion Dam Free Field	CSMIP	24384	37.356	118.988	Mesoz			DOC, Geomatrix					
Larkspur	Ferry Teminal	USGS	1590	37.946	122.508	Holo	Fine	Marine	DOC	A	177	E\F	E1	USGS OFR 94-222
Lawndale	15000 Aviation Blvd	USGS		33.895	118.377	Holo	Coarse	Aeolian	CDMG					
Leona Valley	#3	CSMIP	24307	34.596	118.243	Pleist/Pliocene ?			CDMG					
Littlerock	Brainard Canyon	CSMIP	23595	34.486	117.980	Holo/Pleist/Miocene?			CDMG					
Livermore	VA Hospital, Bldg. 62 (bsmt)	USGS	1226	37.625	121.762	Pleist			DOC					
Loleta		USGS		40.644	124.219	Pleist		Non-marine	DOC					
Loma Linda	VA Hospital, North Ground site	USGS	5229	34.050	117.249	Holo		Alluvium	CDMG	A				UCB EERC 97/01
Loma Linda	VA Hospital, South Ground site	USGS	5229	34.050	117.249	Holo		Alluvium	CDMG	A				UCB EERC 97/01
Lone Pine		CSMIP	44015	36.664	118.094	Holo		Lacustrine	DOC					
Long Beach	15-story Office Bldg	CSMIP	14533	33.768	118.195	Pleist	Coarse	Alluvial Valley	CDMG	A	347	D	C2	UCLA Rpt.62-55, USGS OFR 80-378
Long Beach	5-story CSULB Engineering Bldg	CSMIP	14311	33.783	118.112	Holo	Coarse	Alluvial Fan	CDMG, Geomatrix					
Long Beach	Humanities Bldg. Bsmt.	USGS/CIT	132	33.780	118.110	Holo	Coarse	Marine	CDMG, Geomatrix					

Long Beach	Public Utility Building	USGS/CIT	131	33.769	118.194	Pleist	Coarse	Alluvial Valley	CDMG, Geomatrix				C2	UCLA 62-55
Long Beach	VA Hospital	VA	5106	33.780	118.120	Pleist		Marine	CDMG	A	384	C	C3-D	USGS OFR 80-378
Lucerne		SCE	24											
Malibu	Kilpatrick School	USGS	5079	34.093	118.836	Holo		Alluvial Fan	DOC					
Malibu	Las Flores Canyon	USC	90050	34.045	118.637	Mesoz/Tertiary ?			Dibblee Map					
Malibu Canyon	Monte Nido	USGS	5080	34.0778	118.6929	Tertiary			Dibblee Map					
Mammoth Lakes	Elementary School	USC	36						No match					
Mammoth Lakes	Mammoth H.S. Free Field	CSMIP	54482	37.641	118.963	Pleist		Glacial	DOC, Geomatrix					
Mammoth Lakes	Mammoth H.S. Gym	CSMIP	54301	37.641	118.963	Pleist		Glacial	DOC, Geomatrix					
Mariposa		CSMIP	55067	37.502	119.985	Mesoz			DOC					
Martinez	VA Hospital (bsmt)	USGS	1448	37.993	122.115	Tertiary			DOC	A	395	C	C3	AA 9225-6427
Mendota		CDMG/CSM	56073	36.755	120.382	Holo		Basin	DOC					
Menlo Park	VA Hospital, Bldg.37	USGS	1230	37.468	122.157	Holo	Medium	Alluvial Valley	DOC, Geomatrix	A	265	D	D2C	AA 9225-6427
Mentone	Fire Station	USGS	5162	34.0702	117.1214	Holo		Alluvium	CDMG					
Merced		CSMIP	56071	37.289	120.455	Holo		Lacustrine	DOC					
Milpitas	Industrial Bldg. (2-story)	CSMIP	57502	37.430	121.897	Holo	Aggregate		DOC, Geomatrix	A		D?	D?	UCB EERC-97/01
Modesto		CSMIP	57011	37.666	121.036	Pleist		Marine	DOC					
Mojave	Oak Creek Canyon	CSMIP	34237	35.042	118.377	Holo/Mesoz ?			CDMG					
Mt. Baldy	Elementary School	CSMIP	23572	34.233	117.661	Holo/Mesoz ?			CDMG					
Murrieta Hot Springs	Collins Ranch	CSMIP	13198	33.599	117.132	Mesoz/Holo ?			CDMG					
Napa	Napa College	CSMIP	68150	38.270	122.276	Holo		Alluvium	DOC					
Newport Beach	11-story Hospital	CSMIP	13589	33.624	117.929	Pleist	Coarse	Marine	CDMG	A			C2	UCB/EERC-97/01
Newport Beach	800 - 840 Newport Center Drive	USGS	5246	33.618	117.878	Pleist	Coarse	Marine	CDMG	A	424	C	C1	Law/Crandall 79294
Newport Beach	800 Marguerite	USGS	5285	33.585	117.866	Pleist	Coarse	Marine	CDMG					
North Palm Springs	Fire Station	USGS	5295	33.925	116.548	Holo		Alluvium	CDMG					
North Palm Springs	I10/62	CSMIP	12666	33.915	116.608	Holo/Pleist ?		Alluvium	CDMG					
Oakland	Caldecott Tunnel, Hwy 24	CSMIP	58359	37.857	122.214	Tertiary			DOC					
Ocean Beach		CSMIP	03121	32.749	117.241	Pleist		Marine	DOC					
Olema	Point Reyes	CSMIP	68003	38.043	122.797	Holo		Alluvial Fan	DOC					
Orange*	4000 W. Chapman	CIT	472	33.781	117.892	Holo	Coarse	Alluvial Fan	CDMG	C	235	D	D?	Law/Crandall 85134
Palm Springs	Desert Hospital (4-story)	CSMIP	12299	33.838	116.541	Holo			CDMG	C	311	D	C3-D	Law/Crandall 83237
Palo Alto	Fabian Way and San Antonio Rd	CSMIP	58485	37.423	122.100	Holo		Alluvial Valley	DOC					
Palo Alto	Office Bldg. (5-story)	CSMIP	58484	37.424	122.101	Holo		Alluvial Valley	DOC					
Palo Alto	VA Hospital, Bldg.1 (bsmt)	USGS	1227	37.400	122.140	Pleist	Fine		Geomatrix	A	357	D	D1	USGS OFR 92-287
Palos Verdes	Palos Verdes Resevoir (abutment)	USGS	710	33.774	118.321	Tertiary		Alluvial Valley	CDMG					
Panorama City	Roscoe	USC	90007	34.221	118.441	Holo		Alluvial Fan	CDMG	C	300	D	D	Law/Crandall 79077
Pardee	SCE	MWD												
Pasadena	12-story Commerical/Office Bldg.	CSMIP	24546	34.146	118.146	Pleist		Alluvial Fan	CDMG	C	351	D	D	Law/Crandall 81411
Pasadena	12-Story Office Bldg	CSMIP	24566	34.149	118.151	Holo		Alluvial Fan	CDMG					
Pasadena	6-story Office Bldg.	CSMIP	24541	34.146	118.147	Holo		Alluvial Fan	CDMG	C	351	D	D	Law/Crandall 81411
Pasadena	9-story Commercial Bldg.	CSMIP	24571	34.146	118.143	Pleist		Alluvial Fan	CDMG	B	351	D	D3	Law/Crandall 81411
Pasadena	Brown Gym	CDMG	80046											
Pasadena	CIT Bridge Lab	CDMG	80052											
Pasadena	CIT Calif Blvvd.	CDMG	80047											
Pasadena	CIT Indust. Rel	CDMG	80051											
Pasadena	CIT Kresge Lab	CDMG	80054											
Pasadena	CIT Lura St	CDMG	80048											
Pasadena	CIT Mudd Lab	CDMG	80050											
Pasadena	NASA, JPL Bldg. 179	USGS	5410	34.199	118.173	Holo		Alluvial Fan	CDMG	B	488	C	D2	NUREG/CR-0055, V2
Pasadena	NASA, JPL Bldg. 230	USGS	5412	34.200	118.174	Holo		Alluvial Fan	CDMG	A	488	C	D2	NUREG/CR-0055, V2
Pasadena	USGS/NSMP Office	USGS	5296	34.136	118.127	Pleist		Alluvial Fan	CDMG	A	411	C	D	NUREG-0029, V2
Pasadena*	CIT Millikan Library	CIT	264	34.137	118.125	Pleist	Coarse	Alluvial Fan	CDMG, Geomatrix	A	398	C	D2	NUREG-0029, V2
Pasadena*	JPL	CIT	267	34.200	118.170	Holo	Coarse	Alluvial Fan	CDMG	B	488	C	D2	NUREG/CR-0055, V2
Pasadena*	Seismological Lab	CIT	266	34.149	118.171	Mesoz			CDMG, Geomatrix	B	985	B	B	NUREG/CR-0055, V2
Petrolia	General Store	CDMG	1398	40.324	124.286	Holo			DOC	A	343	D	C2	NUREG/CR-0985, V5
Pleasant Hill	Citizens Savings (3-story)	CSMIP	58348	37.946	122.060	Holo		Alluvium	DOC					
Point Mugu	Naval Air Station	CSMIP	25147	34.1128	119.1202	Holo		Alluvium	Dibblee Map					
Poway	City Hall FF	CSMIP	03499	32.954	117.040	Mesoz			DOC					
Priest Valley		CDMG/CSM	46174	36.191	120.708	Holo		Alluvial Fan	DOC					
Puerta La Cruz	USFS Storage Bldg.	CSMIP	12168	33.324	116.683	Pleist/Mesoz ?			CDMG					
Rancho Cucamonga	Deer Canyon	CSMIP	23598	34.169	117.579	Pleist/Mesoz ?			CDMG					
Rancho Cucamonga		CDMG	5253											
Rancho de Anza	Anza Borrego Park	USGS	5047	33.350	116.400	Holo/Mesoz ?			CDMG					
Redlands	Interstate Van Lines Warehouse (1-story)	CSMIP	23495	34.066	117.214	Holo		Alluvial Fan	DOC					
Redlands	Redlands Fed. Savings (7-story)	CSMIP	23481	34.056	117.178	Holo		Alluvial Fan	DOC					
Redwood City	School Office Bldg (3-story)	CSMIP	58263	37.448	122.265	Tertiary			DOC, Geomatrix	C	585	C	C1?	USGS OFR 77-850

Richmond	Bulk Mail - 2501 Rydin Road	USGS	1439	37.884	122.302	Holo		Alluvial Fan	DOC					
Richmond	Office Bldg. (3-story)	CSMIP	58506	37.978	122.329	Tertiary			DOC					
Rockport		CSMIP	79042	39.740	123.815	Holo		Alluvium	DOC					
Ruth Lake	Matthews Dam	CSMIP	89363	40.369	123.433	Mesoz			DOC					
Sage	Fire Station	CSMIP	12636	33.580	116.931	Mesoz			CDMG					
San Benito		CDMG/CSMI	47288	36.519	121.084	Holo		Alluvial Fan	DOC					
San Bernadino	1-story Commercial Bldg.	CSMIP	23622	34.098	117.293	Holo		Alluvial Fan	DOC					
San Bernadino	3-story Motel	CSMIP	23701	34.163	117.332	Paleocene/Holo ?			CDMG					
San Bernadino	County Bldg. Grounds	USGS	5245	34.1055	117.2892	Holo			CDMG	A	454	C	D	UCB/EERC-97/01
San Bernadino	Hilton Inn (6-story)	CSMIP	23287	34.065	117.279	Holo		Alluvial Fan	DOC					
San Bernadino	Live Oak Resevoir	USGS	656	34.137	117.753	Mesoz			CDMG					
San Bernadino	Lytle Creek - Fire Station	USGS	5409	34.233	117.482	Holo/Mesoz ?			CDMG					
San Bernadino	San Antonio Dam	USGS	287	34.1573	117.6786	Holo/Mesoz ?			CDMG					
San Bernadino	San Berdo, Fire station #10	USGS	5339	34.0919	117.2901	Holo		Alluvium	CDMG					
San Bernadino	San Bernadino Array-Seven Oaks Dam	USGS	5300	34.105	117.104	Holo/Mesoz ?			CDMG					
San Bernadino	Valyermo Forest Station	USGS	5031	34.440	117.850	Holo/Tertiary ?			CDMG					
San Bernadino	Weymouth Filter Plant - ground	USGS	5164	34.114	117.778	Pleist	Coarse	Alluvial Fan	CDMG					
San Bernadino*	Hall of Records	USGS	274	34.105	117.2863	Holo			CDMG	C	460	C	D3	UCLA Rpt. 62-55
San Bruno	Gov't Office Bldg. (9-story)	CSMIP	58394	37.627	122.424	Pleist		Non-marine	DOC	A			C2-D	UCB/EERC-97/01
San Bruno	Office Bldg. (6 story)	CSMIP	58490	37.628	122.424	Pleist		Non-marine	DOC					
San Diego	VA Hospital	VA		32.870	117.230	Pleist		Marine	DOC				B	USGS OFR 79-428
San Francisco	1295 Shafter, Fire Station	USGS	1675	37.7274	122.3851	Mesoz/Holo ?			CDMG	A	770	B		USGS OFR 91-311
San Francisco	Commercial Bldg. (18-story)	CSMIP	58480	37.792	122.400	Holo		Alluvium	DOC				C3	W/C (1973)
San Francisco	SFSU; Thornton Hall	USGS	1116	37.724	122.475	Holo			DOC					
San Francisco	Transamerica Tower	USGS	1239	37.800	122.400	Mesoz			DOC	C	169	E	C3	USGS OFR 80-473
San Francisco	UCSF (6-story)	CSMIP	58479	37.762	122.459	Holo		Aeolian	DOC					
San Jose	Gov't Office Bldg. (13-story)	CSMIP	57357	37.353	121.903	Holo		Alluvium	DOC	A	210	D	D	UCB/EERC-97/01
San Jose	Great Western Savings (10-story)	CSMIP	57355	37.338	121.893	Holo	Fine	Alluvium	DOC, Geomatrix					
San Jose	Lexington Dam	CSMIP	57180	37.202	121.949	Mesoz			DOC, Geomatrix	A	1109	B	B	AA 9225-6427
San Jose	San Jose Interchange; 101/280/680	USGS	1571	37.340	121.851	Holo	Fine	Alluvial Fan	DOC, Geomatrix					
San Jose	Santa Teresa Hills	CSMIP	57563	37.210	121.803	Mesoz			DOC					
San Jose	Town Park Towers (10-story)	CSMIP	57356	37.338	121.888	Holo		Alluvium	DOC, Geomatrix	A	210	D	D	UCB/EERC-97/01
San Juan Bautista	Fire Station	CSMIP	47126	36.846	121.536	Pleist			DOC, Geomatrix					
San Juan Bautista	Hwy 101/156 Overpass	CSMIP	47315	36.862	121.578	Pleist			DOC, Geomatrix					
San Juan Capistrano*		CIT	465	33.489	117.671	Holo/Miocene ?			CDMG					
San Luis Obispo*		CIT	83	35.283	120.666	Holo/Mesoz ?			CDMG	C				NUREG/CR-0055, V2, UCLA Rpt. 62-55
San Martin	Coyote Creek	CSMIP	57217	37.120	121.540	Mesoz			DOC					
San Rafael	Office Bldg (3-story)	CSMIP	68341	38.196	122.819	Mesoz			DOC					
San Rafael	Sewage Plant	CSMIP	58096	37.960	122.499	Holo	Fine	Marine	DOC					
San Ramon	Fire Station	CDMG	57134											
Santa Ana	400 Civic Center Dr.	USGS		33.751	117.870	Holo	Aggregate	Alluvial Fan	CDMG				C2-C3	UCLA 62-55
Santa Ana	Diemer Filter Plant - administration	USGS	698	33.910	117.820	Holo		Fill	CDMG					
Santa Ana	Orange County Engineering Bldg.	USGS/CIT	281	33.750	117.870	Holo	Aggregate	Alluvial Fan	CDMG				C2	UCLA 62-55
Santa Ana	San Joaquin Resevoir (left abutment)	MWD	5257	33.620	117.844	Holo		Fill	CDMG					
Santa Ana	Warner & Greenville	CSMIP	13891	33.716	117.904	Holo	Coarse	Alluvial Fan	CDMG					
Santa Barbara	Freitas	CSMIP	25302	34.4238	119.6989	Pleist			CDMG	B	392	C	D1	NUREG-0029, V2
Santa Cruz	BRAN	UCSC	13	?	?									
Santa Cruz	UCSC	UCSC	15	37.000	122.062	Mesoz			DOC	A	1137	B	C1	AA 9225-6427
Santa Rosa	Commercial Bldg. (5-story)	CSMIP	68387	38.439	122.711	Holo		Alluvium	DOC					
Santa Rosa	Hendley and Tupper	CSMIP	68491	38.437	122.707	Pleist		Alluvium	DOC					
Santa Rosa	Residential Bldg. (14-story)	CSMIP	68489	38.437	122.707	Pleist		Alluvium	DOC					
Shelter Cove	Station A	CDMG	1277	40.040	124.060	Mesoz			DOC					
Shelter Cove	Station B	CDMG	1278	40.030	124.060	Mesoz			DOC					
Sherman Oaks	Union Bank Bldg. (13-story)	CSMIP	24322	34.154	118.465	Tertiary		Alluvial Fan	CDMG, Geomatrix	A	294	D	C2	Law/Crandall 81384
Snow Creek		CSMIP	12630	33.888	116.684	Holo/Mesoz ?			CDMG					
So. San Francisco	Hospital (4-story)	CSMIP	58261	37.660	122.439	Pleist		Non-marine	DOC					
Stockton	Univ. of Pacific	CSMIP	57062	37.981	121.311	Pleist		Marine	DOC					
Sunol	Calaveras Array - Fire Stn.	USGS	1688	37.597	121.880	Pleist			DOC, Geomatrix	A	402	C	D2	USGS 94-552
Taft*	Buena Vista	USGS	1	34.150	119.330									
Tinehama Resevoir	Tinehama Dam	CSMIP	54361	37.052	118.219	Holo		Alluvium	DOC					
Trinity Center		CSMIP	88048	40.982	122.709	Holo		Glacial	DOC					
Turkey	Eregli	ERD		40.980	27.790	Tertiary			MTA-Turkey					
Turkey	Tekirdag	ERD		40.979	27.515	Tertiary			MTA-Turkey					
Upland*	San Antonio Dam	CIT	287	35.799	120.884	Holo/Miocene ?			CDMG					
Vacaville		CSMIP	67068	38.348	121.963	Holo		Alluvial Fan	DOC					

Van Nuys	Holiday Inn (7-story)	CSMIP	24386	34.221	118.471	Holo		Alluvial Fan	CDMG, Geomatrix	C	354	D	D	USGS OFR 80-378
Vasquez Rocks Park		CSMIP	24047	34.490	118.320	Pleist/Oligocene ?			CDMG					
Vernon	CMD Building	USGS/CIT	288	34.000	118.200	Holo	Coarse	Alluvial Fan	CDMG	A	299	D	D2	USGS OFR 82-833
Walnut Creek	Fidelity S&L (10-story)	CSMIP	58364	37.907	122.065	Holo		Alluvial Fan	DOC	A			C1	UCB/EERC-97/01
Watsonville	Telephone Bldg.	CSMIP	47459	36.909	121.756	Holo		Alluvial Fan	DOC					
Westwood	UCLA Factor Bldg	USGS	5405	34.066	118.441	Pleist		Alluvial Valley	CDMG	A	428	C	C2	Law/Crandall 76124
Whittier	7215 Bright Ave (bsmt)	USGS	804	33.977	118.036	Holo		Alluvial Fan	CDMG, Geomatrix					
Whittier	8-story Hotel	CSMIP	14606	33.975	118.036	Holo	fine	Alluvial Fan	CDMG	A			D	UCB/EERC-9701
Winchester	Hidden Valley Farms	CSMIP	13200	33.681	117.056	Mesoz			Geomatrix					
Winterhaven	Sheriff Substation	CSMIP	00022	32.739	114.635	Holo		Alluvial Valley	DOC					
Wrightwood*	Post Office	CIT	290	34.360	117.629	Holo/Mesoz ?			CDMG					
	Aeropuerto Mexicali	UNAM	6616	32.650	115.320									
	ALP (temp)	USGS	4											
	Cachuma Dam (toe)	USGS	106	34.580	119.980	Miocene/Pleist ?			CDMG	A			B	UCLA Rpt. 62-55
	Cash Baugh Ranch	USC	34											
	CHP (temp)	CDMG	46T04											
	Cucapah	UNAM	6617	32.530	115.230	Holo	Aggregate		Geomatrix					
	Del Valle Dam (Toe)	USGS	1265	37.6152	121.7464	Mesoz/Pleist/Miocene ?			CDMG					
	Devers Hill Substation	SCE	5997											
	Edgecumbe Substation Electricrp													
	Elizabeth Lake #	CDMG	24575	34.662	118.387	Pliocene/Holo ?			CDMG					
	Green Church	USC	3											
	GSH													
	Harris Ranch	CDMG	46T07											
	Heart Bar State Park	CSMIP	22T04	34.161	116.799	Mesoz/Holo ?			CDMG					
	Hinds Pumping Plant	MWD/USGS	817	33.710	115.630	Mesoz			DOC					
	Hot Creek	USGS	44											
	Kornbloom Road	USGS												
	LLN	USGS	5											
	Mission Creek Fault	USGS	100											
	MIT (temp)	USGS	6											
	OLF													
	Poe Road	USGS												
	SAHOP Casa Flores	UNAM	6619											
	SGT	USGS	7											
	South Bay Union School	USGS		40.734	124.207	Holo			DOC					
	SUB (temp)	USGS	8											
	TRA (temp)	USGS	9											
	VEW	USGS	10											
	WBS													
	Whitewater Trout Farm	USGS	5072	33.989	116.655	Tertiary/Holo ?			CDMG					
	Woodfords													
	YUB (temp)													

[1] Boring-SMA distance index: A = < 150 m; B = 150 - 450 m; C = 450 - 1600 m

1: Fukushima et al., 2000

2: Shoja-Taheri and Anderson, 1988

Rathje 2000 = personal communication

References

APPENDIX C

Regression Coefficients for Recommended Site Categories

Age Only
Holocene

T (s)	a	+/-	b	+/-	sigma
0.01	-0.25	0.14	-0.17	0.05	0.54
0.02	-0.25	0.14	-0.17	0.05	0.53
0.03	-0.30	0.14	-0.16	0.05	0.54
0.04	-0.47	0.14	-0.18	0.05	0.53
0.05	-0.50	0.14	-0.16	0.05	0.53
0.06	-0.50	0.13	-0.16	0.05	0.53
0.08	-0.48	0.14	-0.14	0.05	0.53
0.09	-0.43	0.14	-0.13	0.05	0.55
0.10	-0.42	0.14	-0.13	0.05	0.55
0.12	-0.37	0.14	-0.13	0.06	0.56
0.15	-0.37	0.14	-0.15	0.06	0.56
0.17	-0.38	0.14	-0.16	0.05	0.55
0.20	-0.39	0.14	-0.17	0.05	0.55
0.24	-0.30	0.14	-0.15	0.05	0.53
0.30	-0.21	0.13	-0.16	0.05	0.52
0.36	-0.11	0.13	-0.13	0.05	0.51
0.40	-0.09	0.13	-0.13	0.05	0.50
0.46	-0.08	0.13	-0.14	0.05	0.49
0.50	0.03	0.13	-0.11	0.05	0.50
0.60	0.07	0.14	-0.11	0.05	0.54
0.75	0.17	0.14	-0.08	0.06	0.56
0.85	0.19	0.15	-0.06	0.06	0.58
1.00	0.23	0.15	-0.04	0.06	0.59
1.50	0.20	0.18	-0.05	0.07	0.69
2.00	0.17	0.19	-0.04	0.07	0.75
3.00	0.32	0.21	-0.07	0.09	0.64
4.00	-0.04	0.22	-0.19	0.09	0.66
5.00	0.45	0.25	-0.09	0.11	0.62
Fa	-0.21	0.12	-0.14	0.05	0.48
Fv	0.14	0.13	-0.09	0.05	0.50

Age Only
Pleistocene

T (s)	a	+/-	b	+/-	sigma
0.01	0.08	0.27	0.00	0.10	0.47
0.02	0.02	0.27	-0.02	0.10	0.46
0.03	-0.03	0.28	-0.01	0.10	0.48
0.04	-0.29	0.28	-0.06	0.11	0.49
0.05	-0.18	0.27	-0.02	0.10	0.46
0.06	-0.22	0.27	-0.04	0.10	0.46
0.08	-0.23	0.26	-0.04	0.10	0.45
0.09	-0.11	0.26	0.00	0.10	0.45
0.10	-0.11	0.27	-0.01	0.10	0.46
0.12	-0.08	0.27	-0.01	0.10	0.47
0.15	-0.10	0.26	-0.02	0.10	0.44
0.17	-0.16	0.26	-0.06	0.10	0.44
0.20	-0.08	0.29	-0.03	0.11	0.49
0.24	0.07	0.28	0.01	0.11	0.48
0.30	0.18	0.28	0.05	0.11	0.48
0.36	0.20	0.28	0.05	0.11	0.49
0.40	0.24	0.29	0.05	0.11	0.50
0.46	0.17	0.31	0.01	0.12	0.53
0.50	0.22	0.31	0.02	0.12	0.53
0.60	0.27	0.32	0.03	0.12	0.54
0.75	0.43	0.33	0.07	0.12	0.57
0.85	0.37	0.34	0.05	0.13	0.58
1.00	0.35	0.33	0.04	0.12	0.56
1.50	0.07	0.35	-0.08	0.13	0.60
2.00	-0.03	0.37	-0.11	0.14	0.64
3.00	-0.06	0.43	-0.21	0.18	0.50
4.00	-0.81	0.49	-0.45	0.20	0.57
5.00	-0.17	0.61	-0.34	0.24	0.59
Fa	0.08	0.25	0.00	0.09	0.42
Fv	0.26	0.29	0.00	0.11	0.50

Age Only
Tertiary

T (s)	a	+/-	b	+/-	sigma
0.01	0.23	0.36	-0.02	0.14	0.62
0.02	0.16	0.36	-0.06	0.15	0.61
0.03	0.14	0.37	-0.03	0.14	0.64
0.04	-0.08	0.38	-0.07	0.15	0.66
0.05	-0.03	0.37	-0.04	0.14	0.64
0.06	-0.05	0.37	-0.04	0.14	0.64
0.08	-0.08	0.36	-0.05	0.14	0.63
0.09	-0.02	0.35	-0.03	0.14	0.61
0.10	-0.05	0.35	-0.03	0.13	0.60
0.12	-0.06	0.35	-0.04	0.14	0.61
0.15	-0.04	0.35	-0.04	0.14	0.61
0.17	-0.03	0.36	-0.06	0.14	0.63
0.20	-0.02	0.36	-0.07	0.14	0.62
0.24	-0.01	0.37	-0.07	0.14	0.64
0.30	0.08	0.37	-0.05	0.14	0.64
0.36	0.02	0.40	-0.07	0.16	0.70
0.40	0.03	0.38	-0.07	0.15	0.66
0.46	0.07	0.37	-0.06	0.14	0.64
0.50	0.06	0.37	-0.08	0.14	0.64
0.60	0.08	0.36	-0.07	0.14	0.63
0.75	0.17	0.37	-0.02	0.14	0.64
0.85	0.17	0.39	-0.01	0.15	0.67
1.00	0.08	0.35	-0.04	0.14	0.61
1.50	-0.04	0.39	-0.05	0.15	0.68
2.00	-0.13	0.42	-0.06	0.16	0.73
3.00	0.27	0.37	-0.01	0.18	0.47
4.00	-0.01	0.36	-0.04	0.18	0.45
5.00	0.32	0.57	0.01	0.32	0.51
Fa	0.04	0.34	-0.06	0.13	0.59
Fv	0.07	0.34	-0.06	0.13	0.58

Age Only
Mesozoic

T (s)	a	+/-	b	+/-	sigma
0.01	-0.18	0.35	-0.10	0.14	0.54
0.02	-0.22	0.35	-0.14	0.14	0.54
0.03	-0.13	0.36	-0.07	0.15	0.56
0.04	-0.20	0.37	-0.05	0.15	0.58
0.05	-0.19	0.36	-0.03	0.15	0.57
0.06	-0.16	0.36	-0.03	0.15	0.56
0.08	-0.16	0.35	-0.02	0.14	0.55
0.09	-0.12	0.35	-0.02	0.14	0.55
0.10	-0.16	0.33	-0.03	0.14	0.52
0.12	-0.20	0.34	-0.07	0.14	0.53
0.15	-0.29	0.36	-0.11	0.15	0.56
0.17	-0.35	0.36	-0.13	0.15	0.57
0.20	-0.39	0.37	-0.14	0.15	0.58
0.24	-0.47	0.37	-0.15	0.15	0.58
0.30	-0.48	0.38	-0.15	0.15	0.59
0.36	-0.40	0.43	-0.12	0.18	0.68
0.40	-0.43	0.45	-0.13	0.18	0.70
0.46	-0.57	0.46	-0.18	0.19	0.73
0.50	-0.55	0.46	-0.17	0.19	0.73
0.60	-0.64	0.47	-0.20	0.19	0.74
0.75	-0.65	0.50	-0.19	0.21	0.79
0.85	-0.63	0.52	-0.16	0.21	0.82
1.00	-0.66	0.53	-0.17	0.22	0.83
1.50	-0.70	0.56	-0.13	0.23	0.88
2.00	-0.69	0.56	-0.09	0.23	0.88
3.00	-0.46	0.61	-0.14	0.27	0.66
4.00	-1.05	0.57	-0.36	0.25	0.62
5.00	-0.13	0.83	0.00	0.40	0.70
Fa	-0.35	0.34	-0.13	0.14	0.54
Fv	-0.56	0.46	-0.15	0.19	0.73

Age + texture
Holo.+ Coarse

T (s)	a	+/-	b	+/-	sigma
0.01	-0.16	0.26	-0.12	0.10	0.51
0.02	-0.14	0.26	-0.12	0.10	0.51
0.03	-0.21	0.26	-0.12	0.10	0.51
0.04	-0.42	0.27	-0.14	0.10	0.52
0.05	-0.35	0.27	-0.08	0.10	0.53
0.06	-0.38	0.27	-0.09	0.10	0.52
0.08	-0.30	0.28	-0.05	0.10	0.55
0.09	-0.20	0.28	-0.02	0.10	0.55
0.10	-0.19	0.28	-0.02	0.10	0.55
0.12	-0.19	0.28	-0.04	0.10	0.55
0.15	-0.14	0.27	-0.04	0.10	0.54
0.17	-0.16	0.27	-0.07	0.10	0.53
0.20	-0.27	0.27	-0.10	0.10	0.54
0.24	-0.16	0.26	-0.09	0.10	0.52
0.30	-0.14	0.25	-0.11	0.09	0.50
0.36	-0.06	0.24	-0.09	0.09	0.48
0.40	-0.08	0.24	-0.11	0.09	0.47
0.46	-0.12	0.24	-0.14	0.09	0.47
0.50	0.01	0.23	-0.11	0.09	0.46
0.60	0.00	0.26	-0.12	0.10	0.51
0.75	0.09	0.28	-0.09	0.10	0.56
0.85	0.12	0.28	-0.07	0.10	0.55
1.00	0.15	0.29	-0.06	0.11	0.57
1.50	-0.07	0.32	-0.15	0.12	0.63
2.00	-0.05	0.35	-0.13	0.13	0.70
3.00	-0.08	0.46	-0.22	0.17	0.63
4.00	-0.71	0.52	-0.43	0.20	0.67
5.00	0.22	0.68	-0.18	0.26	0.68
Fa	-0.11	0.23	-0.09	0.09	0.46
Fv	0.05	0.24	-0.11	0.09	0.48

Age + Texture
Holo.+ Aggregate

T (s)	a	+/-	b	+/-	sigma
0.01	-0.50	0.26	-0.31	0.11	0.51
0.02	-0.48	0.26	-0.31	0.11	0.51
0.03	-0.52	0.26	-0.29	0.11	0.52
0.04	-0.60	0.26	-0.26	0.11	0.51
0.05	-0.69	0.25	-0.27	0.11	0.51
0.06	-0.67	0.25	-0.27	0.11	0.50
0.08	-0.67	0.25	-0.25	0.11	0.49
0.09	-0.65	0.25	-0.25	0.11	0.50
0.10	-0.59	0.26	-0.22	0.11	0.53
0.12	-0.55	0.27	-0.22	0.12	0.54
0.15	-0.58	0.26	-0.25	0.12	0.53
0.17	-0.59	0.27	-0.27	0.12	0.53
0.20	-0.57	0.26	-0.27	0.11	0.51
0.24	-0.48	0.25	-0.25	0.11	0.49
0.30	-0.34	0.23	-0.23	0.10	0.47
0.36	-0.28	0.23	-0.22	0.10	0.46
0.40	-0.30	0.23	-0.24	0.10	0.46
0.46	-0.23	0.24	-0.23	0.10	0.48
0.50	-0.09	0.24	-0.19	0.11	0.48
0.60	0.00	0.26	-0.17	0.11	0.52
0.75	0.07	0.28	-0.16	0.12	0.56
0.85	0.09	0.28	-0.14	0.12	0.56
1.00	0.12	0.28	-0.11	0.12	0.56
1.50	0.14	0.31	-0.11	0.14	0.62
2.00	0.17	0.31	-0.06	0.14	0.63
3.00	0.33	0.32	-0.11	0.15	0.57
4.00	0.13	0.31	-0.16	0.15	0.55
5.00	0.19	0.42	-0.24	0.22	0.65
Fa	-0.39	0.22	-0.24	0.10	0.45
Fv	0.03	0.24	-0.16	0.11	0.48

Age + Depositional Environment

Holo.+L/M

T (s)	a	+/-	b	+/-	sigma
0.01	-0.56	0.31	-0.37	0.14	0.47
0.02	-0.53	0.31	-0.37	0.14	0.48
0.03	-0.57	0.32	-0.35	0.14	0.49
0.04	-0.61	0.33	-0.32	0.14	0.50
0.05	-0.73	0.30	-0.34	0.13	0.47
0.06	-0.68	0.29	-0.31	0.13	0.44
0.08	-0.71	0.32	-0.31	0.14	0.48
0.09	-0.66	0.35	-0.30	0.16	0.54
0.10	-0.64	0.34	-0.28	0.15	0.53
0.12	-0.62	0.36	-0.28	0.16	0.55
0.15	-0.64	0.36	-0.31	0.16	0.55
0.17	-0.60	0.35	-0.30	0.16	0.54
0.20	-0.62	0.33	-0.30	0.15	0.51
0.24	-0.46	0.34	-0.26	0.15	0.53
0.30	-0.36	0.29	-0.23	0.13	0.45
0.36	-0.21	0.31	-0.18	0.14	0.47
0.40	-0.22	0.31	-0.20	0.14	0.48
0.46	-0.18	0.28	-0.19	0.13	0.43
0.50	-0.12	0.28	-0.18	0.13	0.44
0.60	-0.09	0.31	-0.20	0.14	0.48
0.75	0.01	0.31	-0.19	0.14	0.47
0.85	0.08	0.32	-0.15	0.14	0.49
1.00	0.10	0.32	-0.15	0.14	0.49
1.50	0.20	0.34	-0.11	0.15	0.51
2.00	0.16	0.40	-0.11	0.18	0.62
3.00	0.39	0.38	-0.09	0.22	0.47
4.00	0.35	0.38	-0.04	0.22	0.47
5.00	0.14	0.34	-0.24	0.23	0.38
Fa	-0.38	0.30	-0.24	0.13	0.46
Fv	0.01	0.28	-0.17	0.12	0.43

Age + Depositional Environment

Quat. + Alluv

T (s)	a	+/-	b	+/-	sigma
0.01	-0.18	0.16	-0.14	0.06	0.52
0.02	-0.17	0.16	-0.13	0.06	0.52
0.03	-0.27	0.16	-0.14	0.06	0.52
0.04	-0.51	0.16	-0.18	0.06	0.51
0.05	-0.47	0.16	-0.13	0.06	0.51
0.06	-0.50	0.16	-0.15	0.06	0.51
0.08	-0.46	0.16	-0.13	0.06	0.51
0.09	-0.39	0.16	-0.11	0.06	0.52
0.10	-0.37	0.17	-0.11	0.06	0.53
0.12	-0.31	0.17	-0.11	0.06	0.53
0.15	-0.31	0.17	-0.12	0.06	0.53
0.17	-0.34	0.17	-0.15	0.06	0.53
0.20	-0.35	0.17	-0.15	0.06	0.53
0.24	-0.24	0.16	-0.13	0.06	0.51
0.30	-0.12	0.16	-0.12	0.06	0.51
0.36	-0.04	0.16	-0.10	0.06	0.50
0.40	-0.01	0.16	-0.10	0.06	0.51
0.46	-0.04	0.16	-0.13	0.06	0.52
0.50	0.07	0.17	-0.09	0.06	0.52
0.60	0.09	0.18	-0.09	0.07	0.57
0.75	0.16	0.18	-0.08	0.07	0.58
0.85	0.16	0.19	-0.07	0.07	0.60
1.00	0.23	0.19	-0.04	0.07	0.61
1.50	0.10	0.21	-0.09	0.08	0.67
2.00	0.00	0.23	-0.12	0.09	0.74
3.00	0.04	0.28	-0.19	0.11	0.65
4.00	-0.46	0.31	-0.36	0.12	0.67
5.00	0.32	0.37	-0.16	0.15	0.64
Fa	-0.15	0.15	-0.12	0.06	0.47
Fv	0.13	0.16	-0.09	0.06	0.52

NEHRP B

T (s)	a	+/-	b	+/-	sigma
0.01	-0.16	1.26	-0.04	0.51	0.51
0.02	-0.33	1.34	-0.12	0.55	0.52
0.03	-0.19	1.24	-0.02	0.51	0.51
0.04	-0.24	1.19	-0.01	0.49	0.49
0.05	-0.17	1.11	0.05	0.45	0.45
0.06	-0.16	1.10	0.05	0.45	0.45
0.08	-0.17	1.03	0.03	0.42	0.42
0.09	-0.33	0.93	-0.05	0.38	0.38
0.10	-0.19	0.97	0.03	0.40	0.40
0.12	-0.15	0.98	0.03	0.40	0.40
0.15	0.18	1.04	0.18	0.42	0.42
0.17	0.11	1.21	0.12	0.49	0.49
0.20	0.12	1.22	0.15	0.50	0.50
0.24	-0.17	1.20	0.06	0.49	0.49
0.30	-0.41	1.15	-0.02	0.47	0.47
0.36	-0.42	1.49	0.02	0.61	0.61
0.40	-0.52	1.51	-0.02	0.62	0.62
0.46	-0.88	1.50	-0.15	0.61	0.61
0.50	-0.86	1.42	-0.15	0.58	0.58
0.60	-0.74	1.28	-0.12	0.52	0.52
0.75	-0.84	1.58	-0.17	0.64	0.64
0.85	-0.94	1.77	-0.20	0.72	0.72
1.00	-1.03	1.84	-0.22	0.75	0.75
1.50	-1.42	1.77	-0.41	0.72	0.72
2.00	-1.38	2.00	-0.39	0.82	0.82
3.00	-1.77	1.79	-0.65	0.66	0.32
4.00	-2.98	1.41	-1.07	0.52	0.25
5.00	-	-	-	-	-
Fa	-0.25	1.08	0.02	0.44	0.44
Fv	-0.93	1.50	-0.21	0.61	0.61

NEHRP C T (s)	a	+/-	b	+/-	sigma
0.01	-0.11	0.26	-0.08	0.10	0.56
0.02	-0.12	0.26	-0.10	0.10	0.53
0.03	-0.16	0.27	-0.07	0.11	0.56
0.04	-0.33	0.26	-0.11	0.10	0.56
0.05	-0.42	0.26	-0.12	0.10	0.55
0.06	-0.41	0.26	-0.11	0.10	0.55
0.08	-0.43	0.26	-0.13	0.10	0.55
0.09	-0.36	0.27	-0.11	0.11	0.56
0.10	-0.40	0.26	-0.12	0.10	0.56
0.12	-0.37	0.26	-0.11	0.10	0.56
0.15	-0.39	0.28	-0.15	0.11	0.58
0.17	-0.36	0.28	-0.14	0.11	0.59
0.20	-0.40	0.28	-0.15	0.11	0.60
0.24	-0.35	0.29	-0.15	0.11	0.61
0.30	-0.29	0.30	-0.14	0.12	0.63
0.36	-0.25	0.34	-0.13	0.13	0.71
0.40	-0.22	0.33	-0.12	0.13	0.70
0.46	-0.21	0.33	-0.13	0.13	0.69
0.50	-0.15	0.31	-0.11	0.12	0.66
0.60	-0.15	0.34	-0.12	0.13	0.71
0.75	0.05	0.36	-0.05	0.14	0.76
0.85	0.04	0.37	-0.06	0.15	0.78
1.00	0.05	0.37	-0.05	0.15	0.77
1.50	0.06	0.38	-0.03	0.15	0.80
2.00	0.09	0.37	0.02	0.15	0.79
3.00	0.09	0.57	0.00	0.27	0.76
4.00	-0.33	0.57	-0.15	0.27	0.74
5.00	-0.17	0.84	-0.25	0.41	0.75
Fa	-0.27	0.27	-0.13	0.11	0.57
Fv	0.00	0.32	-0.07	0.13	0.68

NEHRP D T (s)	a	+/-	b	+/-	sigma
0.01	0.07	0.22	-0.07	0.08	0.57
0.02	0.04	0.22	-0.07	0.08	0.56
0.03	0.00	0.22	-0.06	0.09	0.57
0.04	-0.18	0.21	-0.09	0.08	0.56
0.05	-0.22	0.21	-0.08	0.08	0.56
0.06	-0.22	0.21	-0.08	0.08	0.56
0.08	-0.23	0.22	-0.08	0.08	0.57
0.09	-0.16	0.22	-0.06	0.09	0.57
0.10	-0.15	0.23	-0.06	0.09	0.59
0.12	-0.10	0.23	-0.05	0.09	0.60
0.15	-0.14	0.23	-0.08	0.09	0.59
0.17	-0.19	0.22	-0.11	0.08	0.56
0.20	-0.16	0.21	-0.10	0.08	0.55
0.24	-0.07	0.21	-0.09	0.08	0.54
0.30	0.07	0.21	-0.05	0.08	0.54
0.36	0.12	0.21	-0.04	0.08	0.53
0.40	0.12	0.20	-0.05	0.08	0.51
0.46	0.13	0.19	-0.06	0.07	0.49
0.50	0.25	0.19	-0.04	0.07	0.50
0.60	0.29	0.20	-0.03	0.08	0.52
0.75	0.41	0.20	0.00	0.08	0.52
0.85	0.41	0.20	0.01	0.08	0.53
1.00	0.37	0.21	-0.01	0.08	0.54
1.50	0.36	0.23	-0.02	0.09	0.59
2.00	0.29	0.25	-0.03	0.10	0.65
3.00	0.47	0.26	0.00	0.12	0.56
4.00	0.01	0.26	-0.16	0.12	0.56
5.00	0.52	0.35	-0.06	0.16	0.61
Fa	0.02	0.19	-0.06	0.07	0.50
Fv	0.34	0.18	-0.02	0.07	0.46

Geotechnical Data

B T (s)	a	+/-	b	+/-	sigma
0.01	-0.03	0.50	0.02	0.22	0.56
0.02	-0.02	0.51	0.00	0.23	0.56
0.03	-0.05	0.50	0.04	0.22	0.56
0.04	-0.12	0.51	0.04	0.23	0.57
0.05	-0.17	0.50	0.04	0.22	0.56
0.06	-0.15	0.50	0.04	0.22	0.56
0.08	-0.20	0.48	0.02	0.21	0.54
0.09	-0.25	0.47	-0.01	0.21	0.53
0.10	-0.27	0.47	-0.01	0.21	0.53
0.12	-0.29	0.49	-0.05	0.22	0.55
0.15	-0.21	0.55	-0.01	0.24	0.62
0.17	-0.18	0.56	-0.01	0.25	0.63
0.20	-0.27	0.54	-0.03	0.24	0.61
0.24	-0.23	0.60	0.00	0.27	0.67
0.30	-0.17	0.59	0.06	0.26	0.67
0.36	-0.16	0.68	0.11	0.30	0.77
0.40	-0.12	0.67	0.11	0.30	0.76
0.46	-0.20	0.66	0.09	0.29	0.74
0.50	-0.15	0.64	0.09	0.28	0.72
0.60	-0.26	0.63	0.05	0.28	0.71
0.75	-0.21	0.67	0.06	0.30	0.76
0.85	-0.19	0.72	0.09	0.32	0.81
1.00	-0.14	0.70	0.12	0.31	0.79
1.50	-0.22	0.73	0.11	0.32	0.82
2.00	-0.31	0.78	0.11	0.35	0.88
3.00	-0.24	0.77	-0.08	0.35	0.63
4.00	-0.81	0.86	-0.28	0.39	0.70
5.00	-0.10	1.06	0.01	0.52	0.63
Fa	-0.15	0.53	0.04	0.24	0.60
Fv	-0.15	0.62	0.10	0.28	0.70

Geotechnical Data

C

T (s)	a	+/-	b	+/-	sigma
0.01	0.10	0.30	-0.04	0.11	0.61
0.02	0.09	0.29	-0.06	0.11	0.59
0.03	0.05	0.30	-0.04	0.11	0.62
0.04	-0.15	0.29	-0.08	0.11	0.60
0.05	-0.19	0.29	-0.08	0.11	0.61
0.06	-0.21	0.29	-0.09	0.11	0.61
0.08	-0.20	0.29	-0.08	0.11	0.59
0.09	-0.15	0.29	-0.06	0.11	0.60
0.10	-0.18	0.29	-0.07	0.11	0.61
0.12	-0.15	0.28	-0.07	0.11	0.59
0.15	-0.20	0.28	-0.12	0.11	0.59
0.17	-0.26	0.28	-0.15	0.10	0.58
0.20	-0.30	0.28	-0.16	0.10	0.57
0.24	-0.25	0.28	-0.16	0.11	0.59
0.30	-0.10	0.30	-0.12	0.11	0.63
0.36	-0.03	0.33	-0.11	0.12	0.69
0.40	0.01	0.32	-0.10	0.12	0.67
0.46	0.04	0.31	-0.09	0.12	0.65
0.50	0.12	0.30	-0.07	0.11	0.63
0.60	0.16	0.33	-0.05	0.12	0.68
0.75	0.35	0.34	0.01	0.13	0.70
0.85	0.29	0.34	0.00	0.13	0.71
1.00	0.20	0.35	-0.02	0.13	0.71
1.50	0.17	0.38	-0.02	0.14	0.79
2.00	0.24	0.38	0.04	0.14	0.78
3.00	0.41	0.47	0.13	0.21	0.69
4.00	-0.12	0.41	-0.04	0.18	0.60
5.00	0.68	0.75	0.18	0.34	0.75
Fa	-0.07	0.27	-0.11	0.10	0.56
Fv	0.24	0.30	-0.03	0.11	0.63

Geotechnical Data

D

T (s)	a	+/-	b	+/-	sigma
0.01	-0.04	0.24	-0.09	0.09	0.57
0.02	-0.06	0.23	-0.09	0.09	0.55
0.03	-0.09	0.24	-0.08	0.09	0.57
0.04	-0.25	0.22	-0.10	0.09	0.54
0.05	-0.31	0.22	-0.09	0.09	0.54
0.06	-0.28	0.22	-0.08	0.09	0.53
0.08	-0.32	0.23	-0.09	0.09	0.54
0.09	-0.24	0.23	-0.07	0.09	0.56
0.10	-0.24	0.24	-0.08	0.09	0.57
0.12	-0.17	0.24	-0.06	0.09	0.58
0.15	-0.17	0.24	-0.06	0.09	0.57
0.17	-0.15	0.23	-0.07	0.09	0.56
0.20	-0.13	0.23	-0.07	0.09	0.55
0.24	-0.06	0.22	-0.06	0.09	0.53
0.30	0.04	0.21	-0.05	0.08	0.51
0.36	0.09	0.21	-0.05	0.08	0.50
0.40	0.08	0.21	-0.06	0.08	0.50
0.46	0.09	0.20	-0.07	0.08	0.49
0.50	0.18	0.20	-0.06	0.08	0.49
0.60	0.20	0.21	-0.07	0.08	0.51
0.75	0.35	0.22	-0.03	0.09	0.52
0.85	0.35	0.22	-0.03	0.09	0.54
1.00	0.35	0.22	-0.03	0.09	0.54
1.50	0.37	0.24	-0.04	0.09	0.58
2.00	0.28	0.27	-0.06	0.11	0.64
3.00	0.42	0.29	-0.04	0.13	0.58
4.00	-0.02	0.31	-0.21	0.14	0.61
5.00	0.30	0.39	-0.20	0.18	0.63
Fa	-0.01	0.20	-0.06	0.08	0.49
Fv	0.28	0.20	-0.05	0.08	0.47

Geotechnical Data

E

T (s)	a	+/-	b	+/-	sigma
0.01	-0.88	0.75	-0.62	0.33	0.41
0.02	-0.87	0.75	-0.62	0.33	0.41
0.03	-0.94	0.76	-0.61	0.33	0.42
0.04	-1.03	0.75	-0.58	0.33	0.41
0.05	-1.27	0.66	-0.63	0.29	0.36
0.06	-1.29	0.64	-0.64	0.28	0.35
0.08	-1.30	0.66	-0.62	0.29	0.36
0.09	-1.35	0.73	-0.64	0.32	0.40
0.10	-1.25	0.77	-0.59	0.34	0.43
0.12	-1.23	0.68	-0.58	0.30	0.38
0.15	-1.09	0.74	-0.55	0.32	0.41
0.17	-1.07	0.72	-0.58	0.31	0.40
0.20	-1.09	0.62	-0.58	0.27	0.34
0.24	-0.91	0.59	-0.54	0.26	0.32
0.30	-1.00	0.68	-0.62	0.30	0.38
0.36	-0.91	0.66	-0.57	0.29	0.36
0.40	-0.86	0.71	-0.55	0.31	0.39
0.46	-0.73	0.80	-0.51	0.35	0.44
0.50	-0.55	0.85	-0.47	0.37	0.47
0.60	-0.24	0.91	-0.39	0.40	0.50
0.75	-0.12	0.79	-0.36	0.35	0.44
0.85	-0.22	0.70	-0.40	0.31	0.39
1.00	-0.28	0.80	-0.42	0.35	0.44
1.50	0.32	0.78	-0.10	0.34	0.43
2.00	0.47	0.69	0.00	0.30	0.38
3.00	0.28	0.97	-0.23	0.48	0.46
4.00	0.20	0.78	-0.21	0.38	0.36
5.00	-0.04	0.48	-0.22	0.25	0.19
Fa	-0.93	0.63	-0.55	0.27	0.35
Fv	-0.21	0.69	-0.36	0.30	0.38

PEER REPORTS

PEER reports are available from the National Information Service for Earthquake Engineering (NISEE). To order PEER reports, please contact the Pacific Earthquake Engineering Research Center, 1301 South 46th Street, Richmond, California 94804-4698. Tel.: (510) 231-9468; Fax: (510) 231-9461.

PEER 2001/10 *Amplification Factors for Spectral Acceleration in Active Regions.* Jonathan P. Stewart, Andrew H. Liu, Yoojoong Choi, and Mehmet B. Baturay. December 2001. $20.00

PEER 2001/09 *Ground Motion Evaluation Procedures for Performance-Based Design.* Jonathan P. Stewart, Shyh-Jeng Chiou, Jonathan D. Bray, Robert W. Graves, Paul G. Somerville, and Norman A. Abrahamson. September 2001. $26.00

PEER 2001/07 *The Rocking Spectrum and the Shortcomings of Design Guidelines.* Nicos Makris and Dimitrios Konstantinidis. August 2001. $15.00

PEER 2001/06 *Development of an Electrical Substation Equipment Performance Database for Evaluation of Equipment Fragilities*. Thalia Agnanos. April 1999. $15.00

PEER 2001/05 *Stiffness Analysis of Fiber-Reinforced Elastomeric Isolators.* Hsiang-Chuan Tsai and James M. Kelly. May 2001. $20.00

PEER 2001/04 *Organizational and Societal Considerations for Performance-Based Earthquake Engineering.* Peter J. May. April 2001. $15.00

PEER 2001/03 *A Modal Pushover Analysis Procedure to Estimate Seismic Demands for Buildings: Theory and Preliminary Evaluation.* Anil K. Chopra and Rakesh K. Goel. January 2001. $15.00

PEER 2001/02 *Seismic Response Analysis of Highway Overcrossings Including Soil-Structure Interaction.* Jian Zhang and Nicos Makris. March 2001. $20.00

PEER 2001/01 *Experimental Study of Large Seismic Steel Beam-to-Column Connections.* Egor P. Popov and Shakhzod M. Takhirov. November 2000. $15.00

PEER 2000/10 *The Second U.S.-Japan Workshop on Performance-Based Earthquake Engineering Methodology for Reinforced Concrete Building Structures.* March 2000. $39.00

PEER 2000/09 *Structural Engineering Reconnaissance of the August 17, 1999 Earthquake: Kocaeli (Izmit), Turkey.* Halil Sezen, Kenneth J. Elwood, Andrew S. Whittaker, Khalid Mosalam, John J. Wallace, and John F. Stanton. December 2000. $20.00

PEER 2000/08 *Behavior of Reinforced Concrete Bridge Columns Having Varying Aspect Ratios and Varying Lengths of Confinement.* Anthony J. Calderone, Dawn E. Lehman, and Jack P. Moehle. January 2001. $20.00

PEER 2000/07 *Cover-Plate and Flange-Plate Reinforced Steel Moment-Resisting Connections.* Taejin Kim, Andrew S. Whittaker, Amir S. Gilani, Vitelmo V. Bertero, and Shakhzod M. Takhirov. September 2000. $33.00

PEER 2000/06 *Seismic Evaluation and Analysis of 230-kV Disconnect Switches.* Amir S. J. Gilani, Andrew S. Whittaker, Gregory L. Fenves, Chun-Hao Chen, Henry Ho, and Eric Fujisaki. July 2000. $26.00

PEER 2000/05 *Performance-Based Evaluation of Exterior Reinforced Concrete Building Joints for Seismic Excitation.* Chandra Clyde, Chris P. Pantelides, and Lawrence D. Reaveley. July 2000. $15.00

PEER 2000/04 *An Evaluation of Seismic Energy Demand: An Attenuation Approach.* Chung-Che Chou and Chia-Ming Uang. July 1999. $20.00

PEER 2000/03 *Framing Earthquake Retrofitting Decisions: The Case of Hillside Homes in Los Angeles.* Detlof von Winterfeldt, Nels Roselund, and Alicia Kitsuse. March 2000. $13.00

PEER 2000/02 *U.S.-Japan Workshop on the Effects of Near-Field Earthquake Shaking.* Andrew Whittaker, ed. July 2000. $20.00

PEER 2000/01 *Further Studies on Seismic Interaction in Interconnected Electrical Substation Equipment.* Armen Der Kiureghian, Kee-Jeung Hong, and Jerome L. Sackman. November 1999. $20.00

PEER 1999/14 *Seismic Evaluation and Retrofit of 230-kV Porcelain Transformer Bushings*. Amir S. Gilani, Andrew S. Whittaker, Gregory L. Fenves, and Eric Fujisaki. December 1999. $26.00

PEER 1999/12 *Rehabilitation of Nonductile RC Frame Building Using Encasement Plates and Energy-Dissipating Devices.* Mehrdad Sasani, Vitelmo V. Bertero, James C. Anderson. December 1999. $26.00

PEER 1999/11 *Performance Evaluation Database for Concrete Bridge Components and Systems under Simulated Seismic Loads.* Yael D. Hose and Frieder Seible. November 1999. $20.00

PEER 1999/10 *U.S.-Japan Workshop on Performance-Based Earthquake Engineering Methodology for Reinforced Concrete Building Structures.* December 1999. $33.00

PEER 1999/09 *Performance Improvement of Long Period Building Structures Subjected to Severe Pulse-Type Ground Motions*. James C. Anderson, Vitelmo V. Bertero, and Raul Bertero. October 1999. $26.00

PEER 1999/08 *Envelopes for Seismic Response Vectors.* Charles Menun and Armen Der Kiureghian. July 1999. $26.00

PEER 1999/07 *Documentation of Strengths and Weaknesses of Current Computer Analysis Methods for Seismic Performance of Reinforced Concrete Members.* William F. Cofer. November 1999. $15.00

PEER 1999/06 *Rocking Response and Overturning of Anchored Equipment under Seismic Excitations.* Nicos Makris and Jian Zhang. November 1999. $15.00

PEER 1999/05 *Seismic Evaluation of 550 kV Porcelain Transformer Bushings.* Amir S. Gilani, Andrew S. Whittaker, Gregory L. Fenves, and Eric Fujisaki. October 1999. $15.00

PEER 1999/04 *Adoption and Enforcement of Earthquake Risk-Reduction Measures.* Peter J. May, Raymond J. Burby, T. Jens Feeley, and Robert Wood. $15.00

PEER 1999/03 *Task 3 Characterization of Site Response General Site Categories*. Adrian Rodriguez-Marek, Jonathan D. Bray, and Norman Abrahamson. February 1999. $20.00

PEER 1999/02 *Capacity-Demand-Diagram Methods for Estimating Seismic Deformation of Inelastic Structures: SDF Systems*. Anil K. Chopra and Rakesh Goel. April 1999. $15.00

PEER 1999/01 *Interaction in Interconnected Electrical Substation Equipment Subjected to Earthquake Ground Motions.* Armen Der Kiureghian, Jerome L. Sackman, and Kee-Jeung Hong. February 1999. $20.00

PEER 1998/08 *Behavior and Failure Analysis of a Multiple-Frame Highway Bridge in the 1994 Northridge Earthquake.* Gregory L. Fenves and Michael Ellery. December 1998. $20.00

PEER 1998/07 *Empirical Evaluation of Inertial Soil-Structure Interaction Effects.* Jonathan P. Stewart, Raymond B. Seed, and Gregory L. Fenves. November 1998. $26.00

PEER 1998/06 *Effect of Damping Mechanisms on the Response of Seismic Isolated Structures.* Nicos Makris and Shih-Po Chang. November 1998. $15.00

PEER 1998/05 *Rocking Response and Overturning of Equipment under Horizontal Pulse-Type Motions.* Nicos Makris and Yiannis Roussos. October 1998. $15.00

PEER 1998/04 *Pacific Earthquake Engineering Research Invitational Workshop Proceedings, May 14–15, 1998: Defining the Links between Planning, Policy Analysis, Economics and Earthquake Engineering.* Mary Comerio and Peter Gordon. September 1998. $15.00

PEER 1998/03 *Repair/Upgrade Procedures for Welded Beam to Column Connections.* James C. Anderson and Xiaojing Duan. May 1998. $33.00

PEER 1998/02 *Seismic Evaluation of 196 kV Porcelain Transformer Bushings.* Amir S. Gilani, Juan W. Chavez, Gregory L. Fenves, and Andrew S. Whittaker. May 1998. $20.00

PEER 1998/01 *Seismic Performance of Well-Confined Concrete Bridge Columns.* Dawn E. Lehman and Jack P. Moehle. December 2000. $33.00